Development of a machine learning based methodology for damage identification on bridges

Rick Milton Delgadillo Ayala

doctoral thesis by

January, 2022

Escola de Camins

Escola Tècnica Superior d'Enginyeria de Camins, Canals i Ports

UPC BARCELONATECH

Development of a machine learning based methodology for bridge health monitoring.

Thesis by publications

Doctoral Thesis by:

Rick Milton Delgadillo Ayala

Directed by:

Prof. Dr. Joan Ramon Casas

Barcelona, January 2022

Universitat Politècnica de Catalunya - BarcelonaTech

Department of Civil and Environmental Engineering

DOCTORAL THESIS

UNIVERSITAT POLITÈCNICA DE CATALUNYA BARCELONATECH

Development of a machine learning based methodology for bridge health monitoring

-thesis by publications-

Rick Milton Delgadillo Ayala

UNIVERSITAT POLITÈCNICA DE CATALUNYA
BARCELONATECH

DEPARTAMENT D' ENGINYERIA CIVIL I AMBIENTAL

PROGRAMA DE DOCTORAT D' ENGINYERIA CIVIL

DOCTORAL THESIS

DEVELOPMENT OF A MACHINE LEARNING BASED METHODOLOGY FOR BRIDGE HEALTH MONITORING

Thesis by publications

This dissertation is submitted for the degree of
Doctor in Civil Engineering

PhD Candidate:

Rick Milton Delgadillo Ayala

MSc, Civil Engineer

Thesis Supervisor:

Joan Ramon Casas Rius

Prof., PhD, Civil Engineer

Escola Tècnica Superior d'Enginyers de Camins, Canals i Ports de Barcelona
(ETSECCPB)

Barcelona, January 2022

PRONABEC
PROGRAMA NACIONAL DE BECAS Y CRÉDITO EDUCATIVO
Beca Generación del Bicentenario

This thesis is subsidized by the Ministry of Education of Peru, through the National Program of Scholarships and Educational Credit PRONABEC - Bicentennial Generation Scholarship.

GENERAL INFORMATION

Title of the thesis

"Development of a machine learning based methodology for bridge health monitoring"

PhD student

Name	Rick Milton Delgadillo Ayala
Academic Record	Civil Engineer (MSc in Structural Engineering)
Institution	Universitat Politècnica de Catalunya (UPC)
Email	rick.milton.delgadillo@upc.edu

Thesis supervisor

Name	Joan Ramon Casas Rius
Academic Record	Catedrático Dr. Ingeniero de Caminos, C y P
Institution	Universitat Politècnica de Catalunya (UPC)
Email	joan.ramon.casas@upc.edu

To my family, my parents and sisters:

Teresa, Nilton, Angela and Karol, for their invaluable love, endless support and encouragement.

"His heart searched for a different way to live for the sake of science and knowledge."

RMDA.

Acknowledgments

I want to express my deepest gratitude to my supervisor, Prof. Joan Ramon Casas. He encouraged me to enroll in this mission that, fortunately, has come to fruition. I really appreciate his wise advice not only professionally but also for my whole life. Working with him is a privilege not only as research or engineer but as a great person.

This research has been possible with the vital financial support provided by the Ministry of education of the government of Peru through the National Program of Scholarships and Educational Credit PRONABEC - Bicentennial Generation Scholarship.

Special thanks to my colleagues at PRONABEC Peru, who provided interesting comments and suggestions, always useful.

I would like to thank to Helmut Wanzel (Vienna Consulting Engineers) for the generous sharing of the bridge data assessed within the present thesis.

I appreciate the support of Prof. Chul-Woo Kim of the Department of Civil and Earth Resources Engineering, Kyoto University, Japan, who shared me the data assessed of the steel Struss bridge used in the present thesis.

This research would not have been impossible without the interest of Professors Guido De Roeck, Edwin Reynders and Geert Lombaert from the Katholieke Universiteit Leuven, who provided me the real monitoring data of the Z-24 bridge used within this study.

Also, I must finish by mentioning Prof. Eleni Chatzi, ETH Zurich, for their valuable sharing of the entire data from numerical benchmark bridge used in the present research.

To my family (in the broadest sense of the word). My parents Teresa and Nilton, who are my motor and motive throughout my life, and to my pretty sisters, Angela and Karol, for always believing in me, helping me and giving me advices.

On a personal note, this thesis would not have been possible without the love, encouragement and support of one important person in my life. Words cannot express my gratitude for the unconditional love and everlasting support of God.

I would also like to thank my friends from twenty-one different countries for showing me life in another way.

Abstract

In recent years the scientific community has been developing new techniques in structural health monitoring (SHM) to identify the damages in civil structures specially in bridges. The bridge health monitoring (BHM) systems serve to reduce overall life-cycle maintenance costs for bridges, as their main objective is to prevent catastrophic failure, cracking, damages, corrosion of steel members among others. In the BHM using dynamic data, there are several problems related to the post-processing of the vibration signals such as: (i) when the modal-based dynamic features like natural frequencies, modes shape and damping are used, they present a limitation in relation to damage location, since they are based on a global response of the structure; (ii) presence of noise in the measurement of vibration responses; (iii) inadequate use of existing algorithms for damage feature extraction because of neglecting the non-linearity and non-stationarity of the recorded signals; (iv) environmental and operational conditions can also generate false damage detections in bridges; (v) the drawbacks of traditional algorithms for processing large amounts of data obtained from the BHM.

This thesis proposes new vibration-based parameters, methods and tools with focus on damage detection, localization and quantification, considering a mixed robust methodology that includes signal processing and machine learning methods to solve the identified problems. The increasing volume of bridge monitoring data makes it interesting to study the ability of advanced tools and systems to extract useful information from dynamic and static variables. In particular, in the field of Machine Learning (ML) and Artificial Intelligence (AI), powerful algorithms have been developed to face problems where the amount of data is much larger (big data). In the present thesis, the possibilities of machine learning techniques (unsupervised algorithms) were analyzed for application to bridge structural analysis taking into account both operational and environmental conditions.

A critical literature review was performed, identifying the problems and limitations that some algorithms present for damage identification, localization and quantification on real bridges. A deep study of the accuracy and performance of a set of algorithms for detecting damage in four case studies of bridges was carried out (three real bridges and one numerical model of a bridge). In the BHM literature review inherent to the vibration-based damage detection, several state-of-the-art methods have been studied that do not consider the nature of the data and the characteristics of the applied excitation (possible non-linearity, non-stationarity, presence or absence of environmental and / or operational effects,) and the noise level of the sensors. This is identified as problematic when applied to BHM. Besides, most research uses modal-based damage characteristics (natural frequencies, mode shapes, and damping) that have some limitations. A poor data normalization is performed by the majority of methods and both operational and environmental variability is not properly accounted for. Likewise, the huge amount of data recorded requires automatic procedures with proven capacity to reduce the possibility of false alarms. On the other hand, many investigations have limitations since only numerical or laboratory cases are studied. All these problems are identified. As a consequence,

a methodology is proposed by the combination of several algorithms to avoid them. Their good performance is checked by the application to several case studies of real bridges.

Finally, the results of all case studies, conclusions and future research lines are presented. The conclusions show a robust methodology based on machine learning algorithms capable to detect, localize and quantify damage. It allows the engineers to verify bridges and anticipate significant structural damage when occurs, under operational and environmental conditions. Moreover, the proposed non-modal parameters show their feasibility as damage features using ambient and forced vibrations in two real bridges. Hilbert-Huang Transform (HHT) in conjunction with Marginal Hilbert Spectrum and Instantaneous Phase Difference shows a great capability to analyze the nonlinear and nonstationary response signals in real bridges for damage identification under operational conditions. The proposed strategy combines algorithms for signal processing (ICEEMDAN and HHT) and machine learning (k-means) to conduct damage detection and localization in bridges by using the traffic-induced vibration data in real-time operation.

Resumen

En los últimos años la comunidad científica ha estado desarrollando nuevas técnicas en monitoreo de salud estructural (SHM) para identificar los daños en estructuras civiles especialmente en puentes. Los sistemas de monitoreo de salud de puentes (BHM) sirven para reducir los costos generales de mantenimiento del ciclo de vida de los puentes, ya que su objetivo principal es prevenir fallas catastróficas, grietas, daños, corrosión de los miembros de acero, entre otros. En el BHM que utiliza datos dinámicos, existen varios problemas relacionados con el procesamiento posterior de las señales de vibración, tales como: (i) cuando se utilizan características dinámicas basadas en modales como frecuencias naturales, forma de modos y amortiguamiento, presentan una limitación en relación a la localización del daño, ya que se basan en una respuesta global de la estructura; (ii) presencia de ruido en la medición de las respuestas de vibración; (iii) uso inadecuado de los algoritmos existentes para la extracción de características de daño debido a que no se toma en cuenta la no linealidad y la no estacionariedad de las señales registradas; (iv) las condiciones ambientales y operativas también pueden generar falsas detecciones de daños en puentes; (v) los inconvenientes de los algoritmos tradicionales para procesar grandes cantidades de datos obtenidos del BHM.

Esta tesis propone nuevos parámetros, métodos y herramientas basados en vibraciones con enfoque en la detección, localización y cuantificación de daños, considerando una metodología robusta y mixta que incluye métodos de procesamiento de señales y aprendizaje automático para resolver los problemas identificados. El creciente volumen de datos de monitoreo de puentes hace que sea interesante estudiar la capacidad de herramientas y sistemas avanzados para extraer información útil de variables dinámicas y estáticas. En concreto, en el campo del Machine Learning (ML) y la Inteligencia Artificial (IA) se han desarrollado potentes algoritmos para afrontar problemas donde la cantidad de datos es mucho mayor (big data). En la presente tesis, se analizaron las posibilidades de las técnicas de aprendizaje automático (algoritmos no supervisados) para su aplicación al análisis estructural de puentes teniendo en cuenta tanto las condiciones operativas como ambientales.

Se realizó una revisión crítica de la literatura, identificando los problemas y limitaciones que presentan algunos algoritmos para la identificación, localización y cuantificación de daños en puentes reales. Se llevó a cabo un estudio profundo de la precisión y rendimiento de un conjunto de algoritmos para la detección de daños en cuatro casos de estudio de puentes (tres puentes reales y un modelo numérico de un puente). En la revisión de la literatura de BHM inherente a la detección de daños basada en vibraciones, se han estudiado varios métodos de última generación que no consideran la naturaleza de los datos y las características de la excitación aplicada (posible no linealidad, no estacionariedad, presencia o ausencia de efectos ambientales y/o operacionales,) y el nivel de ruido de los sensores. Esto se identifica como problemático cuando se aplica a BHM. Además, la mayoría de las investigaciones utilizan características de daño basadas en modales (frecuencias naturales,

formas modales y amortiguamiento) que tienen algunas limitaciones. La mayoría de los métodos realizan una normalización deficiente de los datos y no se tiene en cuenta adecuadamente la variabilidad operativa y ambiental. Asimismo, la enorme cantidad de datos registrados requiere de procedimientos automáticos con capacidad comprobada para reducir la posibilidad de falsas alarmas. Por otro lado, muchas investigaciones tienen limitaciones ya que solo se estudian en casos numéricos o de laboratorio. De esta manera, todos estos problemas están identificados. En consecuencia, se propone una metodología mediante la combinación de varios algoritmos para evitarlos. Su buen desempeño se comprueba mediante la aplicación a varios casos de estudio de puentes reales.

Finalmente, se presentan los resultados de todos los casos de estudio, conclusiones y futuras líneas de investigación. Las conclusiones muestran una metodología robusta basada en algoritmos de aprendizaje automático capaces de detectar, localizar y cuantificar daños. Permite a los ingenieros verificar puentes y anticipar daños estructurales significativos cuando ocurran en condiciones operativas y ambientales. Además, los parámetros no modales propuestos muestran su viabilidad como características de daño usando vibraciones ambientales y forzadas en dos puentes reales. La Transformada de Hilbert-Huang (HHT) junto con el Espectro Marginal de Hilbert y la Diferencia de Fase Instantánea muestran una gran capacidad para analizar las señales de respuesta no lineales y no estacionarias en puentes reales para la identificación de daños en condiciones operativas. La estrategia propuesta combina algoritmos para el procesamiento de señales (ICEEMDAN y HHT) y el aprendizaje automático (k-means) para realizar la detección y localización de daños en puentes mediante el uso de datos de vibraciones inducidas por el tráfico en tiempo real.

Acronyms

SHM – Structural Health Monitoring

BHM – Bridge Health Monitoring

BD – Big Data

DM – Data Mining

AI – Artificial Intelligence

ML – Machine Learning

DP – Deep Learning

SPR – Statistical Pattern Recognition

CAV – Cumulative Absolute Velocity

CAD – Cumulative Absolute Displacement

DVI – Distributed Vibration Intensity

MCVI – Mean Cumulative Vibration Intensity

IVI – Instantaneous Vibration Intensity

AIVI – Amalgamed Instantaneous Vibration Intensity

MCD – Minimum Covariance Determinate

HHT – Hilbert-Huang Transform

EMD – Empirical Model Decomposition

ICEEMDAN – Improved Complete Ensemble Empirical Mode Decomposition with Adaptive Noise

IMF – Intrinsic Mode Functions

VMD – Variational Mode Decomposition

MSD – Mahalanobis Squared-Distance

PCA – Principal Component Analysis

KPCA – Kernel Principal Component Analysis

DC – Damage Condition

DI – Damage Indicator

TW – Time Window

BC – Baseline Condition

CB – Confidence Boundary

IPD – Instantaneous Phase Difference

FE – Finite Element

DMG – Damage

Table of contents

List of Figures

List of Tables

Chapter 1 – Introduction and objectives

1.1. Introduction and motivation

Bridges play a crucial role in our society, regardless of geographical location, for example in the economic development, connecting people, goods and transports. Bridges must be well maintained and managed to preserve safety, durability at a low cost. In this sense, the maintenance and inspection, the permanent quantitative and objective control of the structural condition of bridges must be raised against operational, environmental and accidental factors [1] [2]. This is the main purpose of Structural Health Monitoring (SHM), which is an important field that permits to identify early and progressive structural damage [3] [4]. Likewise, the large amount of data obtained from a bridge monitoring system increasingly requires the implementation of modern techniques and sophisticated algorithms, what derives on other more specific fields currently being developed such as the bridge health monitoring systems (BHMS).

The SHM research area has the general objective of managing infrastructures by detecting structural damage. The SHM process involves the observation of a structural system throughout its useful life using periodic measurements or in real time through a series of sensors, taking into account that a damaged structure produces hidden abnormal changes in structural behavior [5]. Damage identification procedures are carried out by extracting such anomalies using damage-sensitive features and in-depth statistical analysis to discriminate the condition of the actual structure. Some authors [6] [7] mention that the information obtained from long-term SHM monitoring is periodically updated and provides valuable information on the ability of the structure to fulfill its function despite degradation and inevitable aging due to operational and environmental variability. Damage identification procedures can be used to assess the condition of damage and to predict the residual useful life of structures.

To assess the damage condition of a structure, three operational levels are usually targeted: damage detection, diagnosis, and prognosis (Figure 1.1). Nevertheless, damage diagnosis can be subdivided into location, type, and severity; likewise, the hierarchical structure of damage identification can be decomposed in five levels and each one answers the following questions [8].

1. Is the damage present in the system (detection)?
2. Where is the damage (localization)?
3. What kind of damage is present (type)?
4. What is the extent of damage (severity, quantification)?
5. How much useful lifetime remains (prognosis)?

The answers to the proposed questions follow an order and a logical sequence since if the response to the severity of the damage is considered, then the type of damage can be known in advance. On the other hand, the damage prognosis cannot be achieved without a prior understanding of the damage accumulation process [9]. Although it is correct, as mentioned in [8], that damage identification

hierarchy comprises five levels, this thesis focuses mainly on the detection, location and quantification aspects.

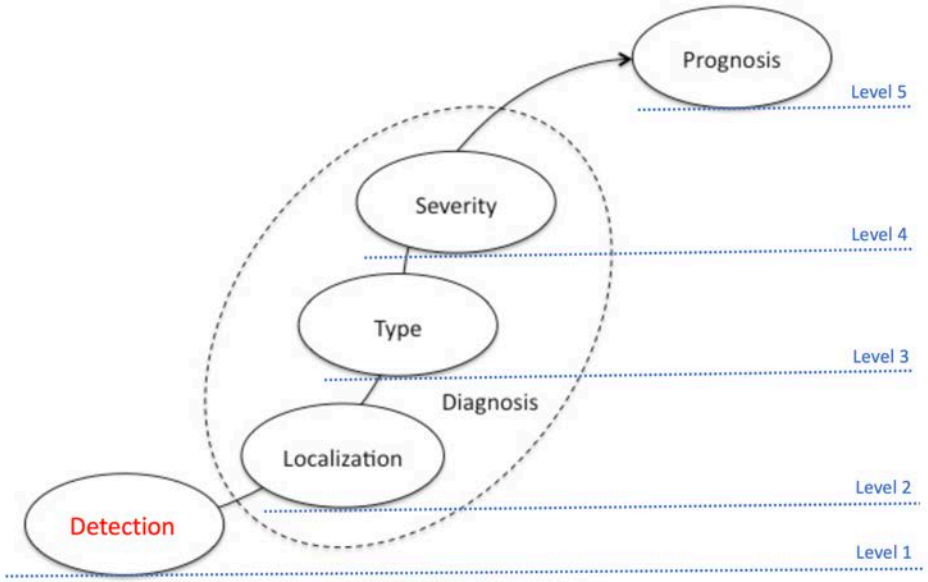

Figure 1.1. Hierarchical structure of damage identification [8].

The previous approach can be applied in many civil infrastructures including bridges. Generally, when bridge damage occurs, the required repair is costly and time consuming. Different types of damage can be cracks [10] (Figure 1.2a), corrosion [11] (Figure 1.2b), absence and deflection of a neoprene pad [12] (Figure 1.2c), faulty expansion joints, impact-induced delamination in composite structures, degradation of structural connections, etc. SHM has several stages such as: collection of reliable data on the current state of the bridge, observation of the evaluation throughout the service life and the characterization of the degradation. In this sense, SHM systems imply the permanent installation of a series and variety of sensors (Figure 1.3), for which the parameters sensitive to damage must be continuously measured (static and dynamic parameters) as well as the environmental parameters (temperature, humidity, wind).

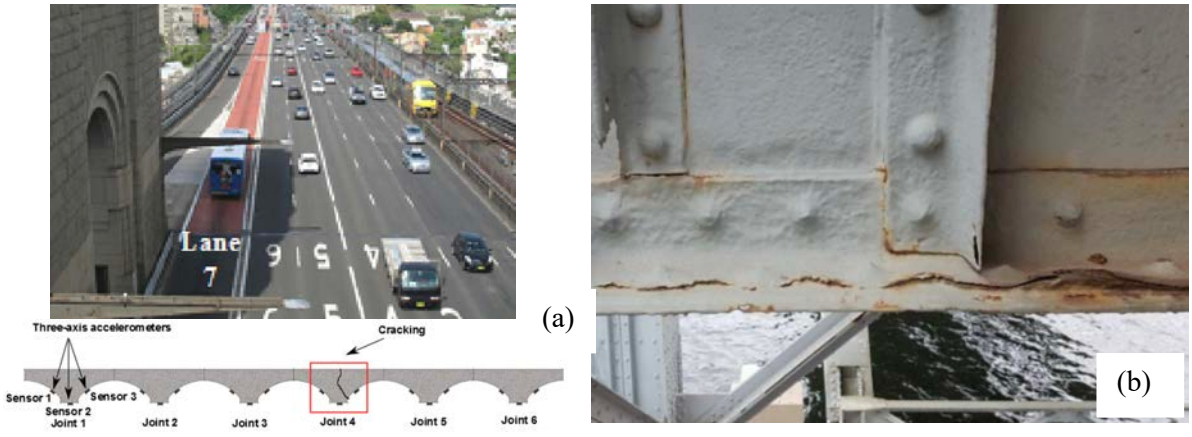

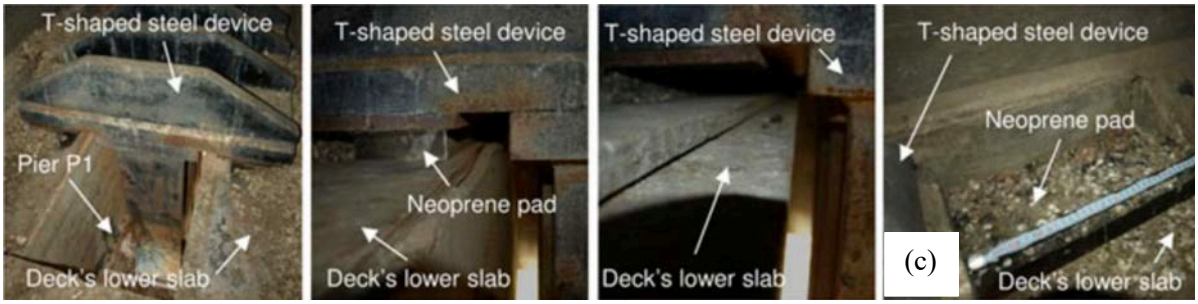

Figure 1.2. Structural damages in bridges (a) Sydney Harbour Bridge, Cracks [10] (b) Old Lidingö Bridge, heavily corroded cross beam [11] (c) Guadiana Bridge, absence and deviation of a neoprene pad [12].

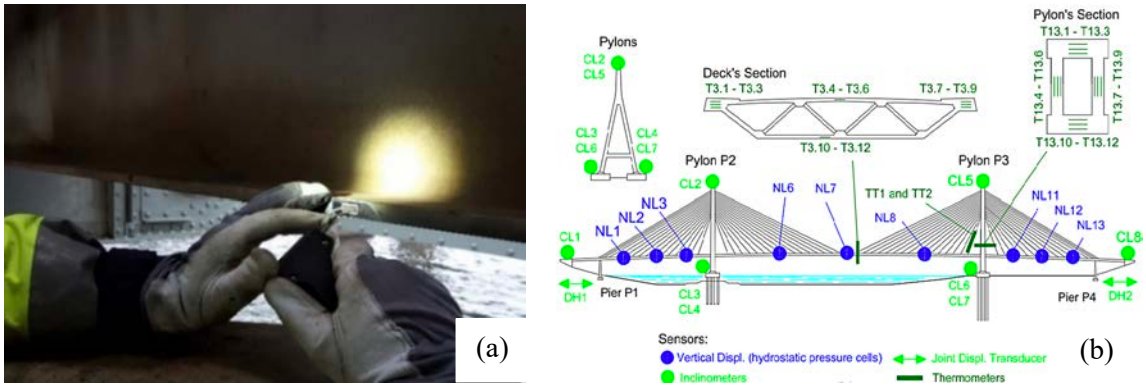

Figure 1.3. Installation of sensors for SHM (a) Old Lidingö Bridge, installing a strain gauge [11] (b) Guadiana Bridge, many kinds of sensor installed (thermometers, inclinometers, etc) [12].

Numerous monitoring and detection SHM approaches have been developed, for instance, physics- and data-based. The first one uses the inverse problem technique to calibrate numerical models (e.g., finite element models). Besides, during the last decades with emerging computing power and sensing technology, the data-based field like Machine learning (ML) has grown enormously, where the algorithms are in the condition of learning and/or modeling the behavior of the structure through data collected over time. Besides, the machine learning algorithms can be divided in supervised and unsupervised. [13] [14] [15]. The supervised algorithms require a set of labeled data for their training and their general objective is to discover the optimal mapping of the inputs to the desired outputs (objective function). That is, these algorithms require a human supervisor to assign a label to each data sample before training [16] [17]. On the other hand, unsupervised learning algorithms require output-only data without any label and their aim is to investigate the statistical distribution of the data to obtain important information about its underlying structure [18].

Considering the transition from research to practice, SHM technology makes a great contribution to caring for the economy and life safety. SHM systems should prove to be a very useful tool to reduce overall maintenance costs within the life cycle of a bridge. For instance, currently, the initial investment for a bridge health monitoring (BHM) system for new bridges ranges from 0.5% to 3% of the total construction cost [19]. The deployed system generates an annual management and maintenance cost

between 5% and 20%. Therefore, BHM systems may require an investment in the order of 4.5% to 9% of the total construction cost of a medium-size bridge during the first 10 years of useful life [20]. Likewise, most of the current infrastructure in North America and Europe is relatively old as it has deteriorated over the years. For example, in the year 2021, 7.5% of the total number of bridges managed by the National Bridge Inventory in the U.S. was considered structurally deficient and 42% of these were over 50 years old. In addition, a recent estimate for the U.S. backlog of bridge repair needs is $125 billion [21]. For this reason, there is a great demand in the evaluation and maintenance of those structures that are gradually suffering damage.

Bridge monitoring must consider robust systems both in the construction stage and during the service life of the structure. For this reason, there are many researchers who recommend and provide the implementation of BHM systems using modern techniques for data collection, processing and analysis [22] - [25]. In addition, these data obtained through monitoring are useful for the detection, location and quantification of damages.

In Europe, for instance, there have been many cases of the abrupt collapses such as: Morandi Bridge [26] in Genoa, Italy in August 2018 (Figure 1.4a), which caused the death of 43 people, that has aroused concern by the authorities and the scientific community to investigate in greater detail the causes of this regrettable fact. As mentioned, [27], the possible causes of bridge collapse include: poor structural design, questionable construction practices, and improperly planned or implemented maintenance. So, it is inevitable to think that maintenance work has dropped significantly in some European countries during the last decade. This can be seen in Figure 1.5. The Figure 1.4b shows a 20-year-old single-arch steel bridge located in Taiwan known as Nanfang'ao, which collapsed in October 2019, injuring 12 people and killing six. According to the investigations, the main cause could have been the corrosion in the suspension cables of the bridge, for which the independent bridge consultant Simon Bourne mentioned to the New Civil Engineer magazine [28] that it must have been necessary to carry out a proactive maintenance and in this way avoid that the cables rust. Likewise, two cases of structural collapses of bridges in Brazil [29] and Peru [30] can be seen in Figure 1.4c and Figure 1.4d respectively. The first case in Brazil occurred during the construction stage of the viaduct, which at that time had a budget of R$ 905 million and caused the loss of two human lives and twenty-two injuries. In the case of Peru, the Topará bridge, whose investment was US $ 33.9 million, collapsed in July 2015 after the passage of a truck that transported scrap metal, in this case it is presumed that the causes have to relationship with a poor structural design.

Figure 1.4. Structural bridge collapses around the world (a) Morandi Highway Bridge, Italy [26] (b) Nanfang`ao Bridge, Taiwan [28] (c) Guararapes Battle Viaduct, Brazil [29] (d) Topará Bridge, Peru [30].

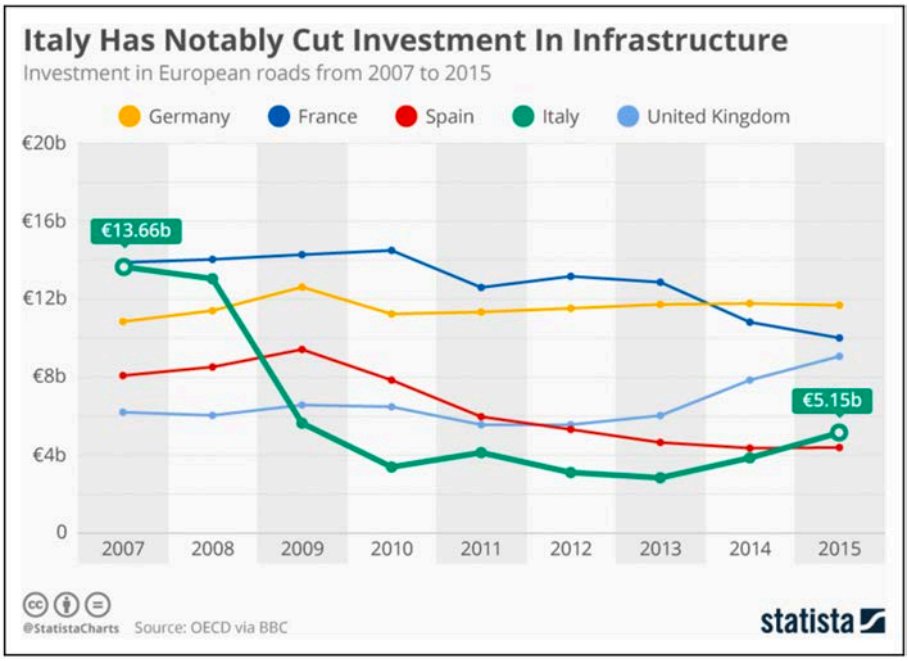

Figure 1.5. The investment in Italian infrastructure, which is related to Genoa bridge collapse [26]. Source: Statista.

Finally, many authors [31] - [33] mentioned that the systems of SHM can be designed in order to:

1. Manage, plan and execute structural monitoring during the construction stage of lightweight structures using resistant materials at low cost;

2. Measure the real structural response to validate the calculations made in the structural design, and thus in the future to improve the design specifications;
3. Detect anomalies, cracks, damages in early stages;
4. Reduce and improve visual inspections with the help of non-destructive testing;
5. Extend the useful life of the structures by placing a real-time monitoring system and thus carry out maintenance work to prevent and reduce management costs, traffic control and downtime;
6. Place SHM systems in order to evaluate the integrity conditions of the structure after the occurrence of damage due to environmental and operational conditions;
7. Implement SHM systems to prevent structural damage due to catastrophic events such as earthquakes, tsunamis, etc. and thus safeguard people's lives.

1.2. Problem Identification

The SHM strategy explores the availability of sensor data and measurements to complement traditional inspection schemes. SHM has emerged as a promising solution due to recent advances in transmission systems, transducers, data acquisition, and signal processing techniques. In addition, within the monitoring of sensitive characteristics, natural frequencies, mode shapes, damping ratios, and modal curvatures are generally considered to detect damage. For instance, the natural frequencies are intrinsically related to the global stiffness of a structure, since if the stiffness decreases it may be an indication of the presence of damage [34] [35]. However, modal parameter-based damage detection techniques contain a number of drawbacks and limitations when applied to bridges. For instance, when the natural frequencies, modes shape and damping are used, they present a limitation in relation to damage location, since they are based on a global response of the structure. According to recent research, the authors [36] [37] have developed exhaustive comparisons in order to identify these problems and provide alternative solutions for the use of other parameters such as non-modal ones. In this sense, the research on this subject is not closed at all and new challenges and developments to solve these problems and to propose efficient non-modal parameters for damage detection and locations are still necessary and worth of further research.

On the other hand, dynamic parameters such as modal frequencies, damping ratios and mode shapes can be easily obtained through conventional time-frequency signal processing such as Fast Fourier Transform (FFT) [38] and short-time Fourier Transform (STFT) [39]. However, these signal processing methods are based on the fact that the signal is linear and stationary. . Besides, there are a few inherent drawbacks of FFT that can affect the performance of system identification and the subsequent damage detection [40]. For example (i) the reduction of data process is particularly obtained by FFT and the structural health condition can be lost during the process [41]. (ii) the time dependency of dynamic parameters cannot be obtained by FFT and considering the signals obtained

from naturally excited structures, it will not be able to capture the evolutionary characteristics that are observed in these signals [42]. The higher frequency modes that are obtained generally represent damages that are local phenomena [43] [44] and the higher frequencies are poorly excited and spaced [45]. In conclusion, damage detection techniques using FFT have relevant drawbacks because the assumption done is that the dynamic process from which the signal is an observation, is linear and stationary. However, the signals obtained from the crossing of vehicles along a bridge do not present these characteristics as the frequency spectrum of the response varies along the crossing due to the vehicle-bridge interaction and also the amplitude of the signal changes depending on the position of the vehicle in relation to the location where the response is recorded. The time dependency of frequency and amplitude of the recorded vibration becomes evident. As a consequence, methods of extraction of modal parameters that assume the linearity and stationarity of the process (as FFT) are not of application to obtain reliable and accurate damage indicators. In this regard, the wavelet transform (WT) [46] [47] and Hilbert–Huang transform (HHT) [40] [48] [49] can analyze non-linear and non-stationary signals and solve these problems efficiently. More research on the accurate implementation of these techniques in real world bridges is still needed in order to check their validity

Additionally, the SHM has two main drawbacks during continuous monitoring. First, several features sensitive to damage are not measured directly, but are estimated from monitoring data using increasingly modern extraction techniques. For example, natural frequencies are obtained from measurements of vibration responses, such as accelerations, which can have estimation errors. Second, the characteristics obtained from monitoring are not only sensitive to changes produced by structural damage, but also to environmental (changes in temperature, humidity, wind speed) and operational (traffic load) conditions. Therefore, in the correct practice of SHM, the accuracy of the estimated features and the environmental and operational variability must be taken into account.

Many environmental factors such as ambient temperature, humidity, wind, affect the vibration parameters since they are features sensitive to damages [6]. However, the variability of environmental factors is very slow compared to the structural change suffered by civil infrastructures [50], since, for example, extreme temperature changes occur during the four seasons of the year. Furthermore, a linear invariant system in time is considered to be a structure that is monitored for a short period of time. But structures generally must be monitored for long periods (days, months, years), since there is a direct non-linear relationship between temperature and stiffness of the materials used. For this reason, it is important to consider temperature variations as the cause of these changes [51] [52].

Researchers have developed different techniques and methods for damage detection on bridges considering dynamic and environmental characteristics monitored during years. One of the most studied cases worldwide is the emblematic bridge Z-24 [53] [54], where progressive damage tests were carried out and taking into account that the bridge operates within its undamaged condition

(baseline condition BC). The bridge was in operation in undamaged situation in both environmental and operational conditions for a year where the natural vibration frequencies were extracted. Figure 1.6 shows the first three frequencies of the Z-24 bridge. The samples obtained from the beginning of the monitoring until August 8, 1998 correspond to the characteristics extracted within the undamaged condition under the operational and environmental variability. From the occurrence of damage (August 8, 1998), the samples obtained correspond to the period of progressive damage, where a decline in vibration frequencies is clearly shown, especially the second. However, the drop in the natural frequencies were not being so evident if the damage had been produced during the winter months, as frequencies even higher than during the past summer could be measured, concluding that the bridge was in good condition because the environmental effect would hidden the structural damaged condition. Only if the environmental effect could be removed, the right conclusion could be achieved.

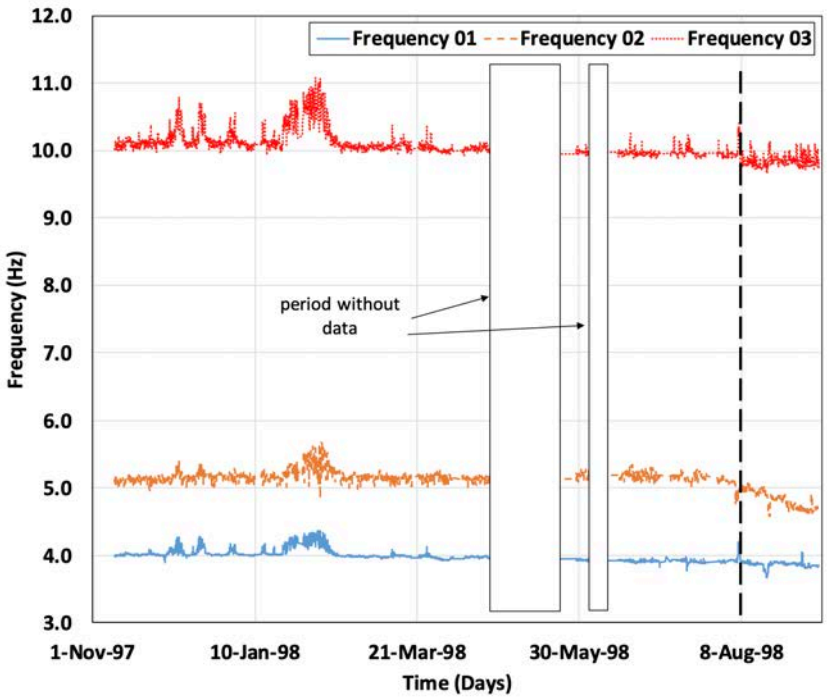

Figure 1.6. Influence of temperature on the modal frequencies obtained from the Z-24 bridge.

In the studies of the Z-24 bridge it is seen how the stiffness is significantly affected, since the jumps observed in the natural frequencies are related to the asphalt layer in cold periods. This problem indicates the need for a correct data normalization process to eliminate the influence of environmental factors. Likewise, it is observed that the changes produced by temperature are greater compared to those caused by structural damage. In this sense, if the process of eliminating these environmental factors is not carried out properly, changes in the structural response characteristics caused by temperature can mask false indications of damage.

In summary, as dynamic response in real bridges in service will be always affected by environmental and traffic effects (inducing non-linearity and non-stationarity in the recorded signals), two main issues appear in the on-site application of damage detection techniques in operating bridges: how to remove the ambient effects and extract accurate damage features feasible for damage detection, location and quantification from short non-linear and non-stationary vibration records.

Numerous applications of damage detection in the civil engineering field can be found. In the majority of them, there is currently a large amount of data obtained from structural monitoring of bridges that needs to be evaluated and analyzed (big data). However, this is a latent problem as traditional damage detection methods are not sufficient to achieve good results when large amounts of experimental data have to be analyzed on-line. In this sense, to overcome these drawbacks and thanks to improvements in computational power and the advancement of sensor technology, machine learning (ML) and artificial intelligence (AI) techniques are being developed with greater attention by the scientific community [14]. However, many big-data methods and tools are available and have been used in several scientific fields, but the most suitable to be applied in the case of damage detection in real world bridges is still an open question.

1.3. Objectives

According to the problems detected in the previous sub-chapter, the main objective of the thesis is the development of a robust and theoretically sound methodology for bridge performance analysis, efficient in early damage detection that can be applied to large volumes of data (big data, many years of monitoring) or in specific measurements (load tests). For this, a methodology is proposed that applies in each case the most appropriate techniques, tools and algorithms depending on the monitoring system characteristics and sensors used (dynamic and / or static) as well as on the nature of the recorded time signals (non-linear and highly non-stationary in the case of operational traffic) and the need to remove the environmental influences, taking into account or not the need of a baseline for damage detection (supervised and non-supervised techniques). To achieve this general objective, these specific objectives are addressed:

1. Review the literature about the relevant state of the art on SHM and BHM and the most used methods and tools available and applied in other scientific fields but with potential for application to the specific case of bridges.
2. Identify the appropriate methods to be used for data processing, analysis and interpretation of results for bridge damage identification, location and quantification. The selected methodology and corresponding tools should take into account the type of data provided by monitoring depending on the characteristics of the applied excitation (possible non-linearity, non-stationarity, presence or absence of environmental and / or operational effects,) and the noise level of the sensors

3. Identify new vibration-based damage features based on the characteristics of the vibration signal and more specific of the damage condition of the sensor location. The objective is to overcome the limitations of the modal-based damage features (natural frequencies, mode shapes and damping) in damage location and quantification.
4. Determine some criteria to set detection thresholds that allow to accurately identify the presence of damage in bridges, under real conditions, both operational and environmental. The huge amount of data recorded requires automatic procedures with proven capacity to reduce the possibility of false alarms.
5. To test the performance of the proposed methodology when applied to both real bridges and numerical models of bridges. The numerical models are used when experimental data is not available with the desired characteristics to check the goodness of the method. In particular, it has not been possible to get experimental data from a real bridge where environmental and operational loads are applied in both original and damaged conditions.

1.4. Organization of the thesis and publications

This present thesis is organized in five chapters in order to fulfil the previous mentioned objectives and goals, plus a chapter on conclusions and future research needs. Moreover, this thesis is presented as a compendium of articles, which were previously published in indexed scientific journals.

Following the present chapter, Chapter 2 gives a general overview of the actual state of knowledge in SHM (Objective 1).

Chapter 3 includes the overall methodology developed for damage detection, localization and quantification on bridges and describes the required tools and their combination for an efficient result (Objectives 2, 3 and 4). To this end, a set of vibration-based damage features are first introduced and defined to produce better damage estimations than modal-based ones. Some of these proposed features are later on re-defined to overcome the mentioned problems of signal non-linearity and non-stationarity. To this end, the HHT is introduced. The procedures for empirical mode decomposition of the signal (EMD) are also presented. Different techniques as CEEMDAN, ICEEMDAN) [49] [55] [56] and Variational Mode Decomposition (VMD) [57] [58] [59] are investigated.

The Implementation of algorithms based on machine learning, artificial intelligence and on the Statistical Pattern Recognition paradigm (SPR), according to the nature of the available data (big or short data) is also introduced in this chapter to deal with the right detection based on statistical patterns of the proposed damage features.

Chapter 4 describes in short, the application of the proposed methodology to 3 real-world bridges) plus a numerical model of a bridge generated as part of COST Action TU1402 [60]. These applications are fully and extensively described later on in chapter 5, which contains the three published journal papers and a conference paper.

In the 3 real-world bridges, artificial and perfectly known damage was created such as: a post-tensioned concrete bridge called S101 (Austria), an arch steel bridge (Japan) and the Z-24 bridge post-tensioned bridge (Switzerland). In all cases, vibration data both in undamaged and damaged conditions was available.

Chapter 5 contains the three published journal papers and one conference paper used as extended version of the results and conclusions of the applications shown in chapter 4.

The list of the journal articles related with this document follows:

[1] Delgadillo, R. M., & Casas, J. R. *Non-modal vibration-based methods for bridge damage identification*. Structure and Infrastructure Engineering, vol. 16, no. 4, p. 676 - 697, August 2019. DOI: 10.1080/15732479.2019.1650080.

[2] Delgadillo, R. M., Tenelema, F. J., & Casas, J. R. *Marginal Hilbert Spectrum and instantaneous phase difference as total damage indicators in bridges under operational traffic loads*. Structure and Infrastructure Engineering, p. 1 – 21. September 2021. DOI: 10.1080/15732479.2021.1982994.

[3] Delgadillo, R. M., & Casas, J. R. *Bridge damage detection via Improved Completed Ensemble EMD with Adaptive Noise and machine learning algorithms.* Structural Control and Health Monitoring, Accepted for publication, January 2022.

The additional conference paper is referenced as:

[1] Rick M. Delgadillo, Joan R. Casas, “A combined kernel-PCA with clustering analysis for bridge damage detection under changing environmental conditions”. In Life-Cycle Civil Engineering: Innovation, Theory and Practice. CRC Press, IALCCE 2021. pp. 1362-1370.

Finally, Chapter 6 describes the main conclusions. In addition, the challenges and future trends in the use of BHM are also included.

Chapter 2 – State of the art review

This chapter is concerned with the presentation and critical analysis of the actual situation on the SHM approach.

2.1. Introduction

Over the years, the civil structures both historical and modern, for instance: bridges, buildings, churches, dams, hospitals were the product of increasingly complex designs. The great rapidity of the increase in techniques and novel materials have helped the development and evolution of cities. In addition, the improvement of construction materials and their performance to resist many external stresses continues to be a challenge for engineering. However, the issue of sustainability and care of the environment is a matter of concern, since today, an attempt is made to reduce the cost and time of construction. For example, larger structures in the world are being built, that require greater maintenance, more sophisticated sensors, and a precise, robust and reliable monitoring system. At the same time, ancient and modern structures go through an aging process from the beginning of their construction and during their service life.

In this sense, the applicability of the Structural Health Monitoring (SHM) field is reviewed in this chapter considering that the improvement in technologies serves to solve the aforementioned problems.

2.2. Structural Health Monitoring (SHM)

The current condition of the structures is susceptible to the combined action of different factors that can progressively deteriorate them and accumulate damage during their useful life. For instance, these factors can be environmental conditions, collisions, extreme events, earthquakes, unanticipated service loads that can affect service capacity and safety [61] [62]. Besides, the natural disasters are still being harmful to bridges. For instance, 30% of Chinese bridge failures from 2009 to 2019 occurred due to natural factors and 70% were due to problems related to design, maintenance, construction and supervision [63]. Likewise in North America and Europe, many bridges were built in 1950 and have more than 50 years of useful life, so they are reaching the end of their expected life [21] [64]. Therefore, the maintenance, inspection and structural health monitoring (SHM) of bridges must be carried out more quickly to avoid tragic events such as human and material losses.

The SHM has been studied particularly in the fields of civil, mechanical and aerospace engineering with the main interest of detection, localization and quantification of damage [65]. SHM consists on the implementation of a strategy as shown in Figure 2.1, combining a variety of technologies and taking advantage of advances in data transmission and acquisition systems, transducers, signal processing techniques, and real-time data analysis. The ability and precision of bridge monitoring systems to identify damage at an early stage will help make better decisions and safeguard human lives. Likewise, they will keep these structures operational and safe. On the other hand, the cost of maintenance and repair will be much less than the cost of a new construction. In this sense, several countries are making great efforts to include structural health systems from the design stage. This is demonstrated in several real case studies to instrument important buildings, bridges and

dams with a continuous monitoring system. For example, Akashi Kaikyo (Japan), Gwangan Bridge (South Korea), Tsing Ma Bridge (China), Indian River Inlet bridge (USA), Pitt River Bridge (Canada) [66]. The author [67] considers several benefits of the implementation of SHM systems to bridges such as: discovers hidden structural reserves, discovers deficiencies timely and increases safety, reduces the uncertainty in structural performance, allows structural management, ensures long-term quality, increase knowledge and it can prevent economic losses and human lives ahead of time. In conclusion, various researchers worldwide are working on improving SHM systems and it is expected that for the next few years the SHM in bridges will be mandatory and will become a standard practice.

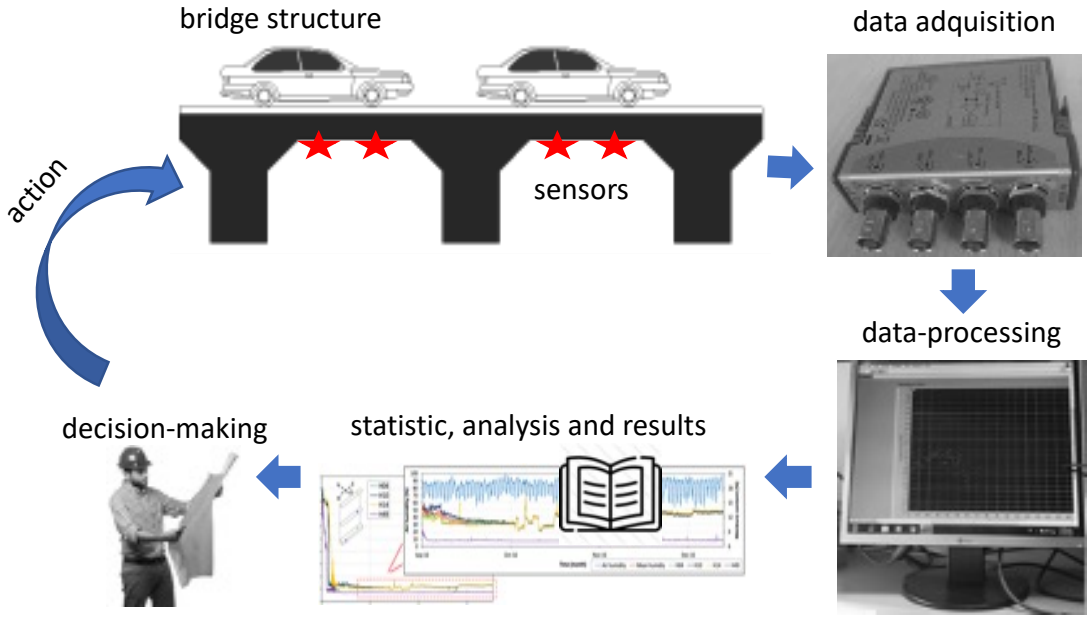

Figure 2.1. The SHM simplified scheme.

The general objective of an SHM system is the detection of damage, however, for example, the installation of reinforcing bars and the repair work of structural elements due to an earthquake also generate structural changes, but this does not mean that there is a structural damage but an improvement. For this reason, the four pillars of structural monitoring to identify damage were proposed by [68], and a few years later, [69] added a very important level to predict useful life. As can be shown:

- Level 1: Damage detection, where the presence of damage is identified.
- Level 2: Damage location, where the location of the damage is determined.
- Level 3: Damage typification, where the nature of damage is determined.
- Level 4: Damage extent, where the severity of damage is assessed.
- Level 5: Prediction of the remaining service life of the structure.

The first four levels show a structural diagnosis and the higher the target evaluation level, the SHM system will provide more information on the current structural state. However, answering each of these levels represents a greater difficulty to obtain information, since it has to be evaluated sequentially. Conversely, the last level is in charge of predicting future behavior, so it is necessary to include deeper knowledge in material fatigue, fault propagation, etc. In this sense, during the last decades, numerous investigations have been carried out to identify structural damages that affect changes in physical properties (mass, stiffness and damping) [70]. For this purpose, the dynamic vibration responses of structures can be used (e.g., natural frequencies, modal shapes, modal curvature and damping) [71] [72] and static responses (e.g., displacements, rotations, forces, stresses) [73] [74]. In this context, the antecedents show the advantages and disadvantages of the different techniques developed in the damage identification field. Several authors conducted an extensive collection of research on BHM up to 2010 [75], 2017 [76], and 2019 [77]. According to [61], damage identification techniques using dynamic parameters can be direct and inverse (or optimization). Direct methods determine the frequency changes of structures and detect structural damage without the need for iterative calculations. On the other hand, the inverse approach is frequently called updating the model in which the structural damage is identified by optimizing the correlation between the frequencies and the modal forms for the theoretical and experimental case. Currently, there are modern techniques using Artificial Intelligence (AI) and Machine Learning (ML) that are developed in greater detail in the following sections.

Finally, the authors [78] conducted an extensive literature review and raised seven Axioms or fundamental principles based on experimental studies that were corroborate for the SHM approach. Axiom II says: "Damage assessment requires a comparison between two systems or states." This means that some approaches "do not require a baseline", for example, routine pattern recognition requires a set of training. However, in the case of novel damage detection, a training set consists of representative characteristics of the normal condition of the structure. To make an optimal diagnosis of structural monitoring, the location and quantification of the damage level is necessary, in this way, the training data must represent all the different damage conditions and not only contain data under normal conditions. In this sense, it is important to use an outlier analysis, which can be compared with a supported criterion and allows to differentiate whether the outlier is statistically probable or unlikely. To sum up, all these aspects have been investigated but still some open issues remain when facing their application to real structures.

In the available literature there are many structural vibration methods that are classified according to their approach, such as: mode shape changes, frequency changes, dynamically measured flexibility, matrix update methods, nonlinear methods, and Neural Networks-based methods. Besides, the application of these methods to real bridge structures has produced inconsistent comparative results and has highlighted a susceptibility to noise, therefore in the present thesis other methods

based on non-modal vibration that were previously studied [36] [37] are used. Conversely, the damage identification methods present certain peculiarities and can be divided into four main areas: time, frequency, time-frequency and modal domains. Table 2.1 depicts a detailed list of classifiers associated with these intrinsic features [79]. From this large number of methods, this thesis presents a more in-depth study about the Time-frequency characteristic considering the Hilbert-Huang Transform (HHT) in the SHM approach.

Table 2.1 Overview of the vibration-based damage features. Adapted from [79].

Time	Time - frequency	Frequency	Modal
Time response / wave form	Wavelet transform	Fourier / power spectra	Natural frequencies
Statistical time series analysis	Hilbert transform	Frequency response function	Mode shape
	Hilbert – Huang transform	Frequency response function curvature	Mode shape curvatures
		Mechanical impedance	Modal damping
		Transmissibility function	Dynamic stiffness
		Anti - resonances	Dynamic stiffness
		Higher harmonics (nonlinear)	Updating methods
		Modulation (nonlinear)	

2.3. Challenges in Bridge Health Monitoring (BHM)

In the last decade, new and innovative methodologies have emerged to face the main problems of SHM in order to become a tool used in the industry. As examples, the following approaches are studied as part of the challenges to damage detection in civil structures:

- Nowadays, technological growth and the advancement of computers have proven to be a useful tool for SHM in general and the BHM in particular. Furthermore, these new methods serve to provide practical means of early warning against structural damage. In this sense, Machine Learning (ML), Artificial Intelligence (AI) and Deep Learning (DL) algorithms have become more feasible and are widely used in detecting structural damage with great precision. One of the most recent investigations describes and discusses the transition from traditional methods to vibration-based ML and DL methods for damage detection in civil engineering [14]. Some researchers used laboratory beams to test machine learning techniques such as artificial neural networks (ANN) and multilayer perceptron (MLP) respectively [80] [81]. The methods were experimentally tested with various induced damage at different locations and depths. The data was used to train a set ANN and MLP with a hidden layer to correlate the location of the damage and the damage severity with changes in natural frequencies. In both cases, the results show that the proposed techniques successfully predicted the minimum levels of damage. On the other hand, one of the most challenging points of BHM is how to extract

characteristics sensitive to damage from the structural response. In this regard, deep learning methods have attracted attention for their ability to effectively extract characteristics sensitive to damage [82]. One of the most important new generative models in unsupervised deep machine learning is the Variational Auto-encoder (VAE). This method is applied for damage identification in a task of bridge under moving vehicle and the results show that the proposed method can accurately identify structural damage [83].

- One of the biggest concerns in detecting damage to actual bridge structures is the presence of environmental and operational factors. For several years, researchers have been motivated that vibration-based methodologies use modal properties as indicators of damage, however it has been reported in several investigations that these properties are sensitive not only to structural damage but to environmental factors such as temperature variations [84]. For instance, the authors [85] [86] use several machine learning algorithms to develop models that evaluate the influence of operational and environmental variability on characteristics sensitive to damage. A new algorithm to identify damage in a structure under the presence of changes in temperature and noise was developed [87]. To this end, the authors presented a new methodology based on the integration of two pattern recognition methods such as Autoencoder and Couple Sparse Coding (CSC). Furthermore, principal component analysis (PCA) is used to reduce the data dimension of frequency response function and compress the data set to build differentiated patterns. For this study [87], a truss bridge and the experimental data of a real bridge were used, where the proposed methodology was verified with great success in the presence of temperature changes, measurement errors, noise and modeling. The detection of structural damage is based on the theory that the modulus of elasticity of materials depends on changes in temperature, while temperature is treated as an input parameter for the system. In conclusion, the authors recommend that temperature should be recorded at various locations in the structure because temperature gradients can potentially affect the accuracy of the results. Some researchers presented the Autoencoder-CSC set through an experimental data validation of an aluminum beam and it was also verified with a 3D FE model of a truss bridge [88]. In this laboratory test, several artificial damages were imposed on the beam as a single and double cut that reduced the stiffness of the cross section. The identification of damage was carried out based on pattern recognition and for this, the frequency response function was studied. The excitations were originated by an impact hammer for damaged and undamaged conditions, and likewise, the Autoencoder and CSC classification algorithms served as unsupervised tools. The proposed methodology was highly effective in detecting structural damage in the presence of environmental variations and other uncertainties.

On the other hand, a deep learning method based on autoencoders was developed in order to detect structural damage, and this new method reduces dimensionality and considers the automatic learning of relationships in its mathematical formulation [89]. The modal and structural stiffness parameters are used to perform pattern recognition. Firstly, the dimensionality of the original input vector was reduced and then multiple hidden layers of a neural network served to preserve the necessary information. As a second step, the reduced characteristics and the stiffness reduction parameters were related using machine learning approach. The inputs to the machine learning model were natural frequencies and modal shapes, while the output was structural damage. The hidden layers in the automatic layer-by-layer encoders were used in the training process. This approach was verified in a numerical and experimental model considering steel frame structures and, according to the authors, this method obtains more efficient results compared with traditional ANN methods.

- Another challenge in the BHM field for damage detection in civil structures is the signal processing, since in most real bridge structures, the signals obtained are non-linear and non-stationary. Therefore, the Hilbert-Huang transform in conjunction with modern empirical mode decomposition techniques are used for damage detection and structural health control. For example, a complete ensemble empirical mode decomposition with adaptive noise (CEEMDAN) technique is investigated to identify the presence, location, and severity of damage on a steel truss bridge model [56]. A prototype bridge is built in the laboratory and subjected to white noise excitations. In addition, various indicators of damage extracted from intrinsic mode functions such as energy, instantaneous amplitude, non-enveloped phase, instantaneous frequency, kurtosis and entropy features with the energy and instantaneous amplitude features are studied for detection, localization and quantification of damages. The results demonstrated the robustness and greater sensitivity of the CEEMDAN method compared to the traditional empirical methods. On the other hand, another recent research considers a mixed approach between CEEMDAN-based HHT and an artificial neural network (ANN) as a very efficient damage detection methodology [90]. This methodology is applied to a steel truss bridge model subject to white noise and four damage parameters are studied such as energy, instantaneous amplitude (IA), unwrapped phase, and instantaneous frequency (IF). The authors conclude that the CEEMDAN-HT-ANN model is efficient in detecting, locating and quantifying structural damage, and that the energy-based damage index demonstrates a more efficient approach compared to the other parameters studied.

Chapter 3 – Proposed methodology and tools for BHM

In the present chapter, the description of the methodology derived to achieve the proposed objectives is presented. The theoretical background and implementation of many algorithms to solve the proposed problems is analyzed in detail.

3.1. Methodology for bridge damage detection, localization and quantification

This section proposes a methodology for damage detection in real bridge structures, which is based on a combination of two approaches: signal processing and machine learning algorithms. The general methodology for damage detection, localization and quantification used in the present thesis is shown in Figure 3.1. As a first step, the different responses that are given in the bridges can be both dynamic and static signals depending on the objective that needs to be achieved in the monitoring studies and the type of sensors and excitation techniques used. These responses are captured by different types of sensors under real conditions such as operational, environmental, load tests, bridge reinforcement, induced artificial damage [91] – [95].

After data acquisition, the processing stage is carried out, which includes the feature extraction and which in turn estimates those that are more representative and sensitive to damage (damage features). In addition, it must be taken into account that the signals to be processed have different intrinsic characteristics depending on the source of the excitation and the stochastic process from where they come from. In fact, the damage detection methods can consider signals such as: linear, non-linear, stationary, non-stationary type or another particular characteristic.

In the next step, the outliers are eliminated trying to preserve the main characteristics of the obtained signals, which allows reducing the dimensionality of the data, which in turn generates lower computational cost. In this case, several authors such as [12] [15] [24] [31] [73] [74] recommend that when large amounts of data are available, symbolic data should be used that represent the main behavior of structure and thus minimize computational level calculations. Once the outliers have been eliminated, algorithms that demonstrate great effectiveness should be used to characterize abnormal structural behaviors, bearing in mind that each case study is different and deserves a different treatment. As is well known in the field of continuous monitoring, a large amount of data is obtained every day that must be treated with special care and implemented various algorithms to achieve reliable and good performance methodologies. For this reason, one of the most recent fields for the processing of large amounts of data is "Big Data (BD)" or data mining that, based on machine learning (ML) and Statistical Pattern Recognition (SPR), allow to improve the detection of structural damage. The supervised and unsupervised algorithms are capable of automatically recognizing the internal structure of the data. For example, results with similar behavior are pooled and different damages are detected, which are usually isolated in small groups [10]. On the other hand, each algorithm has a different concept for clustering, which makes it difficult to use the same evaluation criteria for the different data collected on the bridges. For this reason, the methodology proposed in this research uses statistical tools and various classification algorithms that facilitate the structural damage detection, location and quantification in the case of bridge structures.

Between the statistical processing and the final stage of the flow diagram, the definition of detection thresholds is considered to make the decision whether what is actually being detected as an anomaly is actually the product of structural damage or it may be a false detection generated from other external sources such as environmental or operational conditions or sensor malfunction. In this sense, in order to evaluate the performance of the thresholds, a series of confidence limits must be taken into account with a high level of reliability on the detection index used. During the automatic structural evaluation, a methodology without a baseline is proposed and considering the recommendations of many authors, the detection of damage is achieved through a mobile time-windows procedure [96] - [99].

On the other hand, most of the methodologies implemented for damage detection require the judgment of an expert to analyze the data and make decisions during the continuous monitoring of real bridge structures. However, such a judgment is not always available. Therefore, it is proposed to find the correct combination of algorithms and an efficient methodology so that an analysis can be carried out automatically. Additionally, several case studies in damage detection share the limitation of requiring baseline data, measured while the structure is still in good condition. Such strategies can be effective when applied to newly constructed structures, however, they can fail when used in most constructions that have years of service. In this sense, the methodology proposed in this thesis will take into account all these considerations.

Finally, the majority of damage detection and location investigations have been carried out in laboratory tests. However, when the data from real bridge structures is available and are monitored in real time, various external factors such as operational and environmental arise and they do not allow the structural damage to be clearly identified and located, and make the proposed methodologies limited. In addition, another factor to take into account as a disturbing factor for a correct damage detection in real structures is the presence of noise in the vibration signals acquired as well as the errors inherent in the calibration of the sensors. Therefore, in the present thesis, several real bridges are studied, each one with different particular conditions regarding the testing a structural configuration.

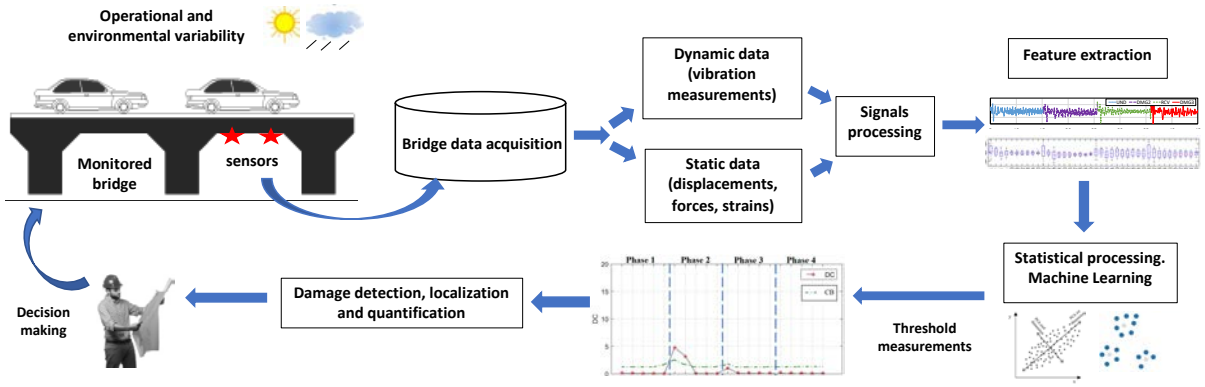

Figure 3.1. Flowchart of the proposed methodology for damage detection, localization and quantification on bridges.

3.2. Vibration-based damage indicators

A different approach to the traditional one is presented in this thesis, since in several investigations the modal-based damage features have proven to be difficult to apply to bridges under real conditions [36] [37]. For example, one of the drawbacks is the low extraction rate of modal properties under ambient excitation. Therefore, techniques based on raw vibration data and new damage characteristics and non-modal performance indicators have a high level of sensitivity to damage and can be easily applied to real bridge structures [49]. These new non-modal parameters are based on other vibration parameters as the vibration intensity measured as amplitudes and also on the specific energy density. Five vibration parameters are proposed and described below, which are extracted from acceleration responses in order to be tested as vibration-based damage features. The application of these parameters to damage detection in real bridge structures can be found in the first journal article published as part of this thesis [49].

1) Cumulative Absolute Velocity (CAV)

This energy-based vibration index was proposed by Kramer [100] and the mean concept involves the summed integral of all absolute acceleration values of the vibration response history denoted as Equation 1. In this regard, CAV represents the area under the absolute accelerogram and this parameter shows a good correlation with structural damage potential.

$$CAV = \int_0^t \left|\ddot{x}(\mathrm{t})\right| dt \tag{1}$$

2) Cumulative Absolute Displacement (CAD)

This CAD is an adaptation of the CAV vibration parameter, but unlike the other parameter, the acceleration signal is first transformed into displacement using integration and band-pass filtering to avoid drift, and can be expressed as:

$$CAD = \int_0^t \left|x(\mathrm{t})\right| dt \tag{2}$$

3) Distributed Vibration Intensity (DVI)

This novel parameter has the concept of vibration intensity, which in simple harmonic motion context can be defined as $(I=a^2/f)$, where a is the acceleration amplitude and f is frequency. In the Equation 3, the Fourier transform is applied to the vibration data and the summation of the vibration intensity values is taken within a frequency range, denoted by (f_i) within the limits m-n. To obtain good results, the frequency range must be selected to encompass the first few vibration modes of the structure, so, DVI can be able to capture the damage sensitivity associated with energy and modal frequency changes.

$$DVI = \sum_{i=m}^{n} 10log_{10}(\frac{\ddot{x}_i^2.(f_i)}{f_i} / I_S) \quad (3)$$

For $m \leq f_i \leq n$ (in Hz)

$$I_S = 10mm^2 / s^3$$

The SI units of vibration intensity are mm^2/s^3 and its logarithmic power form is decibels (dB).

4) Mean Cumulative Vibration Intensity (MCVI)

MCVI is a novel parameter based on vibration intensity (energy / frequency), where the numerator, is the square of the aforementioned vibration parameter CAV, while the denominator is a weighted mean value of Fourier frequency within a specified frequency range. The Equation 4 shows the weighting applied to the discrete frequencies via their corresponding Fourier Amplitude values (FA_i). The most important is that the frequency range selected encompasses the first few modes of vibration of the structure.

$$MCVI = \frac{\int_0^t \ddot{x}(t)^2 dt}{(\sum_{i=m}^{n} FA_i^2.(f_i) \Big/ \sum_{i=m}^{n} FA_i^2)} \quad (4)$$

For $m \leq f_i \leq n$ (in Hz)

5) Instantaneous Vibration Intensity (IVI)

The vibration parameter IVI is also based on the concept of vibration intensity (energy/frequency) and it is designed for use on non-stationary and non-linear data [101]. IVI is represented by the relationship between instantaneous amplitude and frequency obtained via HHT as presented in equation (5)

In addition, in order to guarantee that all obtained physically meaningful IMFs are utilized for damage localization, the sensor obtained IVIs can be combined to provide the Amalgamated Instantaneous Vibration Intensity (AIVI), which consists of mixing the most representative IVIs as presented in Equation (6).

$$IVI_i(t) = a_i^2(t) \big/ \varpi_i(t) \quad (5)$$

$$AIVI_i(t) = \frac{\sum_{i=1}^{N} IVI_i(t)}{N} \quad (6)$$

The CAV, CAD, DVI, MCVI, IVI and AIVI parameters are meaningful depending on the characteristics of the analysed signal. In this sense, Table 3.1 shows the applicability of each defined vibration parameter that can influence the performance of damage identification [49].

Table 3.1 Vibration parameter application classification.

Property	Vibration parameters				
	CAV	CAD	DVI	MCVI	IVI / AIVI
Fourier-based parameter	X	X	✓	✓	X
Non-stationary signal applicability	✓	✓	X	X	✓
Long-duration signal applicability	✓	X	✓	✓	X
Suitability to ambient induced excitation	✓	X	✓	✓	X
Suitability to vehicle-induced excitation	✓	✓	X	X	✓

3.3. Hilbert-Huang Transform in Bridge Health Monitoring (BHM)

To achieve good and reliable results for damage identification on bridges using vibration data, one of the most important steps is to analyze and study the data obtained from monitoring, especially its intrinsic and particular characteristics in order to apply the correct signal analysis in each case. Furthermore, damage sensitive characteristics can be obtained and a statistical analysis must be developed to identify structural damage. In this sense, the majority of authors have used Fourier analysis to extract the main features of vibration measurements. This is theoretically correct if the monitored signal comes from a linear and stationary process. However, if the data contains non-stationary and non-linear vibration signals, the Fourier transform cannot be applied, as explained in section 1.2. Therefore, other methods that take into account variations in amplitude and frequency over time should be used. One of these methods is the Hilbert-Huang Transform (HHT) developed to analyze non-stationary and transient signals, since these are often present in the real world and very often in fields such as mechanics, biomedical, geotechnics [102] - [105]. However, the application of HHT especially in complex and extended civil structures such as bridges is limited [93] [106] due to some problems appearing in the empirical mode decomposition (EMD) of the original signals before the application of the Hilbert transform. This is shown in the next subchapter also indicating the possible solutions to solve the main drawbacks.

3.3.1. Evolution of EMD-based techniques

Despite the major case studies showing EMD as a powerful signal processing tool in the review of literature, it has a significant inherent defect called mode mixing in the IMF [107]. For this reason, a brief introduction will be carried out on the existing methods, EMD, EEMD, CEEMD, CEEMDAN and the proposed improved methods such as ICEEMDAN and VMD which were used in this thesis.

Empirical Mode Decomposition (EMD)

The EMD signal processing method was first proposed by Huang et al. [108] [109], which decomposes a signal into several intrinsic mode functions (IMFs). The original signal can be reconstructed by summation of intrinsic modes, where *x(t)* is the original signal, I_i represent the *I*th IMF and the residue $r_n(t)$ is generally a monotonic function or a constant:

$$x(\mathrm{t}) = \sum_{i=1}^{n} I_i(\mathrm{t}) + r_n(\mathrm{t}) \tag{7}$$

Although several authors have used the EMD method for the identification of damages and the continuous monitoring of different structures [110] – [114], the mode mixing problem can occur in EMD when the signal contains intermittent processes since the EMD make use of all the extrema to construct the envelopes in signals.

First, the EMD method was designed as a process to extract simple oscillatory functions from one or more signals. However, this method has some drawbacks, such as the recurrent emergence of mode mixing due to signal intermittency and a unique intrinsic mode function (IMF) presenting signals of very different scales or signals of similar scale residing in different IMFs [107].

Ensemble Empirical Mode Decomposition (EEMD)

According to previous studies [106] [115] [116], EMD has a main disadvantage in the results of IMFs due to mode mixing, which obtains widely disparate time scales or analogous time scales in separate IMFs. In many cases, this problem is due to signal intermittency that not only can lead to time-frequency alias but also makes IMFs physically meaningless.

Figure 3.2 plots the IMFs and residuals (rows) for a series of experiments obtained from the EMD method (columns). The thin red circles indicate the mode mixing that occurs only in the first four IMFs, as they generally correspond to vibration modes within a frequency range of 25-155Hz. Furthermore, it can be seen that experiment 6 suffers from a high level of mode mixing compared to the other experiments.

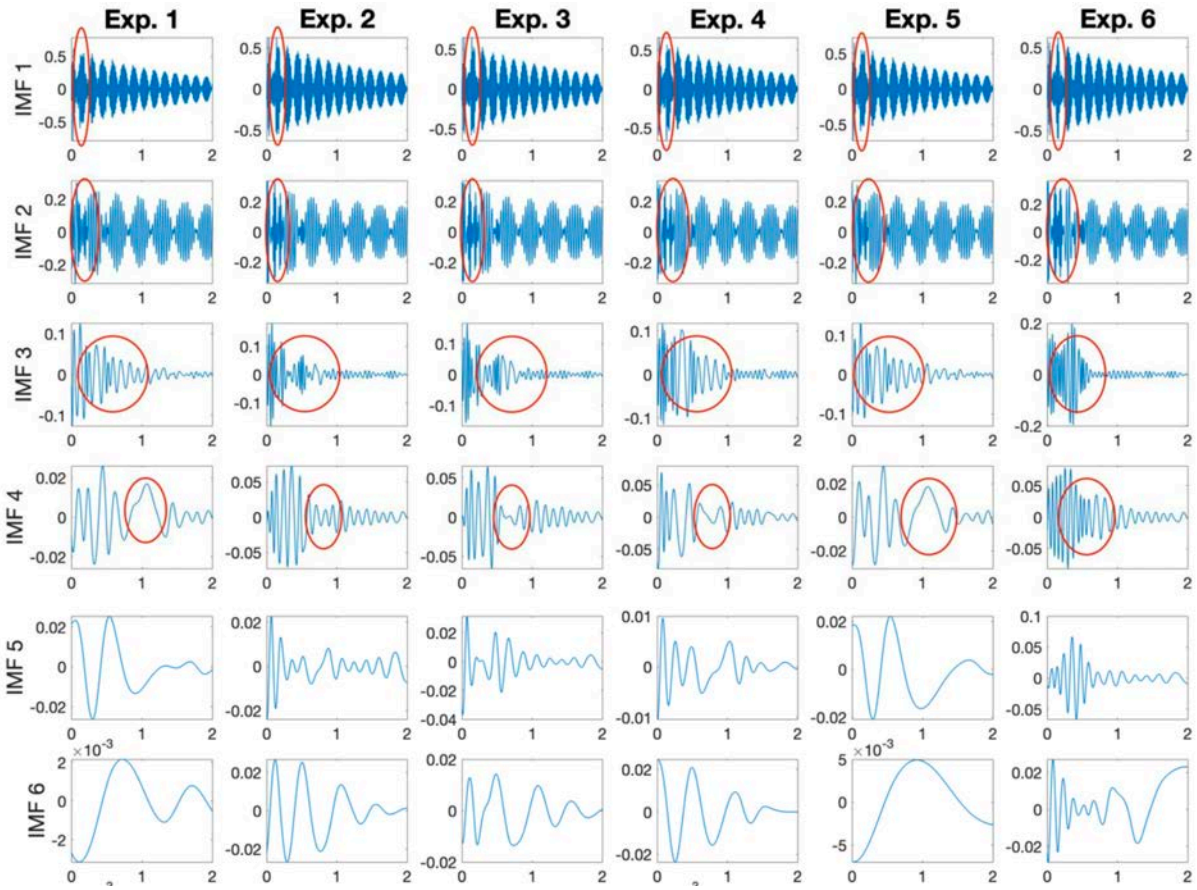

Figure 3.2. Examples of mode mixing occurring in the IMFs. Adapted from [139]

To solve the mode mixing problem explained above, Wu & Huang [107] [117] proposed Ensemble EMD (EEMD) method, which defines the IMF component as a mean of ensemble of trials, having white noise as well as signal. The statistical characteristics of white noise of finite amplitude to improve the scale separation problem is introduced. In reality, when the noise is added to the ensemble it produces a noisy IMFs for each trial. However, it helps all possible solutions to be examined in the ensemble. In fact, the effect of the included white noise is removed by utilizing ensemble mean. Mathematically it can be written as:

$$\mathrm{x}_j(\mathrm{t}) = x(\mathrm{t}) + \omega_j(\mathrm{t}) \qquad \mathrm{j} = 1, 2, \ldots, \mathrm{N} \tag{8}$$

And

$$\mathrm{x}_m(\mathrm{t}) = \sum_{i=1}^{n} C_{ij}(\mathrm{t}) + r_{j,N}(\mathrm{t}) \qquad \mathrm{j} = 1, 2, \ldots, \mathrm{N} \tag{9}$$

Where $x_j(t)$ is the noisy signal of jth trial, $x(t)$ is the original signal, $\omega_j(t)$ is the amplitude of the jth added white noise, $C_{ij}(t)$ is the ith IMF, n is the number of IMFs obtained from EMD method, and N is the number of trials. The residue of added white noise can be written as:

$$\varphi_n = \frac{\varphi}{\sqrt{N}} \tag{10}$$

Where φ_n is the final standard deviation, φ is the amplitude of the white noise and N is the number of trials. Nonetheless, the tolerance in residue noise of the reconstructed signal and the cleaning of the added white noise from the IMF are two problems which occur in EEMD. These disadvantages bring a high computational cost. Thereby, this method is not suitable to be used for continuous monitoring of civil structures [106].

Complementary Ensemble Empirical Mode Decomposition (CEEMD)

In the CEEMD method proposed by Yeh & Shieh [118], the white noise residue present in the IMF is eliminated in a considerable way and its calculation efficiency increases. In the original data, the white noise is added with two opposite polarities: one positive and one negative to generate two sets of ensemble IMFs as shown in the following equation:

$$\begin{bmatrix} M_1 \\ M_2 \end{bmatrix} = \begin{bmatrix} 1 & 1 \\ 1 & -1 \end{bmatrix} \begin{bmatrix} S \\ N \end{bmatrix} \tag{11}$$

Where $S=x(t)$ is the original data, $N=\omega_j(t)$ is the added white noise, M_1 and M_2 are the sum of the original data with positive and negative noise respectively. Although this proposal significantly alleviates the residual noise in the reconstructed signal, there is no guarantee that M_1 and M_2 will produce the same number of modes, making difficult the final averaging. Also, residual noise is present in the modes.

Complete Ensemble Empirical Mode Decomposition with Adaptive Noise (CEEMDAN)

Torres, et al. [119] proposed CEEMDAN method to solve the EEMDs' faults, achieving a negligible reconstruction error and solving the problem of different number of modes for different realizations of signal plus noise. The general idea for this method is the following: (x_j) are generated from (x) and the first mode $\tilde{d}_1 = \bar{d}_1$ is computed exactly as in EEMD, $\bar{d}_n$ is the nth mode of (x). Then, a unique first residue is obtained, independently from the noise realization:

$$r_1 = x - \tilde{d}_1 \tag{12}$$

After that, the first EMD mode is computed from an ensemble of r_1 plus different realizations of a particular noise. The second mode $\tilde{d}_2$ is defined as the average of these modes. The next residue is:

$r_2 = r_1 - \tilde{d}_2$. This procedure continues until a stopping criterion is reached. However, CEEMDAN still has two problems to be solved: (i) the modes contain some residual noise; and (ii) the signal information appears "later" than in EEMD with some "spurious" modes in the early stages of the decomposition. These aspects are finally improved with the ICEEMDAN method as explained below.

Improvements on Complete Ensemble Empirical Mode Decomposition with Adaptive Noise (ICEEMDAN)

Taking into account the drawbacks of the different types of EMD explained above, a controlled noise should be added to the signal in order to create new extrema. Many authors had made an attempt to solve the problem of the appropriate selection for the addition of white noise to solve the mode mixing problem. However, many proposed techniques were not really successful and effective, especially for the signals obtained from real bridges. In this sense, a novel-based Improved CEEMDAN method developed by Colominas et al. [120] is studied in detail in the present thesis for civil structures like bridges. ICEEMDAN method considers two improvements such as residual noise in modes and the spurious modes, as it is explained herein. First, with respect to residual noise in modes, each mode is calculated sequentially, so the final modes are used by CEEMDAN for the computation of the next one. Furthermore, the local means of each realization of signal plus noise are estimated and the true mode is defined as the difference between the current residue and the average.

The ICEEMDAN algorithm is described herein considering $E_k(.)$ as an operator, which produces the k-th mode obtained by EMD, $M(.)$, is also an operator which produces the local mean of the signal and $w^{(i)}$ = is a realization of zero mean unit variance white noise. Taking account, $x^{(i)}=x+w^{(i)}$ being x the original signal and $\leq . >$ the action of averaging throughout the realizations, then the modes for the first EEMD and original CEEMDAN can be expressed as:

$$\tilde{d}_1 = \left\langle E_1\left(x^{(i)}\right)\right\rangle = \left\langle x^{(i)} - M\left(x^{(i)}\right)\right\rangle = \left\langle x^{(i)}\right\rangle - \left\langle M\left(x^{(i)}\right)\right\rangle \tag{13}$$

In order to estimate only the local mean and subtract it from the original signal, the formula can be written as:

$$\tilde{d}_1 = x - \left\langle M\left(x^{(i)}\right)\right\rangle \tag{14}$$

Considering Equations 13 and 14, a reduction in the amount of noise present in the modes is obtained, because the estimation of modes was replaced by the local mean estimations, which demonstrated the best performance previously explained. With respect to spurious modes, analogously to the previous methods like EMD, EEMD obtained a strong overlapping in the scales

for the first two modes (first one extracted adding white noise and the second one adding $E_1(w^{(i)})$). Then, in order to reduce this overlapping, Colominas et al. [120] proposed to use $E_k(w^{(i)})$ and not directly use the white noise to extract the *k*th mode. The sequence of this improved CEEMDAN method consists in:

Step 1. Calculate by EMD the local means of *I* realizations $x^{(i)}=x+\beta_0 E_1(w^{(i)})$, taking account that *I* is the number of realizations of Gaussian white noise added to the signal of interest (*I* is consider usually a few hundred [120]). Then the first residue can be expressed as

$$r_1 = \left\langle M(\mathrm{x}^{(\mathrm{i})}) \right\rangle \tag{15}$$

Where $\beta_0 = \varepsilon_0\, std(x)/std(E_1(w^{(i)}))$; β_0 is chosen such that ε_0 is exactly the reciprocal of the desired signal-to-noise ratio (SNR) between the first added noise and the analyzed signal; the SNR is considered as a quotient of standard deviations.

Step 2. At the first stage *(k=1)* calculate the first mode:

$$\bar{d}_1 = x - r_1 \tag{16}$$

Step 3. Estimate the second residue as the average of local means of the realizations $r_1+\beta_1 E_2(w^{(i)})$ and define the second mode:

$$r_1 = \left\langle M(\mathrm{x}^{(\mathrm{i})}) \right\rangle \tag{17}$$

Step 4. For $k=3,\ldots,N$ calculate the *k*th residue

$$r_k = \left\langle M(r_{k-1} + \beta_{k-1}\, \mathrm{E}_k(w^{(\mathrm{i})})) \right\rangle \tag{18}$$

Step 5. Compute the *k*th mode

$$\bar{d}_k = r_{k-1} - r_k \tag{19}$$

Step 6. Go to step 4 for next *k.*

Constants $\beta_k=\varepsilon_k\, std(r_k)$ are chosen to obtain a desired signal-to-noise ratio (SNR) between the added noise and the residue to which the noise is added.

Variational Mode Decomposition

Apart from EMD and the following improvements, another potential method to decompose signals is called Variational Mode Decomposition (VMD), and was developed by Dragomiretskiy

and Zosso [57]. The VMD is an adaptive and non-recursive decomposition method that transforms a mode decomposition problem into a variational solution problem. Furthermore, several investigations have found that the VMD method overcomes certain drawbacks in the EEMD method since it is more robust to noise and avoids the modal aliasing of the EMD approach [121]. The multicomponent signal can be decomposed by VMD into an ensemble of quasi-orthogonal band-limited IMFs with specific sparsity properties in the spectral domain. The IMF are obtained via an optimization problem trying to minimize the objective function:

$$\min_{\{u_k\},\{\omega_k\}} \left\{ \sum_k \left\| \partial_t \left[(\delta(t) + \frac{j}{\pi t}) * u_k(t) \right] e^{-j\omega_k t} \right\|_2^2 \right\} \quad \text{subject to} \sum_k u_k = f \tag{20}$$

Where, δ is the Dirac distribution, ∂_t represents the partial differential equation of a system, where t is the time variable, u_k = *k*th IMF and ω_k = center pulsation around which the *k*th IMF is mostly compact. f is the signal to be decomposed. The bandwidth of each mode is estimated by the squared H^l Gaussian norm of its shifted signal with only positive frequencies. Furthermore, an unconstrained optimization problem is fitted with a quadratic penalty and Lagrangian multipliers λ in order to transform the Equation 20. Then the modified Lagrangian is:

$$L(u_k, \omega_k, \lambda) = \alpha \sum_k \left\| \partial_t \left[\left(\delta(t) + \frac{j}{\pi t} \right) * u_k(t) \right] e^{-j\omega_k t} \right\|_2^2 + \left\| f - \sum u_k \right\|_2^2 + \left\langle \lambda, f - \sum u_k \right\rangle \tag{21}$$

The penalty factor $\hat{\alpha}$ is named as balancing parameter of the data-fidelity constraint. The Equation 21 is solved by the alternative direction multipliers method called ADMM. In this way, the decomposed modes and the center frequency are obtained in each change operation. Thus, mathematically, each mode obtained from the solutions in the spectral domain can be expressed by the following formula:

$$\hat{u}_k(\omega) = \frac{\hat{f}(\omega) - \sum_{i \neq k} \hat{u}_i(\omega) + \left(\hat{\lambda}(\omega)/2 \right)}{1 + 2\alpha(\omega - \omega_k)^2} \tag{22}$$

In this thesis, a series of additional damage indices are developed based on the ICEEMDAN and VMD decomposition techniques as explained later.

3.3.2. Hilbert-Huang Transform (HHT)

The Hilbert-Huang Transform (HHT) is an advanced method developed by Huang and colleagues [108] [109] and the main advantage is its precision to analyze non-linear and non-

stationary signals. The HHT includes two steps. Firstly, several intrinsic mode functions (IMFs) can be obtained using a method to decompose into a finite set of intrinsic oscillatory components, as an example the more used is called empirical mode decomposition (EMD) method. However, nowadays, the efficiency of other new approaches is widely used (ICEEMDAN, VMD). Then, the instantaneous frequency. amplitude and phase can be obtained through the Hilbert transform (HT) and yield a time–frequency representation (Hilbert spectrum) for each IMF analyzed.

The results of the IMFs $\{c_i(\tau)\}$ are input into Hilbert Transform as follows:

$$H[c_i(t)] = \frac{1}{\pi}\int_{-\alpha}^{\alpha} \frac{c_i(\tau)}{t-\tau} d\tau \tag{23}$$

The analytic signal $z(t)$ in Equation 24 is formed by Hilbert Transform $H[c_i(t)]$ in conjunction with $\{c_i(\tau)\}$, where $a_i(t)$ and $\theta_i(t)$ are the instantaneous amplitudes and phases shown in Equation 25 and 26 respectively.

$$z(\mathrm{t}) = c_i(\mathrm{t}) + \mathrm{jH}\left[c_i(\mathrm{t})\right] = a_i(\mathrm{t})\,\mathrm{e}^{j\theta_i(\mathrm{t})} \tag{24}$$

$$a_i(\mathrm{t}) = \sqrt{c_i^{\,2}(\mathrm{t}) + \mathrm{H}^2\left[c_i(\mathrm{t})\right]} \tag{25}$$

$$\theta_i(\mathrm{t}) = \arctan\left(\frac{\mathrm{H}\left[c_i(\mathrm{t})\right]}{c_i(\mathrm{t})}\right) \tag{26}$$

The Equation 27 shows the instantaneous frequencies $\{\omega_i(t)\}$ of each IMFs, which are determined by differentiating the instantaneous phase function.

$$\varpi_i(\mathrm{t}) = \frac{d\theta_i(\mathrm{t})}{dt} \tag{27}$$

Compared to other theoretical and experimental research, damage detection based on real studies using the HHT approach is quite limited. The authors [115] used the EMD to identify the locations of damage and the times of its occurrence in a benchmark built in a laboratory. The simulation results demonstrated that the appearance of spikes in EMD can be detected if the measured signal has very little signal contamination or is free from noise contamination The evaluation of the dynamic condition in a bridge in Texas using the HHT approach was performed by [122] [123]. In this case, three damage scenarios were applied such as: intact, moderate damage and severe damage to a concrete column substructure. The piles were excavated and broken to simulate flood and earthquake damage to a bridge substructure. The HHT method served to obtain a quantitative difference between the instantaneous frequencies of the damaged structures and the healthy state.

The authors [124] examined instantaneous phase, marginal Hilbert spectrum, and joint time-frequency analysis for HHT data in an experimental bridge model subjected to three levels of damage. The results show that there is a phase difference between each level of damage for the sensor close to damage. Therefore, it seems that the phase difference is another important indicator for detecting and locating damage under transient vibration loads. Numerical and experimental cases of frame structures under environmental excitations were studied by [125], who used an improved HHT technique and developed a scheme for the detection of damage in real structures. [101] applied the HHT approach to identify and locate the progressive damage imposed on a real bridge structure. In this case, the HHT technique was used because the response to forced vibration was quite short, non-linear and non-stationary. Finally, the authors used an instantaneous vibration intensity (IVI) and amalgamated instantaneous vibration intensity (AIVI) parameters to identify and locate the damage. Furthermore, the evolution of the EMD method during these last ten years and its application to civil structures is studied in detail.

3.3.3. Damage indices based on HHT

By employing Improved Completed Ensemble Empirical Mode Decomposition with Adaptive Noise (ICEEMDAN) and Variational Mode Decomposition (VMD) and HHT to the derived IMF´s, in addition to the instantaneous frequency, amplitude and phase, two key features are extracted from the intrinsic mode functions and the application of the Hilbert transform. These parameters are marginal Hilbert spectrum (MHS) and the instantaneous phase difference (IPD), that includes the relationship between instantaneous amplitude and frequencies.

1) Marginal Hilbert Spectrum (MHS)

The Marginal Hilbert spectrum $h(\omega)$ is similar to the Fourier spectrum [124] [126] for stationary signals and measures the total amplitude contribution from each IMFs component value of determined signal during a time duration *T*. The MSH is obtained by integration over time of the Hilbert amplitude spectrum $H(\varpi, t)$ and it can be represented as:

$$h(\omega) = \int_0^T H(\omega, t)\,\mathrm{dt} \tag{28}$$

2) Instantaneous Phase Difference (IPD)

Taking into account that the HHT method uses the individual IMFs to calculate the instantaneous frequency, instantaneous phase and amplitude, the Equation 29 can be computed using a total instantaneous phase obtained by the sum of the instantaneous phases for each IMF. In this sense, the total number of rotations of the measured signal *x(t)* in the complex plane can be written as Equation 29. The total number of rotations in the complex plane for a unique time value *t* is multiplied by 2π,

because the $\theta(t)$ is unwrapped with radian phases in time. $I_i(t)$ is the i-th IMF, as defined previously in Equation 7.

$$\theta(\mathrm{t}) = \sum_{i=1}^{n} \arctan\left(\frac{H\left[I_i(\mathrm{t})\right]}{I_i(\mathrm{t})} \right) \tag{29}$$

A reference point (o) on the structure bridge can be chosen and the phase difference of a point p, relative to this reference point is simply performed as:

$$\phi_P(\mathrm{t}) = \theta_p(\mathrm{t}) - \theta_0(\mathrm{t}) \tag{30}$$

Where, the "phase difference" considers the total phase at any point p on a bridge relative to a reference point 0 and $\phi_P(t)$ gives the relative phase relationship of a travelling structural wave for a given state of a bridge. In conclusion, bearing in mind the idea of damage detection, $\phi_P(t)$ is able to detect a change in the speed at which energy travels through the structure when a damage is present. As mentioned by several authors [124] [127] [128], and based on laboratory tests, the tracking of changes in the wave speed of response measurements considering Equation 30 can be an effective method for damage identification and localization and this will be further investigated here for the case of real bridges.

Finally, nowadays, there is little research that uses a mixed approach between the Hilbert-Huang Transform (HHT) and machine learning (ML) algorithms to detect damage in real bridges [56] [90]. For instance, recently, the authors [90] developed a mixed methodology of HHT, CEEMDAN and Artificial Neural Network (ANN) in order to identify the damage and classify its severity in a laboratory-scale model of a steel truss bridge. They proposed several damage indicators (DI) that include instantaneous amplitude (IA), instantaneous frequency (IF), unwrapped phase and energy but using white noise excitations Therefore, one of the main objectives of this thesis is to check the joint effectiveness of the HHT, damage indices and the ML algorithms when applied to several real bridge structures. To this end, the concepts of ML and big data analysis are presented in the following chapter

3.4. Big Data and Statistical pattern recognition for BHM

The current condition of the civil structures is susceptible to environmental actions, material deterioration, aging and multiple hazards that can occur in structures located in rural and urban areas. To avoid irreparable events, human losses and damage to structures, recent advances in sensor technology and modern techniques have made it possible to explore Big Data (BD) concepts to find appropriate solutions. The storage of the large volume of high-dimensional data obtained from SHM is a relatively new research topic known as Big Data [129]. The concept of BD has received remarkable attention when dealing within the civil engineering works like bridges [130] [131]. The different

investigations concerning to SHM and big data show that the strategies used in both fields have the same objectives and challenges. Table 3.2 compares the steps to follow in both big data and SHM.

In addition, the challenges inherent to BD applied to real bridges include the damage detection and localization through the data processing obtained during several years of monitoring. Big data together with trends in artificial intelligence (AI), machine learning (ML) and statistical pattern recognition (SPR) [132] serve to "learn" the behavior of civil structures such as bridges and then help engineers to make decisions about the future maintenance and repair scenarios.

Table 3.2 Pipelines for big data and forward approaches to SHM. Adapted from [130].

Big data	**Forward SHM**
Recording	Acquisition
Cleansing	Normalization
Aggregation	Data fusion
Modelling	Prediction
Interpretation	Classification

Taking account the Axioms of SHM [78], damage assessment requires a comparison between two states of the system and each SHM approach requires a baseline system (as mention in Axiom II). From this concept, the level of damage detection that is studied is dependent on the way in which the training data set is defined. In this sense, both the combination of normal and damaged conditions of a bridge as well as only the normal conditions are factors that can be studied considering the data set available. Therefore, in the present thesis, the SHM and BD approaches are posed in the context of a pattern recognition problem that is composed of four parts: operational evaluation, data acquisition, feature extraction and statistical modeling for feature classification, as illustrated in Figure 3.3.

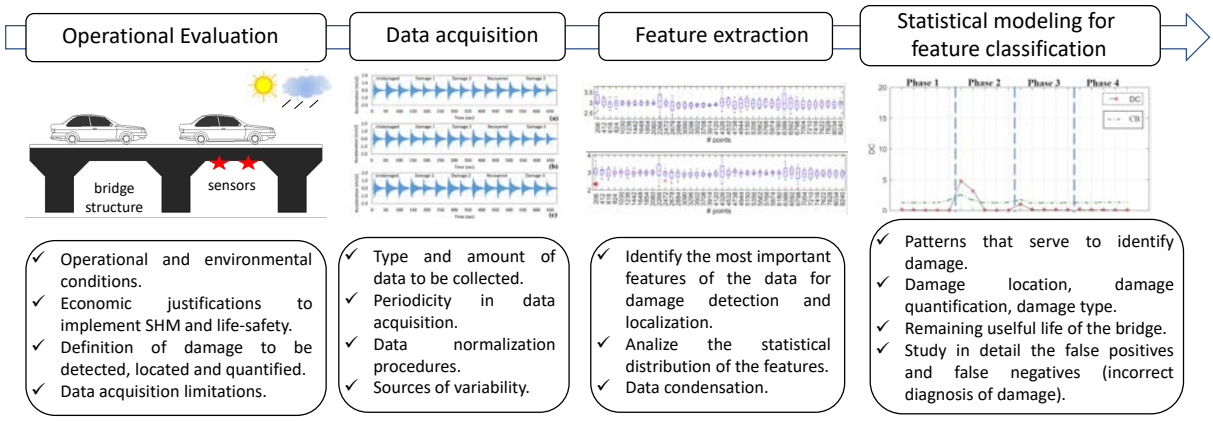

Figure 3.3. The SHM process based on the Statistical Pattern Recognition (SPR).

1) Operational evaluation

The first step to implement an SHM system defines the most appropriate methodology and procedure for monitoring and identifying damage to be used, that is, taking into account its advantages and limitations. This first stage of the SHM process considers an operational evaluation and attempts to answer four essential questions [3]:

- What is the main motivation for implement SHM? And how are the economic and human security conditions justified to implement the structure's monitoring system?
- How is damage defined for the structural system and, for multiple damage scenarios, which cases are the most concern?
- What are the operational and environmental conditions under which the structural system of interest operates?
- What are the limitations on acquiring data in the operational environmental?

Additionally, this first process begins to impose limitations on how to carry out this task and identify the main challenges such as: (i) bridges are considered structures of great economic cost, therefore, unlike other structural systems of less magnitude, it is more difficult to incorporate lessons learned to define anticipated damage. (ii) these civil structures suffer a slow degradation with normal use such as: corrosion, fatigue, damage due to sudden changes in temperature (freezing, thermal damage), loss of prestressing forces, degradation of connectivity induced by vibrations. (iii) the structural designs are carried out using events with a low probability of occurrence but high impact, such as: hurricanes, debris flow, earthquakes, floods.

2) Data acquisition

The second phase of the SHM process includes data acquisition, normalization and cleaning of data, this is a very important stage as it affects the correct identification of damage. Data acquisition includes:

- Planning and selection of excitation methods (forced / environmental).
- Data transmission (wired / wireless).
- The type of sensing hardware (tension, acceleration, displacement, etc.).
- Network (number and location of sensors).
- Time intervals for each case study and acquisition hardware, data transfer speed and storage capacity.

A very important aspect is that damage-induced changes in the data collected by the sensors can be distinguished from changes obtained by environmental and operational conditions, since these can mask structural damage. For this reason, the data that is collected must be normalized to make comparisons and not give false detections of damage.

In general, sources that affect response and that are other than damage cannot be completely eliminated, but they can be detected and minimized. Therefore, it is very important to make the appropriate measurements so that in later stages these sources can be statistically quantified and accurate thresholds for damage detection can be set. Finally, data cleansing is another stage that must be taken great care. For instance, during the feature selection process, the data rejected or taken into account are defined by an empirical procedure, that is, based on previous experience in data acquisition. Thus, nowadays, there are numerous data cleaning techniques such as signal processing, filtering and sampling [14].

3) Feature extraction

This stage considers the study of many features sensitive to damage, which are intended to identify and differentiate between the damaged and undamaged structural condition of a structure (bridges). Among these characteristics sensitive to damage are modal parameters, quasi-static strains, local flexibilities and other vibration-based parameters as previously defined in the present thesis. In addition, a characteristic sensitive to damage will change to a greater or lesser extent when different levels of damage occur. Methods involving comparisons with analytical models use Finite Element (FE) approaches to introduce faults through computer simulation and the structure can then be analysed in its damaged state. This comparison is made to identify which parameters are most sensitive in distinguishing between damaged and undamaged systems. Actual damage tests such as fatigue, induced damage, corrosion and changes in temperature cause the structure to degrade and damage to accumulate, thus, these can be very useful to identify characteristics.

The development of the innovative technologies used for SHM allows obtaining and storing large amounts of data (big data). In this sense, it is convenient that the data can be condensed to make comparisons of many sets of features, since the characteristics are related and assembled during the useful life of the structure. Likewise, data reduction techniques are increasingly innovative and robust to identify the sensitivity of features to structural changes in operational and environmental conditions. However, in the feature extraction phase of real SHM applications, care must be taken as both environmental and operational effects can mask damage-related changes in features, and hence the actual damage level cannot be determined. According to past research [11] [33], it is known that the more sensitive a feature is to damage, the more sensitive it is to changes in environmental and operational factors. In conclusion, more innovative and robust procedures should be developed for feature extraction that have the following properties as shown in Table 3.3.

Table 3.3 Main properties of damage-sensitive features. Adapted from [11] [33]

Sensitivity	A feature only has to be sensitive to damage and not to other external factors.
Computational requirements	Embedded systems should facilitate minimal processor cycles and minimal assumptions.

Dimensionality	The selected feature vector should not have a significant loss of information and should have the lowest dimension. If this is not fulfilled, high dimensionality shows undesirable complexity in statistical models and storage mechanisms.
Consistency	Feature's magnitude should change monotonically with damage level.

4) Statistical modeling for feature classification

The last stage of SPR-based SHM includes statistical modelling of the extracted features to improve the damage detection process. At this stage, machine learning algorithms are implemented to normalize the monitoring data and study the distributions in order to determine the structural condition. In the literature review, several algorithms are considered, however the present thesis only refers to the most advanced ones (Section 3.5). ML algorithms are classified into: novelty detection, classification (outputs are discrete class labels) and regression (respects the prediction of continuous quantities). The first belongs to the group of unsupervised algorithms, while the last two belong to supervised learning.

3.5. Machine learning techniques for bridge damage analysis

Machine learning (ML) is an application of artificial intelligence (AI) that aims to improve damage detection in BHM and give systems the ability to learn and improve automatically from experience. ML algorithms can self-learn the behavior of monitoring data and can then make predictions of possible future damage, without human intervention or assistance. Figure 3.4 shows the classification of machine learning algorithms [133] [134]. In the SPR-BHM approach, pattern recognition (SPR) is a field that uses various algorithms to label data as healthy or damaged

Furthermore, the application of ML algorithms to cases of real structures is focused on improving damage detection in variable operating and environmental conditions under which the structural response is measured. In the BHM state-of-the-art several algorithms have been reported that have an output-only approach related to data normalization, extraction and damage identification. However, in the present thesis, only a methodology that uses the algorithms of PCA, KPCA, *k*-means is considered. They are exposed in the following sections.

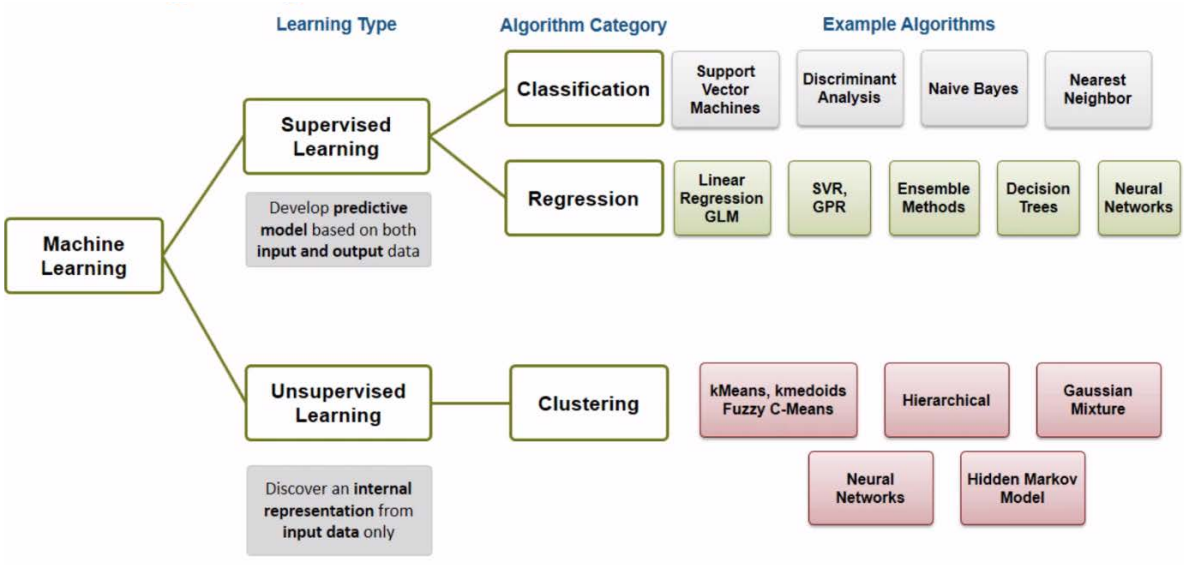

Figure 3.4. Algorithms used in Machine Learning. Adapted from [133].

3.5.1. Supervised and unsupervised machine learning algorithms

Machine learning algorithms find natural patterns in data that generate insight in order to make better decisions and predictions. As shown in Figure 3.4, machine learning algorithms are divided into 2 groups: supervised and unsupervised, and this depends on the type of data being analyzed. For instance, a supervised learning algorithm takes a known set of input data (the training set) and known responses to the data (output), and trains a model to generate reasonable predictions for the response to new input data [133]. Many applications in SHM use supervised machine learning and analyze existing data for the output that it is trying to predict. Supervised learning techniques are very useful when the prior knowledge about possible structural damage is available. In addition, all supervised learning techniques can be used as form of classification or regression to develop predictive models.

The classification models predict discrete responses and classify input data into categories, for instance, a medical diagnosis of cancer serves as a classification task since the input to the system is classified into either ‘‘cancer” or ‘‘no cancer”; whether an email is genuine or spam, or whether a damage is structural or not in SHM [14]. The regression models predict continuous responses and the goal is to model the relationship between a numerical output and a number of inputs. For instance, changes in temperature or fluctuations in power demand or during the monitoring period in SHM, besides, the typical applications include electricity load forecasting and algorithmic trading. The only difference between regression and classification is the format of the output. Therefore, taking account the Axiom III [78], the supervised machine learning approach allows to characterize damage as type and severity up to the level 3 of damage identification. The Support Vector Machines (SVM), Principal Component Analysis (PCA), Kernel Principal Component Analysis (KPCA), Naive Bayes classifier (NB) and Decision Trees (DT) are the most commonly algorithms that belong to this category.

On the other hand, unsupervised learning algorithms require output-only data without any labeling and find hidden patterns or intrinsic structures in data. The principal objective is to investigate the distribution of the data in order to obtain useful information regarding its underlying structure. Taking into account Axiom III [78], with this approach it is possible to reach a maximum level 2 of damage identification (implies the location). In addition, the overall goal is to achieve damage detection, clustering and dimensionality reduction. In this sense, these unsupervised algorithms first establish a reference condition of the structure considering appropriate characteristics extracted from the data, for example, they can be measured or obtained from a numerical model. Then, a statistical pattern recognition (SPR) process is used and the most important characteristics extracted from the new data are compared with those observed in the reference condition (no damage). At this stage, damage detection thresholds can be defined, since if there are significant anomalies or deviations, the algorithm has correctly identified this novelty, which finally indicates that the structure presents an anomalous behavior that may be the product of the damage. Examples of unsupervised learning techniques are k-means clustering, Gaussian Mixture Models (GMM), Variational Auto-encoder (VAE) and Generative Adversarial Networks (GAN).

Finally, there are some algorithms that are flexible, that is, they can be used in both the supervised and unsupervised approach, for example, Artificial Neural Networks (ANN), Genetic algorithms (GA), Hidden Markov Models (HMM). Some of these algorithms are described in more detail in the following sections of the present thesis.

1) Supervised machine learning algorithms

Principal Component Analysis (PCA)

PCA is one of the oldest multivariable statistical methods and well-known linear method for data analysis, which is used for mapping multidimensional data and as a dimensional reduction tool [135]. This method was first coined in early 1900's by Pearson [136] as an analogue of the principal axis theorem in mechanics and later developed in early 1930's by Hotelling [137]. PCA performs a decomposition of eigenvalues in a sample covariance matrix. This process produces both eigenvalues and eigenvectors corresponding to each value (Figure 3.5). Furthermore, a large number of interrelated variables can be represented into low-dimensional uncorrelated variables by an orthogonal projection with minimal redundancy, in which the new reduced coordinates are known as principal components.

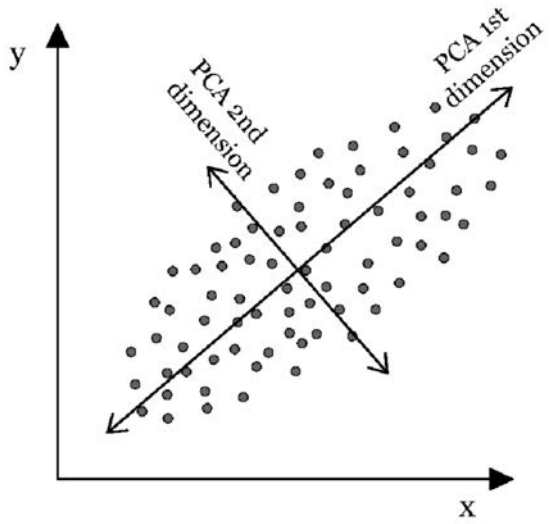

Figure 3.5. Axes in a Principal Component Analysis (PCA). Adapted from [11].

Damage sensitivity features collected from bridge structures subjected to environmental conditions can be processed by PCA to extract the main factors driving the variances in the data set [138] [139]. In the present thesis, PCA is used to extract the differences and similarities in the original data set rather than reducing the dimensions of the original data set. These results are shown in two investigations where PCA is used to eliminate environmental factors (temperature), and then a methodology for damage identification in a numerical bridge was proposed [94] [95].

Mathematically, Z denotes a *nxp* data set of *n* damage sensitivity feature collected from *p* observations with $n<p$. In [94], one damage sensitive parameter such as instantaneous phase is chosen as the feature, this damage parameter is represented by *n* and *p* represents the amount of time the instantaneous phase is collected. It can be expressed as:

$$Z = \begin{bmatrix} X_{1,1} & \cdots & X_{1,p} \\ \vdots & \ddots & \vdots \\ X_{n,1} & \cdots & X_{n,p} \end{bmatrix} \tag{31}$$

PCA transforms the data set *X* into a new *mxp* data set *Y* with smaller dimensions which characterizes most of the variances in the original data set. In this regard, a transform matrix T is used to relate Y and Z, which has dimensions *mxn* as shown in Equation 32.

$$Y = TX \tag{32}$$

Where *Y* is the score matrix and it represents a new set of data which combines the scores of each observation obtained for the factors affecting the original data set. The factors which represent the environmental effects are one of the principal components. The first principal component is represented by which present most of the variance in the original data set (normally environmental effects), and the second component accounts for the second most variance, and so on [138].

T is the loading matrix and its rows correspond to the eigenvectors of the covariance matrix of *X*. The singular value decomposition can be applied to obtain the eigenvectors of the covariance matrix of *X*. This relationship can be computed as:

$$\frac{1}{p-1} XX^T = U \frac{\sum^2}{p-1} U^T \tag{33}$$

U = orthonormal matrix $(UU^T = I)$ whose columns represent the eigenvector of the covariance matrix of *X* (hence $T = U^T$), and the summary is obtained by

$$\sum = \begin{bmatrix} \sum_1 & 0 \\ 0 & \sum_2 \end{bmatrix} \tag{34}$$

The singular values are represented by $\sum_1 diag(\sigma_1, \sigma_2, \ldots, \sigma_m)$ and $\sum_2 diag(\sigma_{m+1}, \sigma_{m+2}, \ldots, \sigma_n)$. The $\sum_1$ and $\sum_2$ are organized in descending order $(\sigma_1 \geq \sigma_2 \geq \ldots \geq \sigma_m \geq \sigma_{m+1} \geq \ldots \geq \sigma_n \rightarrow 0)$. Finally, the damage detection can be obtained considering the analysis of the only first few rows of the score matrix (first few principal components in PCA method). Therefore, the number of principal components should be chosen carefully in order to avoid the false detections.

Kernel Principal Component Analysis (KPCA)

The KPCA algorithm is the nonlinear extension of the linear principal component analysis (PCA) developed by [140]. This KPCA algorithm is a statistical tool commonly used to fit a nonlinear model to the features sensible to damages in the undamaged state. Moreover, this algorithm can be used to compare the predictions of a model and the characteristics observed in the field of structural health monitoring on bridges [50].

Nowadays, many parameters used as damage sensitivity features in real bridges are affected by environmental conditions (e.g. temperature, humidity, wind). Figueiredo et al. [141] proposed an approach to damage detection in a bridge known as Z24 taking into account that the bridge operates within its undamaged condition (baseline condition BC) under operational and environmental factors. As a first step, the unsupervised learning stage was carried out to infer the heterogeneity of the data in different operational and environmental conditions. Then, the next step was to establish a procedure to incorporate prior knowledge of the baseline data into the damage detection process. A daily Damage Index (DI) was implemented, corresponding to the minimum Mahalanobis Squared-Distance (MSD) coefficient of two models with a de-fined threshold for the 95% confidence region. Therefore, the performance of the classifier was observed taking into account the existence of known damaged structural responses. Reynders et al. [50] developed an improved output-only method based on the KPCA in order to eliminate nonlinear operational influences and environmental conditions on Z24

bridge. They have previously confirmed the non-linear relationship between natural frequencies and ambient temperature. The authors used two parameters automatically determined from the learned model based on Gaussian KPCA and the results demonstrated satisfactory improvements in data normalization for damage identification. The authors [142] adopted PCA and KPCA algorithms for data compression and the median values of principal components were defined for damage feature extraction in a six-bay truss bridge model. Afterwards, a fuzzy c-means (FCM) clustering algorithm is used to categorize these features for structural damage detection. This method could effectively identify the bridge damages simulated by loosening the bolted joints of the truss bridge structure.

KPCA is formulated in the following way. Mathematically, a training data matrix $X \in^{\sim mxn}$ is considered for normal condition data. Where n = feature vectors; m = environmental and operational factors when the bridge is undamaged. Moreover, $Z \in^{\sim kxn}$ represents a test data matrix, where k = number of feature vectors from the undamaged or/and damage states. The data normalization consists as follows: (i) the loadings matrix, U, is obtained from X; (ii) the test matrix Z is mapped onto the feature space $\sim r$ and reversed back to the original space $\sim n$, where r = number of factors or principal components. Finally, (iii) the residual matrix E is obtained as the difference between the original and the reconstructed test matrix.

For the feature classification, a feature vector f *(f = 1, 2,...,l)* is considered and its residual uncorrelated with environmental and operational conditions can be computed as:

$$e_f = U_1 U_2^T \Phi(\mathrm{z}_f) \tag{35}$$

U_1 = contains the r largest eigenvectors; U_2 = comprises the $(m - r)$ shortest eigenvectors and the compact form $U = [U_1\ U_2]$ represents the eigenvectors matrix partitioned. Furthermore, $\Phi(z_f)$ represents a nonlinear mapping of the output sequence, z_f, onto a possible very high-dimensional. In addition, the r principal components can be obtained by test the minimal percentage of the variance Γ (0.99 can be adopted) to explain the variability in the matrix X [50]. Note that due high-dimensional in feature space of the KPCA, the Γ and r may be larger than the values used in linear PCA. Then, an eigenvector matrix A can be used in order to determine Φ, as follows:

$$U = \tilde{\Phi} A \tag{36}$$

$$\tilde{\Phi} = \frac{1}{\sqrt{m}}\left[\Phi(\mathrm{x}_1)...\Phi(\mathrm{x}_m)\right] \tag{37}$$

All solutions are summarized in solve a standard eigenvalue problem as mention in Equation 37, where Λ = diagonal matrix containing the ranked eigenvalues λ_i and K = kernel matrix expressed by the formula 39.

$$KA = A\Lambda \tag{38}$$

$$K = \tilde{\Phi}^{T}\,\tilde{\Phi} \in \tilde{}^{\,mxm} \tag{39}$$

A kernel function can be represented by the inner product of the form $\Phi(x_i)^T \Phi(x_j)$ and a Gaussian kernel or radial basis function (RBF) defines a single parameter by the equation 40. Where $\sigma > 0$ is the bandwidth of the RBF kernel and can be obtained using the Shannon's information entropy in the inner product matrix *K*.

$$k(\mathrm{x}_i, \mathrm{x}_j) = \exp\left(-\frac{\left\| \mathrm{x}_i - \mathrm{x}_j \right\|^2}{2\sigma^2} \right) \tag{40}$$

2) Unsupervised machine learning algorithms

Cluster technique is one of the most used unsupervised machine learning approach with the main objective to divide the input dataset into clusters with similar examples. In cluster analysis, data is partitioned into groups based on some measure of similarity or shared characteristic. Clusters are formed so that objects in the same cluster are very similar and objects in different clusters are very distinct. The clustering algorithms fall into two broad groups: hierarchical and nonhierarchical (Figure 3.6). The first approach produces nested sets of clusters by analyzing similarities between pairs of points and grouping objects into a binary, hierarchical tree. Some algorithms of this category are agglomerative and divisive. Several investigations using this method have been developed for damage identification on bridges [31] [73] [96], the authors describe clustering methods as well as the definition of the hierarchy and its use for damage detection are extensively described.

The second group is made up of the following algorithms: *k*-means, k-Medoids, dynamic cloud and fuzzy C-means. These techniques have been used in recent years for damage detection, localization and quantification on bridges [97] – [99] [143]. Taking into account the literature review, Santos et al [74] implemented two approaches together: cluster algorithms and symbolic data to achieve a single-value novelty index (NI) to be able to detect structural changes in multi-sensor data-sets. To achieve the capability of NI and to corroborate the proposed theory, data obtained from Samora Machel bridge was used. During structural monitoring, refurbishment works were performed, such as repairing/replacement of concrete, replacement of suspension cables, hangers and supports. The methodology was implemented to perform a real-time assessment using a single-value NI for multiple time windows (TW). A cluster analysis technique was proposed by Santos et al. [97] for damage identification in a real bridge, and they utilized a statistical process considering interquartile ranges as part of symbolic data analysis. The algorithms used are able to allocate data objects to any number of predefined clusters, irrespective of whether this amount has really been observed in the structural system. This strategy was applied to vibration data (frequencies, mode shapes and damping

ratio). A cable-stayed bridge was utilized as case of study for damage identification [12], the authors used a combination of two statistical learning methods such as neural networks and clustering methods in order to detect early damages. Diez et al. [10] proposed a clustering-based approach to join datasets with similar behaviors and then detect structural changes on the Sydney Harbour Bridge. The approach presented has a peculiarity of considering the vibration signals caused by passing vehicles to detect and locate damaged junctions using *k*-means clustering algorithm. The results showed correlations between joints, locating a damaged joint and another with a defective instrumented sensor.

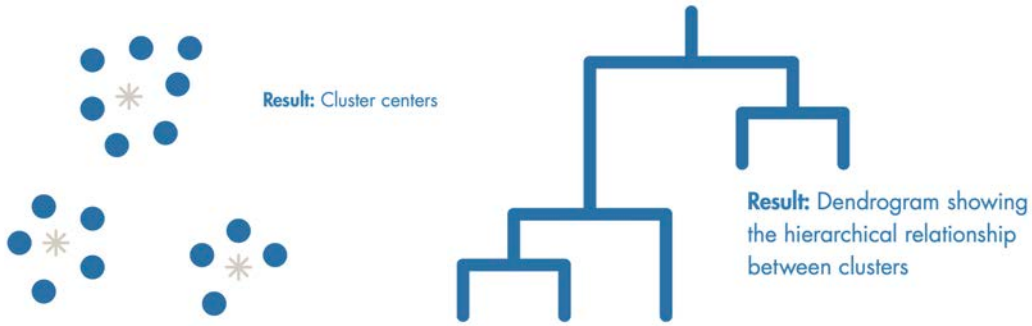

Figure 3.6. Nonhierarchical and hierarchical (dendrogram) clustering examples. Adapted from [133].

Clustering methods provide a variety of algorithms with desirable characteristics for the discovery of intrinsic properties contained in the data. As an un-supervised machine learning algorithm, clustering does not require the definition of reference/training data. Instead, they have the capability to "understand" the intrinsic features by trying to find the most compact and separated set of clusters [91]. In the present thesis, the most used and powerful unsupervised machine learning algorithm like *k*-means is used and therefore, its background is introduced in the following [55] [91].

K-means

k-means clustering is a partitioning method that splits data into k mutually exclusive clusters, and returns the index of the cluster to which it has assigned each observation. Unlike hierarchical clustering, *k*-means clustering operates on actual observations (rather than the larger set of dissimilarity measures), and creates a single level of clusters. The distinctions mean that *k*-means clustering is often more suitable than hierarchical clustering for large amounts of data.

According [11], *k*-means algorithm minimizes within-cluster sum of squares and mathematically can be computed as Equation 41, where n data points are partitioned into k mutually exclusive clusters in which each data point belongs to the cluster with the nearest mean. The variance between groups has to be maximized while the total variance within the group is minimized, this means that the squared error function J in equation 40 must be minimized, where, n = number of data points, k = number of clusters and c = centroid of cluster j.

$$J = \sum_{j=1}^{k} \sum_{i=1}^{n} \left\| x_i^{(j)} - c_j \right\|^2 \tag{41}$$

The sequence of this *k*-means method consists in:

1. Cluster the data into *k* groups where *k* is predefined.
2. Select *k* data points at random for the centroids.
3. Assign objects to their closest centroid according to the Euclidean distance function.
4. Calculate the centroid or mean of all data points in each cluster.
5. Repeat steps 2), 3) and 4) until the same data points are assigned to each cluster in consecutive runs.

The main objective of cluster analysis is to minimize the distance within the cluster that maximizes the distance between clusters, it is simply performed as:

$$W(\mathrm{P}_k) = \frac{1}{2} \sum_{k=1}^{K} \sum_{c(\mathrm{i})=\mathrm{k}} \sum_{c(\mathrm{j})=\mathrm{k}} d_{ij} \tag{42}$$

Where a given partition containing *K* clusters is considered, $P_K = \{C_{1, \ldots,} C_K\}$; *c(i)* = many-to-one allocation rule that assigns object *i* to cluster *k*, based on a dissimilarity measure d_{ij} defined between each pair of data objects, *i* and *j*.

Cluster validity

Mathematically, the clustering procedures obtain a certain number of partitions in an arbitrary way, however, within the cluster analysis, high dissimilarity values and results that are not optimal can be obtained. In this sense, the optimal number of clusters must be studied in detail. Some authors [144] have suggested using a quantitative evaluation known as cluster validations to find the optimal value of clusters. One of the most widely used validity indices in SHM is called silhouette statistics (SIL). The construction of silhouette statistic consists in assigning a fixed number of clusters K to the ith observation, and can be expressed with the following formula:

$$s(\mathrm{i}) = \frac{b(\mathrm{x}_i) - \mathrm{a}(\mathrm{x}_i)}{\max\left\{a(\mathrm{x}_i), \mathrm{b}(\mathrm{x}_i)\right\}} \in [-1, 1] \tag{43}$$

Where $b(x_i)$ = distance to nearest neighboring cluster's center, $a(x_i)$ = average distance between the *i*th object of cluster *C* and the remaining *j* objects. By finding the average of silhouette widths for all samples, the average silhouette width can be computed as:

$$SIL = \frac{1}{K} \sum_{i=1}^{K} s(\mathrm{x}_i) \tag{44}$$

Where K = clustering partitions and the value of silhouette coefficient varies from 0 to 1. Finally, a larger silhouette width indicates better clustered data.

Chapter 4 – Application and results

In the present chapter, the methods and tools described in the previous chapter are applied to check their accuracy and reliability in the damage detection. The idea is to check the performance of the new vibration-based damage features as well as to apply the most appropriate tools in each specific application, depending on the characteristics of the gathered data. Also, the application is carried out trying to follow the increasing level of complexity of the different tools applied. As the main objective of the thesis is that the proposed detection techniques could provide accurate results for real bridges, the application is carried out in response data from three real-world bridges where artificial and perfectly known damage was created, so the performance of the approaches can be perfectly checked.

4.1. Application of new vibration-based parameters for bridge damage identification

Currently, traditional methods for detecting structural damage use modal methods considering vibration frequencies, mode shapes, damping ratios as sensitive features to damage. Nevertheless, the present example shows an alternative novel approach for damage identification based on the non-modal based parameters defined in Chapter 3. Firstly, only ambient vibration (linear and stationary) is studied using several empirical parameters described in Section 3.2 (CAV, DVI, MCVI) and in the paper presented in chapter 5.1. These non-modal parameters are applied to measured vibration response data obtained from progressively damages in a real bridge named S101 located in Austria. After that, the application of these parameters and others as defined in Section 3.2 and in Chapter 5 (Section 5.1), is extended to the case of traffic generated vibrations (non-linear and non-stationary). To this end, previously to their application, the dynamic signals are decomposed by means of the HHT. The bridge selected for this second part is a steel arch bridge in Japan.

The S101 bridge (Figure 4.1a) was a post-tensioned concrete bridge located near Vienna in Austria that had a main span of 32m, two 12m side spans, deck cross-section 7.2m wide and double-webbed t-beam, whose webs had a width of 0.6 m [145] [146]. The columns, beams and the deck slab were built with concrete material of 2400 kg/m3 density and the Young's modulus of 24.8 GPa. In 2008, it was decided to replace the S101 bridge due to insufficient carrying capacity and deteriorating structural condition being identified from visual inspection data. However, before demolition, a progressive damage test under ambient excitation was conducted on this bridge (Figure 4.1b).

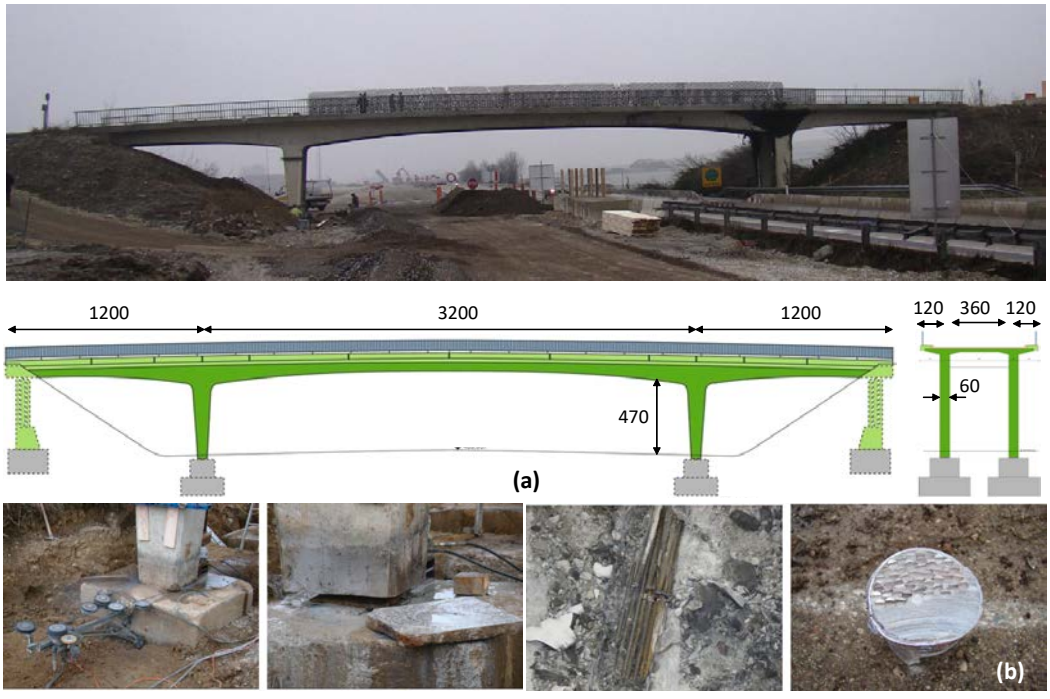

Figure 4.1. (a) View of the S101 Bridge and bridge dimension (dimensions in centimeters); (b) Progressive damage of column and tendons on bridge S101. Adapted from [145] [146].

A complete description of the progressive damage scenarios and monitoring as well of the results obtained from this example is available in Section 5.1 where the journal paper 1 is included. Here, only the main results and conclusions are described.

The Euclidean Distance evolution of the CAV-based symbolic data objects throughout the duration of the progressive damage test is presented in Figure 4.2a. All damage scenarios were evaluated considering the Y-axis as a linear representation of time. It can be observed that an enhanced divergence from the undamaged state occurs at the sensors located at the damaged North Pier during the pier settlement test. After the pier is returned to its original positions, the Euclidean distance returns close to normal. This is to be expected, as the pre-stressed tendons should supply enough compression to close the majority of cracks caused by the pier settlement, effectively reversing the simulated damage. The Mahalanobis squared distance (MSD) evolution of the vibration parameter DVI throughout the duration of the progressive damage test is presented in Figure 4.2b. It can be observed that an enhanced divergence from the undamaged state occurs across the bridge during the pier settlement test, but particularly so at the sensors located at the damaged North Pier. The MSD evolution of the vibration parameter MCVI throughout the duration of the progressive damage test is presented in Figure 4.2c. It can be observed that an enhanced divergence from the undamaged state occurs on the North side of the bridge during the pier settlement test, with no exact location of damage identified. For the severed pre-stressed tendons, MCVI provides a strong indication of damage for the 3rd tendon cut, but no others.

The results of the application to this real bridge demonstrate the robustness of the proposed damage features for damage identification using measurements of ambient excitations. Moreover, this investigation has demonstrated that the novel empirical vibration parameters assessed are suitable for damage detection, localization and quantification.

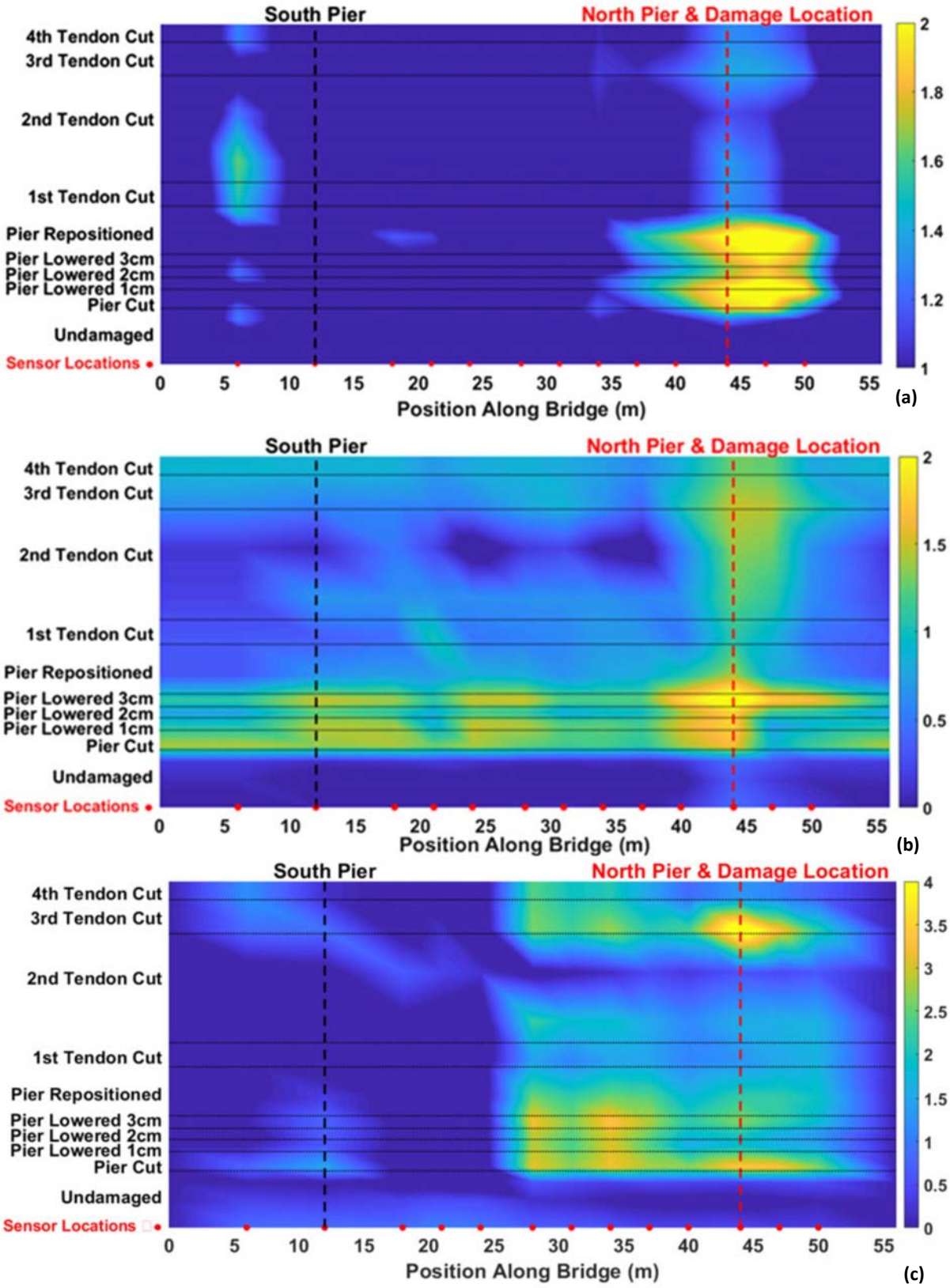

Figure 4.2. Evolution of damage parameters (a) CAV (b) DVI (c) MCVI.

Two methods of outlier detection were employed: MSD for the Gaussian distributed parameters DVI and MCVI, and Euclidian Distance of the symbolic data objects from the lognormal distribution of the energy-based CAV. Regarding the three assessed parameters, CAV portrayed the strongest indication of damage for the pier settlement test, while DVI was able to identify both types of damage, pier settlement and simulated stiffness loss.

In the second application, several damage parameters such as CAV, CAD, IVI, AIVI were used to detect damage in a Japanese bridge.

The Warren truss bridge was located in Japan and all the experimental study was carried out by Chang & Kim [147]. The structure consists of a single span 59.2m, 8.2 m maximum height, and 3.6 m width, designed for a single lane. Figure 4.3a depicts the real bridge that was constructed in 1959, besides, after 2012 it was demolished and replaced by a new one. A dynamic load test was carried out before the bridge was removed, using artificial damages (Figure 4.3d) and only a one van-type vehicle (Figure 4.3b) crossed along the bridge. The experimental setup consists of a sensor network to measure vertical accelerations as shown in Figure 4.3c. Further details of the bridge as well as the produced damage scenarios and tests carried out are presented in Section 5.1.

Figure 4.3. Illustration of (a) the Warren truss bridge (b) recreation vehicle used in the test (c) location of the 8 accelerometers and artificial damages (d) experimental programme of the artificial damage. [Adapted from reference 147].

The non-modal vibration-based damage characteristics CAV, CAD, IVI and AIVI are detailed and selected for the evaluation of high energy and short duration non-stationary signals induced by the passage of the vehicles. That is, as a first step, signal decomposition methods are used because the signals recorded from this load test are non-linear and non-stationary in nature. Then, the Hilbert-Huang Transform (HHT) and the parameters based on vibration intensity are applied. Additionally, new damage features such as instantaneous frequency, instantaneous amplitude and instantaneous

vibration intensity derived from the application of HHT are proposed and their performance in detecting and localizing damage investigated.

Figure 4.4a presents the CAV values obtained at all sensor for the condition states (healthy and damaged states). All values are normalized to the largest undamaged value and the damage 3 (DMG3) condition yields a significant change in CAV at Sensor 4, which is the damage location. However other condition states are less separable by eye. Besides, Figure 4.4b is used to portray the percentage variation from baseline for sensors 1-5 for damage 2 (DMG2), recovery (RCV) and damage 3 (DMG3). From here it is clearer that the spikes associated with DMG2 & DMG3 are located at the point of damage, while the percentage variation of the RCV state is less pronounced, indicating that the recovery process succeeded in realigning bridge behavior to near baseline. Figure 4.4c depicts the CAD values obtained at all 8 sensor locations and for all condition states, which are normalized to the largest undamaged value. Again, it is clear that DMG3 yields a significant change in CAD at Sensor 4, which is the location of damage. Figure 4.4d represents the percentage variation from baseline for sensors 1-5 for DMG2, RCV & DMG3, which shows clear damage at sensors 3 & 4 for damage states DMG2 & DMG3 respectively. Both sensors are located at the point of damage, indicating a successful damage location assessment. Moreover, the RCV state is close to baseline, which correctly indicates no damage present. Finally, the Figure 4.4e presents the AIVI values obtained at all sensor locations, where DMG3 is again the most obvious divergent. Furthermore, the percentage variation of sensors 1-5 is presented in Figure 4.4f. The damage detection behavior is similar to previous analyzed cases, where two principal damage locations are identified by AIVI.

As a conclusion, all empirical vibration parameters assessed (CAV, CAD, IVI and AIVI) identified the required damage events, with CAD providing the greatest resolution regarding the damage location. The parameters based on vibration energy showed significant increase throughout the time range for all sensors close to damage. In contrast with a sensor away from undamaged state, where no appreciable change in vibration magnitudes were observed with increasing levels of damage. To evaluate the damage using the AIVI parameter, it is not only necessary to find the maximum peak points, but it is important to analyze the behavior of the intensity during the entire time of the forced load test. From the comparison with the damage identification based on modal-based parameters carried out by [147], it is observed that all the vibration parameters assessed appear to outperform the modal frequency changes. In this regard, with AIVI's percentage differences producing the best overall.

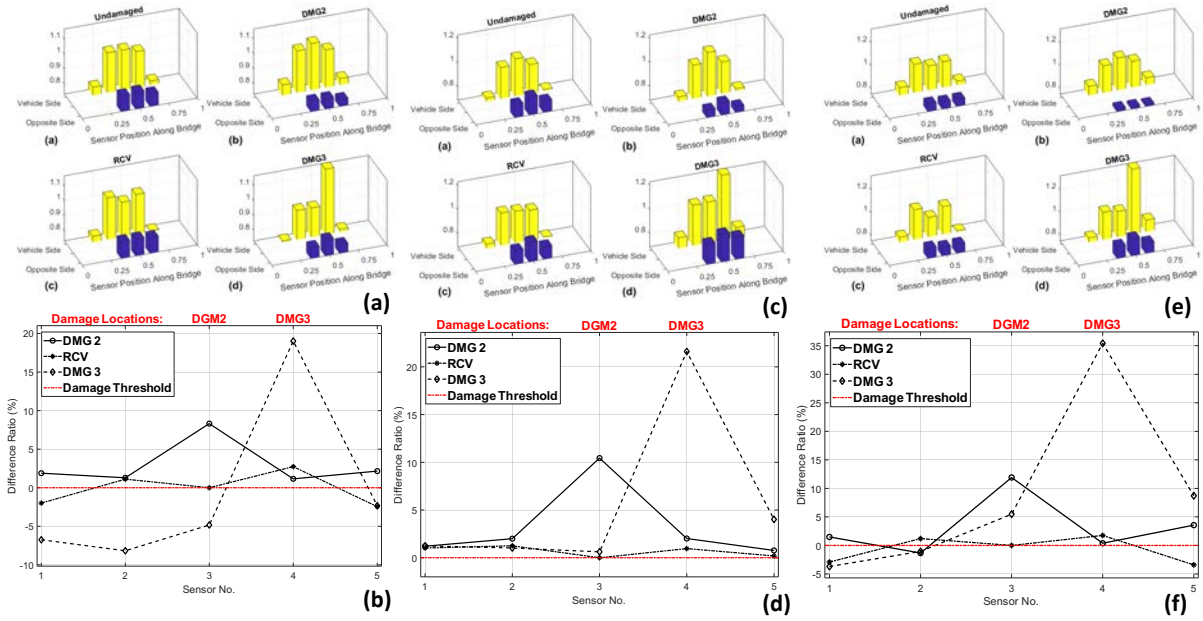

Figure 4.4. Comparison of values per sensor for all damage scenarios (a) Normalized CAV (b) CAV percentage variation from baseline (c) Normalized CAD (d) CAD percentage variation from baseline (e) Normalized AIVI (f) AIVI percentage variation from baseline.

As a final conclusion of this first application, in both bridges the use of the non-modal based damage parameters allows a correct damage identification and localization by analyzing the results of each sensor. However, the possibility of robust damage quantification was not possible based on these parameters in the case of the forced vibrations. For this reason, new vibration-based damage features will be applied in Section 4.2 seeking for their ability to quantify the damage. Also, machine learning and artificial intelligence techniques must be implemented for automatic damage identification since in this first application, it is treated in a comparative way between healthy and damaged conditions (supervised detection). In addition, there is no presence of environmental variability as temperature changes since both tests were carried out in a short time interval. Therefore, the next step is to propose unsupervised automatic detection algorithms (clustering) as well as methods to remove the influence of ambient temperature, which is developed in the next application presented in Section 4.3.

4.2. Feasibility of Marginal Hilbert Spectrum and Instantaneous Phase Difference as total damage indicators

At present, the trends and challenges in the development of signal processing tools are increasingly being used with an emphasis on real bridge structures. Therefore, it is important to study new damage parameters from vibration signals. This application focuses on the study of the non-linear and non-stationary dynamic response of bridges under operating loads [92], but analyzing the performance of new vibration-based damage features that may be obtained as a result of the application of HHT, such as Marginal Hilbert Spectrum (MHS) and Instantaneous Phase Difference

(IPD) as defined in subsection 3.3.3. They are proposed as total damage indicators, in the sense, that by using them it is possible to detect, locate and also quantify damage These new damage parameters are applied and corroborated in two bridges: the Japanese bridge described in the previous section (see Figure 4.3) and a numerical model of a two-span steel bridge. The full results of the application are described in the journal paper presented in Section 5.2 and only the main parts are summarized herein.

Taking into account the mathematical formulation of these new damage parameters explained in section 3.3.3, Figure 4.5a plots the results of the MHS for sensor 1 located far from the damage on the steel arch bridge. In the undamaged condition, it has a frequency of 3.0 Hz, and the maximum frequency decreases as the damage is more severe (2.82 Hz and 2.72 Hz for damage 1 and damage 2, respectively). Also, in the recovered state, the frequency increases slightly (2.92 Hz). However, damage 3 (DMG03) produces an increase in peak frequency (3.20 Hz), which does not physically indicate the presence of damage. Similarly, sensor 2 does not show a clear pattern in frequency changes that could be correlated with the presence of damage (Figure 4.5b). On the other hand, Figures 4.5c and 4.5d show a different behavior for sensors 3 and 4 respectively, where the damage was located in the exact position of these sensors. The frequency reduction in sensor 3 from the undamaged state (baseline) to damage levels 1, 2, and 3 are 6%, 10%, and 2% respectively. For sensor 4, from the baseline to damage 1, 2 and 3, the reduction is 5%, 9% and 17% respectively, which is also correlated with the extension and intensity (value of 5% for half of the cut compared to 9% for the cut) and the location of the damage (sensor 4 is located right where the damage 3 is present). Therefore, the results of the MHS damage parameter show that the sensors located in the damage are capable of identifying, locating and quantifying structural damage.

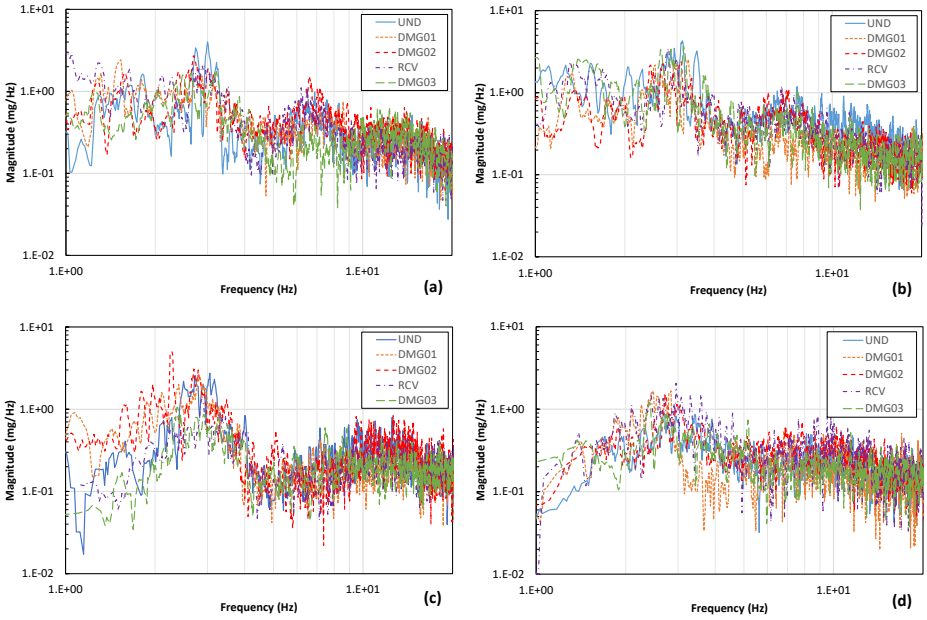

Figure 4.5. Marginal Hilbert spectra using ICEEMDAN (a) sensor 1 (b) sensor 2 (c) sensor 3 (d) sensor 4.

Additionally, the other damage parameter known as instantaneous phase difference (IPD) was studied. For example, the results of the IPD of sensors 2 and 5 are shown in Figures 4.6a and 4.6b respectively, where in both cases they do not show any clear trend with a damaged and recovered state present in the bridge, since they are far from the damage location. However, Figure 4.6c shows the evolution of the IPD for sensor 3, where the results in the bridge are significantly lower when damage is present compared to the healthy condition (baseline). Also, the recovered state (RCV) is close to the baseline, correctly indicating that no damage is present. Figure 4.6d corresponds to sensor 4 and shows a similar trend, since the values have a greater decay compared to the baseline when damage 3 occurs. In the recovered state (RCV), the behavior is clearly evident since the values follow the path of the baseline. Therefore, both sensors indicate a successful location of the damage. As reported in Section 5.2 also this parameter provides a clear indication of the severity of the damage present (damage quantification).

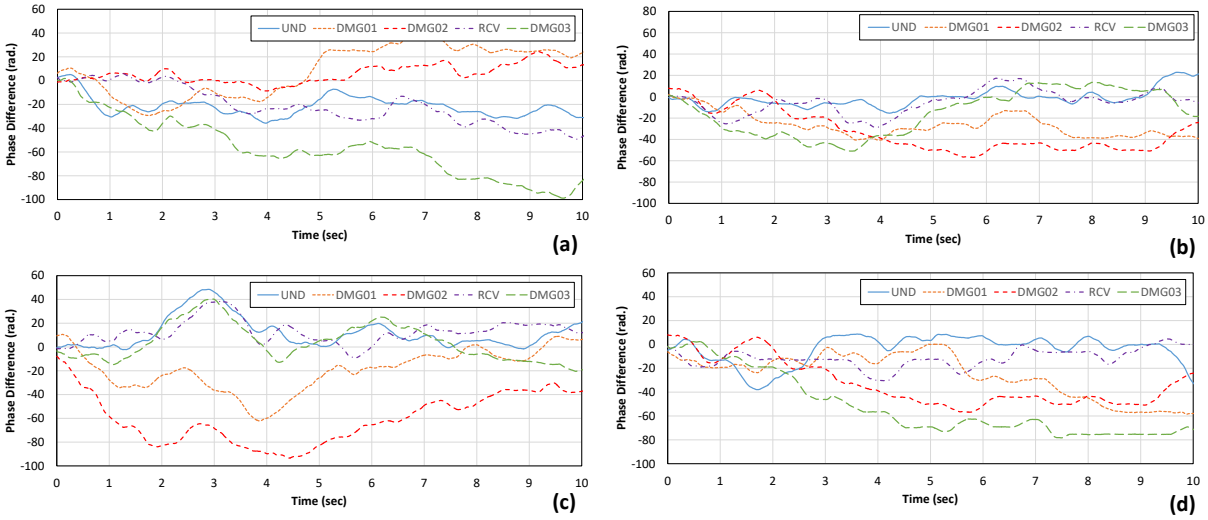

Figure 4.6. Mean phase difference values using ICEEMDAN (a) sensor 2 (b) sensor 5 (c) sensor 3 (d) sensor 4.

As second case study, a numerical model bridge is studied. This numerical model represents the superstructure of a two-span continuous steel beam bridge subjected to changing operational and environmental conditions. Figure 4.7 plots a description of the FE model of the bridge which was developed by [60] and it is presented considering different damaged states. The bridge deck is represented by a two-dimensional finite element (FE) model as shown in Figure 4.7a. It consists of a two-span continuous beam with equal span lengths of 10m. The cross section is rectangular with constant thickness b = 0.1m and height h = 0.6m. It is assumed to be made from low carbon structural steel (Grade S235). For this numerical bridge, cracks on the beam surface are considered and they are modelled by reducing Young's modulus on certain finite elements. In particular, six damage scenarios grouped in two damage regions are imposed for damage detection as shown in the Figure 4.7b. The location of sensors is described in the Table 4.1. The vibration is due to the crossing of a single vehicle at a constant speed along the deck (forced vibration).

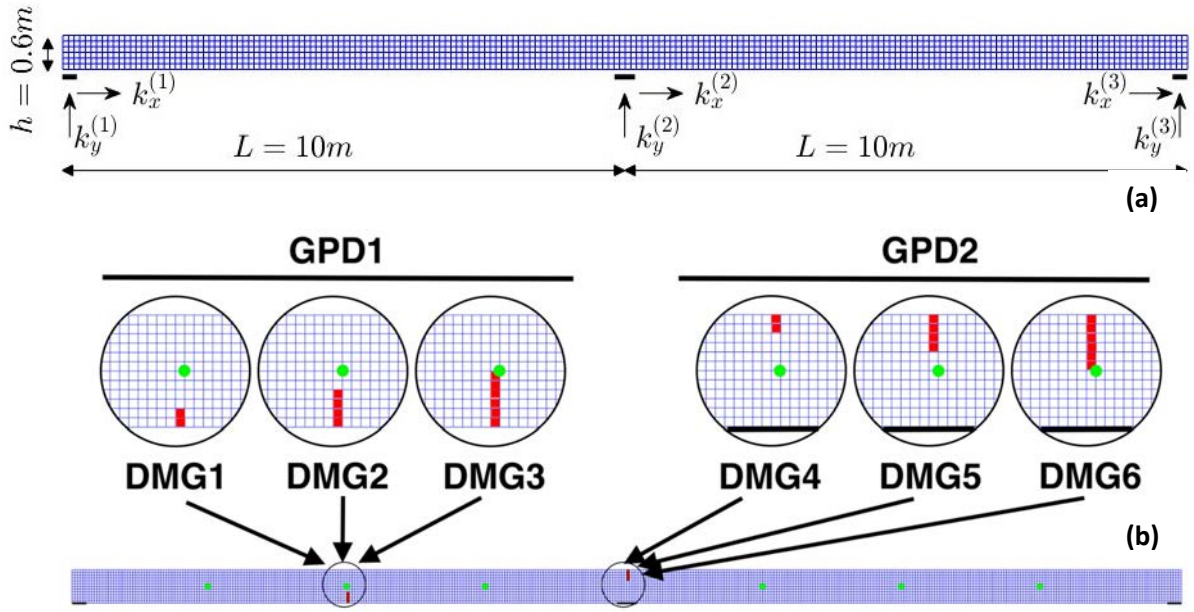

Figure 4.7. Numerical bridge (a) geometry of the two-span steel beam on elastic boundaries in the longitudinal and vertical directions (b) sensors (in green) & damage locations (in red) on steel beam.

Table 4.1 Sensors located along the numerical bridge.

Sensors	Description	Location along the neutral axis of the beam (y=0.3m)
S-01	At 1/4L from the left-hand support	x = 2.5m
S-02	At the middle of the left-span	x = 5.0m
S-03	At 3/4L from the left-hand support	x = 7.5m
S-04	At 3/4L from the right-hand support	x = 12.5m
S-05	At the middle of the right span	x = 15.0m
S-06	At 1/4L from the right-hand support	x = 17.5m

Figure 4.8 plots the MHS for the undamaged and damaged scenarios grouped in a single subplot for each sensor and considering the group of damage GPD1, where DMG1, DMG2 and DMG3 damages are grouped in GPD1 as can be shown in Figure 4.7b. It can be seen that for the baseline (blue lines) the marginal spectrum shows a peak frequency ranged from 30 to 32 Hz. This frequency range is close to the natural frequency corresponding to the first asymmetrical mode of vibration (29 Hz). It is also noticeable that for all sensors, when damage occurs, the peak value of energy increases while the frequency corresponding to this peak reduces. This behavior indicates the presence of damage as noted by many authors [120] [127] [128].

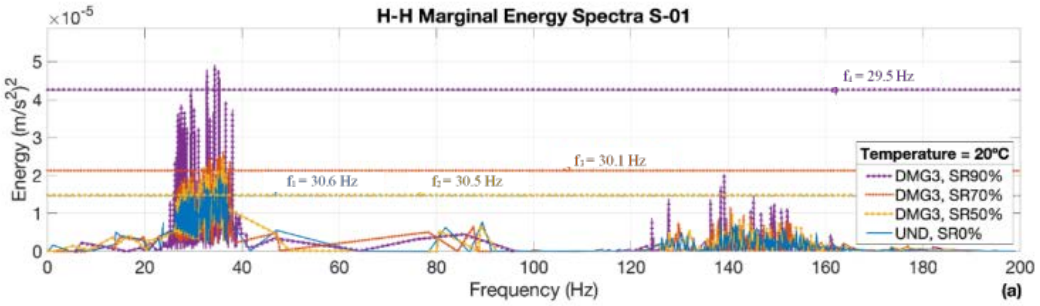

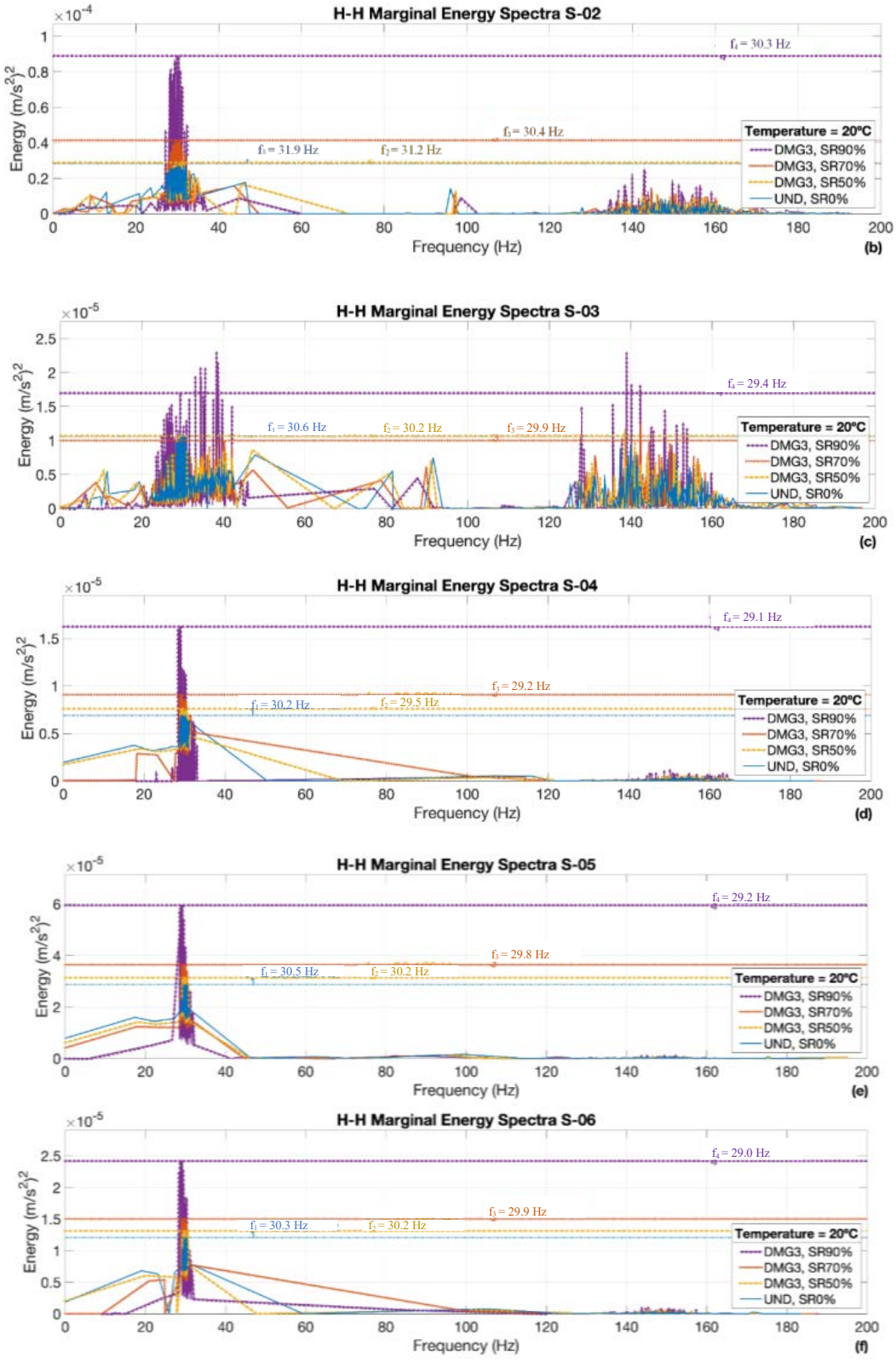

Figure 4.8. Marginal Hilbert Spectra for all sensors and for GPD1.

Figure 4.9 depicts the instantaneous phase difference (IPD) for the undamaged and damaged scenarios of GPD1 at each sensor. It clearly shows a decrease of the phase difference in all sensors due to the presence of damage in the system. It can be also observed how the values reflect the severity of

damage inferred by different values of the percentage of stiffness loss as the graph for the most severe damage scenario DMG3, Stiffness reduction of 90% tends to be located below the other damage configurations. The phase difference from different sensors can detect, locate and quantify (in terms of intensity) the damage.

The conclusion of this case study is that results for damage detection obtained in both cases for the 2 proposed parameters are very satisfactory. On one hand, for all sensors, the peak frequencies extracted from the MHS are reduced when damage occurs due to stiffness loss. On the other hand, all sensors detect a reduction of the instantaneous phase difference when damage occurs due to the decrease in the wave speed of the response measurements. In addition, those sensors located closer to the zones where damage occurs show a more noticeable reduction than the sensors placed more far away. Both, in the numerical case study and in the real bridge, the results illustrate that the MHS is able not only to detect and localize the damage, but also to ascertain the extension and intensity of the damage. In the case of the IPD, this damage indicator correctly detected, localized and quantified the intensity of the damage, but not its extension. Therefore, the spectral peak frequency and the instantaneous phase difference have shown as useful features to identify, locate and quantify damage in bridges under operational loads.

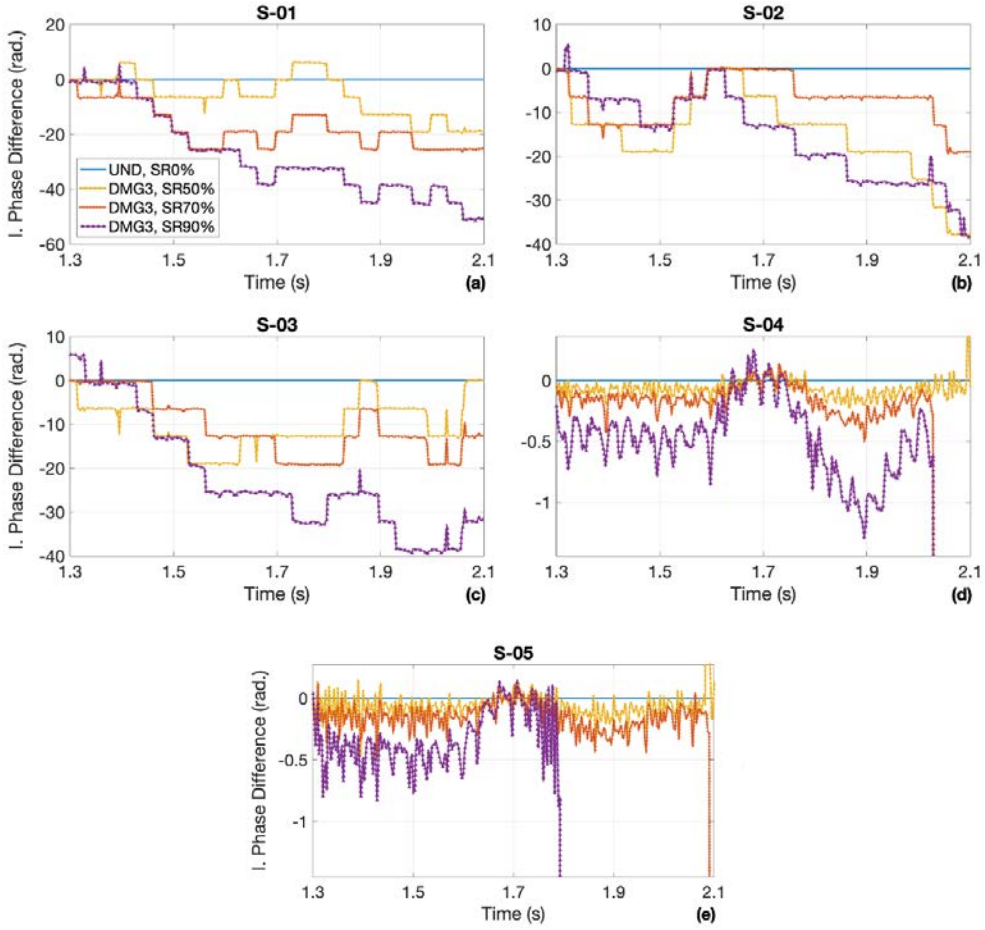

Figure 4.9. Instantaneous phase difference for each sensor and damage scenario corresponding to GPD1.

4.3. Application of un-supervised damage detection under changing environmental conditions

New trends in damage identification applied to bridges bring with them new challenges such as considering environmental variability. In the two examples described before, no temperature changes were present due to the short duration of the tests and its influence in the performance of the damage indicators was not obtained. Therefore, in the present application it is foreseen the possibility of a robust methodology for damage detection considering environmental changes and ambient vibration (not traffic) and using unsupervised machine learning techniques such as clustering. The application is carried out in a real bridge. The Figure 4.10a shows the well-known bridge called Z24 (Switzerland) that was studied dynamically tested for a period of 1 year under temperature changes and ambient vibration and later on artificially damaged with new dynamic tests carried out. This is a post-tensioned concrete box girder bridge with a main span of 30 m and two side-spans of 14 m (Figure 4.10b-d). The Z24 bridge was monitored for approximately one year and a long-term continuous monitoring program between November 1997 and August 1998 was carried out. The bridge was monitored by a long-term continuous vibration system, where the data was acquired hourly through two kinds of measurements: ambient vibration response and environmental conditions. During the long-term monitoring test, several progressive damage scenarios were imposed to the structural system of the bridge before its demolition (Figure 4.10e).

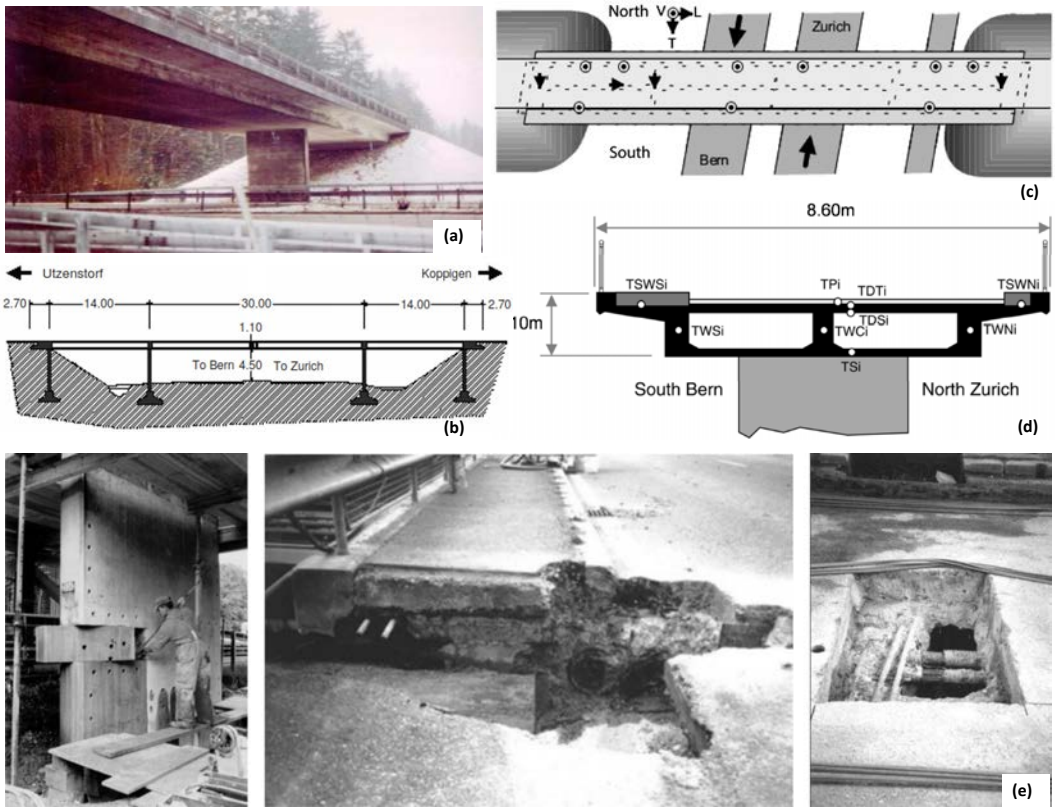

Figure 4.10. The Z-24 Bridge (a) side view and (b) longitudinal section. Acceleration sensor's locations (c) cross-section and (d) location of the thermocouples (e) damage scenarios carried out in the Z-24 Bridge; left to right: pier settlement, failure of anchor heads, and tendon rupture. Adapted from [33].

More detailed data on the monitoring system implemented, the damage scenarios and the results and conclusions of this case study can be obtained from the conference paper listed in Section 5.3

Many researchers have pointed out the issues and limitations of PCA method, since it does not correctly consider the effects of environmental factors on the modal parameters because this relationship is in general nonlinear [50] [53] [148]. Hence, in pursuit of better damage detection the kernel principal component analysis (KPCA) as described in Sub section 3.5.1 has been used in this case. For this purpose, the data sets were divided in three groups: training data, monitoring data in undamaged state and monitoring data in damaged condition. The model was constructed using 3500 data points for training phase and the rest of the data were used for monitoring in undamaged and damaged state. Figure 4.11a depicts the gradual development of the damage indicator (DI) and the red squares correspond to the artificial damages imposed to Z24 bridge during the last month of monitoring. Figure 4.11b gives a mobile window that contains samples in the two conditions of the bridge: undamaged and damaged. Figure 4.11c plots the damage indicators and all the mobile windows during the whole monitoring period. Then, the clustering unsupervised k-means algorithm generates the DC values for each mobile window, as shown in Figure 4.11d. In this case the values of DC demonstrate the real behavior of the bridge differentiating the loss of stiffness from the healthy condition. Besides, a confidence boundary (CB) was proposed as an indicator that warns with a pre-defined confidence level about structural damage if crossed by the damage feature indicator. A complete description of the application of the clustering algorithm and the obtained results can be found in Section 5.3. In conclusion, the kernel PCA algorithm presented good performance and capability for output-only damage detection. Its capability to identify the non-linear behavior of modal parameters due to changes in environmental conditions is fully proven. With regard to the statistical machine learning algorithms and clustering, this example shows a good capability for damage identification using the *k*-means algorithm (as described in Sub section 3.5.1). The proposed strategy demonstrates the success for detecting misfits without generating false detections in the case where the vibration data comes from a stationary process due to the ambient vibration in the bridge during the long time period of analysis. However, the next challenge is to see if the unsupervised machine learning algorithm will still work in the case of a forced vibration caused by the traffic in a real bridge. In this case, instead of environmental variability, the operational variability is the main issue. This is analyzed in the next application shown in Section 4.4.

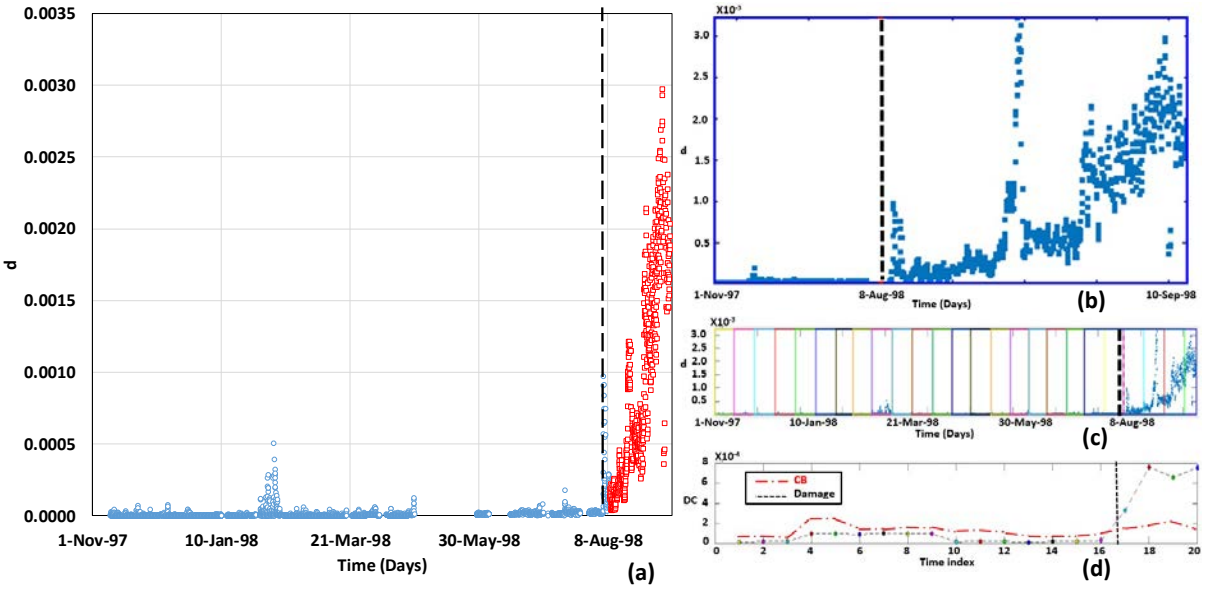

Figure 4.11. Damage detection procedure (a) damage indicator from the undamaged/baseline and damaged condition (b) damage indicator in a time-window (c) sequence of mobile windows (d) DC values obtained from each window.

4.4. Unsupervised damage detection under operational variability

According to the research presented, the proposed unsupervised detection considering Machine learning algorithms (clustering such as *k*-means) gives good results when temperature affects the results but its influence is successfully removed by appropriate normalization techniques as KPCA. The unsupervised technique is here applied to the traffic induced vibration of the steel arch bridge described in Section 4.1 (Figure 4.3). As the amplitude and frequency of the recorded signal is changing with the vehicle crossing, in this case instead of the natural frequencies of the bridge (as in the case of bridge Z24), the instantaneous frequency obtained with the HHT is proposed as the damage feature. The machine learning method was used for automatically classifying the damages using a moving windows process sequentially applied to the structural response of the bridge Moreover, a confidence boundary is defined in order to allow unsupervised damage detection with a certain level of confidence (suppression of false alarms).

The feature extraction is carried out using a symbolic data analysis. This analysis consists in the reduction of the data in more generic types and less voluminous information in contrast with classical data used in SHM applications. Symbolic data objects (SDO) use time intervals in statistical quantities such as interquartile intervals (IQR) or histograms. Interquartile intervals are used in this application.

The full description of the strategy for damage detection and localization is available in the journal paper displayed in Section 5.4. The sequence of the damage detection procedure is depicted in Figure 4.12 for sensor 3. In Section 5.4 similar figures for the rest of the sensors can be obtained. Figure 4.12a shows the instantaneous frequency obtained in sensor 3. An algorithm of time-window (TW) was used

to successively model, classify and identify the several damage scenarios, and the symbolic objects describing 40 seconds of normalized instantaneous frequency were considered along with time windows (5 SDO per TW) (Figure 4.12b). The sequential application of the *k*-means algorithm described in Section 3.5.1 is used to analyze each time window. The damage condition (DC) and confidence boundary (CB) obtained at each TW and for each analyzed set-in sensor 3 are depicted in Figure 4.12c. The figure clearly shows a damage detection (mismatch that exceeds the confidence boundary CB) when DMG2 occurs at a position close to sensor 3.

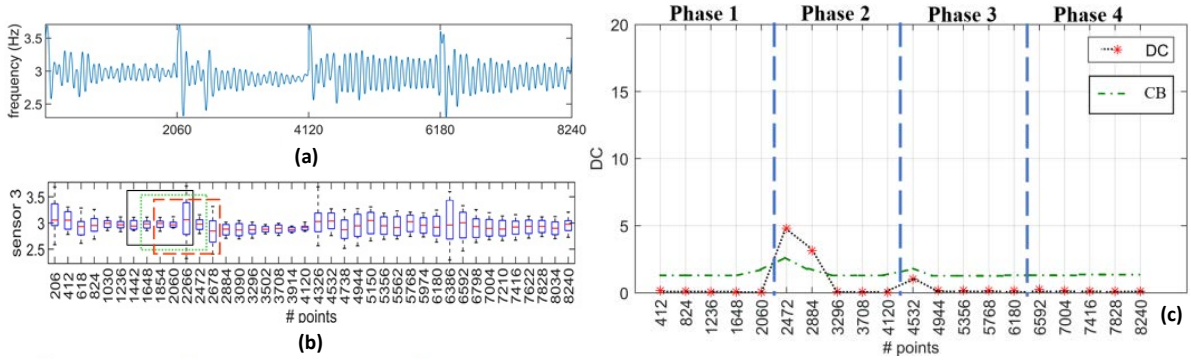

Figure 4.12. Damage detection procedure (a) instantaneous frequency for sensor 3 considering all damage states (b) sequence of mobile windows (c) Damage Condition (DC) values obtained from each window and the definition of confidence boundary (CB).

From the analysis of the results obtained in all sensors, the following conclusions can be drawn. A clustering-based approach to group data of instantaneous frequencies with similar behavior on bridge was developed, and then used to detect and localize structural damages. The *k*-means clustering algorithm was capable to allocate data objects to any number of predefined clusters. Additionally, the symbolic data objects (SDO) based on interquartile intervals were able to accurately generalize the data-set of instantaneous frequencies. The SIL cluster validity index demonstrated its ability to suggest the number of distinct structural behaviors (clusters in the analyzed data set) monitored on the bridge. In conclusion, the results show that the proposed mixed method was effective and can endow better results in bridge health monitoring in order to damage identification, localization and quantification for bridge under operational status.

Chapter 5 – Published Articles

This chapter reproduces the published articles produced in this thesis. Each paper follows its own numbering of sections, figures, tables, equations and references.

Journal Paper I:

Rick M. Delgadillo, Joan R. Casas, "Non-modal vibration-based methods for bridge damage identification", Structure and Infrastructure Engineering, vol. 16, no. 4, p. 676 – 697, July 2019. DOI: 10.1080/15732479.2019.1650080

- Area: Civil & Structural Engineering
- Quartile: Q1 (2019)
- JCR Impact Factor: 2.620 (2019)
- Number of cites: 6 (Scopus)

Journal Paper II:

Rick M. Delgadillo, Fernando J. Tenelema, Joan R. Casas, "Marginal Hilbert Spectrum and instantaneous phase difference as total damage indicators in bridges under operational traffic loads", Structure and Infrastructure Engineering, p. 1-21, September 2021. DOI: 10.1080/15732479.2021.1982994.

- Area: Civil & Structural Engineering
- Quartile: Q1 (2019)
- JCR Impact Factor: 2.620 (2019)
- Number of cites: - (Scopus)

Conference Paper I:

Rick M. Delgadillo, Joan R. Casas, "A combined kernel-PCA with clustering analysis for bridge damage detection under changing environmental conditions". In Life-Cycle Civil Engineering: Innovation, Theory and Practice. CRC Press, IALCCE 2021. pp. 1362-1370.

Journal Paper III:

Rick M. Delgadillo, Joan R. Casas, "Bridge damage detection via Improved Completed Ensemble EMD with Adaptive Noise and machine learning algorithms", Structural Control and Health Monitoring, January 2022, Accepted for publication.

- Area: Civil and Structural Engineering
- Quartile: Q1 (2020)
- JCR Impact Factor: 4.990 (2020)
- Number of cites: - (Scopus)

5.1. Journal Paper I

Non-modal vibration-based methods for Bridge Damage Identification

Published in Structure and Infrastructure Engineering, vol. 16, no. 4, p. 676 – 697, July 2019. DOI: 10.1080/15732479.2019.1650080

Rick M. Delgadillo [1], Joan R. Casas [1]

[1]Department of Civil and Environmental Engineering, Technical University of Catalonia (UPC), c/ Jordi Girona 1-3, 08034 – Barcelona, Spain

Received: 18 March 2019; Revised: 2 July 2019; Accepted: 4 July 2019

Abstract: Many methods of damage identification in bridge structures have focused on the use of either numerical models, modal parameters or non-destructive damage tests as a means of condition assessment. These techniques can often be very effective but can also suffer from specific pitfalls such as, numerical model calibration issues for nonlinear and inelastic behaviour, modal parameter sensitivity to environmental and operational conditions and bridge usage restrictions for non-destructive testing. The present paper covers alternative approaches to damage identification of bridge structures using empirical parameters applied to measured vibration response data obtained from two field experiments of progressively damaged bridges subjected to ambient and vehicle induced excitation, respectively. Numerous non-modal vibration-based damage features are detailed and selected for the assessment of either the ambient or vehicle induced excitation data based on their inherent properties. The results of the application to 2 real bridges, one under ambient vibration and the other of forced vibration demonstrate the robustness of the proposed damage features for damage identification using measurements of ambient and vehicle excitations. Moreover, this investigation has demonstrated that the novel empirical vibration parameters assessed are suitable for damage detection, localization and quantification.

Keywords: Structural health monitoring; bridges; damage identification; vibration parameters; Hilbert–Huang Transform; ambient excitation; forced vibration

1. Introduction

Structural damage and degradation of bridges is dangerous and costly occurrence. Once identified, repair works should be carried out promptly, as maintenance costs dramatically increase when damage is left unattended; therefore, it is vital that bridge owners conduct necessary visual inspections and structural integrity testing on a regular basis. However, due to the large quantity of bridges in the network, this is impractical. Instead of directly inspecting every bridge, sensors can be used to indirectly infer the presence of damage using theoretical relationships, such as that of modal frequency and stiffness. Numerous modal parameters have been proposed in this sense, some of which are presented and discussed in (Moughty & Casas, 2017). However, also other non-modal parameters have been considered. The majority of them are found and discussed in Kramer (1996), such as RMS acceleration, Arias Intensity, Cumulative Absolute Velocity (CAV) and others. In general, these parameters were defined to represent the frequency content, amplitude or duration of a ground motion, Nonetheless, nowadays they can be used to detect damages in real civil structures obtaining successful outcomes, as seen later in the present paper.

In this context, Kim et al. (2013) utilized conventional dynamic properties as a damage-sensitivity derived from linear system parameters of a time series model. They found MTS (Mahalanobis Taguchi System) is able to enhance the identification of structural changes due to damage. (Goi & Kim, 2017) proposed a novel damage indicator automatically derived from a set of multivariate autoregressive models on an actual steel truss bridge. This damage indicator demonstrated that the modal information included in a multivariate system could help to improve damage detection performance. (Zhou et al., 2015) carried out a real experiment on a free-free steel beam excited by a shaker (structural forced dynamic response data). Mahalanobis Square Distance (MSD) approach was developed in order to detect the damage levels. The authors claimed that the MSD is effective for damage detection using frequency-based raw data. Additionally, this approach may function in operational conditions. (Nguyen et al., 2014b) improved Mahalanobis Square Distance method with a controlled data generation scheme based on Monte Carlo simulation methodology. The effectiveness was demonstrated using a benchmark structure data from a building model with several damage levels.

The use of modal parameters as damage sensitive features have found that their performance may suffer from their sensitivity to environmental and operational conditions which can mask damage events. Additionally, the non-stationarity of some vibration signals creates a problem when using standard modal techniques based on Fourier transforms, as linear stationarity is assumed. Finally, Table 1 gives some advantages and disadvantages of the techniques applied to modal parameters in order to detect damages in real civil structures.

Table 1. Advantages and Disadvantages of damage detection methods based on modal parameters.

Method	Advantages	Disadvantages	Reference
Mahalanobis Taguchi System (MTS)	serve to emphasize change of the damage-sensitive feature due to damage	An expert judgment is needed to select the initial parameters	(Kim et al., 2013)
Mahalanobis Square Distance (MSD)	Its simplicity and computational efficiency	MSD fails when nonlinearities are present in observations	(Zhou et al., 2015)
Autoregressive models	Can be used to extract damage-sensitive features	The appropriate order estimation of an AR model is a complex issue	(Laory et al., 2013) (Goi & Kim, 2017)
MSD with Minimum Covariance Determinate (MCD)	Produces high resolution of structural condition variation and reduce uncertainty regarding external sources of excitation	Do not present a computational efficiency since this process takes multiple iterations	(Moughty & Casas, 2017)

In applications not using modal parameters, and instead using displacement/strain measurements as features for damage identification, (Tondreau & Deraemaeker, 2014) proposed a damage sensitive feature in two experimental applications using ambient dynamic strain measurements. In this case, all the damage scenarios were correctly located without false alarms. (Sun et al., 2016) proposed a damage detection method by analysing dynamic displacement of bridge structures under moving vehicle, which is represented by the numerical simulation of a beam model. The results showed both reliability and efficacy of this method in damage detection of bridge structures. Also, according to statistical hypothesis testing criteria, (Ou et al., 2017) covered a problem focused on the damage detection via the use of statistical and modal damage detection methods for a small-scale wind turbine. In conclusion, the statistical-based methods outperform modal-based ones, succeeding in the detection of induced damage, and they can be very well integrated into maintenance processes.

(Fassois and Kopsaftopoulos, 2013) outlined several statistical time series methods for vibration based structural health monitoring using a laboratory truss structure. The proposed methods achieved the detection, the location and the quantification of damages. However, they were limited by the specific type of model employed and for the adequate user experience. Moreover, (Kankanamge & Dhanapala, 2016) utilized the wavelet analysis for identification of modal properties and damage detection in two case studies: a single-span steel girder bridge in Holland, Michigan and a cable-stayed bridge in mainland China. The results showed that Continuous Wavelet Transform (CWT) method is a very effective tool, which is able to provide reliable results both in modal parameters identification and damage detection. (Ding and Chen, 2013) analysed the multi-scale wavelet transform coefficients of curvatures of mode shapes in order to indicates the damage location in a simply supported beam bridge. The results showed that the peaks of the wavelet transform coefficients indicate the damage location. (Hester & Gonzalez, 2012) utilized the wavelet energy content to detect damage in a simply supported bridge beam model, which proved to be more sensitive to damage.

The recent advances in Artificial Intelligence based damage identification methods are increasingly being used for their great performance. For instance, (Laory et al., 2013) proposed a

methodology for damage detection that combines moving principal component analysis (MPCA) with four regression-analysis methods applied in three case studies. The results indicate that the combined methods perform better than each individual method in terms of damage detectability and time to detection. (Nguyen et al., 2014a) used several variants of Principal Component Analysis (PCA) for detection and localization of damage on the Champangshiehl bridge and the precast panels. The results demonstrated that the damages were better distinguished in both cases.

Some researchers have applied other innovative techniques for analysis of bridge vibration data and damage identification. For instance, (Santos et al., 2013) implemented a strategy to detect structural damage using a symbolic data analysis in order to reduce raw vibration data through a statistical process utilizing Interquartile Ranges. The researchers obtained good results from the baseline-free strategy proposed, and this allowed to detect the structural changes regardless the modal quantities used (modal parameters) in real-time (without resorting to the entire data set).

This paper, which is an extended version of the paper by Moughty and Casas (2018b), presents a number of empirical vibration parameters designed to be suitably applicable as damage indicator features to the specific vibration signals that are typical from either long-duration, low-energy stationary ambient vibration or short-duration, high-energy non-stationary vehicle-induced signals.

2. Empirical vibration parameters

2.1. Vibration Parameters

This section introduces the five vibration parameters that are extracted from acceleration responses that will be tested as vibration-based damage features:

(1) Cumulative Absolute Velocity (CAV)

It is an energy-based vibration parameter proposed by Kramer (1996). It is the summed integral of all absolute acceleration values of the vibration response history:

$$CAV = \int_0^t \left|\ddot{x}(t)\right| dt \tag{1}$$

In reality, this parameter represents the area under the absolute accelerogram and CAV presents a good correlation with structural damage potential. Figure s1(a) and s1(b) shows an acceleration record and the corresponding values of CAV as they evolve over time.

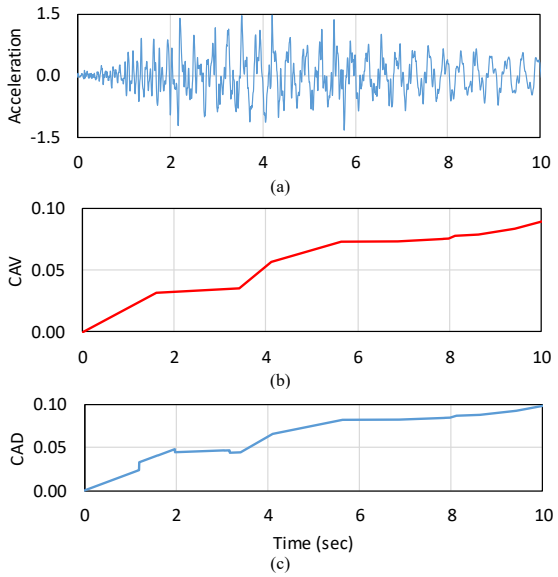

Figure 1. Illustration of the definitions of vibration parameters (a) acceleration time series (b) CAV (c) CAD.

(2) Cumulative Absolute Displacement (CAD)

It is an adaptation to the above CAV vibration parameter; however, in this case the acceleration signal is first transformed into displacements using integration and band- pass filtering to avoid drift. Figure 1(c) shows the CAD integral in the evaluated time:

$$CAD = \int_0^t |x(t)|\, dt \tag{2}$$

(3) Distributed Vibration Intensity (DVI)

It is a novel vibration parameter that is based on the concept of vibration intensity, which in simple harmonic motion context can be defined as $(I=a^2/f)$, where a is acceleration amplitude and f is frequency. The SI units of vibration intensity are mm^2/s^3 and its logarithmic power form is decibels (dB). For the distributed variant employed herein, a Fourier transformation is applied to the vibration data and the summation of the vibration intensity values is taken within a frequency range, denoted by (f_i) within the limits m-n in Equation (3). It is important that the frequency range selected encompasses the first few modes of vibration of the structure; in the present study, the frequency range is taken as $(m\text{-}n = 1Hz - 20Hz)$. In this way, DVI may capture the damage sensitivity associated with energy and modal frequency changes.

$$DVI = \sum_{i=m}^{n} 10 log_{10}\left(\frac{\ddot{x}_i^2 .(f_i)}{f_i} / I_S\right) \tag{3}$$

$$\text{For } m \le f_i \le n \text{ (in Hz)}$$

$$I_S = 10mm^2 / s^3$$

(4) Mean Cumulative Vibration Intensity (MCVI)

It is the second of three parameters based on the concept of vibration intensity (energy / frequency). In MCVI, the energy portion, i.e. the numerator, is the square of the aforementioned vibration parameter CAV, while the denominator is a weighted mean value of Fourier frequency within a specified frequency range. As per Equation (4), the weighting is applied to the discrete frequencies *(f_i)* via their corresponding Fourier Amplitude values *(FA)*.

As highlighted for DVI, it is important that the frequency range selected encompasses the first few modes of vibration of the structure; in the present study, the frequency range is taken as *(m-n = 1Hz – 20Hz)*.

$$MCVI = \frac{\int_0^t \ddot{x}(t)^2 dt}{\left(\sum_{i=m}^{n} FA_i^2 .(f_i) \Big/ \sum_{i=m}^{n} FA_i^2\right)} \quad (4)$$

$$\text{For } m \le f_i \le n \text{ (in Hz)}$$

(5) Mean Cumulative Vibration Intensity (MCVI)

It is the last vibration parameter that is based on concept of vibration intensity (energy / frequency), however, in this case the vibration parameter is designed for use on non-stationary and non-linear data, such as the vehicle induced excitation case assessed in the present study. IVI is the product of two Hilbert-Huang Transform (HHT) (Huang et al., 1998) parameters; instantaneous amplitude and instantaneous frequency, which are commonly presented together in a Hilbert-Huang Spectrum. However, this method of representation is not easily quantifiable. A more objective representation of instantaneous amplitude and frequency can be obtained via IVI, whose calculation is summarized in following explanatory paragraphs. For a more in-depth explanation on IVI's calculation and application, the reader is referred to (Moughty & Casas, 2018a).

The first step is to decompose the raw non-stationary and non-linear vibrations signals into different Intrinsic Mode Functions (IMFs) using Empirical Mode Decomposition (EMD). In the present study, an advanced method of EMD is used to improve the acquisition performance of IMF, known as Improved Complete Ensemble Empirical Mode Decomposition with Adaptive Noise (ICEEMDAN) and proposed by (Colominas et al., 2014). The authors proposed substantial

improvements to obtain components with less noise and more physical meaning. The resulting IMFs $\{c_i(\tau)\}$ are input into the Hilbert Transform:

$$H[c_i(t)] = \frac{1}{\pi}\int_{-\alpha}^{\alpha} \frac{c_i(\tau)}{t-\tau} d\tau \tag{5}$$

The resulting Hilbert Transform $H[c_i(t)]$ is grouped with $\{c_i(\tau)\}$ to form an analytic signal $z(t)$ (Equation 6) whose constituents $a_i(t)$ and $\theta_i(t)$ (instantaneous amplitudes and phases), can be expressed by Equation (7) & Equation (8) respectively. Instantaneous frequencies $\{\varpi_i(t)\}$ of each IMF are determined by differentiating the instantaneous phase function in Equation (9). Equation (10) expresses how the vibration parameter IVI is obtained by combining the instantaneous amplitudes and frequencies.

$$z(t) = c_i(t) + jH[c_i(t)] = a_i(t)e^{j\theta_i(t)} \tag{6}$$

$$a_i(t) = \sqrt{c_i^2(t) + H^2[c_i(t)]} \tag{7}$$

$$\theta_i(t) = \arctan\left(\frac{H[c_i(t)]}{c_i(t)}\right) \tag{8}$$

$$\varpi_i(t) = \frac{d\theta_i(t)}{dt} \tag{9}$$

$$IVI_i(t) = a_i^2(t)/\varpi_i(t) \tag{10}$$

Finally, note that IVI can be obtained for each particular sensor. Therefore, in order to guarantee that all obtained physically meaningful IMFs are utilized for damage localization, the sensor obtained IVIs can be combined to provide the Amalgamated Instantaneous Vibration Intensity (AIVI), which is studied in more detail in the results section.

2.2. Application Suitability of Vibration Parameters

The variables of each bridge monitoring campaign, such as monitoring duration, excitation method, number and type of sensors can differ widely from project to project. This may be due to the influence of external conditions associated with each bridge, such as the traffic volume and type, socioeconomic factors and the financial budget available. The result being that the vibration data

obtained may attain different properties that may render some damage sensitive features, such as those presented here, unsuitable for application.

For instance, long duration vibration data may not be suitable for the vibration parameter IVI, as the computation effort of the EMD process would be substantial. Furthermore, Fourier-based damage sensitive features, such as modal parameters are unsuitable for non-stationary vibration data that would be typical of vehicle induced excitation bridge testing. The proposed methods studied here were applied when the traffic was closed, that is, when there was no normal traffic excitation. In addition, these methods are useful when there is only environmental vibration and for a controlled load test. For this reason, Table 2 is provided to give a breakdown of the applicability of each of the selected vibration parameters to specific vibration properties that may influence their damage identification performance.

Table 2. Vibration parameter application classification

Property \ Vib. Para.	CAV	CAD	DVI	MCVI	IVI/AIVI
Fourier-Based Parameter	✗	✗	✓	✓	✗
Non-Stationary Signal Applicability	✓	✓	✗	✗	✓
Long Duration Signal Applicability	✓	✗	✓	✓	✗
Suitability to Ambient Induced Excitation	✓	✗	✓	✓	✗
Suitability to Vehicle Induced Excitation	✓	✓	✗	✗	✓

3. Damage identification method

The damage identification methodology employed is dependent on the quantity of extracted vibration parameters and their origin. For instance, in an ambient condition test data, vibration parameters are continuously extracted every minute over the duration of the progressive damage test, while for a vehicle induced excitation test, vibration parameters are extracted for each vehicle crossing only. This provides two very differently sized datasets. In the vehicle induced excitation case, the method of damage detection is simple like-for-like comparison, while ambient excitation case requires the application of an outlier detection algorithm suited to the probability distribution of each vibration parameter. For Gaussian distributed vibration parameters, such as DVI and MCVI, the MSD multivariate outlier detection algorithm is employed. It uses mean and covariance data to train and assess dataset continuity. MSD is calculated as follows:

$$D_{\varsigma} = \left(\left\{\bar{X}\right\}_{\varsigma} - \left\{X\right\}\right)^{T} \left[\Sigma\right]^{-1} \left(\left\{X\right\}_{\varsigma} - \left\{\bar{X}\right\}\right) \tag{11}$$

Where $\{X\}_\varsigma$ is the potential outlier, $\{\bar{X}\}$ is the mean of the training data and $[\Sigma]$ is the covariance matrix of the training data. In addition to the MSD, the Minimum Covariance Determinate (MCD) estimator is also employed to enhance robustness and reduce uncertainty regarding sources of ambient excitation by identifying and removing outliers from the training data prior to MSD. The FAST MCD algorithm by (Rousseeuw & Van Driessen, 1999) is employed in this study.

For non-Gaussian distributed vibration parameters such as the energy-based parameter CAV, its value can never be less than zero and has no theoretical maximum. As such, it distribution fit can be taken as Log-Normal, which is unsuitable for use with MSD. Instead, symbolic data objects are obtained from the Log-Normal distributions of overlapping windowed CAV datasets of 30min duration with 6 min overlap. Symbolic data objects are representative values of a larger data set that can be used in an SHM context, as demonstrated by Santos et al. (2013). In the present study, the overlapping Log-Normal distributions of CAV are reduced to their symbolic data objects of; Median and Interquartile Range. Using these two symbolic objects as a two-dimensional damage feature vector, changes to the CAV distribution can be calculated using pairwise Euclidean distance as follows:

$$E.dist = \sqrt{\left(X_{UD} - X_{Dam}\right)^2 + \left(Y_{UD} - Y_{Dam}\right)^2} \tag{12}$$

Where X_{UD} and X_{Dam} represent the first symbolic data object for the undamaged and damaged cases, respectively, and Y_{UD} and Y_{Dam} represent the second symbolic data object for the undamaged and damaged cases, respectively. The damage identification method used in the case of the forced vibration is based on the Improved Complete Ensemble Empirical Mode Decomposition with Adaptive Noise (ICEEMDAN) as presented in Moughty and Casas 2018a.

4. Case studies

4.1. Ambient Excitation - S101 Bridge

The S101 was a post-tensioned concrete bridge located near Vienna in Austria that had a main span of 32m and two 12m side spans. The deck cross-section was 7.2m wide double-webbed t-beam, whose webs had a width of 0.6 m. The height of the beam varied from 0.9 m in the mid-span to 1.7 m over the piers, as can be seen in Figure 2. The columns, beams and the deck slab were built with concrete material of 2400 kg/m^3 density and the Young's modulus of 24.8 GPa. In 2008, it was decided to replace the S101 Bridge due to insufficient carrying capacity and deteriorating structural condition being identified from visual inspection data. Before demolition, a progressive damage test

was conducted on the S101 Bridge across 3 days in 2008 though the completion of a number of sequential actions, which are presented in Table 3.

Overall, the damage applied can be divided into two main stages; (1) simulated pier foundation settlement, (2) bridge deck stiffness loss through the severing of four pre-stressed tendons. During the test the bridge was closed to traffic, meaning that excitation was mainly ambient, although one traffic lane beneath the bridge was kept in use. As for environment sources of excitation, very little temperature variation was observed throughout the test duration as sub-zero temperatures were kept within a 3 to 4 degree range due to persistent heavy cloud cover (VCE, 2009). Vibration data was recorded by 13 accelerometers located on one side of the bridge deck, with a sample rate of 500 Hz. Vibration recordings from the sensors did not cease throughout the progressive damage test. For the present study, the measured data was discretized into 66 sec long segments of 33,000 samples.

Figure 2. View of the S101 Bridge and bridge dimension (dimensions in centimeters)

Table 3. Damage actions applied to the S101 Bridge

Damage State	Damage Actions
1	Undamaged
2	North-Western (NW) pier cut through
3	NW pier lowered by 1cm
4	NW pier lowered by 2cm
5	NW pier lowered by 3cm
6	Support plates inserted & pier returned to origin
7	First pre-stressed tendon cut over NW pier
8	Second pre-stressed tendon cut over NW pier
9	Third pre-stressed tendon cut over NW pier
10	Forth pre-stressed tendon cut over NW pier

4.2. Vehicle-Induced Excitation - Steel Truss Bridge

The data have been obtained from a progressive damage test conducted on a Japanese bridge that was subjected to a moving vehicle excitation (Kim et al., 2013). The bridge in question was a simply-supported steel truss bridge that spanned 59.2m with a width of 3.6m and a max height of 8m. In the bridge, the truss members were built by beam elements and were assigned with steel material properties (density 7900 kg/m^3 and Young's modulus 200 GPa). Likewise, the deck was built of concrete material with the density 2400 kg/m^3 and elasticity modulus of 21 GPa. It was scheduled to be replaced in 2012, before which a progressive damage test was carried out while the bridge was closed to the public. Dynamic response was recorded from 8 uniaxial accelerometers, positioned as per Figure 3(b) and measuring the vertical acceleration, with sample rates of 200Hz.

The induced damage scenarios consist of severing vertical members of the truss structure in the locations presented in Figure 3(b). The progression of the damage states is described in Table 4 and presented in Figure 4. The damage actions began with the partial intersection of the mid-span vertical member (DMG1), before its full intersection was completed (DMG2). After which, the damaged member was reconnected (RCV) with a welded flange. Finally, the vertical member at 5/8th span was completed severed (DMG3).

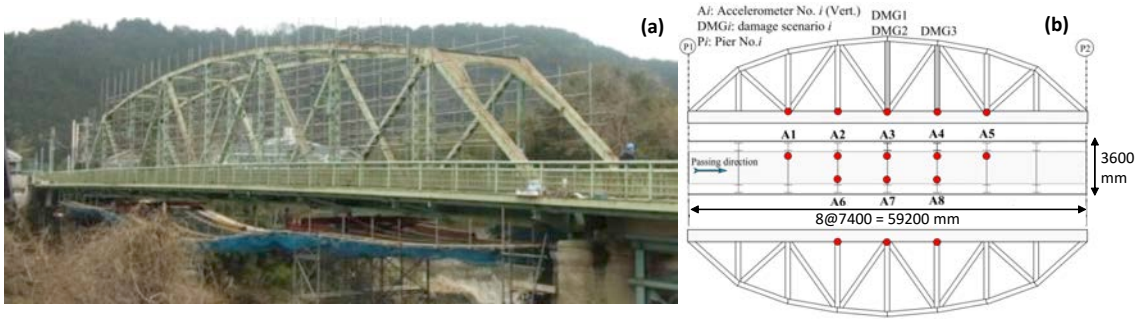

Figure 3. Steel truss bridge (a); sensor & damage locations (b)

Table 4. Damage actions conducted on the Steel Truss Bridge

Damage State	Description of Damage Actions
1	Undamaged
2	Half cut in vertical member at mid-span
3	Full cut in vertical member at mid-span
4	Mid-span member reconnected
5	Full cut in vertical member at 5/8th span

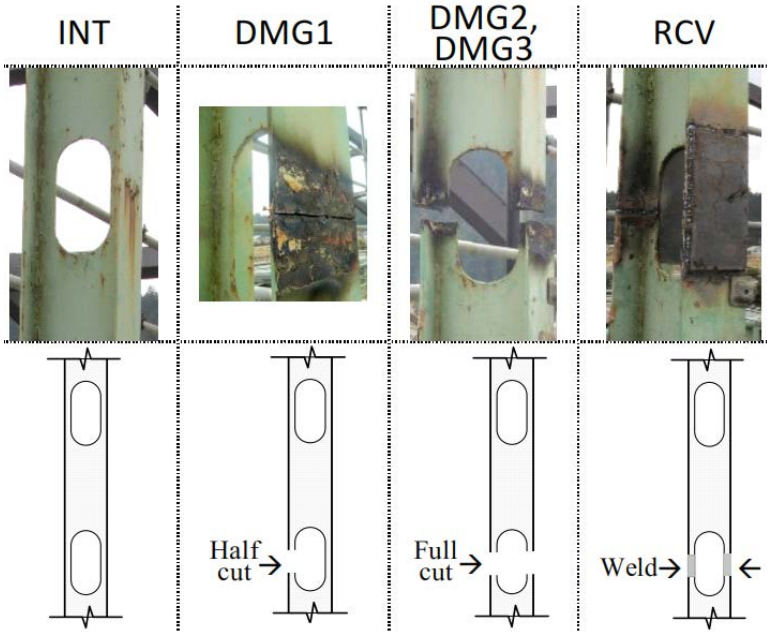

Figure 4. Steel truss bridge damage scenarios

For each damage scenario, a 21kN double-axle truck crossed the bridge 3 times at approximately 40km/h. The weight of the vehicle was enough to excite the bridge and to obtain the vibration parameters. In addition, each damage scenario could be carried out normally considering that the 21kN was not excessive. A sample time-history of acceleration response is presented in Figure 5 with the section of forced vibration shaded in grey. The forced vibration response is quite short in duration and highly non-stationary, as such it is unsuitable for Fourier-based transformation, therefore, this section of the signal is taken as the input for the parameter IVI.

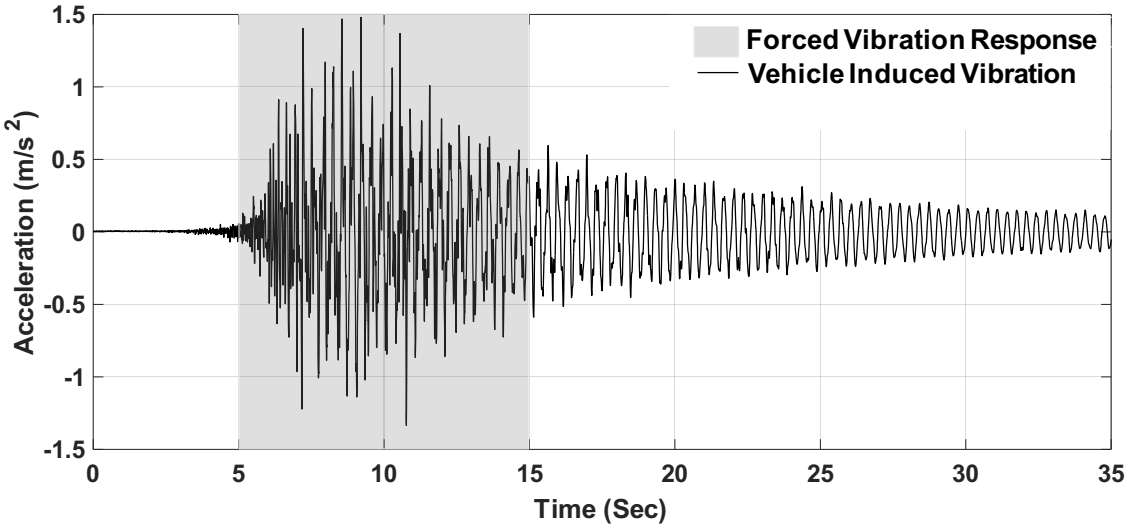

Figure 5. Example of vehicle induced vibration response

5. Results

5.1. Ambient Excitation - S101 Bridge

The damage identification assessment results for the S101 Bridge under ambient excitation are presented herein for the three vibration parameters that were deemed suitably applicable to such conditions as per the criteria set out in Table 2.

(1) CAV

The Euclidean Distance evolution of the CAV-based symbolic data objects (Median & Interquartile Range) throughout the duration of the progressive damage test is presented in Figure 6. For this purpose, all the damage scenarios presented in Table 3 were evaluated considering the Y-axis as a linear representation of time. It can be observed that an enhanced divergence from the undamaged state occurs at the sensors located at the damaged North Pier during the pier settlement test. After the pier is returned to its original positions, the Euclidean distance returns close to normal. This is to be expected, as the pre-stressed tendons should supply enough compression to close the majority of cracks caused by the pier settlement, effectively reversing the simulated damage. The succeeding damage events that entail the severing of 4 pre-stressed tendons generate little change in CAV distribution through time. Although this may seem like a missed damage event, it may also indicate that a sufficient level of compression is still present in the remaining pre-stressed tendons to maintain normal structural behaviour without severely cracked sections.

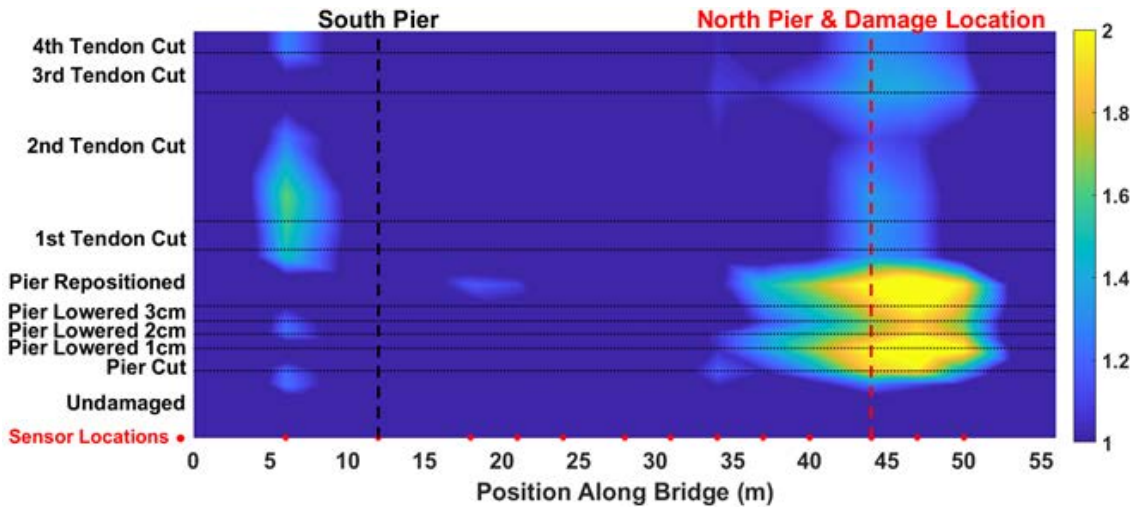

Figure 6. Evolution of CAV through time at each sensor using the Euclidian Distance of the chosen symbolic data objects of median and interquartile range of overlapping windowed CAV Lognormal distributions.

(2) DVI

The MSD evolution of the vibration parameter DVI throughout the duration of the progressive damage test is presented in Figure 7. It can be observed that an enhanced divergence from the

undamaged state occurs across the bridge during the pier settlement test, but particularly so at the sensors located at the damaged North Pier. Similarly to CAV, the divergence of CAD reduces upon pier repositioning, however, as the pre-stressed tendons are severed, damage is once again highlighted at the North Pier.

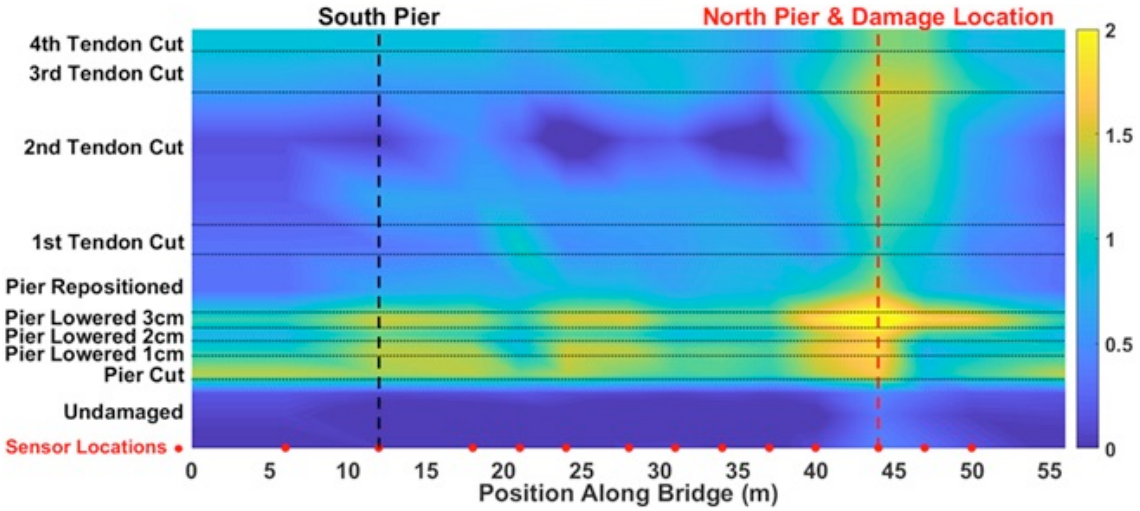

Figure 7. Evolution of DVI through time at each sensor using Mahalanobis Squared Distance.

(3) MCVI

The MSD evolution of the vibration parameter MCVI throughout the duration of the progressive damage test is presented in Figure 8. It can be observed that an enhanced divergence from the undamaged state occurs on the North side of the bridge during the pier settlement test, with no exact location of damage identified. For the severed pre-stressed tendons, MCVI provides a strong indication of damage for the 3rd tendon cut, but no others.

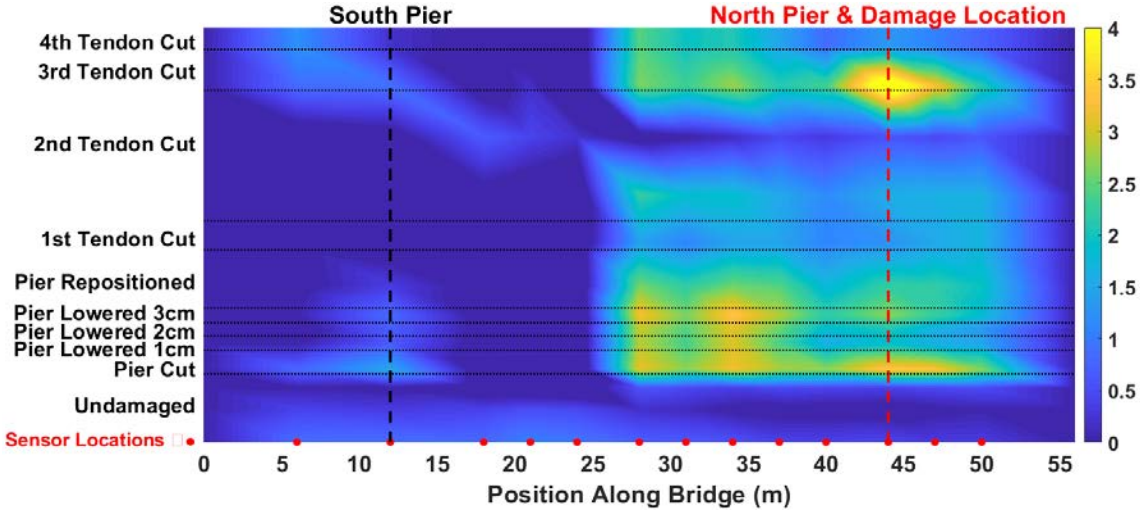

Figure 8. Evolution of MCVI through time at each sensor using Mahalanobis Squared Distance.

5.2. Vehicle-Induced Excitation – Steel Truss Bridge

In this section, an exhaustive analysis of Instantaneous Vibration Intensity parameter (IVI) is developed. IVI utilizes the time-frequency-energy representation of the well-known Hilbert Spectrum in a novel manner that provides more quantifiable measure of signal variations. In this study, the IVI's obtained for each vehicle crossing are analysed across a 10s duration that captures the forced vibration response of the bridge under the vehicle load (see case study number 2). For the undamaged condition, Figure 9 shows an example of Hilbert-Huang Spectrum that is obtained for the first 3 IMFs of Sensor 1 in the steel truss bridge described in the case of study. The time–frequency variation shows energy concentration around 3Hz, 6.8Hz and 13.3Hz, which represent the first, second and fifth vibrational mode as per Kim, et al. (2014). However, considering only this information is difficult to ascertain changes in structural behaviour. For this reason, a more quantitative representation known as IVI is presented in Figure 10. This relation obtained from Equation (10) considers both instantaneous frequencies and amplitudes.

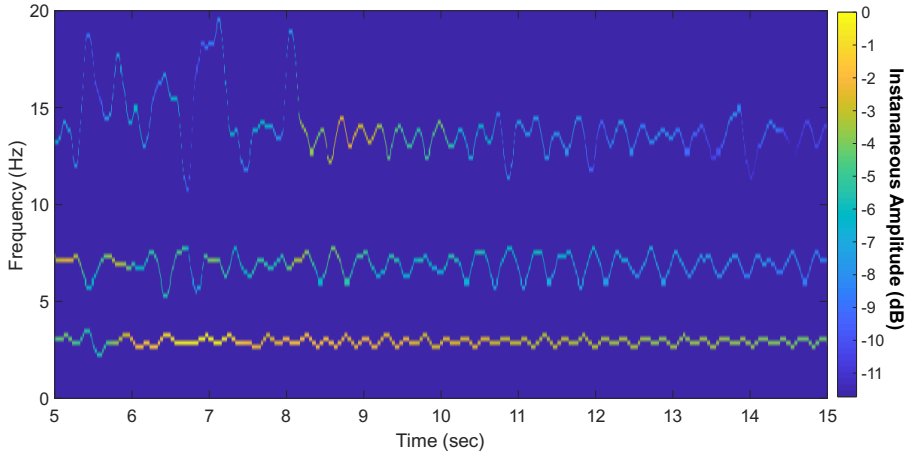

Figure 9. Hilbert-Huang Spectrum for first 3 IMFs

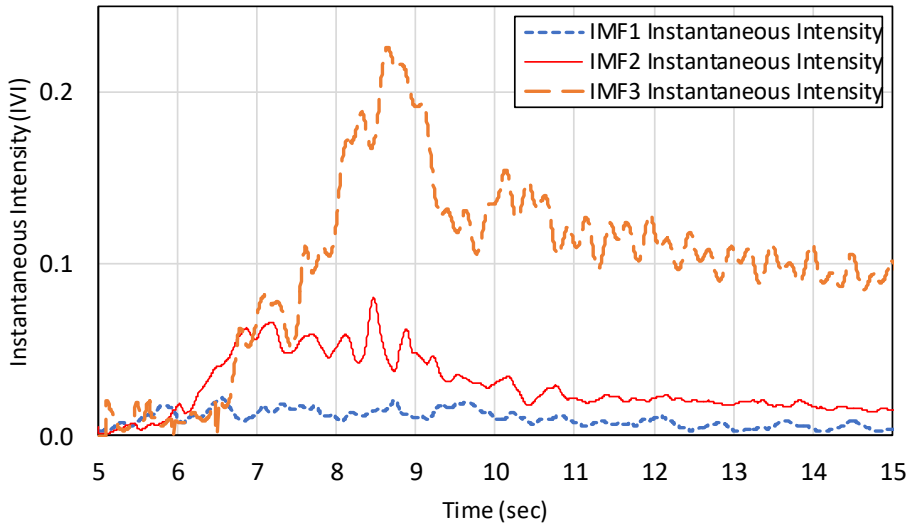

Figure 10. Instantaneous Vibration Intensity from first 3 IMFs

Previous studies presented by (Moughty & Casas, 2017) and (Moughty & Casas, 2018a) show that some IMFs extracted from the acceleration data are physically meaningful. For this purpose, it must be taken into account that three of the IMFs extracted from the tests that will be used here, correspond to the three natural vibration frequencies of the bridge and, therefore they are related to the IVI parameter.

5.2.1 Analysis based on individual IMF´s

As in this case each analyzed IMF corresponds to a natural frequency of the bridge, the analysis starts with the results obtained for each IMF separately. In this sense, Figure 11 shows the changes of IVI at each sensor along the bridge for frequency 1 (IMF 3) and bearing in mind that the intensity increases as greater damage occurs since the IVI parameter is closely related to the amplitude and frequency. Figures 11 (a) to Figure 11 (e) display an interesting behavior for the first five sensors along the bridge, and it is clearly shown that the closer the sensor to the location where damage occurs, the better the sensor manages to capture the behavior of the bridge structure from an undamaged state, moderate damage (DMG 2), recovery (RCV) and severe damage (DMG 3). Furthermore, in location of critical sensors as 3 and 4, the Figure 11 (c) and Figure 11 (d) plot a greater increase of IVI and a shift to the left due damage 2 and damage 3 respectively. Additionally, the analysis of the maximum peaks shows a considerable increase of $\Delta 1=0.08$ and $\Delta 2=0.13$ between the un-damaged and damaged scenarios, which demonstrate the presence of damage close to them. On the other hand, sensors 7 and 8 located on the other side of the cross section of the bridge show slight variation between un-damaged and damaged cases ($\Delta 3=0.03$ and $\Delta 4=0.03$), which means that they can not detect damage because the damage is not close to them, as can be shown in Figure 11 (g) and Figure 11 (h) respectively. In addition, the sensor 6 do not show different behavior between un-damaged and damaged cases (Figure 11f).

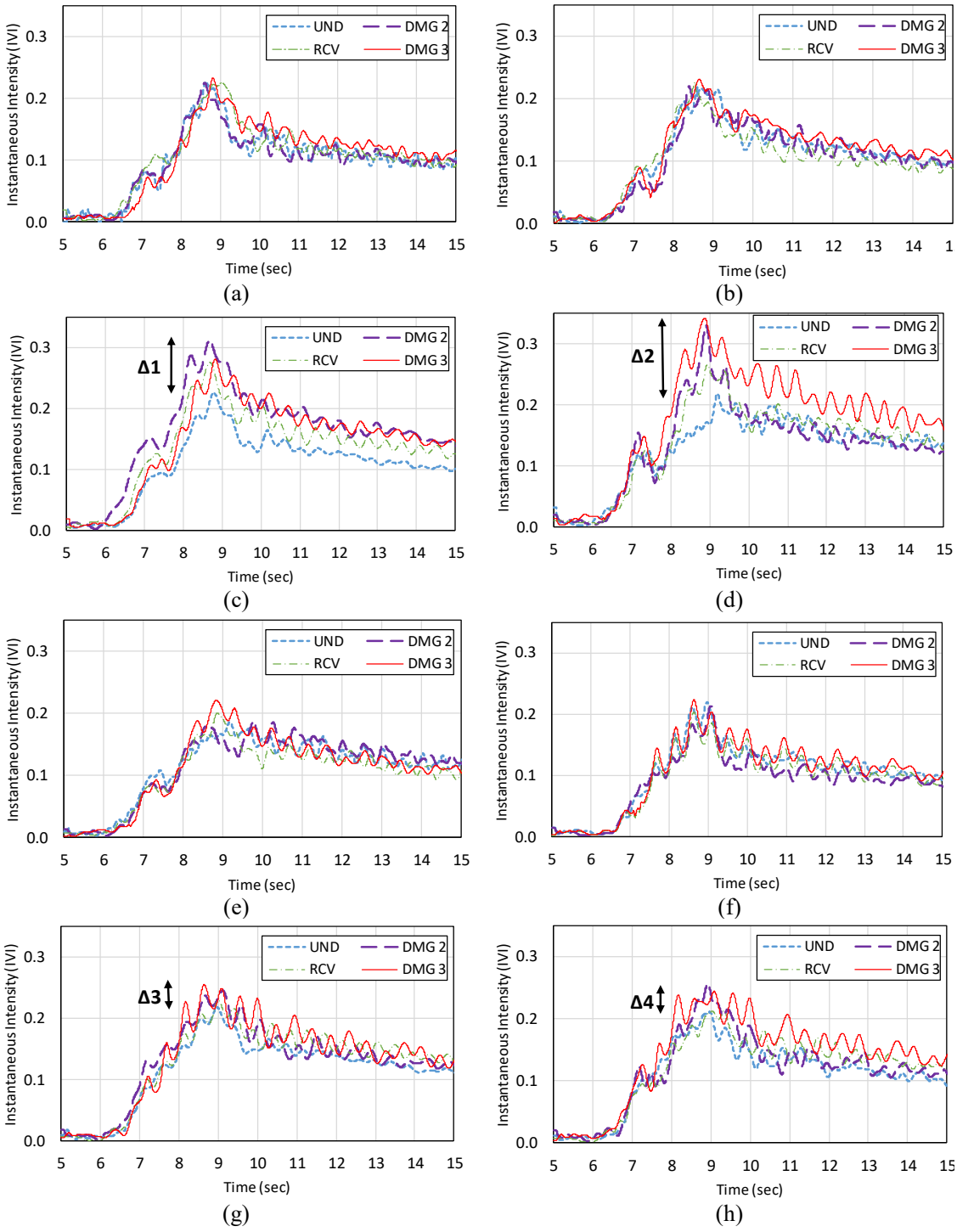

Figure 11. Variation of Instantaneous Vibration Intensity parameter (IVI) for frequency 1 (IMF 3) at each sensor location along the bridge during all damage states: (a) sensor 1 (b) sensor 2 (c) sensor 3 (d) sensor 4 (e) sensor 5 (f) sensor 6 (g) sensor 7 (h) sensor 8.

Further on, Figure 12 (a) and Figure 12 (b) plot the changes of IVI at each sensor considering two damage states (DMG 2 and DMG 3) for the fundamental frequency (IMF 3). In the first case, the sensor 4 obtains a maximum peak of 0.33 and all instantaneous intensities registered by sensor 3 are

amplified, which indicates that the damage 2 (DMG 2) occurs in this location as shown in Figure 3. In the second case, it is clearly evident how the intensities in sensor 4 are amplified exactly in the position where the damage 3 occurred (DMG 3). In conclusion, the instantaneous vibration intensity referred to the first vibration frequency is able to identify and locate the damage in the exact position where the sensor is located.

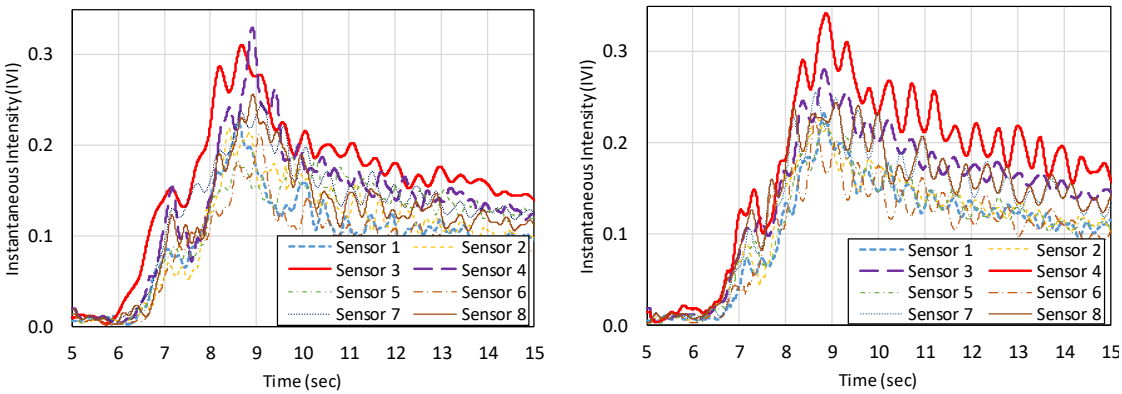

Figure 12. Variation of Instantaneous Vibration Intensity (IVI) parameter for frequency 1 in two damage scenarios: (a) damage 2 (DMG 2) (b) damage 3 (DMG 3).

In this part, the results obtained from the analysis carried out previously are verified, in which IVI parameter obtained good performance to detect and locate the damage in the bridge. Figure 13 shows the analysis of instantaneous frequencies for the most critical sensors 3 and 4 where damage 2 and 3 occurred respectively. Figure 13 (a) shows that the frequency 1 (IMF 3) captured by the sensor 3 has a very clear behavior and the signal does not present noise, whereby this frequency can be correctly identified. In the first case, when the condition of bridge goes from the undamaged state to damage 2 (DMG 2) the average frequency 1 decreases from 3.0 Hz to 2.85 Hz. In the recovered damage scenario, the bridge shows a slight increase in average frequency from 2.85 Hz to 2.95 Hz. Finally, for the most critical damage 3 (DMG 3), the average frequency decreases from 2.95 Hz to 2.90 Hz. In the present study, good instantaneous frequencies results were obtained in contrast with reference analysis developed by Kim et al. (2014). In the same way, Figure 13 (b) depicts the frequencies obtained in each damage scenario for sensor 4, and it presents the same behavior between undamaged, damaged and recovered bridge condition (e.g. increase and decrease of frequency).

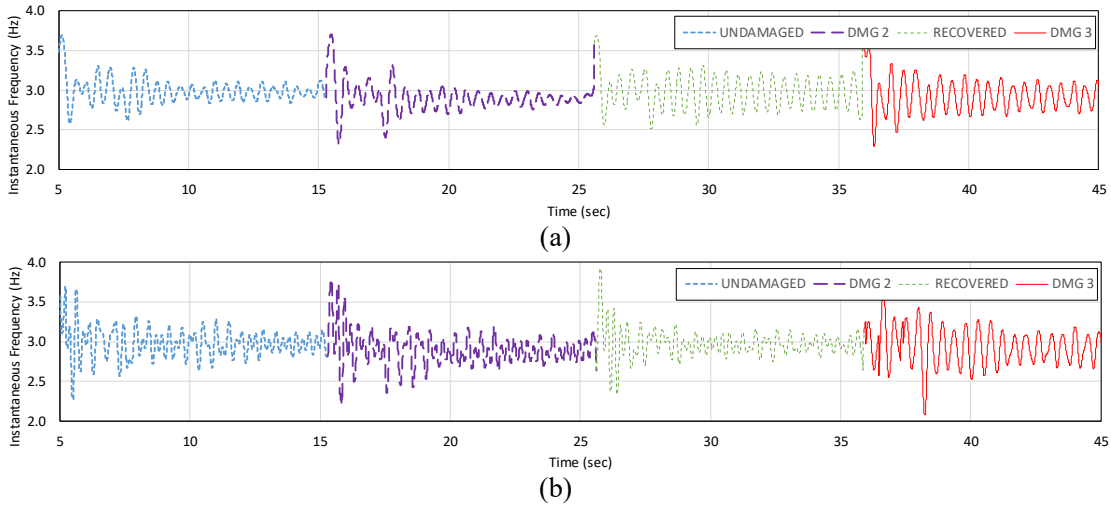

Figure 13. Variation of Instantaneous frequencies 1 (IMF 3) at each damage stages (a) sensor 3 (b) sensor 4.

Additionally, instantaneous amplitude analysis is performed for the most critical sensors 3 and 4 where damage 2 and 3 occurred respectively, this can be shown in Figure 14. For sensor 3, Figure 14 (a) shows that the instantaneous amplitude in the undamaged state (UND) has a maximum peak of 0.62. However, when damage 2 occurs (DMG 2) the maximum peak increases to 0.83 getting a maximum variation of $\Delta 1 = 0.21$. Then, the recovered state of the structure (RCV) occurs when the bridge has a behaviour of returning to its initial state (undamaged). Finally, in the third damage (DMG 3) the maximum amplitude peak increases in value. In the same way, the analysis of the sensor 4 (Figure 14b) shows a similar behaviour like presented in sensor 3, since the damage 3 occurs in location of sensor 4. In addition, in this state, the maximum peak reaches a value of 0.96, which produces a maximum variation of $\Delta 2 = 0.32$.

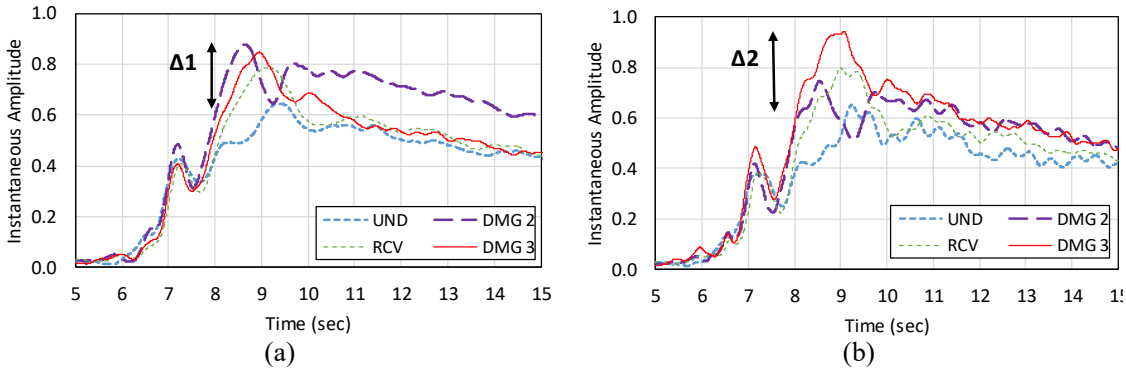

Figure 14. Variation of Instantaneous amplitudes for IMF 3 at each damage stages (a) sensor 3 (b) sensor 4.

On the other hand, Figure 15 (a) to Figure 15 (h) shows the behaviour of IVI in each sensor for the second vibration frequency (IMF 2). In this case, the maximum peaks do not help to identify the damage, nonetheless, when damage occurs the tendency to increase of IVI is maintained.

Furthermore, a clear signature of damage is not identified and this could be due to noise presented in frequencies and amplitudes. This is clearly understood since the IVI has a direct relationship with the instantaneous vibration frequencies and amplitudes (as shown in equation 10).

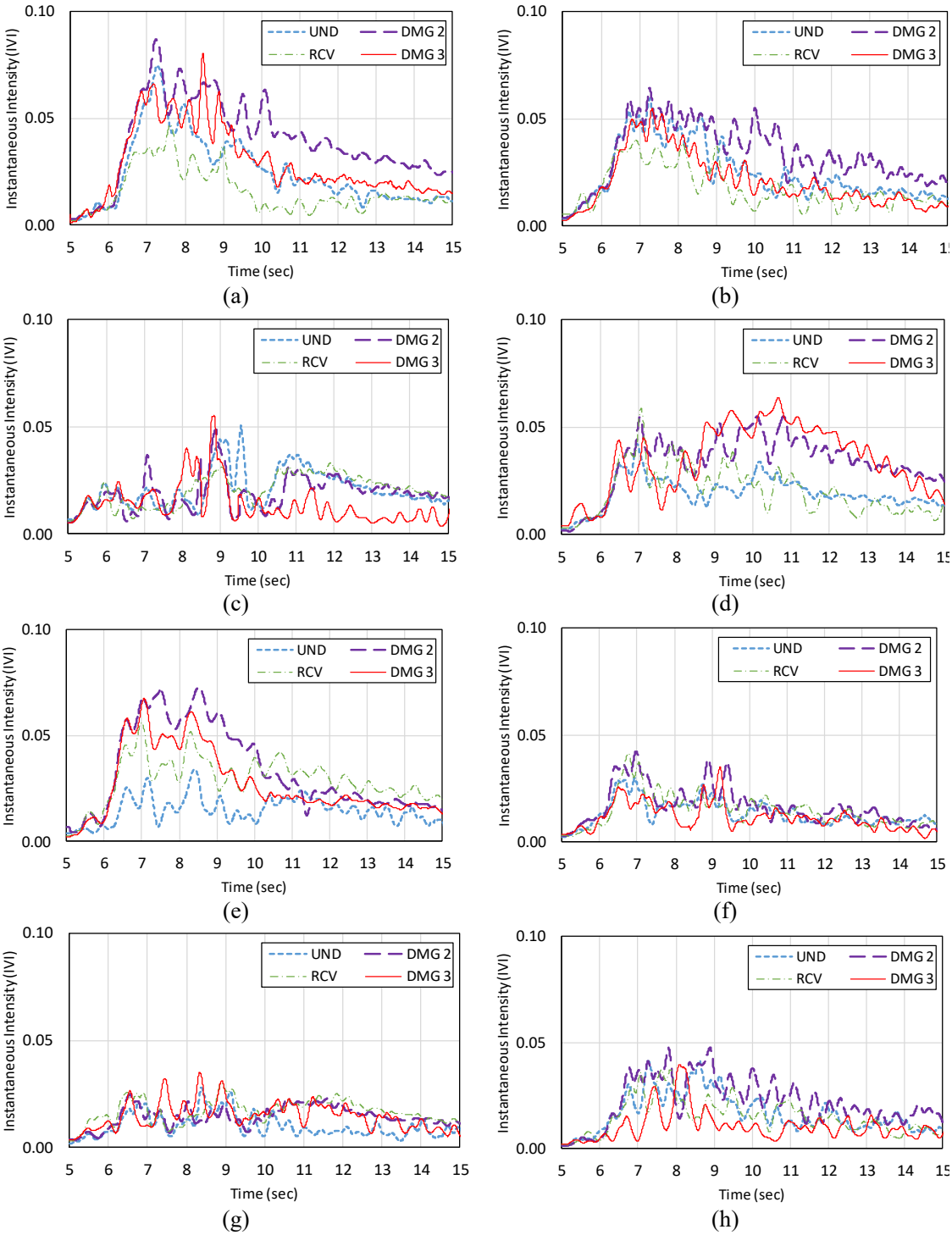

Figure 15. Variation of Instantaneous Intensity parameter (IVI) for frequency 2 (IMF 2) at each sensor locations along the bridge during all damage states: (a) sensor 1 (b) sensor 2 (c) sensor 3 (d) sensor 4 (e) sensor 5 (f) sensor 6 (g) sensor 7 (h) sensor 8.

Figure 16 (a) and (b) provide the variation of the instantaneous frequency 2 (IMF 2) for the most critical sensors 3 and 4 respectively. In this regard, both sensors can not be used to identify the presence of structural damage over time. In the same way, this behaviour does not represent the physical condition of the four damage scenarios already studied. In conclusion, the second frequency of vibration (IMF 2) is not able to recognize the structural damage due to the presence of high noise level in the signals.

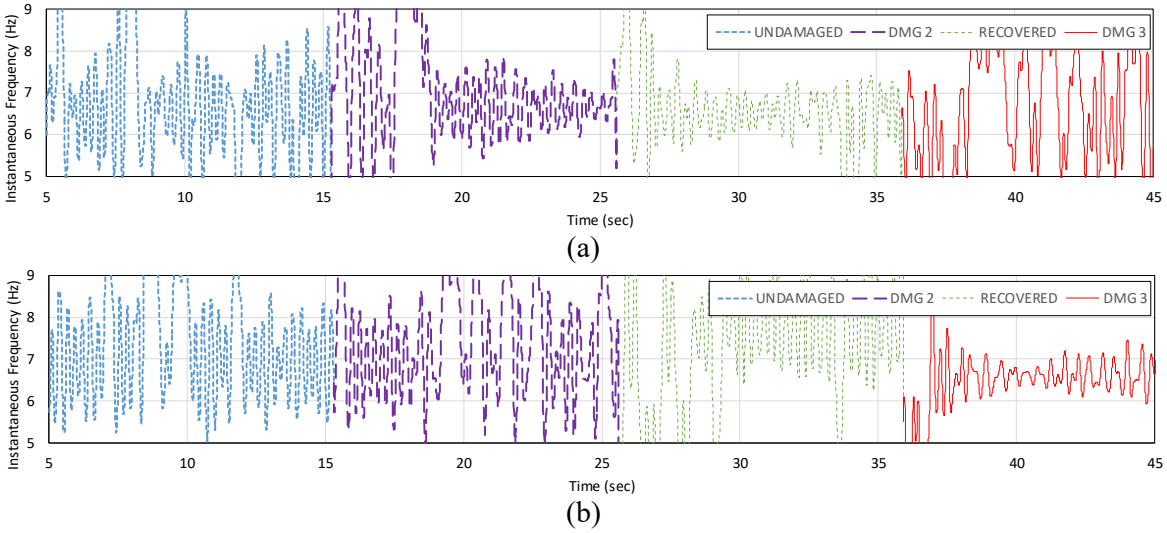

Figure 16. Variation of Instantaneous frequencies 2 (IMF 2) at each damage stages (a) sensor 3 (b) sensor 4.

The study of the instantaneous amplitude for the second vibration frequency is shown in Figures 17 (a) and (b) for sensors 3 and 4 respectively. Taking as reference that the IVI parameter depends on the instantaneous amplitude, it is verified that this is not useful to identify and locate the damage because in both cases there is no maximum reference peak, furthermore, there is no trend that can be useful for evaluate the undamaged and damaged condition of the bridge.

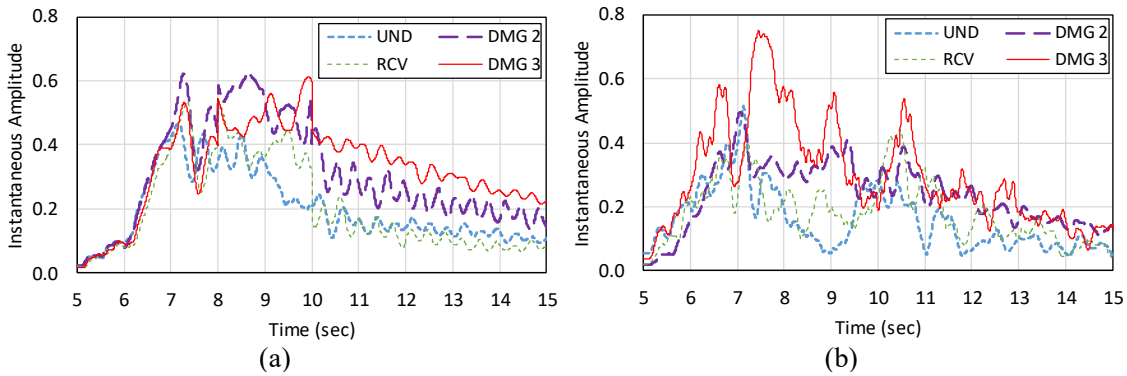

Figure 17. Variation of Instantaneous amplitudes for IMF 2 at each damage stages (a) sensor 3 (b) sensor 4.

In the same way, the instantaneous intensity related to the fifth vibration frequency (IMF 1) is shown from Figure 18 (a) to Figure 18 (h) for all sensors. The results show that the IVI parameter

does not present a well-established damage feature and presents a high variability. For this reason, the exact position of the damage can not be located. Bearing in mind the same analysis for IMF 2, Figure 19 and Figure 20 plot the instantaneous frequency and amplitude respectively. Thereby, the IVI parameter from IMF1 can not be used to identify the damage because the frequencies as well as amplitudes are highly variable.

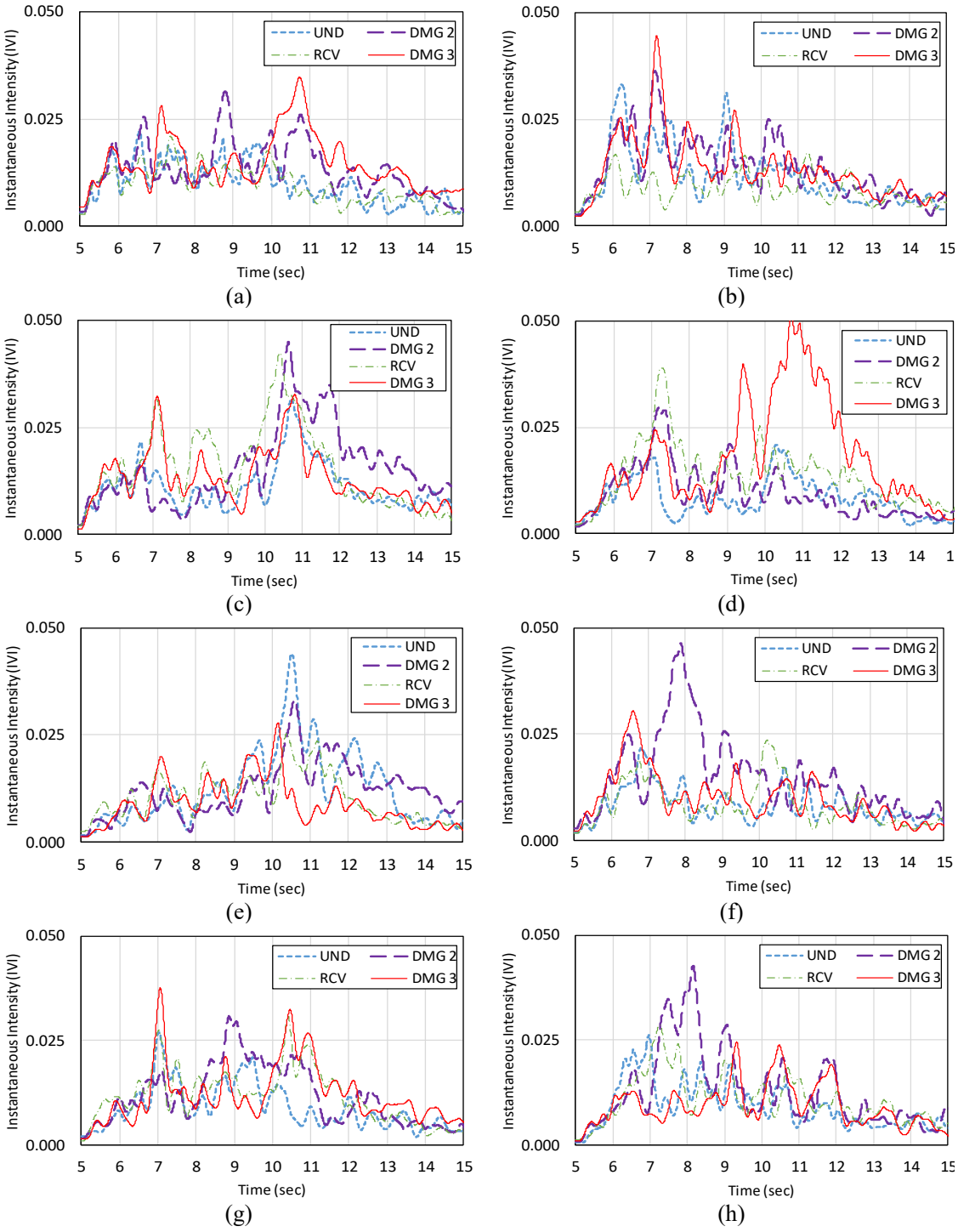

Figure 18. Variation of Instantaneous Intensity parameter (IVI) for frequency 5 (IMF 1) at each sensor locations along the bridge during all damage states: (a) sensor 1 (b) sensor 2 (c) sensor 3 (d) sensor 4 (e) sensor 5 (f) sensor 6 (g) sensor 7 (h) sensor 8.

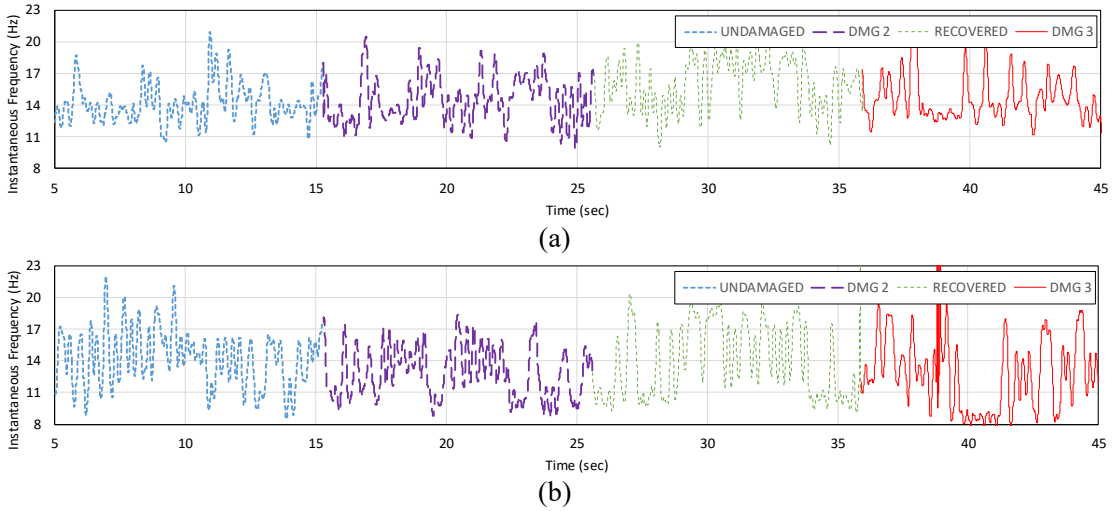

Figure 19. Variation of Instantaneous frequencies 2 (IMF 1) at each damage stages (a) sensor 3 (b) sensor 4.

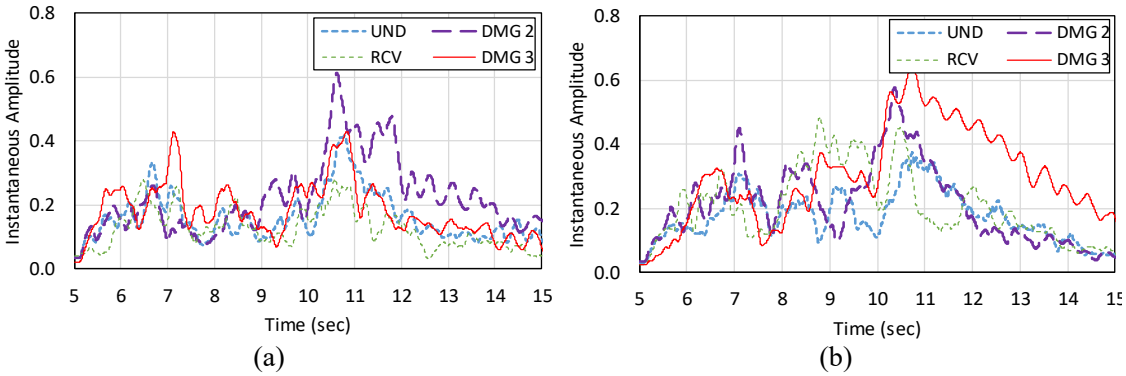

Figure 20. Variation of Instantaneous amplitudes for IMF 1 at each damage stages (a) sensor 3 (b) sensor 4.

As a conclusion of this analysis, only the case of IMF 3, corresponding to the first vibration mode, reported accurate results regarding detection and location of damage.

5.2.2 Analysis based on total IMF (AIVI)

The approach of this study also includes a more complete and deep analysis to the one presented by (Moughty & Casas, 2018a). For this purpose, a further analysis of instantaneous vibration intensity is performed in order to detect and locate the damage on the bridge. Thus, the IVI parameter is modified in the Amalgamated Instantaneous Vibration Intensity (AIVI) which uses the combination of the detected IMFs of the first, third and fifth natural frequencies. In addition, the influence of different damages on all sensors are considered and studied.

Figure 21 shows the variation of AIVI parameter over time. For instance, sensor 1 (Figure 21a) shows normal behavior in all four damage scenarios and this can be verified because imposed damage was far away. A similar behavior was found in sensors 2, 5 and 6 as shown in Figure 21 (b), Figure

21 (e) and Figure 21 (f) respectively. However, taking into account the undamaged state of the bridge as reference, in Figure 20(c) the sensor 3 presents a slight variation ($\Delta 1=0.03$) caused by the total cut in a vertical member at 5/8th-span (DMG 2). Furthermore, the maximum damage was identified (DMG 3) for sensor 4 as shown Figure 21 (d) and this is presented in the large increase of AIVI parameter ($\Delta 2=0.12$) that clearly reflects the severity and intensity of the damage, and in this way, it can be measured and compared with the rest of the sensors. Moreover, Figure 20(g) and Figure 21 (h) display a slight increase of AIVI parameter in the location of the sensors 7 and 8 due to the damages 2 and 3 respectively. For damage 2, the sensor 7 is able to capture a variation of $\Delta 3=0.02$ and sensor 8 increases in intensity by a value of $\Delta 4=0.04$ because of damage 3. This slight variation can be explained since sensors 7 and 8 are located in front of sensors 3 and 4 taking as reference the cross section of the bridge (as shown in Figure 3). In this way the value of AIVI becomes only slightly modified because the damage is not close to them.

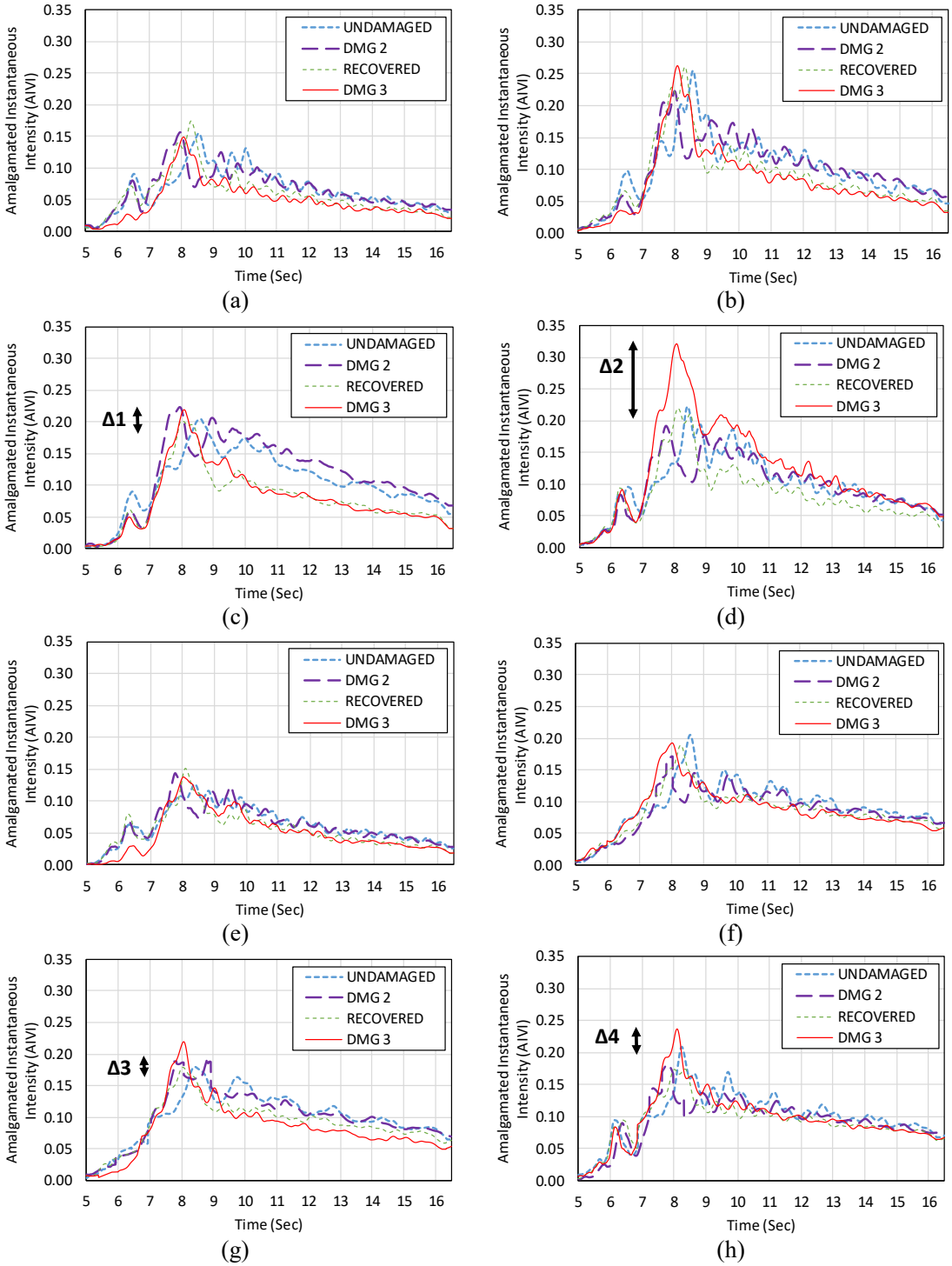

Figure 21. Vertical variation of Amalgamated Instantaneous Vibration Intensity (AIVI): (a) sensor 1 (b) sensor 2 (c) sensor 3 (d) sensor 4 (e) sensor 5 (f) sensor 6 (g) sensor 7 (h) sensor 8.

Figure 22 (a) and Figure 22 (b) show the behavior of the most critical positions: sensor 3 and 4 on one side and sensor 7 and 8 on the other side of the bridge. In this case, the evolution of the intensity over time indicates that the damage and the recovery can be detected automatically and AIVI vibration parameter improves the sensitivity to the detection of damage when compared to the results

obtained with IVI in the previous section. Finally, all the sensors captured the recovery behaviour (RCV scenario) and this is shown when the AIVI values try to return to the undamaged state.

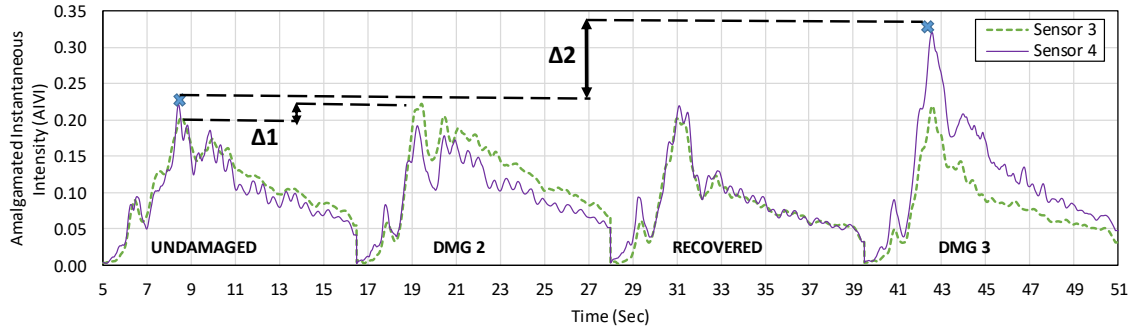

(a)

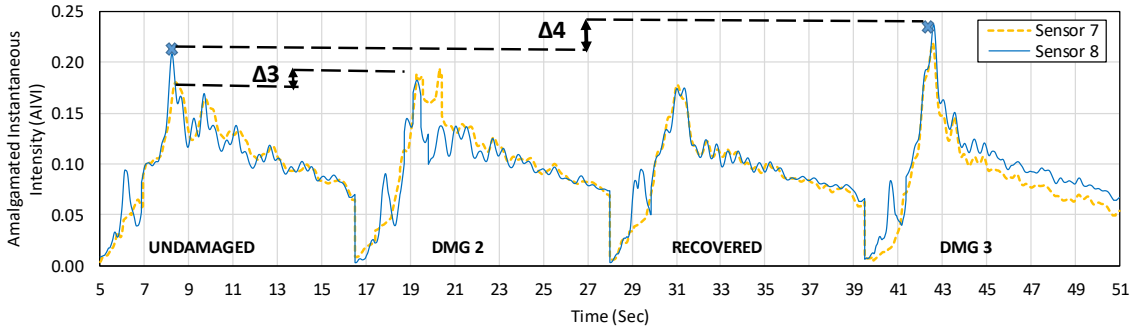

(b)

Figure 22. Comparison of AIVI parameter between critical sensors located in the damages: (a) sensor 3 and sensor 4 (b) sensor 7 and sensor 8.

The present study expands this inquiry to show the different phases of AIVI variation during the excitation time induced by the vehicle. For this purpose, Figure 23 (a) shows stationary values of all sensors for initial undamaged condition (IP1=Initial Position). This state displays a maximum value aligned for all sensors in 8.6 seconds. Besides, in forced vibration time interval, a larger instantaneous intensities induced by the vehicle passage could be observed. The instantaneous values are significantly higher for damaged cases compared with the undamaged state (healthy) bridge structure. In the beginning (5-8.6 s approximately), the Figure 23 (b) plots the AIVI values for damage level 2 which increase relatively (DMG 2) and these were moved to the left compared with undamaged state. All the sensors show that maximum intensity values are shifted to the left 1 second approximately, from the initial position (IP1) to the final position (FP1). This behaviour is observed after the vehicle has passed over the sensor 3 location, where the second damage occurred (DMG 2). Figure 23 (c) provides the recovery state (RCV). The maximum peaks of instantaneous intensity try to move to the right from a final position (FP1) to another final position (FP2). From this behaviour, it can be understood that bridge structure attempts to return to its undamaged initial condition. Afterwards, as shown in Figure 23 (d), the tendency of the peaks is to move to the left. This is reasonable since in this scenario the greatest damage occurred (DMG 3) and the most critical sensor 4, unlike others, suffers significant changes of AIVI due to damage occurring in this position. The maximum peaks

move to the left from a final position (FP2) to another final position (FP3) and the time shift is around 0.5 seconds.

As a final caveat, a maximum increase of 0.2 to 0.32 in AIVI parameter was obtained during 1 second approximately, it could be recognized after all the damage scenarios imposed to bridge structure. All this behaviour of induced excitation in the bridge can be understood because for each damage scenario, the forced vibration data that the vehicle generated were taken as the average between the three passages at 40km/h approximately.

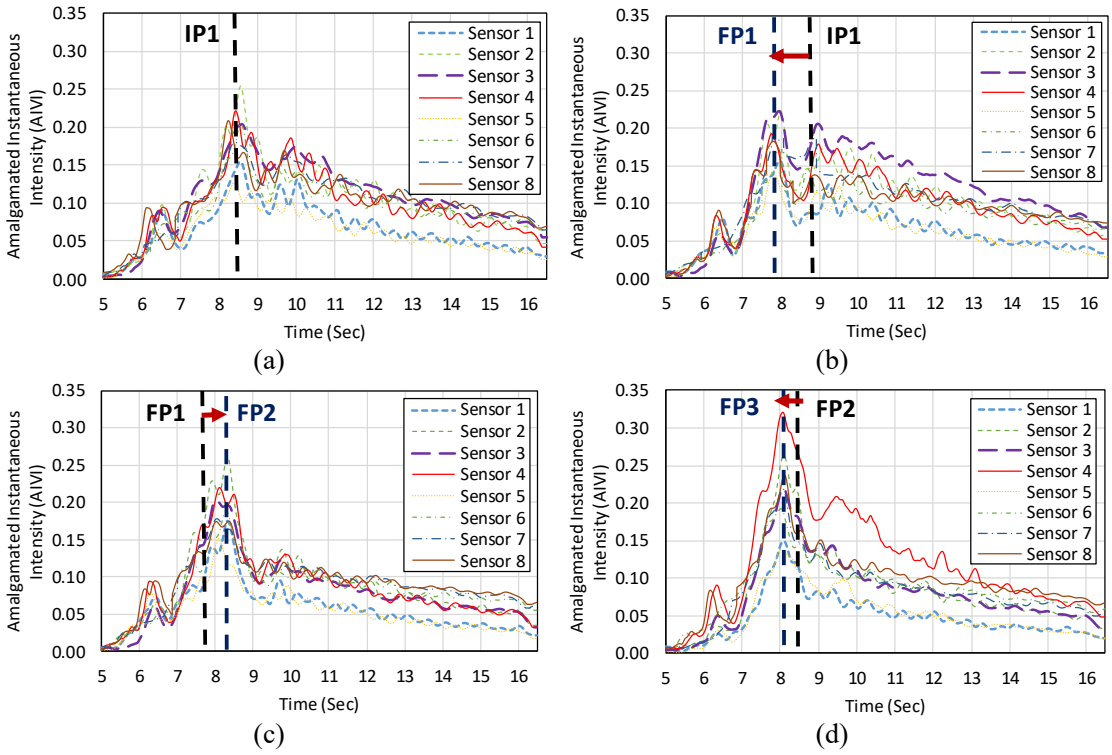

Figure 23. Maximum peak variation in four damage scenarios over time of AIVI parameter (a) undamaged (UND) (b) damage 2 (DMG 2) (c) recovered (RCV) (d) damage 3 (DMG 3).

For more detail, the present study also suggests to consider other damage feature parameters that can be extracted from Amalgamated Instantaneous Vibration Intensity. Figure 24 shows a second maximum point candidate to analyse structural damages. In this case, the pattern of the AIVI parameter is similar to the one presented in Figure 23. According to Figure 24 (a), the second maximum point is located at 9.9 seconds for undamaged condition. Then, second peaks follow a well-known trend, these move from right to left (IP1 to FP1) due to first damage like can be seen in Figure 24 (b). After that, the bridge structure recovers and attempts to return to its initial state of undamaged condition (Figure 24c). Furthermore, the final position (IP1) moves to another final position (FP2). Subsequently, the Figure 24(d) plots the extreme scenario for damage DMG 3 where the amalgamated instantaneous intensity goes to final position (FP3), and this final state shows clearly a higher variation that exists in the AIVI parameter captured by all the sensors.

Therefore, the horizontal and vertical changes experienced by Amalgamated Instantaneous Vibration Intensity parameter (AIVI) serve to identify and locate the damage in the bridge, and this trend improves when the maximum peaks are analysed in detail. It is shown that AIVI (all IMF´s together) is a better suited parameter for damage identification than IVI (IMF´s separately). The results obtained by (Chang & Kim, 2016), when analysing the same test but in the free vibration part of the acceleration signal, are similar to the ones obtained here. In fact, in their study the analysis based on a single frequency was as effective as when using multiple ones, because it was sensitive only to certain specific damage scenarios. Therefore, AIVI will be used in the next section to compare its performance with the other selected parameters in the case of forced vibration.

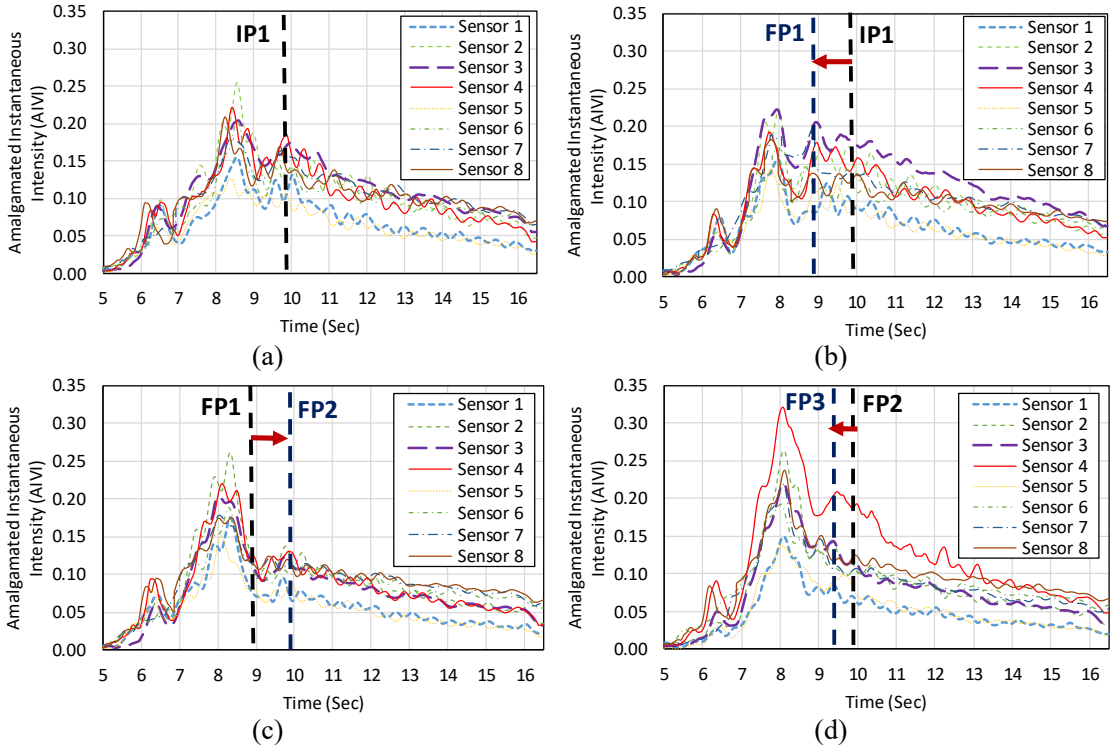

Figure 24. Second peak variation of AIVI parameter in four damage scenarios over time (a) undamaged (UND) (b) damage 2 (DMG 2) (c) Recovery (RCV) (d) damage 3 (DMG 3).

5.2.3 Comparison of vibration parameters from forced vibrations

The damage identification assessment results for the Steel Truss Bridge under vehicle induced excitation are presented herein for the three vibration parameters that were deemed suitably applicable to such conditions as per the criteria set out in Table 2: CAV, CAD and AIVI. In addition, a damage indicator parameter is employed to quantify the changes per sensor per damage scenario. This is called Cumulative Difference Ratio (CDR) as presented in (Moughty & Casas, 2018a). CDR is presented in Equation (13), in the case of parameter AIVI, where $\sum_{i=1}^{n}(AIVI_{Dami})$ and $\sum_{i=1}^{n}(AIVI_{UDi})$ are the

cumulatively summed values of AIVI across time for the damaged state and undamaged state, respectively. A similar equation applies in the case of CAV and CAD.

$$CDR(\%) = \frac{\sum_{i=1}^{n}(AIVI_{Dami}) - \sum_{i=1}^{n}(AIVI_{UDi})}{\sum_{i=1}^{n}(AIVI_{UDi})} x100 \qquad (13)$$

(1) CAV

Figure 25 presents the CAV values obtained at all 8 sensor locations (as per Figure 3) for the condition states of; Undamaged, DMG2, RCV & DMG3. All values are normalized to the largest undamaged value. It is evident from Figure 24(d) that the DMG3 condition yields a significant change in CAV at Sensor 4, which is the damage location. However other condition states are less separable by eye. For this reason, Figure 26 is used to portray the percentage variation from baseline for sensors 1-5 for DMG2, RCV & DMG3. From here it is clearer that the spikes associated with DMG2 & DMG3 are located at the point of damage, while the percentage variation of the RCV state is less pronounced, indicating that the recovery process succeeded in realigning bridge behaviour to near baseline.

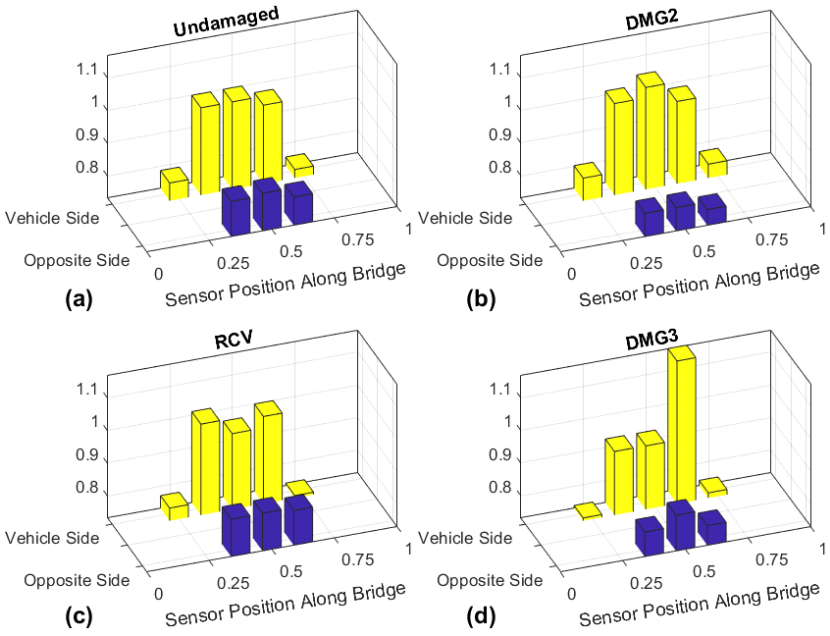

Figure 25. Normalized CAV values per sensor for damage scenarios; (a) Undamaged, (b) DMG2, (c) RCV & (d) DMG3.

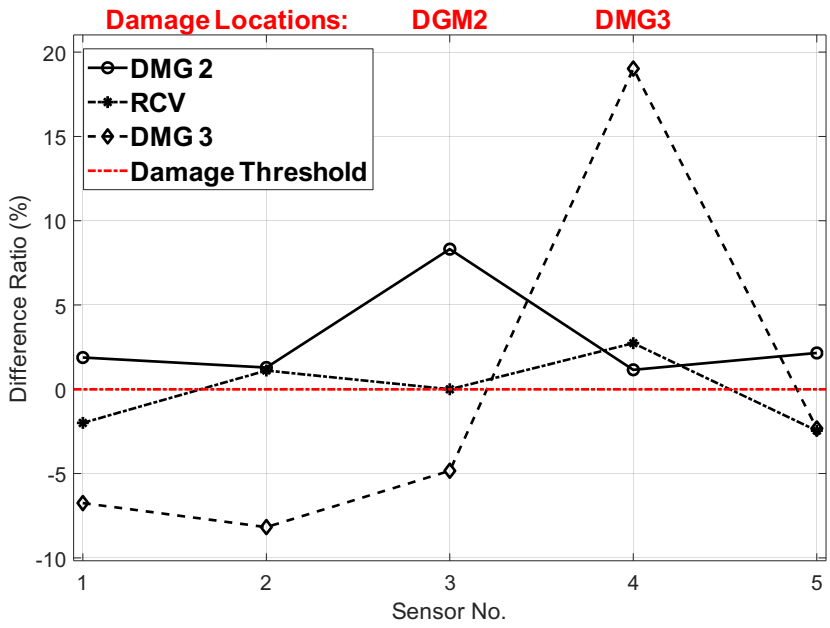

Figure 26. CAV percentage variation from baseline at sensors 1-5 for damage scenarios; DGM2, RCV & DMG3.

(2) CAD

Figure 27 presents the CAD values obtained at all 8 sensor locations (as per Figure 4.) for the condition states of; Undamaged, DMG2, RCV & DMG3. All values are normalized to the largest undamaged value. Again, it is clear that DMG3 yields a significant change in CAD at Sensor 4, which is the location of damage. In Figure 28, the percentage variation from baseline for sensors 1-5 for DMG2, RCV & DMG3 is given, which shows clear damage at sensors 3 & 4 for damage states DMG2 & DMG3, respectively. Both sensors are located at the point of damage, indicating a successful damage location assessment. Furthermore, the RCV state is close to baseline, which correctly indicates no damage present.

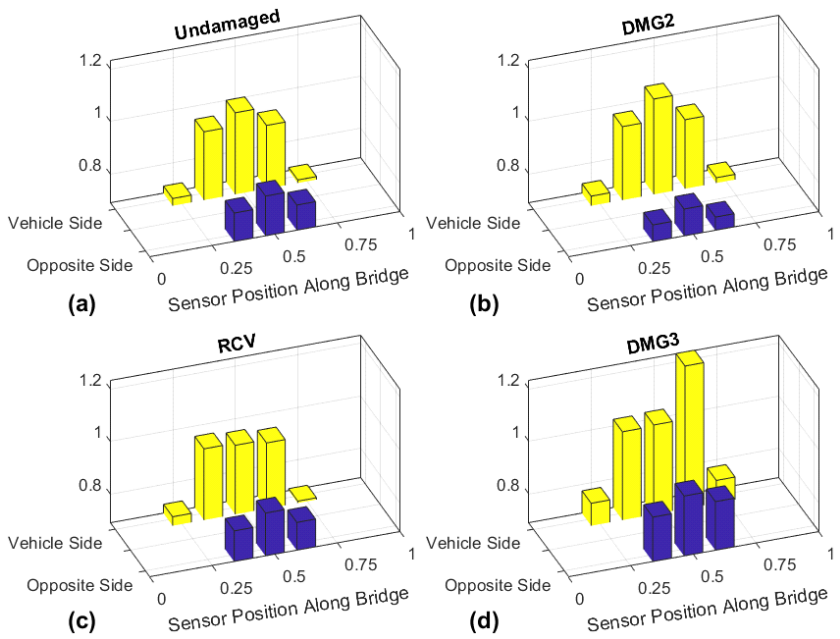

Figure 27. Normalized CAD values per sensor for damage scenarios; (a) Undamaged, (b) DMG2, (c) RCV & (d) DMG3.

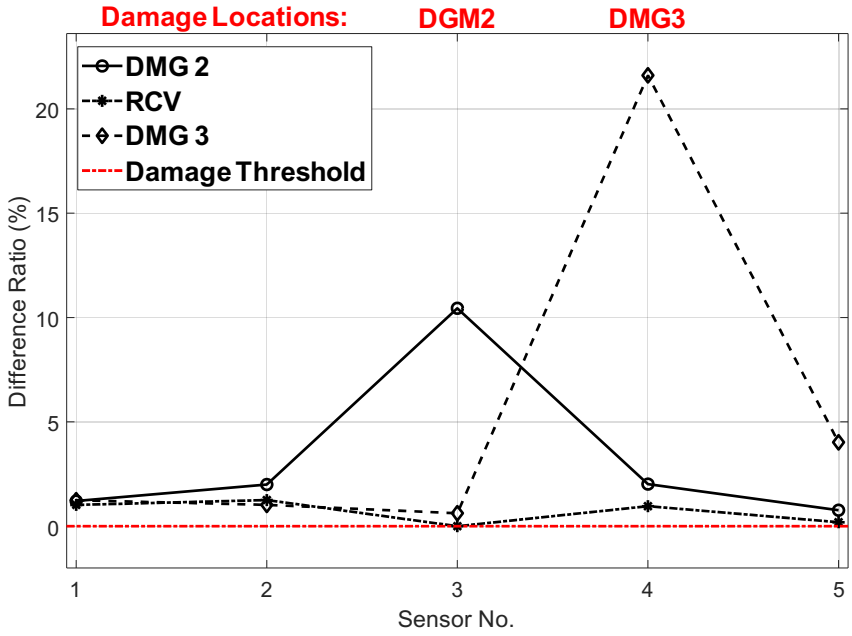

Figure 28. CAD percentage variation from baseline at sensors 1-5 for damage scenarios; DGM2, RCV & DMG3.

(3) AIVI

Figure 29 presents the AIVI values obtained at all 8 sensor locations (as per Figure 4.) for the condition states; Undamaged, DMG2, RCV & DMG3, of which, DMG3 is again the most obvious divergent. The percentage variation of sensors 1-5 is presented in Figure 30 for the condition states of; DMG2, RCV & DMG3. It is evident that the two damage locations are identified by AIVI, those being sensors 3 and 4 for condition states DMG2 & DMG3, respectively.

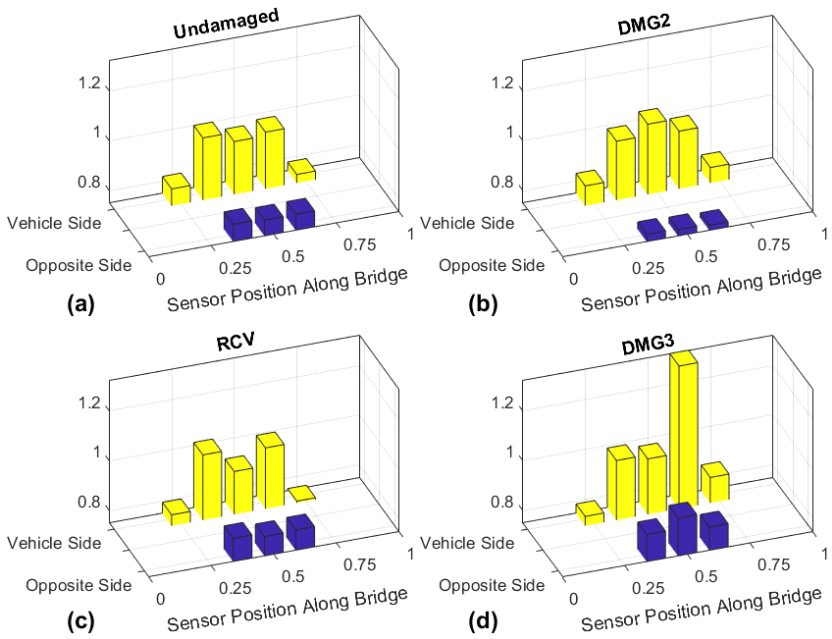

Figure 29. Normalized AIVI values per sensor for damage scenarios; (a) Undamaged, (b) DMG2, (c) RCV & (d) DMG3.

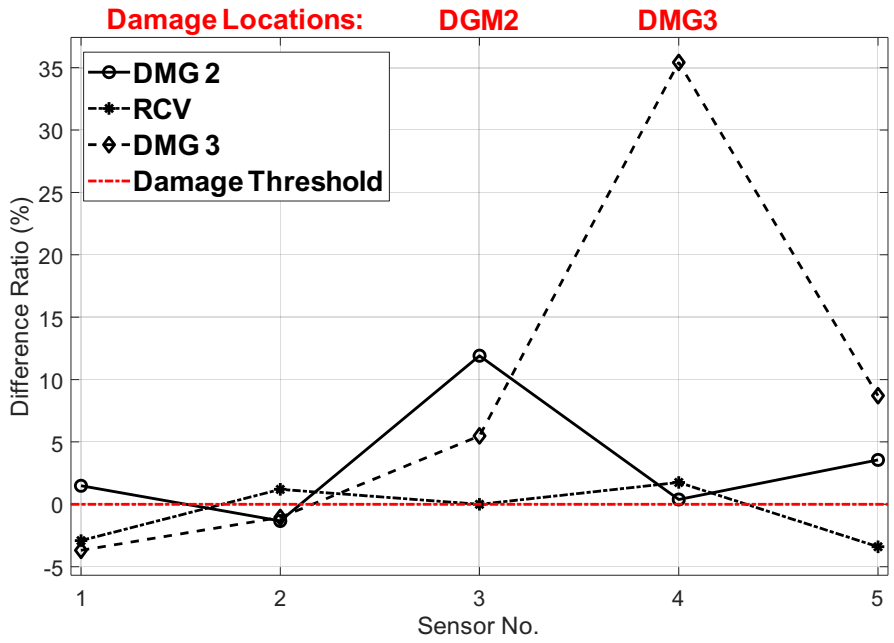

Figure 30. AIVI percentage variation from baseline at sensors 1-5 for damage scenarios; DGM2, RCV & DMG3.

5. Discussion

Based on the results of the present study, some recommendations for practical cases and advice for practitioners on the best method to use depending on the characteristics of the recorded data are presented in Figure 31 and discussed herein.

1. In the ambient induced excitation case study, two methods of outlier detection were employed; MSD for the Gaussian distributed parameters DVI & MCVI, and Euclidian Distance of the symbolic data objects from the LogNormal distribution of the energy based CAV. Of the three parameters assessed, CAV portrayed the strongest indication of damage for the pier settlement test, while DVI was able to identify both types of damage, pier settlement and simulated stiffness loss.
2. In the vehicle induced excitation case study, all empirical vibration parameters assessed (CAV, CAD, IVI & AIVI) identified the required damage events, with CAD providing the greatest resolution regarding the damage location, as displayed by the singular spikes in Figure 27.
3. The parameters based on vibration energy showed significant increase throughout the time range for all sensors close to damage. In contrast with a sensor away from undamaged state, where no appreciable change in vibration magnitudes were observed with increasing levels of damage.
4. To evaluate the damage using the AIVI parameter, it is not only necessary to find the maximum peak points, but it is important to analyse the behaviour of the intensity during the entire time of the forced load test. According to the exhaustive evaluation of instantaneous intensity, the first fundamental frequency, unlike the second and fifth, is the one that obtained better and clear results to identify and locate the damage on the bridge.
5. To evaluate the damage identification capability of the vibration parameters assessed under vehicle induced excitation, the percentage variation observed at the damage location for condition states; DMG2, RCV & DMG3 are given in Table 5 and can be compared against modal frequency changes for each damage scenario in Table 6, courtesy of Kim et al. (2014). From the comparison, all of the vibration parameters assessed appear to outperform the modal frequency changes in this regard, with AIVI's percentage differences producing the best overall.

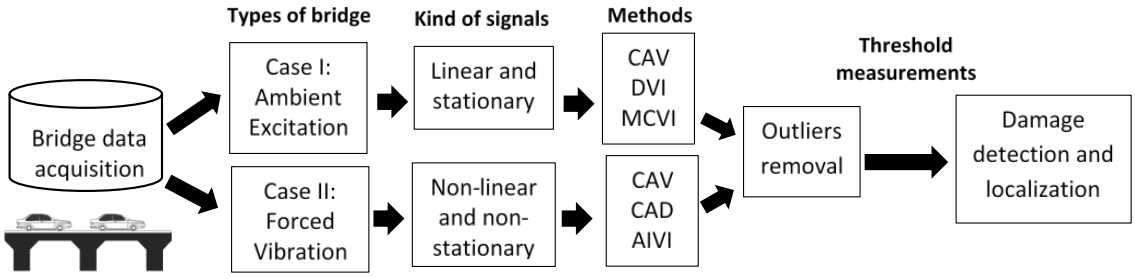

Figure 31. Flowchart to choose the most appropriate method in the damage identification.

Table 5. Vibration parameter variation for total number of sensors and damage scenarios

Vibration Parameter	DMG2	RCV	DMG3
CAV	+9.1%	+0.1%	+19.8%
CAD	+10.2%	-0.1%	+22.2%
AIVI	+12.3%	-0.1%	+35.8%

Table 6. Modal frequency variation (Kim et al., 2014)

Mode	DMG2	RCV	DMG3
1st B. Mode	-2.67%	-0.13%	+0.31%
2nd B. Mode	+0.20%	-0.25%	-5.67%
3rd B. Mode	-0.21%	-0.87%	-9.05%
4th B. Mode	+0.22%	-0.72%	-6.87%
5th B. Mode	+0.58%	+0.19%	-0.16%

6. Conclusions

The present paper describes a set of novel vibration parameters such as CAV, CAD, DVI, MCVI, IVI and AIVI and their feasibility as damage features to detect damage using ambient and forced vibrations in two real bridges. Bridge data can be obtained from ambient or forced vibration, that at the same time may present some particularities such as linearity and stationarity. For instance, in the first bridge analyzed, the signals are linear and stationary, however in the second case, the bridge is subjected to a forced vibration, which produces non-linear and non-stationary signals. The developed strategy consists of using non-modal vibration-based methods. The results presented in this paper, have demonstrated that many of the novel empirical vibration parameters assessed are suitable for damage identification (detection, localization & quantification), provided that they are applied to a suitably applicable vibration signal type, as per the criteria set out in Table 1 and Figure 31, and provided that a suitable outlier detection method is chosen based on the distribution type of the extracted vibration parameter. Some practical recommendations for application of the proposed techniques are listed in the discussion section.

However, it should be pointed out that in both bridge data analysed, operational and environmental effects are not considered in the present study. To include those effects in the damage detection performance of the defined vibration parameters is the subject of further research.

Acknowledgements

The first author gratefully acknowledges for the scholarship in support of his PhD studies to the Ministry of Education of Peru with the National Scholarship and Educational Loan Program PRONABEC - President of the Republic Scholarship. The authors would like to thank Prof. Chul-Woo

Kim of the Dept. of Civil and Earth Resources Engineering, Kyoto University, Kyoto, Japan for the generous sharing of the steel truss bridge data assessed within this study.

References

1. Colominas, M.A., Scholtthauer, G., & Torres, M.E. (2014). Improved complete ensemble EMD: A suitable tool for biomedical signal processing. *Biomedical Signal Processing and Control*, 14, 19–29.
2. Chang, K.C., & Kim, C.W. (2016). Modal-parameter identification and vibration-based damage detection of a damaged steel truss bridge. *Engineering Structures*, 122, 156–173.
3. Ding, K., & Chen, T. P. (2013). Study on Damage Detection of Bridge Based on Wavelet Multi-Scale Analysis. In *Advanced Materials Research* (Vol. 639, pp. 1010-1014). Trans Tech Publications.
4. Fassois, S. D., & Kopsaftopoulos, F. P. (2013). Statistical time series methods for vibration based structural health monitoring. In *New trends in structural health monitoring* (pp. 209-264). Springer, Vienna.
5. Goi, Y., & Kim, C. W. (2017). Damage detection of a truss bridge utilizing a damage indicator from multivariate autoregressive model. *Journal of Civil Structural Health Monitoring*, 7(2), 153-162.
6. Huang, N. E., Long, S. R. & Shen, Z. (1996). The mechanism for frequency downshift in nonlinear wave evolution. In *Advances in applied mechanics* (Vol. 32, pp. 59-117C). Elsevier.
7. Hester, D., & González, A. (2012). A wavelet-based damage detection algorithm based on bridge acceleration response to a vehicle. *Mechanical Systems and Signal Processing*, 28, 145-166.
8. Kankanamge, L., & Dhanapala, Y. S. S. (2016). Application of Wavelet Transform in Structural Health Monitoring.
9. Kim, C.W., Kitauchi, S. & Sugiura, K. (2013). Damage detection of a steel bridge through on-site moving vehicle experiments. In *Proceedings of the Second Conference on Smart Monitoring, Assessment and Rehabilitation of Civil Structures (SMAR2013), Istanbul, Turkey*.
10. Kim, C.W., Chang, K.C., Kitauchi, S., McGetrick, P.J., Hashimoto, K. & Sugiura K., (2014). Changes in modal parameters of a steel truss bridge due to artificial damage. *Safety, Reliability, Risk and Life-Cycle Performance of Structures and Infrastructures-Proceedings of ICOSSAR, New York,* 16-20.
11. Kramer, S. L. (1996). *Geotechnical Earthquake Engineering*. Prentice-Hall, Upper Saddle River, New Jersey.
12. Laory, I., Trinh, T. N., Posenato, D., & Smith, I. F. (2013). Combined model-free data-interpretation methodologies for damage detection during continuous monitoring of structures. *Journal of Computing in Civil Engineering*, 27(6), 657-666.

13. Moughty, J. J. & Casas, J. R. (2017). A state of the art review of modal-based damage detection in bridges: development, challenges, and solutions. *Applied Sciences,* 7(5), 510.
14. Moughty, J.J. and Casas, J.R. 2018a, Damage Identification of Bridge Structures using the Hilbert-Huang Transform. In *Life Cycle Analysis and Assessment in Civil Engineering: Towards an Integrated Vision: Proceedings of the Sixth International Symposium on Life-Cycle Civil Engineering (IALCCE 2018), 28-31 October 2018, Ghent, Belgium* (pp. 1-8). CRC Press.
15. Moughty, J.J. & Casas, J.R. 2018b. Noninvasive Empirical Methods of Damage Identification of Bridge Structures using Vibration Data. In *Life Cycle Analysis and Assessment in Civil Engineering: Towards an Integrated Vision: Proceedings of the Sixth International Symposium on Life-Cycle Civil Engineering (IALCCE 2018), 28-31 October 2018, Ghent, Belgium* (pp. 1-8). CRC Press.
16. Nguyen, V. H., Mahowald, J., Maas, S., & Golinval, J. C. (2014a). Use of time-and frequency-domain approaches for damage detection in civil engineering structures. *Shock and Vibration, 2014.*
17. Nguyen, T., Chan, T. HT., & Thambiratnam, D. P. (2014b). Controlled Monte Carlo data generation for statistical damage identification employing Mahalanobis squared distance. *Structural Health Monitoring*, 13(4), 461-472.
18. Ou, Y., Chatzi, E. N., Dertimanis, V. K., & Spiridonakos, M. D. (2017). Vibration-based experimental damage detection of a small-scale wind turbine blade. *Structural Health Monitoring,* 16(1), 79-96.
19. Rousseeuw, P. J., & Driessen, K. V. (1999). A fast algorithm for the minimum covariance determinant estimator. *Technometrics*, 41(3), 212-223.
20. Santos, J., Cremona, C., Orcesi, A., & Silveira, P., (2013). Baseline-free real-time novelty detection using vibration-based symbolic features. *Experimental Vibration Analysis for Civil Engineering Structures (EVACES), 28-30 October, Ouro, Brazil*.
21. Sun, Z., Nagayama, T., Su, D., & Fujino, Y. (2016). A damage detection algorithm utilizing dynamic displacement of bridge under moving vehicle. *Shock and Vibration, 2016.*
22. Tondreau, G., & Deraemaeker, A. (2014). Automated data-based damage localization under ambient vibration using local modal filters and dynamic strain measurements: Experimental applications. *Journal of sound and vibration*, 333(26), 7364-7385.
23. Vienna Consulting Engineers, V.C. (2009). *Progressive Damage Test S101 Flyover Reibersdorf* (Report No. 08/2308). Vienna, Austria.
24. Zhou, Y.-L., Figueiredo, E., Maia, N., Sampaio, R. & Perera, R. (2015). Damage detection in structures using a transmissibility-based Mahalanobis distance. *Structural Control and Health Monitoring*, 22(10), 1209-1222.

5.2. Journal Paper II

Marginal Hilbert Spectrum and instantaneous phase difference as total damage indicators in bridges under operational traffic loads

Published in Structure and Infrastructure Engineering, pp. 1 - 21, September 2021. DOI: 10.1080/15732479.2021.1982994.

Rick M. Delgadillo [1], Fernando J. Tenelema [1], Joan R. Casas [1]

[1]Department of Civil and Environmental Engineering, Technical University of Catalonia (UPC), c/ Jordi Girona 1-3, 08034 – Barcelona, Spain

Received: 3 April 2021; Revised: 25 August 2021; Accepted: 13 September 2021

Abstract: The challenges and future trends in the development of signal processing tools are being widely used for damage identification in bridges. Therefore, it is important to analyse the vibration signals in order to attain effective damage characterization. In this paper, the non-linear and non-stationary dynamic response of bridges under operational loads is studied. First, the signals are decomposed into intrinsic mode functions (IMF) by a novel Improved Completed Ensemble EMD with Adaptive Noise technique (ICEEMDAN). Hilbert-Huang transform is used to obtain their corresponding Hilbert spectra. The marginal Hilbert spectrum (MHS) of each IMF and the instantaneous phase difference (IPD) are proposed as total damage indicators (DI), in the sense that they are able to detect, localize and quantify damage under transient vibration due to traffic. The methodology was tested in two case studies: (i) a numerical model of a two-span steel bridge (ii) a dynamic test conducted on a real steel arch bridge subjected to a series of artificial damages. The experimental and real case results from the damage indices based on the extracted features demonstrate the robustness and more sensitivity of the novel Improved Completed Ensemble EMD with Adaptive Noise technique (ICEEMDAN) in addressing the damage location.

Keywords: Hilbert-Huang Transform (HHT), Empirical Mode Decomposition (EMD), damage identification, Marginal Hilbert spectrum (MHS), Phase Difference (PD), transient vibration, traffic loads.

1. Introduction

Observations of many damages, such as material deterioration, inappropriate usage, environmental conditions and issues related to aging are being studied by structural health monitoring (SHM). For many decades, the civil engineering community has been deeply developing multiple SHM systems via vibration-based techniques for several structures such as bridges. Actually, recent advances in sensor and information technologies have improved the performance in big data (Entezami et al., 2020), monitoring (Spiridonakos et al., 2016), and damage identification (Delgadillo & Casas, 2020; Moughty & Casas, 2017) in bridges. The main dynamic signal processing techniques are fast Fourier transform (FFT) (Diez et al., 2016), wavelet transform (WT) (Li et al., 2019) and Hilbert-Huang transform (HHT) (Delgadillo & Casas, 2020; Chen et al., 2014). The Hilbert-Huang transform allows energy-time-frequency resolution for analysing data from non-stationary and nonlinear processes. The first mathematical formulation of this method was proposed by Huang et al., 1996. The main step in HHT technique consists in decompose the original signal in several intrinsic mode functions (IMF). However, over time, different improvements have been developed in the decomposition of signals starting with the EMD (Huang et al., 1996) technique and now an improved algorithm named ICEEMDAN is used (Colominas et al., 2014). Shi et al. 2005 proposed two methods from measured data containing damage events in a structure. Simulations results based on EMD together with Hilbert transform were proposed to determine the natural frequencies and damping ratios before and after damage. Wu et al. 2009 developed a new method based on HHT to monitor the health of large civil structures under unknown excitation. Both Hilbert-Huang spectrum and marginal spectrum analysis based on HHT are utilized for damage assessment. Roy et al. 2019 considers the problem of long-term monitoring taking into account that a direct comparison of the vibration signals or modal properties at different periods of time may not be sufficient to identify the damages and their exact locations. In this sense, the extraction of the morphologies of the changes in the response signals is very important when analysing the vibration signals. In addition, the correlation between the vibration signals and the type, location, and intensity of structural damage should be thoroughly studied. For this purpose, the authors used EMD technique and HHT to calculate damage indices (DI) using experimental tests conducted on a cantilever steel beam prototype, and the results indicate that the proposed method is effective and feasible. Roveri & Carcaterra, 2012 developed a novel HHT based method for damage detection of bridge structures with cracks under a traveling load. The technique demonstrated good capability to identify the presence and the location of the damage along the beam using a single point measurement. Some authors (Delgadillo & Casas, 2019; Delgadillo & Casas, 2020) studied the performance of novel ICEEMDAN and HHT for damage identification and localization in real steel bridges under operational conditions. It was concluded that HHT and the improved EMD obtain accurately the instantaneous frequency and amplitude and the instantaneous vibration intensity (IVI) as damage indicators.

In addition, the HHT technique is conformable with response signals of the forced-vibration type that are commonly nonlinear and nonstationary in the case of bridge structures due to the vehicle-bridge interaction. (Kunwar et al. 2013; Readdy & Krishna, 2015) proposed damage detection using the HHT technique on bridges structures. Kunwar et al. 2013 examined an instantaneous phase and marginal Hilbert spectrum of transient vibration loads to evaluate three damage cases and healthy condition of an experimental bridge model. The results showed the efficiency to detect and locate damage using the phase difference parameter. The research carried out by Kunwar, 2017 showed an improvement in the study of damage localization using acceleration response through vibration parameters. The present paper shows the feature extraction using an improved EMD technique (ICEEMDAN) and the performance of two damage features (marginal Hilbert spectrum (MHS) and instantaneous phase difference (IPD)) to identify, localize and quantify damage in bridges.

The method is applied to identify damage in a numerical bridge and in a real truss bridge under operational conditions. Nowadays, numerical structures are commonly used for performance evaluation in the context of SHM, since they help researchers to study and evaluate the effectiveness of several SHM methods. Besides, the scarcity or sometimes the absence of appropriate forced-vibration experimental data on real damaged structures make numerical models the key for reliably reproducing the actual dynamic behaviour of the structure either under operational or ambient excitations. Consequently, in this paper, the TU1402 numerical bridge (Tatsis & Chatzi, 2019) has been selected as a case study. The utilization of this numerical model is based on the fact that no experimental data is available from an original and damaged bridge subjected to vehicular traffic when the damage appears in a continuous 2-span bridge, as opposed to the second case study, where a different configuration (arch bridge) is analysed.

2. Proposed Approach

A general method which requires two steps in analysing the dynamic response is proposed as follows. The first step is to pre-process the data by the novel EMD method called Improved Completed Ensemble Empirical Mode Decomposition with Adaptive Noise (ICEEMDAN). With this technique, the raw data is decomposed into a number of intrinsic mode functions (IMF). The second step is to, apply the Hilbert Huang transform to the decomposed IMFs and construct the energy-frequency-time distribution (Hilbert spectrum). In addition to the instantaneous frequency and amplitude, the marginal Hilbert spectrum and instantaneous phase difference are also obtained, which are proposed and investigated as damage indicators (DI) (Figure 1).

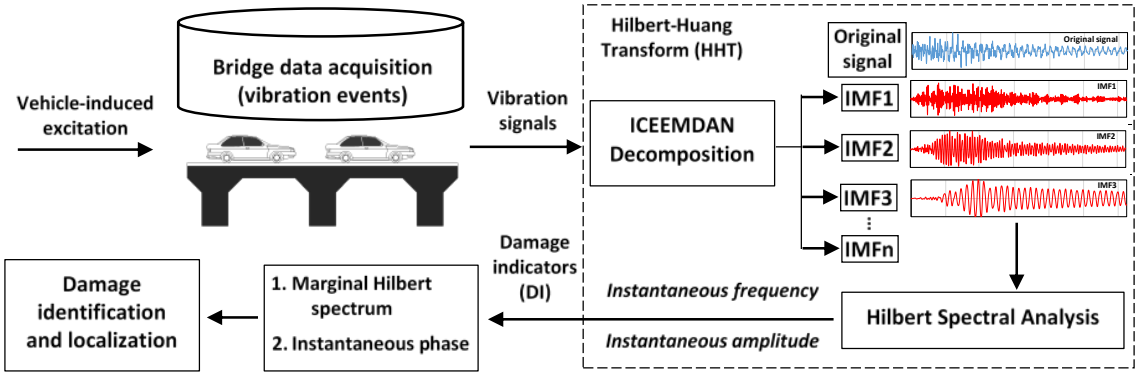

Figure 1. Structure of the proposed method.

2.1. Improvements on Complete Ensemble Empirical Mode Decomposition with Adaptive Noise (ICEEMDAN)

The ICEEMDAN method developed by Colominas et al. 2014 was proposed in order to add controlled noise to create new extrema in the studied signals. This algorithm is forced to focus in some specific values of the scale-energy space, since the local mean is "forced" to stick to the original signal in some parts where new extrema are created with exception in the rest of the signal (where no creation of extrema occurred). First, with respect to residual noise in modes, each mode is calculated sequentially, so the final modes are used by ICEEMDAN for the computation of the next one. Furthermore, the local means of each realization of signal plus noise are estimated and the true mode as the difference between the current residue and the average should be defined.

2.2. Hilbert Huang Transform

The Hilbert Huang Transform (HHT) is an advanced algorithm, which is being used widely in SHM field in order to process nonstationary and nonlinear signals. The HHT method involves two steps: (i) decomposition of the original data into different simple intrinsic modes of oscillation and (ii) performing Hilbert transform to each simple mode (Hilbert spectrum analysis).

In this article, two damage indices based on the Marginal Hilbert Spectrum (MHS) and unwrapped phase extracted by ICEEMDAN technique are used to detect, locate, and classify the severity of the damage. Their definition is presented below.

The marginal Hilbert spectrum $h(\omega)$ measures the total amplitude contribution from each IMF component value of the signal over the time duration T and is obtained by integration over time of the Hilbert amplitude spectrum ($H(\omega,t)$). As mentioned in Huang et al. 1998 and Kunwar et al., 2013, in a similar way that Fourier spectrum is adequate to analyse linear and stationary time signals, the marginal Hilbert spectrum is well suited for non-linear and non-stationary signals. In both cases, a reduction in peak frequency may indicate damage. Mathematically, it is expressed as:

$$h(\omega) = \int_0^T H(\omega, t)\,\mathrm{dt} \tag{1}$$

Apart from the calculation of the instantaneous frequency, HHT of individual IMFs gives the instantaneous phase and amplitude. A total instantaneous phase is obtained by the sum of the instantaneous phases for each IMF. Equation (2) gives the total number of rotations of the measured signal *x(t)* in the complex plane. The total number of rotations in the complex plane for a unique time value *t* is multiplied by 2π because the $\theta(\mathrm{t})$ is unwrapped with radian phases in time.

$$\theta(\mathrm{t}) = \sum_{n=1}^{N} \arctan\left(\frac{H\left[I_n(\mathrm{t})\right]}{I_n(\mathrm{t})}\right) \tag{2}$$

In a bridge structure, $\theta_p(\mathrm{t})$ represents the value of a phase function at a location *p.* Therefore, if a point on the bridge structure is chosen as a reference point, the phase function relative to the reference point can be expressed as

$$\phi_P(\mathrm{t}) = \theta_P(\mathrm{t}) - \theta_o(\mathrm{t}) \tag{3}$$

Where $\phi_P(\mathrm{t})$ represents the relative phase relationship of a travelling structural wave for a given state of a bridge. The "phase difference" considers the total phase at any point *p* on a bridge relative to a reference point *0.* Therefore, bearing in mind the idea of damage detection, $\phi_P(\mathrm{t})$ will alter the speed at which energy travels through the structure.

As mentioned by several authors (Kunwar et al., 2013; Pines & Salvino 2002; Salvino et al., 2003), and based on laboratory tests, the tracking of changes in the wave speed of response measurements considering Equation (3) can be an effective method for damage identification and localization and this is further investigated here for the case of a real bridge instead of a laboratory model.

3. Case studies: Description

3.1. Numerical model

As part of COST Action TU1402 on Quantifying the Value of SHM, a numerical model described in Tatsis & Chatzi, 2019 was generated. The model represents the superstructure of a two-span continuous steel beam bridge subjected to changing operational conditions. In this section, a

description of the FE model of the bridge is firstly presented considering different damaged states. Then, a modal analysis is carried out to identify the natural frequencies and vibration modes of the superstructure. Lastly, a time history analysis using Newmark integration method is carried out to obtain the displacement and acceleration time histories at six measurement points (called "sensors") when a load moves on the deck. The acceleration records are used to check the performance of the method and the damage features proposed in this paper for damage detection.

3.1.1 Geometry and material properties

The bridge deck is represented by a two-dimensional finite element (FE) model as shown in Figure 2. It consists of a two-span continuous beam with equal span lengths of 10m. The cross section is rectangular with constant thickness b = 0.1m and height h = 0.6m. It is assumed to be made from low carbon structural steel (Grade S235). The material has a Young's modulus E = 215GPa, Poisson's ratio ν = 0.3 and density ρ = 7850 kg/m^3 at ambient temperature of T = 20ºC.

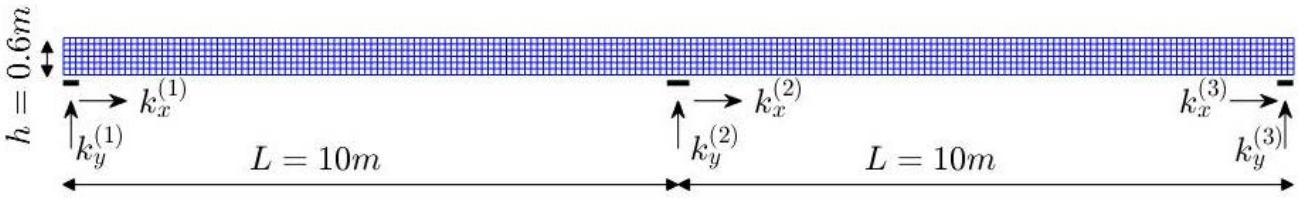

Figure 2. Geometry of the two-span steel beam on elastic boundaries in the longitudinal and vertical directions.

3.1.2 Elastic supports

In this case study, three identical and equally spaced elastic supports are considered. Two elastic supports are located at both ends in a width of 0.3m and another is located at the midpoint of the beam in a width of 0.4m. These supports are modelled as point supports with the following horizontal and vertical stiffness: $k_x = 10^7$ kN/m in the *x* longitudinal direction, and $k_y = 10^{12}$ kN/m in the *y* vertical direction.

3.1.3 Element type and Gauss quadrature rule

The bridge superstructure is a thin member with a small z dimension (0.1m thick) compared to the in-plane x and y dimensions (20m and 0.6m, respectively). Besides, it is only subjected to in-plane loading. Generally, structures that meet these two conditions are considered to be in a state of plane stress in which the normal stress σ_z and the shear stress γ_{yz} are assumed to be zero. Therefore, a two-dimensional FE model is constructed for the plane stress problem using isoparametric quadrilateral elements whose formulation is characterized by using the same shape functions to interpolate the displacement field and nodal coordinates (geometry), as explained by Oñate, 2013.

These elements have two degrees-of-freedom (DOFs) per node corresponding to vertical and horizontal displacements. Therefore, the model was discretized using four-node bilinear quadrilateral elements (QUAD4: 4-Node and 8-DOFs) and 2x2 Gauss quadrature rule, resulting in 200 and 6 elements in x and y directions (1200 elements, 1407 nodes and 2814 DOFs in total).

3.1.4 Damage scenarios and sensors

Structural damage can be inferred as a reduction of bridge bending stiffness causing a change of the dynamic behaviour (Huang et al., 1996). For this case study, cracks on the beam surface are considered. Cracks are modelled by reducing Young's modulus on certain finite elements. In particular, six damage scenarios grouped in two damage regions are imposed for damage detection as shown in the Figure 3.

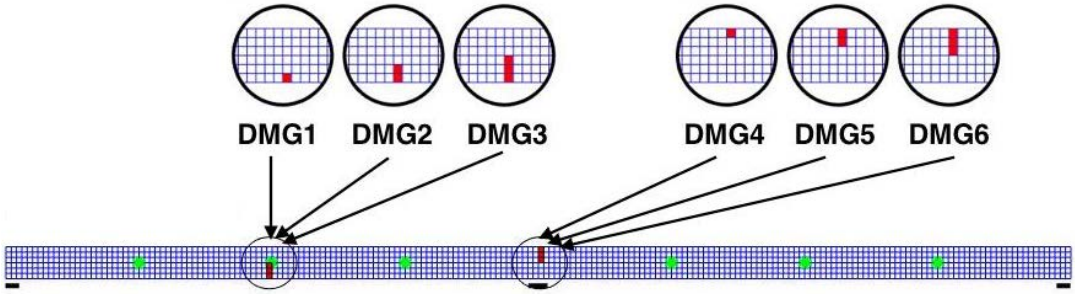

Figure 3. Sensors (in green) & damage locations (in red) on steel beam.

In each case, damage differs from each other in the number of the mesh elements affected, as shown in Figure 3, simulating the extent of damage. Damaged zone has a constant width of 0.1m and the height ranges from 0.1 to 0.3m. The description of the six damage scenarios is summarized in Table 1.

Table 1. Description of damage states performed on the numerical steel beam.

Damage states	Number of damaged mesh element	Damaged location
Undamaged (UND)	0	-
Damaged 1 (DMG1)	1	At the bottommost edge of the mid-left span section
Damaged 2 (DMG2)	2	
Damaged 3 (DMG3)	3	
Damaged 4 (DMG4)	1	At the uppermost edge of the mid-support section
Damaged 5 (DMG5)	2	
Damaged 6 (DMG6)	3	

Six measurement points called “sensors” are considered to provide information about the displacements and accelerations over time in both x and y directions. The location of these sensors is described in the Table 2 and shown in figure 3.

Table 2. Measurement points or sensors located along the beam.

Sensors	Description	Location along the neutral axis of the beam (y=0.3m)
S-01	At 1/4L from the left-hand support	x = 2.5m
S-02	At the middle of the left-span	x = 5.0m
S-03	At 3/4L from the left-hand support	x = 7.5m
S-04	At 3/4L from the right-hand support	x = 12.5m
S-05	At the middle of the right span	x = 15.0m
S-06	At 1/4L from the right-hand support	x = 17.5m

The six damage scenarios are classified in two groups of damage (GPD) in order to study the sensitivity of the method to localize and quantify the damage in terms of extension (number of elements damaged) and intensity (percentage of stiffness reduction (SR)). The corresponding groups of damage are described in Table 3. Group of damage 1 (GPD1) considers the effect of severity of damage for the maximum crack depth (DMG3) by simulating the damage severity with different stiffness reduction, from 50 to 90 %, while Group of damage 2 (GPD2) investigates the influence of the crack extension for a given percentage of stiffness reduction (SR=90%).

Table 3. Groups of damage (GPD).

Group of damage	Damage scenarios	Stiffness reduction SR (%)
GPD 1 (x=5m)	UND	-
	DMG3	50
	DMG3	70
	DMG3	90
GPD 2 (x=10m)	UND	-
	DMG4	90
	DMG5	90
	DMG6	90

3.1.5 Modal analysis

The effective modal mass is a good measure to evaluate this significance of each mode of vibration, as described by Wining & Klein, 1996. For this case study, the number of modes to be considered are those providing more than 90% of the cumulative Effective Mass Participation Factor (EMPF) The first 20 natural frequencies and the mass normalized mode shapes (Yan et al., 2014) of the undamaged structure, mobilizing a EMPF of 100% in the longitudinal and 90 % in the vertical directions are shown in Figure A.1 and Table A.1 of the appendix. The first 20 natural frequencies range from 18.6 to 654.3 Hz. The lowest natural frequency of 18.6 Hz corresponds to the first horizontal mode of vibration in which the motion is entirely longitudinal. The first vertical mode of vibration is symmetric at a frequency of 26.1 Hz (mode 2) and asymmetric at 28.9 Hz (mode 3).

The next modal parameter to be determined in order to calculate the time-history for the travelling load is the damping ratio required to compute the damping matrix. The Rayleigh damping

formulation (Chopra, 2017) is assumed expressing the damping matrix C as a linear combination of the mass and stiffness matrices, M and K respectively, that is

$$C = \alpha M + \beta K \tag{4}$$

Where α and β are real scalars calculated with the technique proposed by (Chowdhury & Dasgupta, 2003) for systems with large number of degrees of freedom. The objective was to estimate a rational value of α and β establishing an increase of the damping ratio, ξ, with each of the subsequent modes as the assumption of constant damping ratio for all modes will not be realistic for particular systems where higher mode contribution is significant. Therefore, two reference modes of vibration are needed to calculate α and β. The EMPF is a crucial factor when calculating damping of a structure as modes contributing largely to dynamic responses are found on the basis of the EMPF. For our case study, the first dominant frequency in the y-direction takes place in mode 3 (f_3 = 28.996Hz) with an EMPF, F_{iy}, of 70.16% expressed in percentage, while the second dominant frequency occurs in mode 8 (f_8 = 156.012Hz) with an approximated F_{iy} of 12.08%. These are the two reference modes selected to compute α and β in such a way so that the modal damping ratios ξ related to the third and eighth natural frequencies are ξ_3 = 3% and ξ_8 =10%, respectively. These damping ratios are very high for a standard steel bridge, but have been selected high in order to check that the proposed methodology is even able to detect damage in highly damped structures, where the signal to noise ratio (SNR) can be much lower. After using the technique proposed by (Chowdhury & Dasgupta, 2003), the Rayleigh coefficients are found: α = 4.59982 and β = 0.00019.

3.1.6 Loading

A deterministic moving load (LC1) is considered to derive a time-history analysis simulating traffic. A weight of a standard car truck (3 tons) travelling at constant velocity of v = 3m/s (10.8 km/h) is considered. A speed of 3m/s is quite satisfactory in order to identify noticeable changes in the dynamic behaviour of the structure, although it does correspond to a very low speed for real traffic situations. As shown in Figure 4, the vehicle weight is modelled as a concentrated vertical point load. This is a simplified model of a real vehicle interacting with a real bridge, but it will be appropriate for the verification of the method jointly with the complementary results obtained from the real bridge described in the section 3.2.

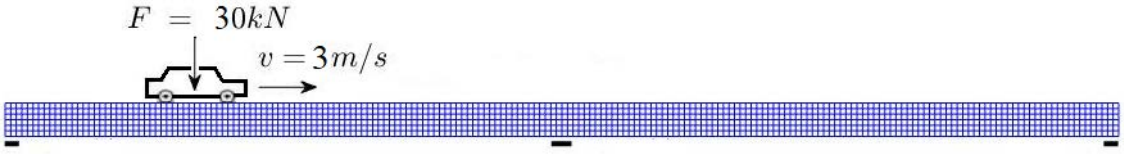

Figure 4. Loading in the form of a moving concentrated vertical force (force: F=30kN, speed: v = 3m/s).

It should be noted that the way the time-dependant point load was modelled and the corresponding forces introduced in the FEM mesh is the main reason for the forcing frequencies to be conditioned by the vehicle speed and the mesh element size in longitudinal direction. That is to say, considering a vehicle speed of *v* and a mesh element length of *b* causes the bridge superstructure model to face an input force with frequencies $f = v/b,\ 2v/b,\ 3v/b,\ 4v/b$ and so on, having a greater influence in the dynamic response those frequencies close to natural frequencies. The highest possible frequency, $n*v/b$, where n is an integer, should be less than the half sampling frequency used for the time history analysis. The ratio of the moving load speed and mesh element length (v/b) is a key factor to accurately determine the forcing frequencies. For instance, if *b* remains constant while varying *v,* a low speed may cause the appearance of closely spaced spectral modes, some of which may correspond to non-physical modes. In contrast, a high speed can cause no dynamic change when damage occurs as long as the damaged element is small. A similar interpretation could be done for the value of *b*. However, this value is obtained in advance after a mesh convergence analysis in order to provide accurate results. In our study case, an element length of b = 0.1m was set. Moreover, to take into account the influence of low and high frequencies the first and second bending modes were considered, thus covering a frequency range of 26-29Hz and 146-156Hz, respectively. Finally, a speed of *v* = 3m/s was found quite satisfactory to obtain a frequency band around 30Hz and 150Hz, thus reducing the number of non-physical modes.

3.1.7 Time History Analysis

The implicit Newmark integration schema (Newmark, 1959) is used to solve the differential equations of motion in modal coordinates. Then the mode superposition method (Rao, 2017) is used to estimate the final dynamic responses in terms of a few numbers of significant eigenmodes. The Newmark's method using $\gamma = 1/2$ and $\beta = 1/6$, known as the Newark's linear acceleration method is used here (Clough & Penzien, 1975). The Newmark's linear acceleration method is stable as long as the time step to solve the differential equations of motion fulfils the following condition:

$$\Delta t_c \leq \frac{1}{\omega_{\max}} \sqrt{\frac{4}{\left(\gamma + \frac{1}{2}\right)^2 - 4\beta}} \tag{5}$$

Where ω_{max} is the maximum angular frequency to be considered. As a first approach, $\omega_{max} = 2\pi f_{max}$ corresponds to the 20th mode of vibration with a natural frequency of 654.3Hz, approximately. Numerically, the Equation 5 can be expressed as Equation 6 and considering $\gamma = 1/2$ and $\beta = 1/6$:

$$\Delta t_c \leq \frac{2\sqrt{3}}{\omega_{\max}} = \frac{\sqrt{3}}{\pi f_{\max}} = \frac{1.732}{654.334\pi} = 0.00085\,\text{s} \tag{6}$$

Therefore, a time step of Δt_c = 0.0001 seconds is considered for independently solving each differential equations of motion in modal coordinates. On the other hand, one must also set an output time-step size, Δt_{out}, which should be small enough to provide sufficient resolution for time-history analysis. According to table A.1 in the appendix, the two first vertical modes represent a participation factor of 83 %, with a maximum frequency of 156 Hz. Therefore, to avoid aliasing and according to the Nyquist criterion, a sampling frequency of 400 Hz (equivalent to an output time step = 0.0025 s) was decided for the acceleration records. For both groups of damage, the total length of the acceleration records is set to 6.67 seconds corresponding to the time it takes the vehicle to travel the entire bridge (forced vibration).

Figure 5 shows the y-axis acceleration-time history responses recorded form each sensor location (rows) and for each damage scenario (columns) of GPD1. They look as highly non-linear and non-stationary. One also can see high accelerations right at the moment when the excitation force is applied to an area provided with elastic supports, especially at the beginning. However, accelerations in these areas are disregarded by only considering forced vibration responses over a study time interval time 1.3 and 2.1 seconds for all sensors. Hence, a time interval of 0.8 seconds represented by a black rectangle in Figure 5 is taken into account for damage identification.

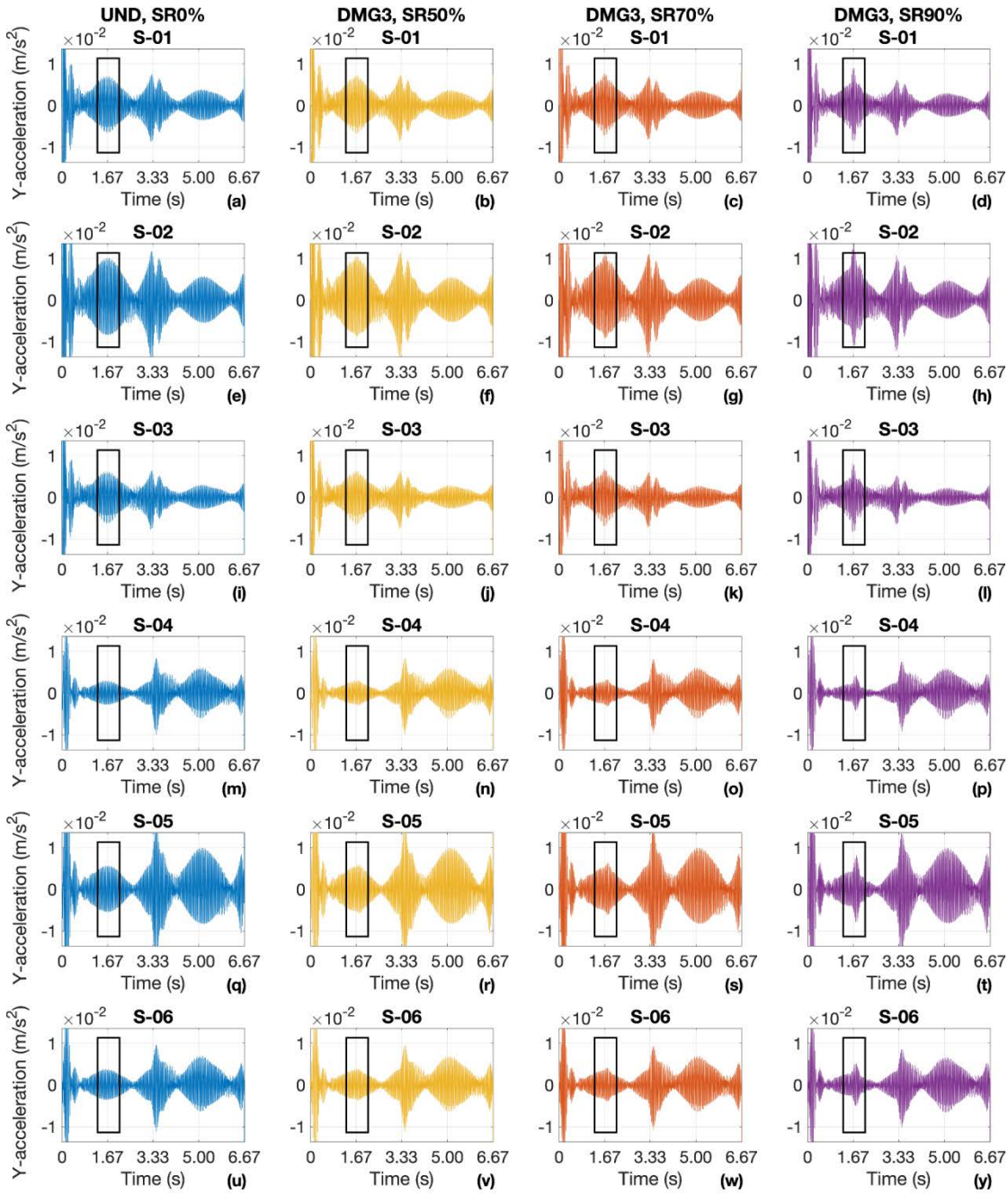

Figure 5. Y-axis acceleration time-history responses at each sensor location for group of damage 1 (GPD1) and time interval used for damage detection (black rectangle).

Figure 6 shows the y-axis acceleration time-history responses at each sensor location (rows) and for each damage scenario (columns) of GPD2. It can be noticed that when damage occurs at the mid-support section, no signal change is seen before 10 seconds just when the moving load crosses the mid-support section. In this Figure, an important increase in accelerations can be seen from 3.1 to 3.5 seconds, hence, this time interval of 0.4 seconds is considered for damage identification.

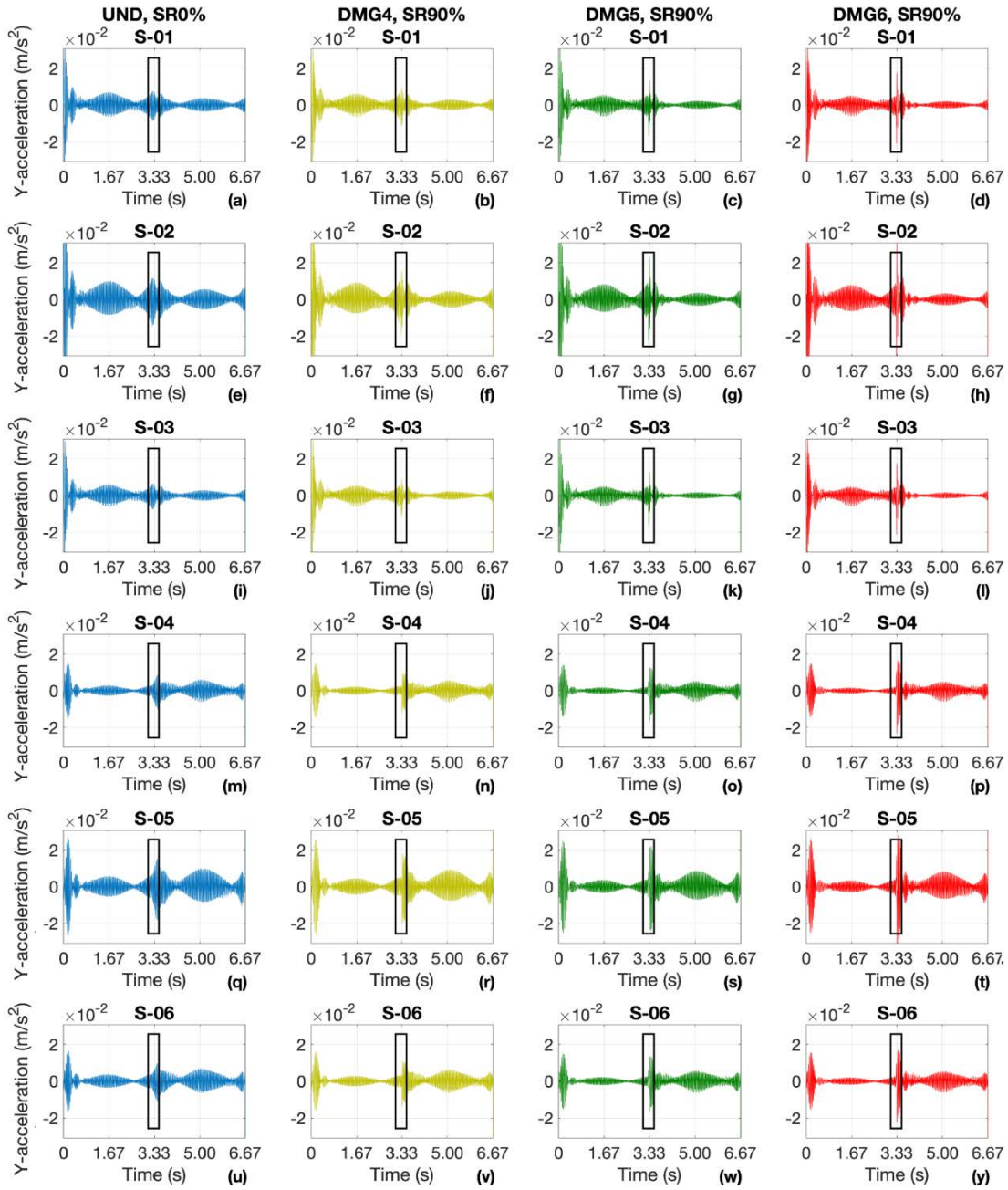

Figure 6. Y-axis acceleration time-history responses at each sensor location for Group of damage 2 (GPD2) and time interval used for damage detection (black rectangle).

3.2. Steel Warren arch bridge

3.2.1 Description of the bridge

The simply supported bridge was a steel arch of the Warren truss type composed of a main span of 59.2 m, 3.6 m width and 8.2 m height, as shown in Figure 7a. The bridge, before complete demolition, was instrumented and subjected to a progressive damage test by (Kim et al. 2014). These data sets are unique in the sense that they consider the operational condition both in healthy and damaged condition in a real bridge. A two-axle recreation vehicle with 21kN of weight (Serena model; Nissan Motor Co. Ltd.) was used for experiments, as presented in Figure 7b, and during the

experiment, the bridge was excited by this vehicle. Eight uniaxial accelerometers captured the vibrations of the bridge, with sample rates of 200Hz and labelled as sensors A1, A2,…,A8 (Figure 7c). Five of these sensors were located at the damaged side (A1-A5) and the other three at the opposite side (A6-A8).

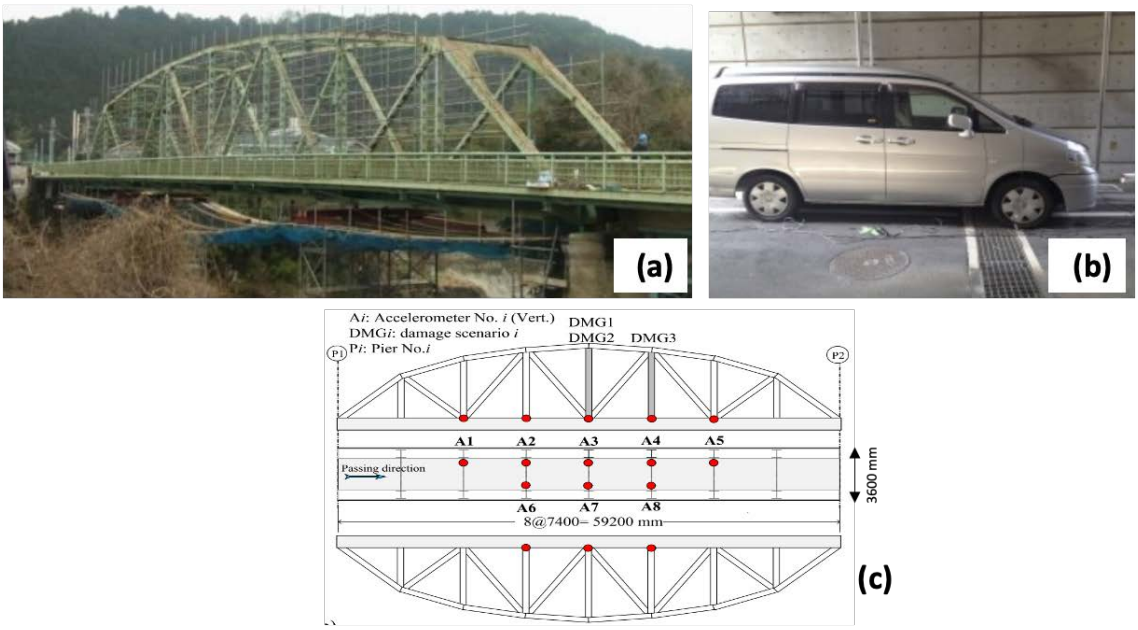

Figure 7. Warren truss bridge (a) longitudinal section (b) recreation vehicle (c) location of the 8 accelerometers and artificial damages.

3.2.2 Damage scenarios

Five progressive damage tests were carried out in short time period before the demolition of the bridge, as summarized in Table 4 and sketched in Figure 8. The location of these artificial damages was depicted in Figure 7c. Firstly, when the structure is in healthy condition and with no artificial damages, is consider like intact (UND). Then, two damage scenarios were imposed to bridge consecutively (i) a partial intersection of the mid-span vertical element was applied using an oxyacetylene cutting torch, this state was named (DMG1) and it could represents a low stress redistribution in the bridge structure as shown in Figure 8b; (ii) the second damage imposed represents a high stress redistribution, which consists in a full intersection of the same member (DMG2) and it can be shown in Figure 8c. Physically speaking, the previous cuts were obtained to imitate patterns of typical damages in bridges like corrosion or overloading. After the first damages (DMG1 and DMG2), the full cut was recovered and it was denoted as the RCV state, as can be observed in Figure 8d. This recovery state consists in weld steel plates and a jack was used to reduce the gap in the cut member. However, after that, the bridge was not guaranteed to be restored to its original undamaged state. Conversely, the RCV scenario simply served as a reference point to the following damage scenario. Finally, the Figure 8c show the DMG3 scenario, where a full cut was imposed in the vertical member located at the 5/8th-span (Figure 7c).

Table 4. Progressive damage test scenarios.

Damage states	Description of damage actions
1	Undamaged (UND)
2	Half cut in vertical member at mid-span (DMG1)
3	Full cut in vertical member at mid-span (DMG2)
4	Mid-span member reconnected (RCV)
5	Full cut in vertical member at 5/8th span (DMG3)

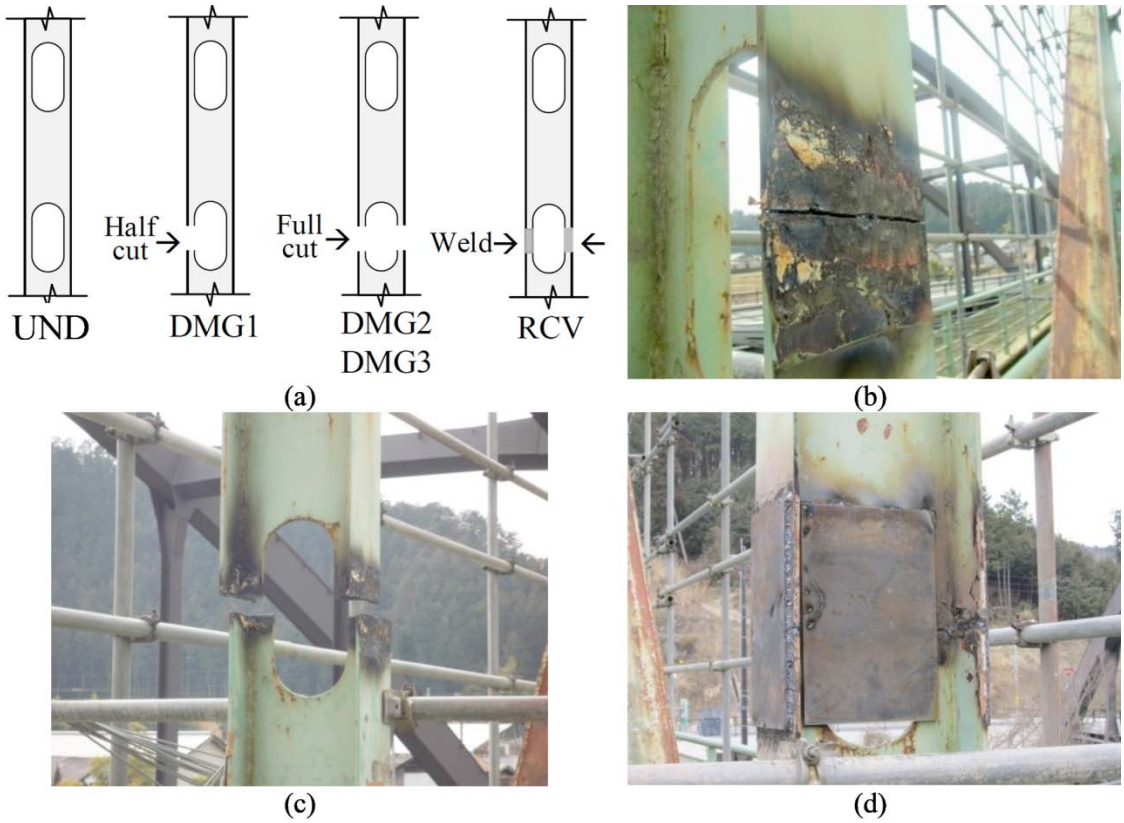

Figure 8. Damage scenarios carried out in the steel truss bridge (a) sketch (b) Half cut in vertical member (DMG1) (c) Full cut in vertical member (DMG2 and DMG3) (d) Mid-span member reconnected (RCV).

During the experimental tests, the average speed in each damage scenario was calculated as 36-41km/h. Nonetheless, the speed of around 40 km/h was considered because it was the most common in all the tests realized by (Chang and Kim, 2016). With respect to environmental conditions, the temperature was not recorded, because there were no temperature variations during the short duration of the tests. The distance over the bridge was covered in about 10 s. The vertical acceleration responses captured by the accelerometers placed in the bridge consists of two parts as shown in Figure 9, (i) tanking account the first 10 seconds approximately, the feature of the signal is considered a forced vibration, which is quite short in duration and looks highly nonlinear and non-stationary; and (ii) after the 10 seconds, the bridge vibrated freely.

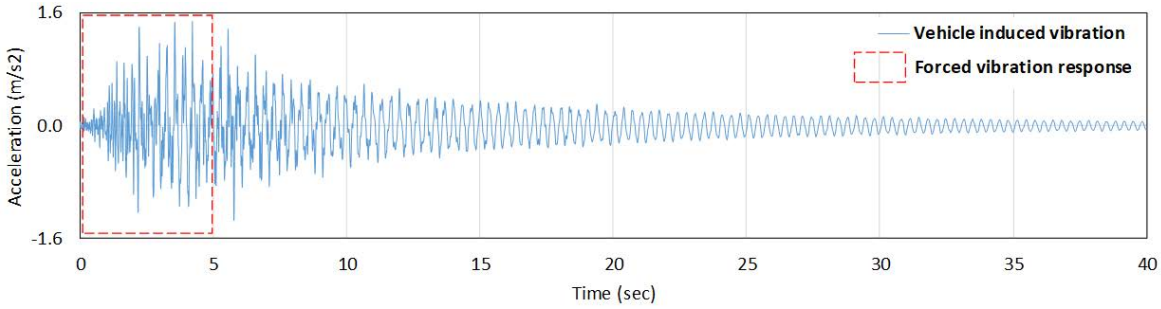

Figure 9. Time history of bridge acceleration response in sensor 1.

4. Case studies: results and discussion

4.1. Numerical bridge

As mentioned previously (see Section 3.1 above), two groups of damage (GPD1 and GPD2) were investigated to show the influence of damage location, extension and intensity.

4.1.1 IMFs using ICEEMDAN method

The first step of HHT method is to decompose the acceleration time histories into a finite number of intrinsic mode functions (IMFs) which are sorted from high to low frequencies. In general, the first IMFs can be associated to a physical meaning by representing a simple oscillatory mode of the bridge. For both groups of damage and sensors, the ICEEMDAN method (Colominas et al., 2014) as described in section 2.1 was used with the following parameters: an ensemble of I = 500 realisations and a total of N = 5000 shifting operations.

Figure 10 illustrates the forced vibration response and the first four IMFs obtained in sensor S-02 and for GPD1. Each column represents a different damage configuration. The first row represents the original signal, while the following rows represent the signal decomposition into IMFs ordered from highest to lowest frequency. It can be seen that for all damage scenarios the first three IMFs carry the most oscillating components (from Figure 10e to 10p), while the rest of IMFs have a low contribution. On the other hand, for GPD2, the forced vibration signal and the first four IMFs obtained from ICEEMDAN method at sensor S-02 are shown in Figure 11.

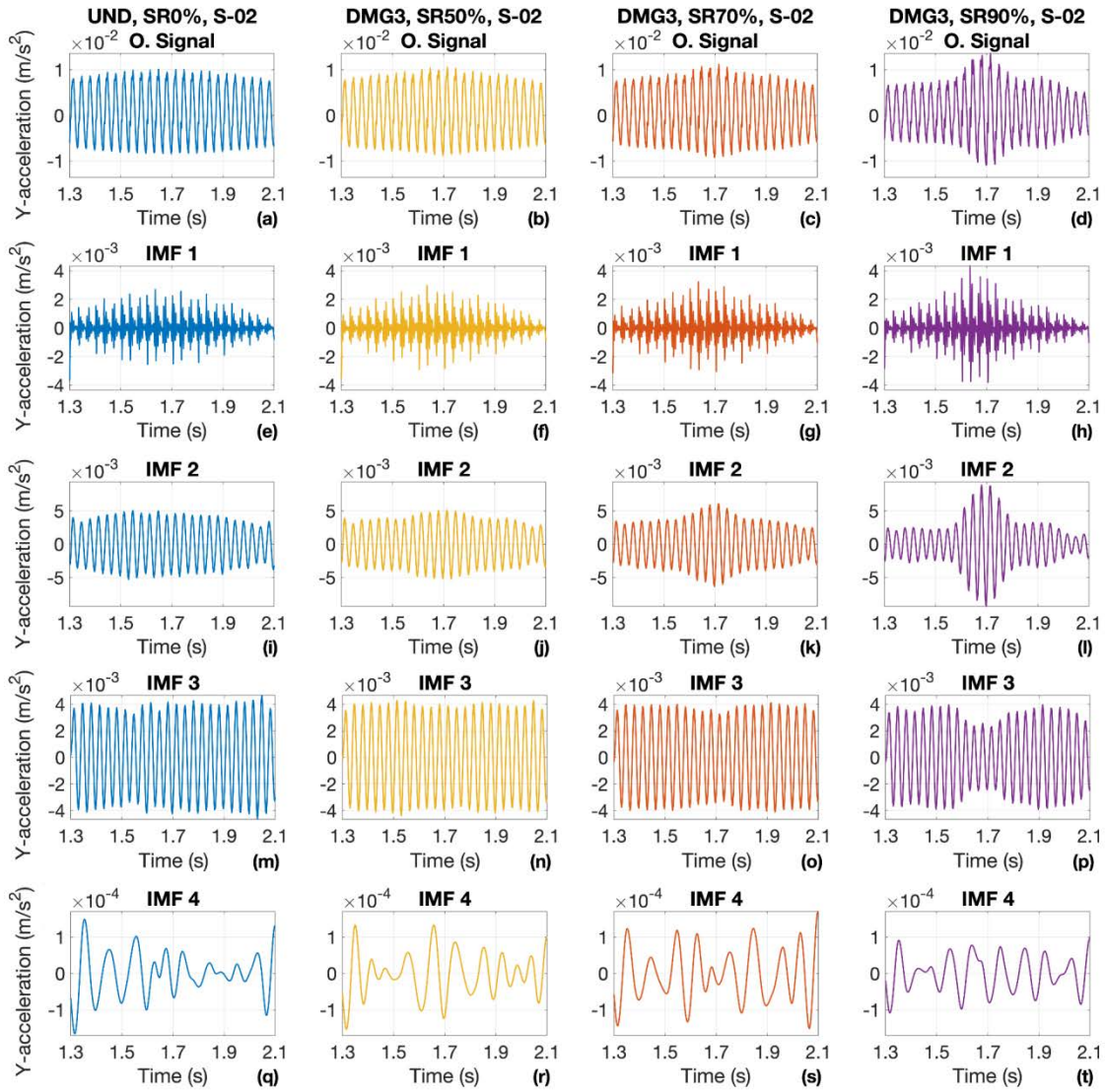

Figure 10. Forced vibration acceleration and the first four IMFs obtained from ICEEMDAN method in sensor S-02 and GPD1.

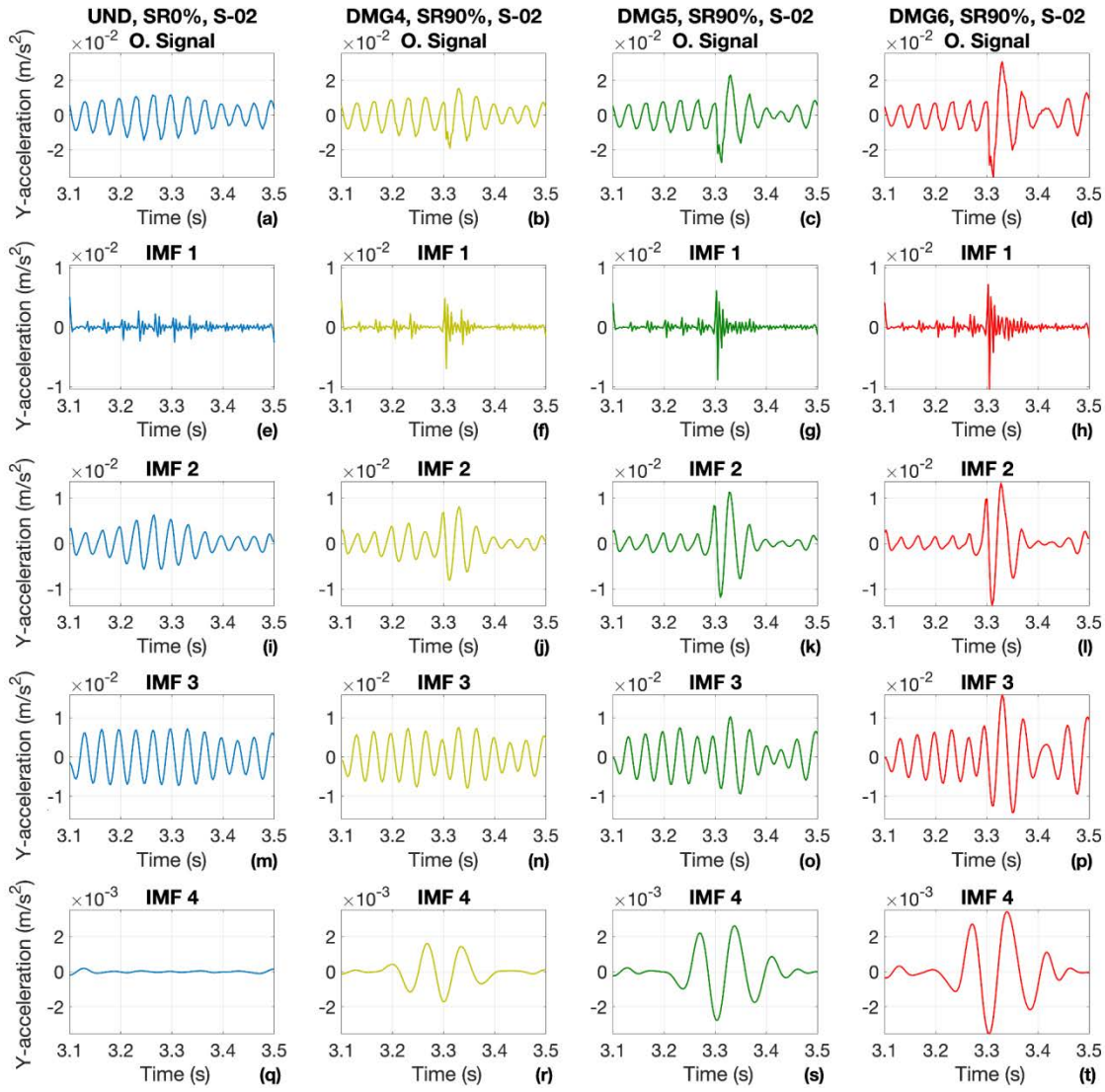

Figure 11. Forced vibration signal and the first four IMFs obtained from ICEEMDAN method in sensor S-02 and GPD2.

4.1.2 Analysis of instantaneous frequencies and amplitudes

The instantaneous (time-dependant) frequencies and amplitudes are obtained from the physically meaningful IMFs using the Hilbert Transform. For GPD1, Figures 12 and 13 illustrate the instantaneous frequencies and amplitudes for all sensors respectively (each sensor per row and each scenario per column for all damage scenarios). Figure 12 shows high oscillations around the frequency of 150 Hz for IMF1 due to the mode-mixing problem, while a more constant instantaneous frequency around 30 Hz is shown in IMF2 and IMF3 for sensors S-01, S-02 and S-03 and only in IMF2 for sensors S-04, S-05 and S-06. Figure 13 depicts the fact that the instantaneous amplitude increases at t = 1.7s due to structural damage, significantly expanding as the level of damage grows, in particular, for IMF1 and IMF2. Similar results are shown in figures A.2 and A.3 in the appendix for the case of GPD2.

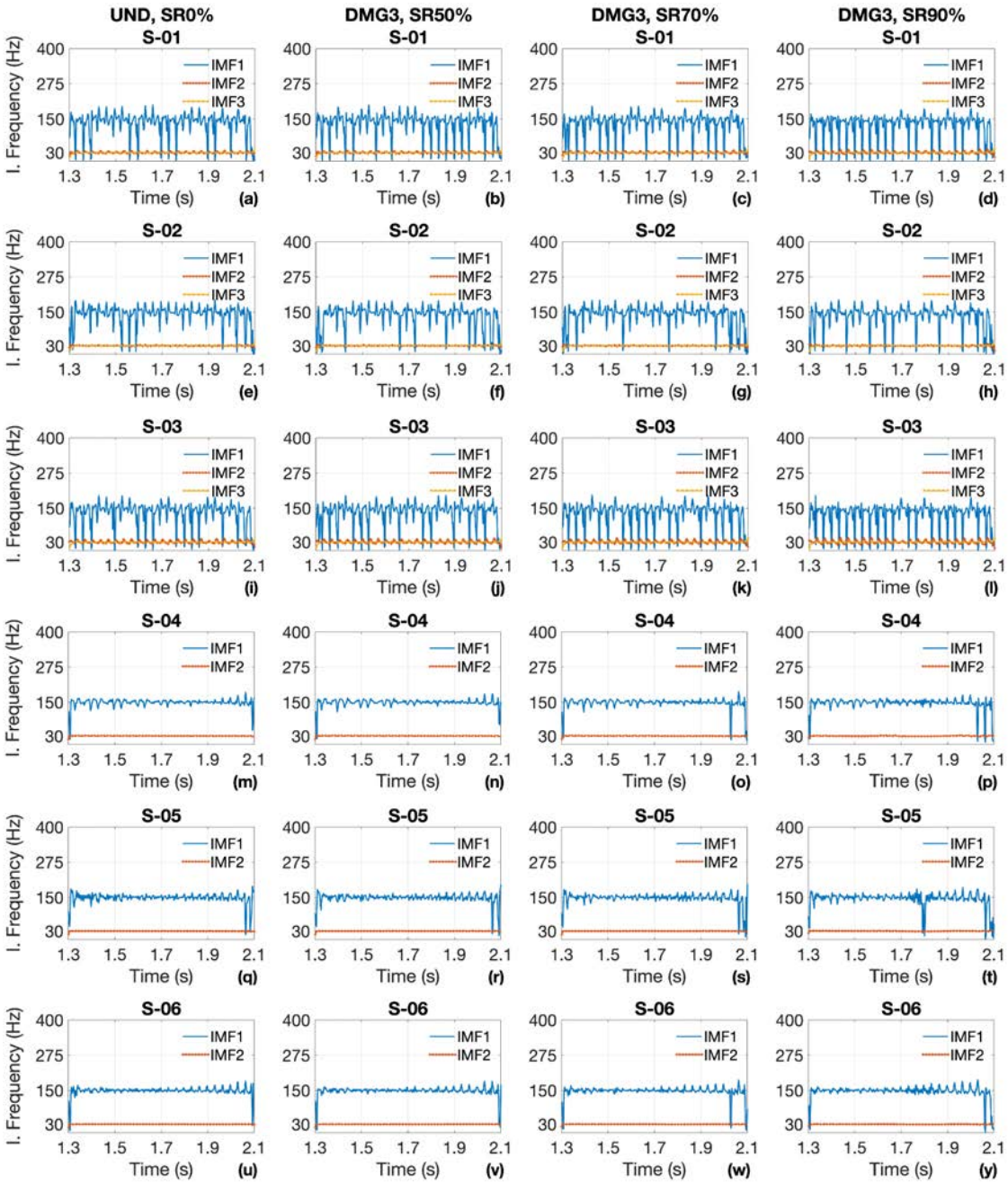

Figure 12. Instantaneous frequency for all sensors and Group of damage 1 (GPD1).

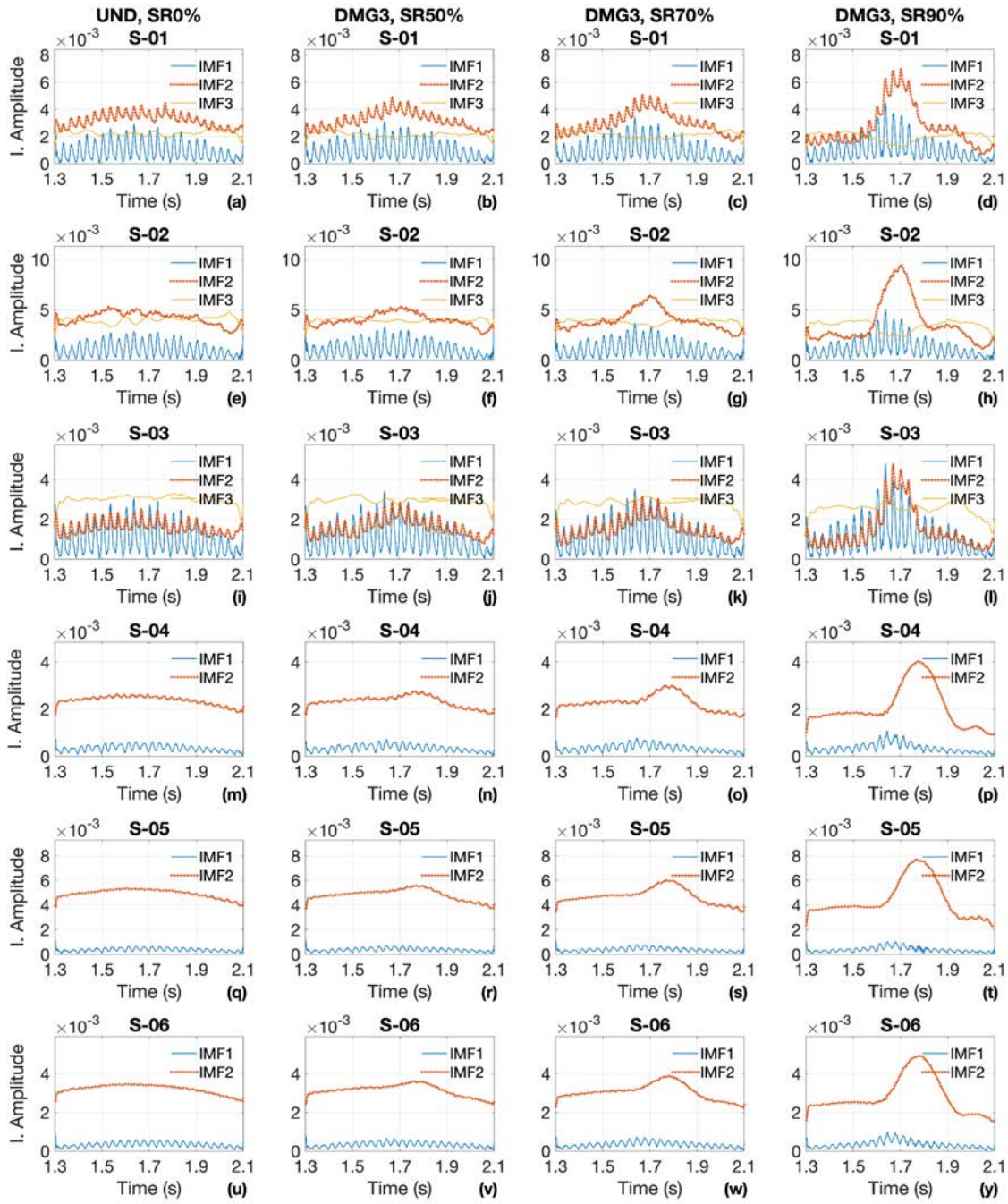

Figure 13. Instantaneous amplitude for all sensors and Group of damage 1 (GPD1).

4.1.3 Marginal Hilbert Spectrum

The marginal Hilbert spectrum gives an indication of the total energy that each frequency value contributes with. And, contrary to the Fourier spectrum representation, in the marginal spectrum a large amount of accumulated energy at a certain frequency (spectral peak frequency) implies that there is a higher probability for a wave to have appeared locally over the entire time span. As shown in Equation (1), the Hilbert spectrum measures in a probabilistic sense the contribution of the frequencies presents in the whole interval of analysis to the total amplitude (Salvino et al., 2003). In

practice, (Kim et al. 2014) observed that the point where the marginal Hilbert spectrum has a maximum depends on the changes in the stiffness of the bridge, therefore, the presence of damages is related with a reduction in peak frequency. Furthermore, the lowest peak frequency corresponding to the first peak value of magnitude is worth to be analyzed for damage detection as proposed by Kunwar et al., 2013.

Figure 14 plots the marginal Hilbert spectrum for the undamaged and damaged scenarios grouped in a single subplot for each sensor and considering the group of damage GPD1. It can be seen that for the baseline (blue lines) the marginal spectrum shows a peak frequency ranged from 30 to 32 Hz. This frequency range is close to the natural frequency corresponding to the first asymmetrical mode of vibration (29 Hz). It is also noticeable that for all sensors, when damage occurs, the peak value of energy increases while the frequency corresponding to this peak reduces. This behavior indicates the presence of damage as noted by many authors (Kunwar et al., 2013; Salvino et al., 2003; Pines & Salvino, 2002; Salvino et al., 2014).

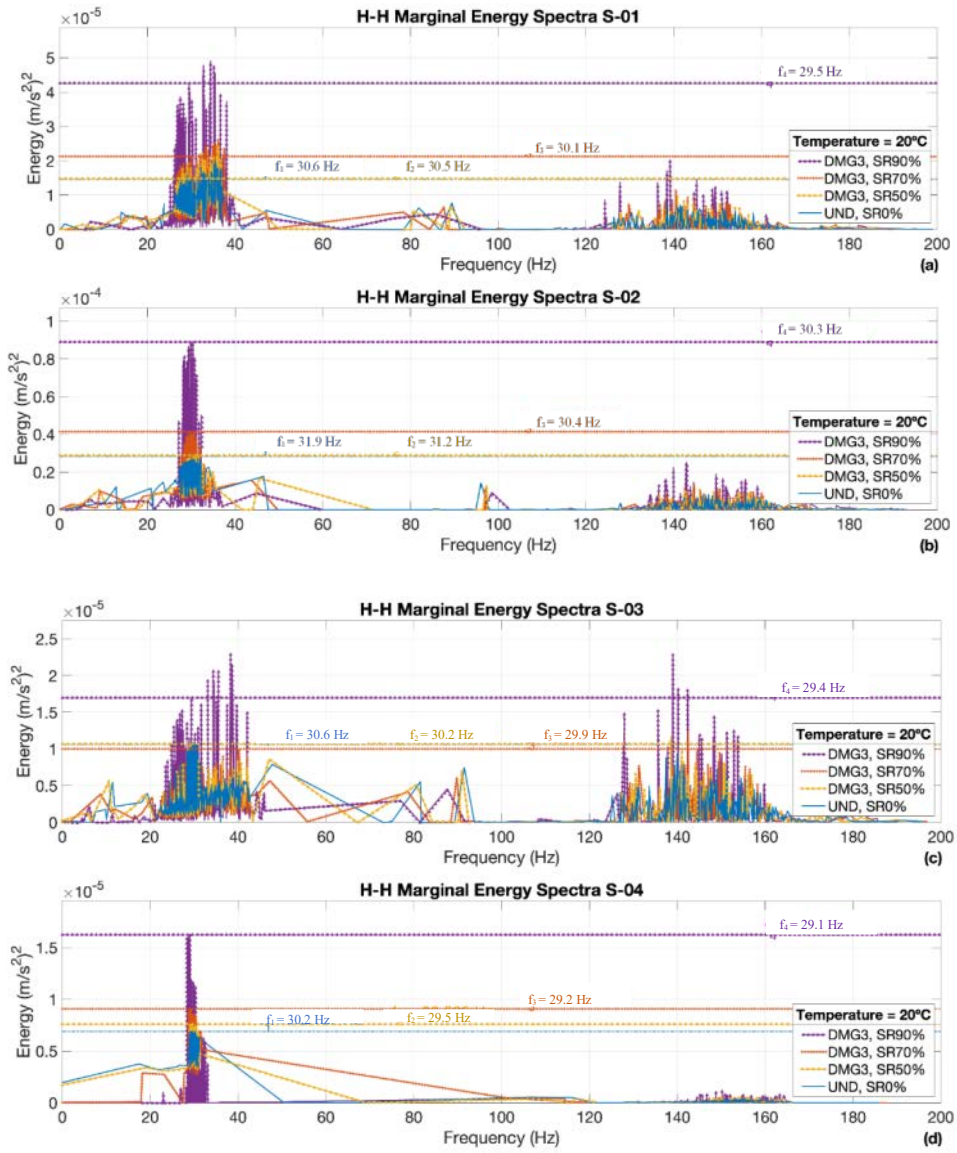

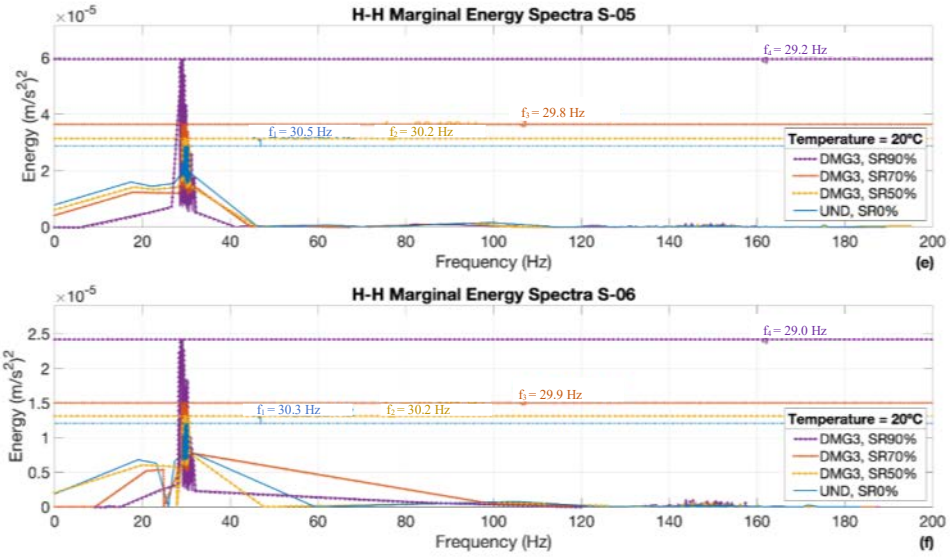

Figure 14. Marginal Hilbert Spectra for all sensors and for GPD1.

The values of frequency corresponding to the peak and the percentage of frequency reduction obtained for each damage scenario and sensor are presented in Table 5. All values shown in Table 5 decrease when damage occurs. The peak frequency steadily decreases as the severity of damage increases in all sensors. Therefore, all sensors can detect and quantify the intensity of damage.

It is also noticeable that when the stiffness reduction (SR) is more than 50%, the largest difference in frequencies occurs in sensor S-02 placed in the exact damage location. Therefore, according to the values from Table 5, one can conclude for GPD1 that damage is closer to sensor S-02, which is where the greatest differences in frequency reduction are found. From this perspective, the marginal Hilbert spectrum aids also to locate the damage. In summary, this damage feature is able to detect, locate and quantify the severity of damage.

Table 5. Peak frequencies values using ICEEMDAN for all sensors and GPD1.

Sensors	UND	DMG3, SR50%		DMG3, SR70%		DMG3, SR90%	
	Peak Frequency [Hz]	Peak Frequency [Hz]	Frequency Reduction [%]	Peak Frequency [Hz]	Frequency Reduction [%]	Peak Frequency [Hz]	Frequency Reduction [%]
S-01	30.6	30.5	0.37	30.1	1.64	29.5	3.67
S-02	31.9	31.2	2.21	30.4	4.68	30.3	5.18
S-03	30.6	30.2	1.25	29.9	2.44	29.4	3.94
S-04	30.2	29.5	2.18	29.2	3.38	29.1	3.77
S-05	30.5	30.2	1.26	29.8	2.52	29.2	4.44
S-06	30.3	30.2	0.41	29.9	1.28	29.0	4.38

Figure 15 plots the marginal Hilbert spectrum for the undamaged and damaged scenarios grouped in a single subplot for each sensor and considering the group of damage GPD2. The peak frequencies values and the percentage of frequency reduction obtained for each damage scenario and

sensor are presented in Table 6. All values shown in this table decrease when damage occurs. Again, the peak frequency steadily decreases as the damage depth increases in all sensors. Therefore, all sensors can detect the extension of damage.

It is also noticeable that, the largest decreases in frequencies occurs in sensor S-03 and S-04 which are the closest to where damage occurs. In this case, the method is able to detect, locate and quantify (in terms of extension) the damage. In conclusion, according to the results from MHS, damage can be identified, located and quantified both in extension and intensity.

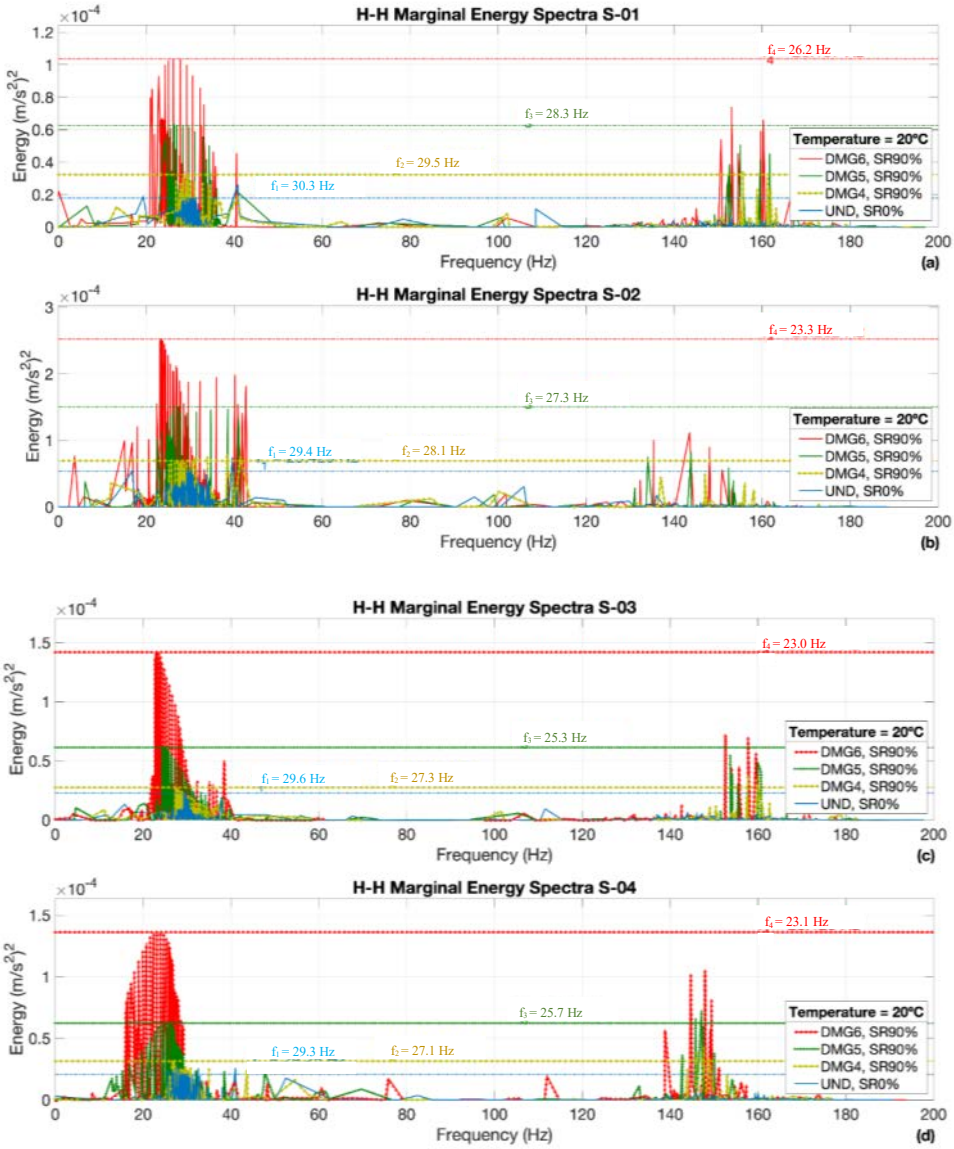

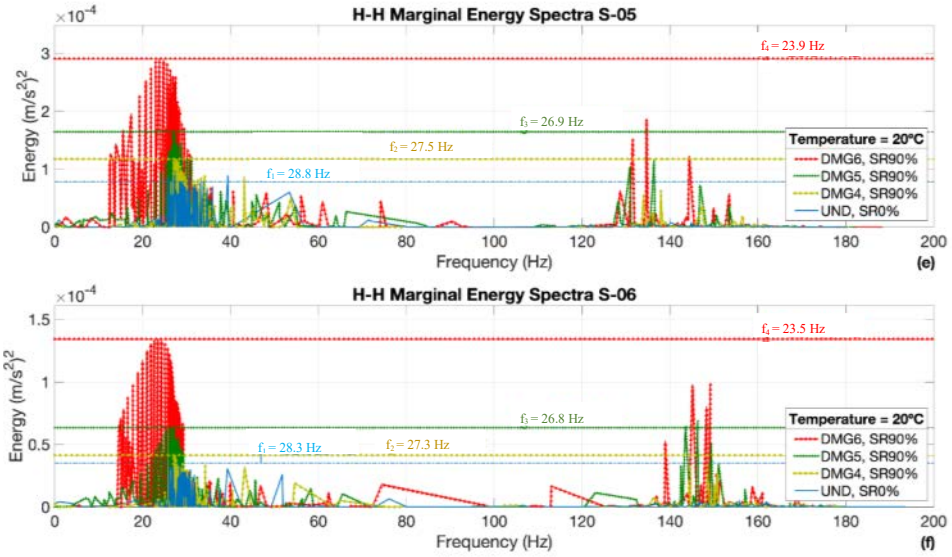

Figure 15. Marginal Hilbert Spectra for all sensors and for GPD2.

Table 6. Peak frequencies values using ICEEMDAN for all sensors and GPD2.

Sensors	UND	DMG4, SR90%		DMG5, SR90%		DMG6, SR90%	
	Peak Frequency [Hz]	Peak Frequency [Hz]	Frequency Reduction [%]	Peak Frequency [Hz]	Frequency Reduction [%]	Peak Frequency [Hz]	Frequency Reduction [%]
S-01	30.3	29.5	2.61	28.3	6.92	26.2	15.66
S-02	29.4	28.1	4.81	27.3	7.79	23.5	25.02
S-03	29.6	27.3	8.13	25.3	16.94	23.0	28.49
S-04	29.3	27.1	8.09	25.7	13.77	23.1	26.46
S-05	28.8	27.5	4.82	26.9	7.05	23.9	20.68
S-06	28.3	27.3	3.69	26.8	5.74	23.5	20.57

4.1.4 Instantaneous phase difference

As explained in section 2.2, the sum of the instantaneous phase angle for each meaningful IMF represents the total number of rotations of the acceleration signal in the complex plane. Then, the instantaneous phase angle is unwrapped with radian phases to obtain a monotonously increasing phase for all time t, $\theta(t)$, representing the phase of the travelling structural waves of the acceleration signals (Salvino et al., 2014). On the other hand, the instantaneous phase difference is the instantaneous phase relative to a reference point, $\phi_p(t)$ representing the changes in wave speed through each individual structural element (Salvino et al., 2014). Therefore, when damage occurs the amplitude increases, the wave speed reduces and hence the phase difference decreases. In addition, according to the references (Kunwar et al., 2013; Salvino et al., 2003; Pines & Salvino, 2002), the values of the instantaneous phase difference change as the damage are produced and this in turn modifies the speed and the path that the energy travels through the structure. In addition, this parameter is very convenient because does not include vibration amplitude for damage detection (Kunwar et al., 2013). Hence, time-dependant phase difference is used as a damage sensitive feature.

Sensor S-06 is chosen as the reference point as it is located far away from the damage zone leading to larger visibly phase difference values at all times.

Figure 16 depicts the instantaneous phase difference, $\phi_P(t)$, for the undamaged and damaged scenarios of GPD1 at each sensor. It clearly shows a decrease of the phase difference in all sensors due to the presence of damage in the system. It can be also observed how the values reflect the severity of damage inferred by different values of the percentage of stiffness loss as the graph for the most severe damage scenario DMG3, SR90% tends to be located below the other damage configurations. This is more evident at 1.7 seconds for sensors S-01, S-02 and S-03, just at the exact time when the vehicle passes over the damaged zone. In addition, at this point in time, the IP difference suddenly increases, what gives an indication on where the damage is located. The shapes of the IP difference corresponding to sensors S-01, S-02 and S-03 differ from the ones in sensors S-03, S-04, S-05 due to the number and shape of the IMFs selected for the application of the HHT-damage detection method, as seen in Figure 12. In summary, the phase difference from different sensors can detect, locate and quantify (in terms of intensity) the damage.

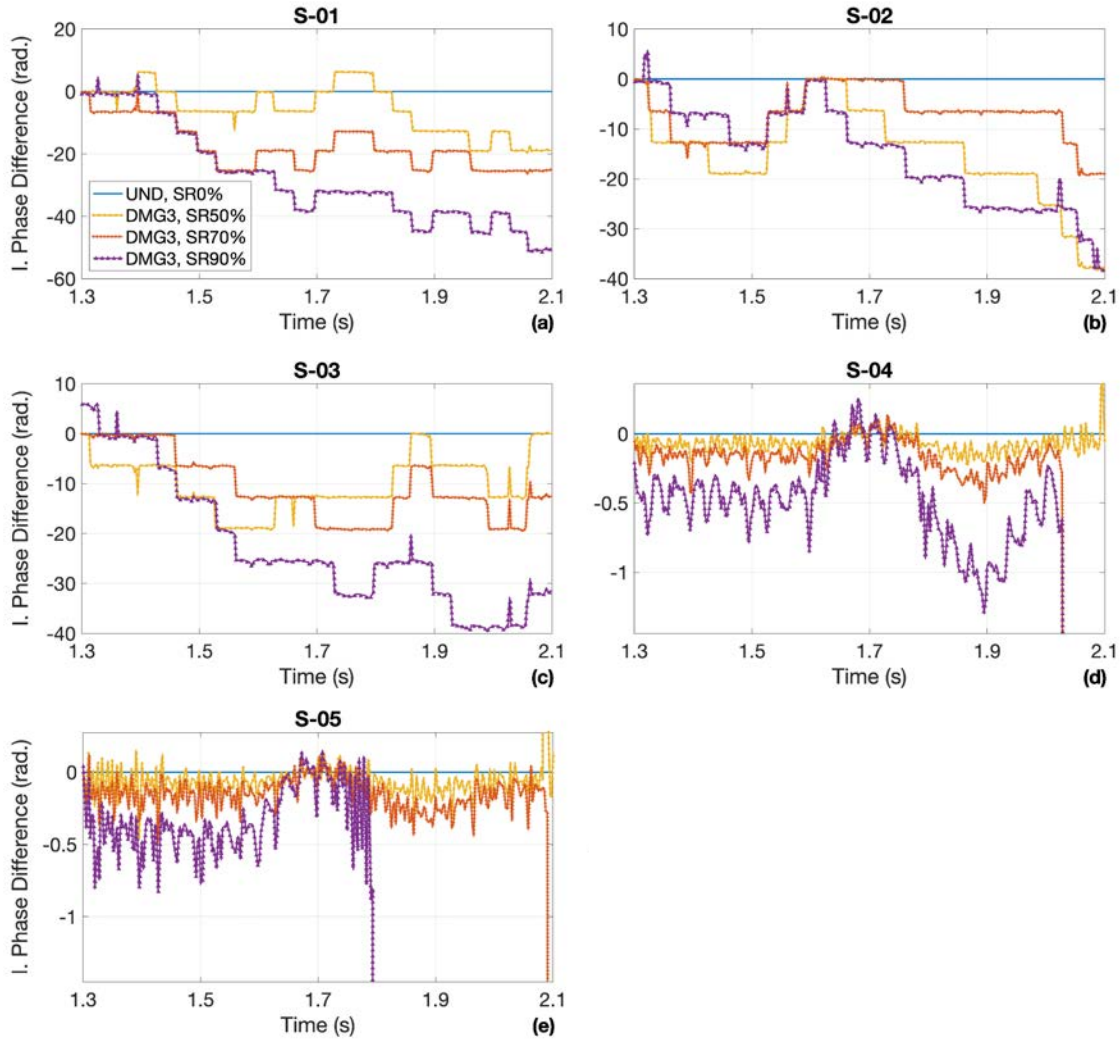

Figure 16. Instantaneous phase difference for each sensor and damage scenario corresponding to GPD1.

Figure 17 plots the instantaneous phase difference for the undamaged and damaged scenarios of GPD2 at each sensor. Again, it clearly shows a decrease of the phase difference for damaged states compared with the healthy condition, in all sensors. However, none of them is able to detect the effect of damage depth (damage extension) as there is not a clear trend of one curve above or below the other. Also, there is not a clear change in the curves after 3.4 seconds, when the moving load passes through the damage zone at the intermediate support. Therefore, in this case, all sensors indicate a successful damage detection, but none of them detects damage location and reflects how the damage extension grows.

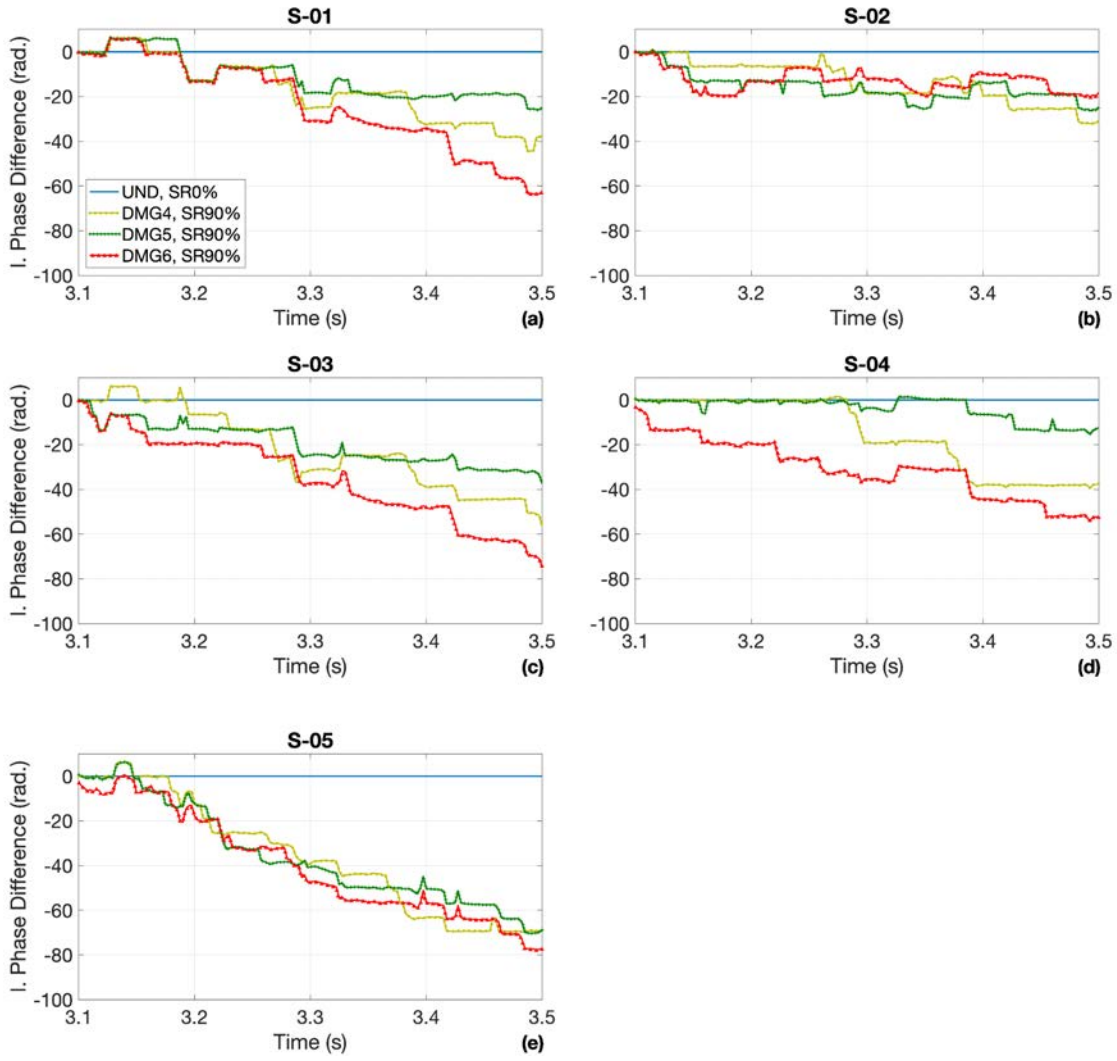

Figure 17. Instantaneous phase difference for each sensor and damage scenario corresponding to GPD2.

4.2 Steel arch bridge

After the promising results for damage detection, location and quantification (both in extension and severity) obtained for the numerical model, the next step is to check this performance in the case of a real bridge. In this sense, Figure 18 shows the superposition of vertical vibration data of three

runs recorded by all the sensors (A1,…,A8) for each damage scenario. Sensors 3 and 4 are exactly on the position where the severe and critical damages occurred, and, sensor 1 is further away from all damages. Figure 18 shows data for 15 runs over 670-s time and the data analysis was obtained for each run separately, that is, time starts and ends at zero during forty seconds for each run respectively, as shown in Figure 9. However, only the first 10 seconds of each run corresponding to the forced vibration part when the vehicle is within the bridge is considered in the analysis.

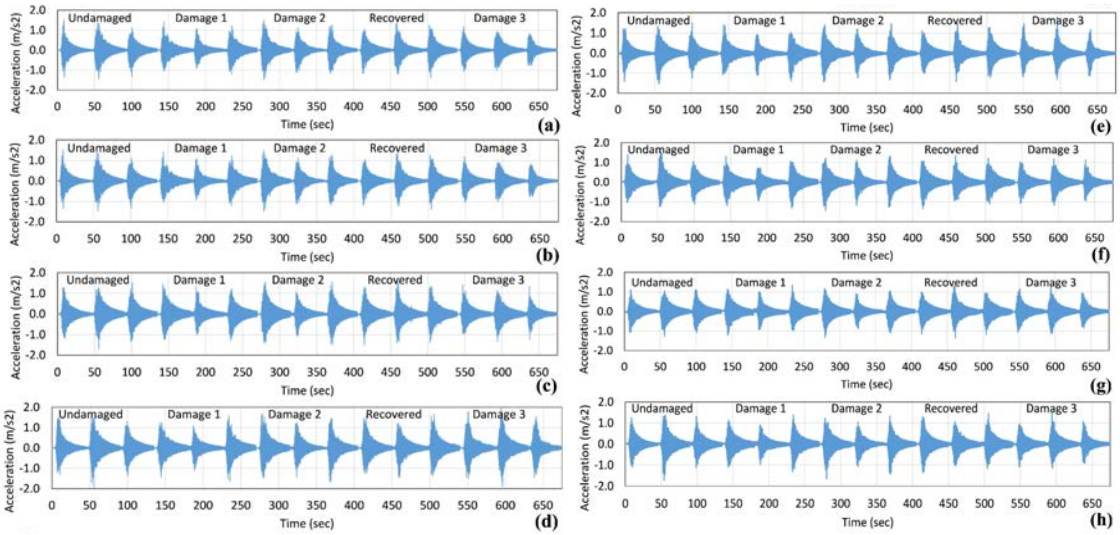

Figure 18. Steel truss bridge vertical acceleration data for 15 runs (a) sensor 1 (b) sensor 2 (c) sensor 3 (d) sensor 4 (e) sensor 5 (f) sensor 6 (g) sensor 7 (h) sensor 8.

4.2.1 Hilbert spectral analysis

(Moughty & Casas, 2018; Delgadillo & Casas, 2021) obtained the Hilbert Spectrum for this bridge in a previous study. However, as explained there, it was difficult to ascertain changes in structural behaviour from such representation in the case of this bridge and only those sensors closer to the damage showed a noticeable change between the original and damaged conditions. The time-frequency analysis presented in the previous studies (Kunwar et al., 2013; Moughty & Casas, 2018; Delgadillo & Casas, 2021) just gives an initial indication for damage identification. A more quantitative representation, so-called Instantaneous Vibration Intensity (IVI), obtained from the instantaneous frequencies and amplitudes, was proposed as a damage signature and its applicability in the detection of damage through the definition of the so-called Cumulative Difference Ratio (CDR) was demonstrated in the investigation (Moughty & Casas, 2018). Preliminary results were also shown in Delgadillo & Casas, 2021 about the feasibility of new damage indicators as the marginal Hilbert spectrum and the phase difference. This new damage features are further and fully investigated in this paper with the information gathered in all sensors.

4.2.2 Marginal Hilbert spectrum

Kim et al. 2014, developed an investigation concerning the first several mode shapes and natural frequencies of the bridge, identifying the first fundamental frequency as 2.98 Hz. In this regard, the Hilbert marginal spectra is used and studied herein like a potential damage parameter and the first frequency peak obtained is around 3.0 Hz for all sensors and artificial damage levels. The Hilbert marginal spectral (log-log scale) for sensors 1 to 8 are shown in Figures 19 to 21. Table 7 summarizes all first peak frequencies around 3 Hz obtained from those figures.

For sensor 1 located away from damages, the Hilbert marginal spectra show a very narrow and constant frequency peak at 3.0 Hz in the undamaged condition (Figure 19 a). This first measured peak frequency is close to the natural frequency of the bridge determined by several authors (Delgadillo & Casas, 2020; Chang et al., 2016; Moughty & Casas, 2018). Also Figure 19 a depicts the damages consequently applied in the member located at mid-span, and the peak frequency decreases as the damage is more severe (2.82 Hz and 2.72 Hz for damage 1 and damage 2 respectively). Furthermore, in the recovered state the frequency increases slightly (2.92 Hz). However, damage 3 (DMG03) produces an increase in the peak frequency (3.20 Hz), which physically does not indicate the presence of damage. Similarly, sensor 2 does not show a clear pattern in the frequency changes that could be correlated to the presence of damage (Figure 19 b).

Table 7. Peak frequency values spectrum using ICEEMDAN for sensors 1 to 8.

Damage states	Frequency (Hz)								Frequency reduction (%)		
	sensor1	sensor2	sensor3	sensor4	sensor5	sensor6	sensor7	sensor8	sensor3	sensor4	
Baseline	3.00	3.10	3.00	3.00	3.04	2.75	2.88	3.00			
Damage 01	2.82		2.90	2.82	2.84	2.89	2.72	2.97	3.40	6	5
Damage 02	2.72		2.92	2.70	2.72	2.81	2.62	2.81	3.10	10	9
Recovered	2.92	2.84	2.90	2.95	2.88	3.02	2.81	3.40	3	2	
Damage 03	3.20		2.85	2.94	2.50	2.95	2.91	2.98	2.92	2	17

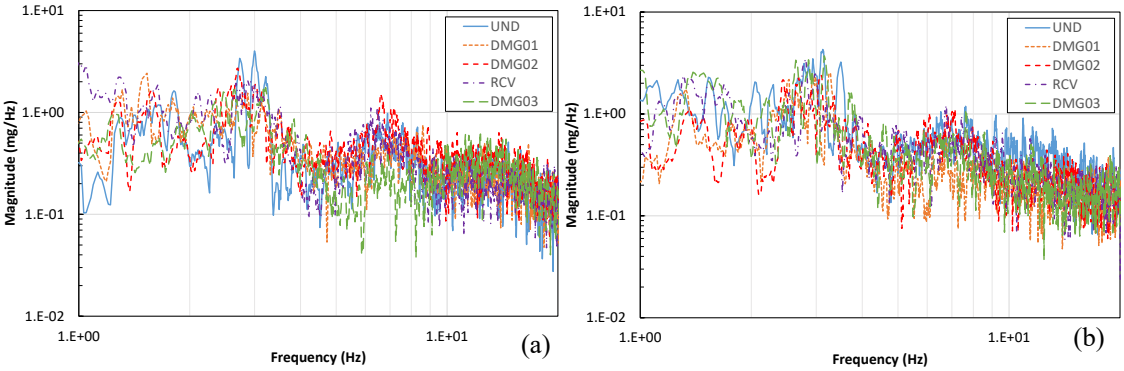

Figure 19. Marginal Hilbert spectra using ICEEMDAN (a) sensor 1 (b) sensor 2.

A completely different behaviour is observed for sensors 3 and 4 (see Figure 20 and table 7). The percentage reduction for frequencies in sensor 3 from baseline to damage levels 1, 2 and 3 are 6 %, 10 % and 2 % respectively. The percentage variation considering the baseline and recovered state (RCV) is very small. The results in this sensor are fully correlated with the damages. In fact, DMG01 and DMG02 are provoked in the member where sensor 3 is located. However, DMG03, being of the same order as DMG02 shows a lower frequency reduction due to the distance between the damaged member and the sensor location. Also, as seen in the case of the numerical model, the reduction in frequency is related to the severity of the damage (compare the value of 6% and 10 % reduction with the fact that the first value corresponds to half-cut of the member, and the second to the full cut). For sensor 4, from baseline to damage 1, 2 and 3 the reduction is 5%, 9% and 17% respectively, which is also fully correlated with the extent, intensity (5 % value for half-cut compared to 9 % for full cut) and location of damage (sensor 4 is located just where damage 3 is present).

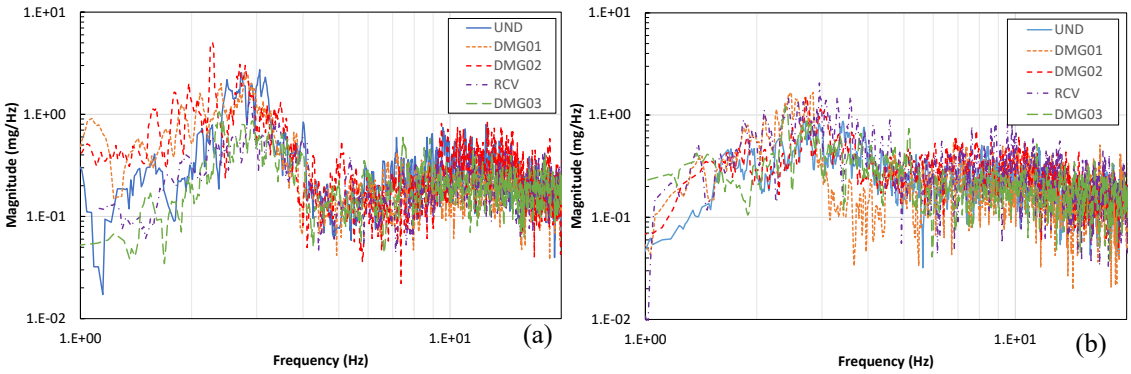

Figure 20. Marginal Hilbert spectra using ICEEMDAN (a) sensor 3 (b) sensor 4.

Regarding the rest of the sensors (figure 21 and Table 7) the peak frequency values for baseline and the artificial damages range from 2.0 to 4.0 Hz and the frequency reduction does not present a clear and significant trend. The conclusion is that these sensors are not able to detect the damages as they occurred away and in the opposite side of their position. In conclusion, as was the case for the numerical model, the peak frequency values obtained from the MHS, are a good damage indicators, not only to detect the damage but also to find its location and to guess its intensity.

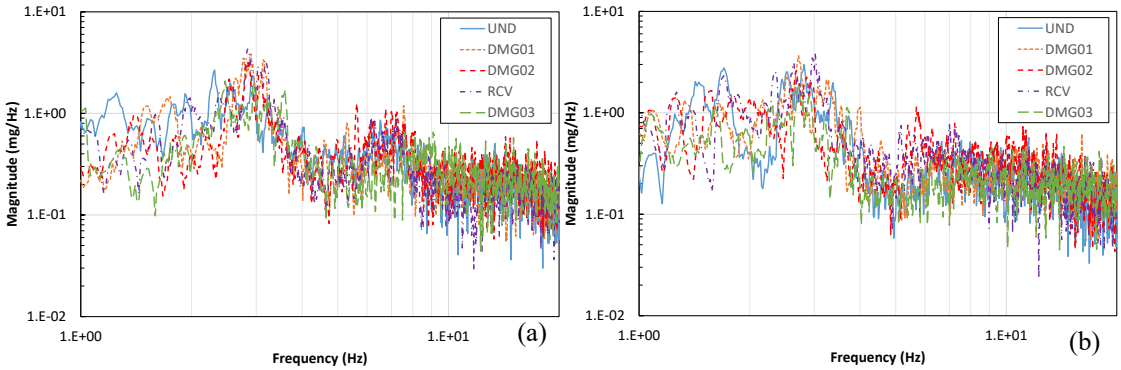

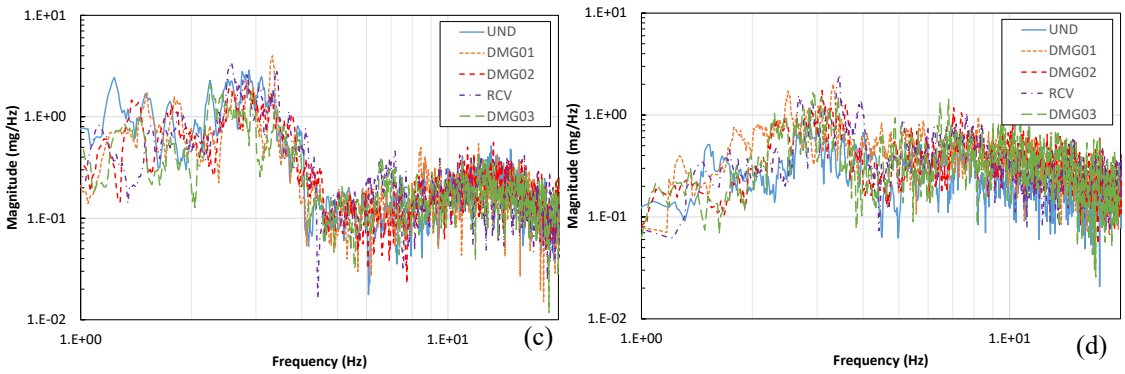

Figure 21. Marginal Hilbert spectra using ICEEMDAN (a) sensor 5 (b) sensor 6 (c) sensor 7 (d) sensor 8.

4.2.3 Instantaneous phase difference

A sensor in the bridge (sensor 1) is selected as reference, and the phase difference at all locations (sensors 1 to 8) with respect to the reference point are calculated using the Equation (3) (Figures 22 and 23). The phase difference is obtained as the mean of 3 different runs for each damage scenario.

Figure 22 (a) shows the results for sensor 3. The phase difference values on the bridge are significantly lower when damage is present in comparison with the healthy condition (baseline). In the beginning (0-1.0 s approximately), the phase difference values for damage 1 and 2 decrease rapidly in comparison with the baseline. DMG2 gives larger reduction earlier in time and the phase difference is always higher than for DMG1, as it should be, confirming, as in the case of the numerical case study, that this damage indicator is also sensible to the intensity of damage. At around 5 s, when the vehicle passes over the exact location of sensor 3 (close to damage 2), the phase difference values suffer the largest reduction. In addition, the recovered state (RCV) is close to baseline, which correctly indicates no damage present. DMG3 is almost not noticeable at this sensor because of its location far from where damage occurs.

Figure 22 (b) corresponds to sensor 4. The results show a similar trend. For example, when damage 3 occurs, the values have a greater decay in comparison with the baseline. In the recovered state (RCV), the behaviour is clearly evident since the values follow the path of the baseline. The maximum difference for damage 3 occurs at the time around 7 s, just when the vehicle is close to the sensor 4. Therefore, both sensors indicate a successful damage location. Again, here more intensity of damage (DMG01 and DMG02) derives on larger phase differences.

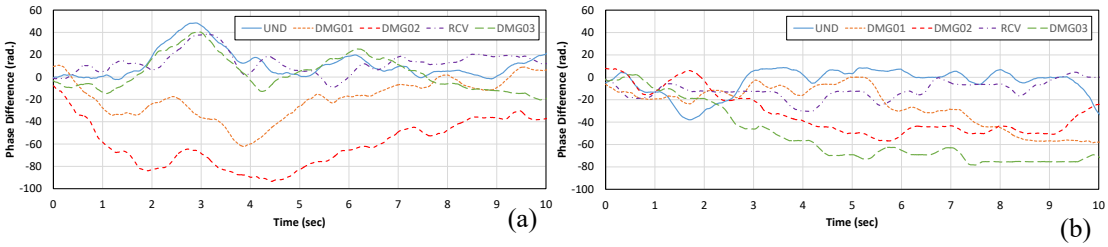

Figure 22. Mean phase difference values using ICEEMDAN (a) sensor 3 (b) sensor 4.

The rest of the sensors (Figure 23) unlike sensors 3 and 4, they do not show any clear trend with damaged and recovered state present in the bridge as they are located far from the damaged area. In conclusion, also in this case, the phase difference shows a good performance in detecting, localizing and quantifying the damage in terms of intensity. Regarding the quantification of the extension, unfortunately the damage scenarios do not provide this possibility as they are all produced in only a cross-section.

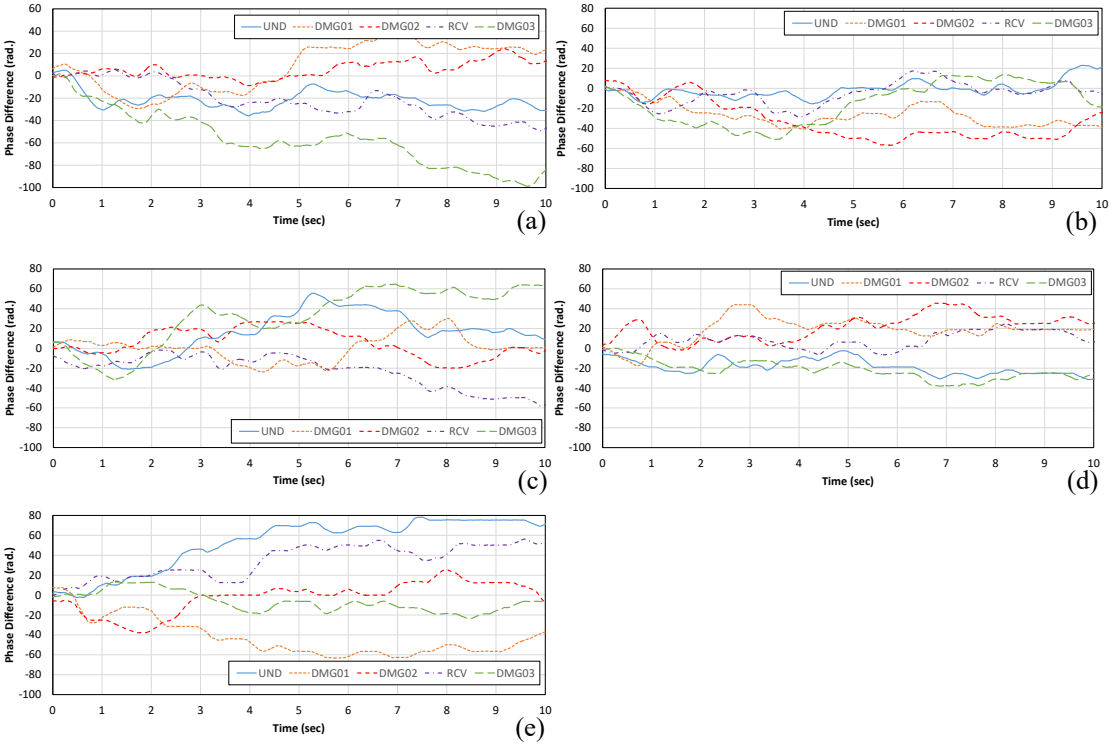

Figure 23. Mean phase difference values using ICEEMDAN (a) sensor 2 (b) sensor 5 (c) sensor 6 (d) sensor 7 (e) sensor 8.

5. Conclusions

Two parameters obtained from the HHT, the marginal Hilbert spectrum (MHS) and the instantaneous phase difference (IPD) are proposed as damage indicators for bridges under traffic loads, where recorded data is characterized by high non-linearity and non-stationarity. To derive accurate results using HHT, the paper proposes signal analysis and feature extraction through an

improved EMD named Improved Completed Ensemble Empirical Mode Decomposition with Adaptive Noise (ICEEMDAN). This method has two major advantages in the decomposition of signals: the avoidance of the spurious modes and the reduction in the amount of noise contained in the modes

To verify the efficiency of the ICEEMDAN-HHT method and the feasibility of the marginal Hilbert spectrum (MHS) and instantaneous phase difference (IPD) as damage indicators, a numerical model of a bridge and a real steel arch bridge subjected to traffic loading were used to analyse different damaged states. Results for damage detection obtained in both cases are very satisfactory. On one hand, for all sensors, the peak frequencies extracted from the Hilbert marginal spectrum are reduced when damage occurs due to stiffness loss. On the other hand, all sensors detect a reduction of the instantaneous phase difference when damage occurs due to the decrease in the wave speed of the response measurements. In addition, those sensors located closer to the zones where damage occurs show a more noticeable reduction than the sensors placed more far away. Both, in the numerical case study and in the real bridge, the results show that the MHS is able not only to detect and localize the damage, but also to ascertain the extension and intensity of the damage. In the case of the IPD, this damage indicator correctly detected, localized and quantified the intensity of the damage, but not its extension. Therefore, the spectral peak frequency and the instantaneous phase difference have shown as useful features to identify, locate and quantify damage in bridges under operational loads. The main advantages of the two proposed damage features are an algorithm easy to program and intuitive as well as the possibility to be obtained from load tests in the bridge since they are well suited for transient signals. As disadvantages, in the case of the MHS, in certain cases, it could be difficult to set a clear peak frequency. This fact could negatively affect the calculation of the percentage of frequency reduction leading to a wrong comparison of the results obtained for different damage scenarios. In the case of IPD, the results may depend on the number of Intrinsic Modes Functions (IMFs) selected and their importance in the overall dynamic response of the bridge. Therefore, it is relevant to always consider the most significant and representative IMFs produced by applying the HHT.

Acknowledgements

The first author acknowledges the financial support received from Peruvian Ministry of Education with the Bicentennial Generation Scholarship (PRONABEC program) for the great support on his PhD studies. The authors wish to express their sincere gratitude to Prof. Eleni Chatzi, ETH Zurich, for providing the detailed numerical bridge data. The authors also thank the Prof. Chul-Woo Kim, Kyoto University, for having granted access to the experimental datasets of the steel arch bridge.

References

[1] Chang, K. C., & Kim, C. W. (2016). Modal-parameter identification and vibration-based damage detection of a damaged steel truss bridge. *Engineering Structures*, *122*, 156-173.

[2] Chen, B., Zhao, S. L., & Li, P. Y. (2014). Application of Hilbert-Huang transform in structural health monitoring: a state-of-the-art review. *Mathematical Problems in Engineering*, *2014*.

[3] Chopra, A. K. (2017). Dynamics of structures. theory and applications. *Earthquake Engineering*.

[4] Chowdhury, I., & Dasgupta, S. P. (2003). Computation of Rayleigh damping coefficients for large systems. *The Electronic Journal of Geotechnical Engineering*, *8*(0), 1-11.

[5] Clough, R. W., & Penzien, J. (1975). Dynamics of Structures. McGraw-Hill.

[6] Colominas, M. A., Schlotthauer, G., & Torres, M. E. (2014). Improved complete ensemble EMD: A suitable tool for biomedical signal processing. *Biomedical Signal Processing and Control*, *14*, 19-29.

[7] Delgadillo, R., M., & Casas, J. R. (2019). SHM of Bridges by Improved Complete Ensemble Empirical Mode Decomposition with Adaptive Noise (ICEEMDAN) and Clustering. In proceedings *Enabling Intelligent Life-cycle Health Management for Industry Internet of Things (IIOT) 2019*.

[8] Delgadillo, R. M., & Casas, J. R. (2020). Non-modal vibration-based methods for bridge damage identification. *Structure and Infrastructure Engineering*, *16*(4), 676-697.

[9] Delgadillo, R., M., & Casas, J. R. (2021). Damage detection in a real truss bridge using Hilbert-Huang Transform of transient vibrations. 10th International Conference on Bridge Maintenance, Safety and Management (IABMAS 2020), 11 – 15 April 2021, Sapporo Convention Center, Japan (pp.1-8).

[10] Diez, A., Khoa, N. L. D., Alamdari, M. M., Wang, Y., Chen, F., & Runcie, P. (2016). A clustering approach for structural health monitoring on bridges. *Journal of Civil Structural Health Monitoring*, *6*(3), 429-445.

[11] Entezami, A., Sarmadi, H., Behkamal, B., & Mariani, S. (2020). Big data analytics and structural health monitoring: a statistical pattern recognition-based approach. *Sensors*, *20*(8), 2328.

[12] Huang, N.E. et al.(1998). The empirical mode decomposition and the Hilbert spectrum for nonlinear and non-stationary time series analysis. Proceedings of the Royal Society of London. Series A: mathematical, physical and engineering sciences, vol. 454, no 1971, p. 903-995.

[13] Huang, N. E., Long, S. R., & Shen, Z. (1996). The mechanism for frequency downshift in nonlinear wave evolution. *Advances in applied mechanics*, *32*, 59-117C.

[14] Kim, C. W., Chang, K. C., Kitauchi, S., McGetrick, P. J., Hashimoto, K., & Sugiura, K. (2014). Changes in modal parameters of a steel truss bridge due to artificial damage. In *Proceedings of the 11th International Conference on Structural Safety and Reliability, (ICOSSAR)* (pp. 3725-3732).

[15] Kunwar, A., Jha, R., Whelan, M., & Janoyan, K. (2013). Damage detection in an experimental bridge model using Hilbert–Huang transform of transient vibrations. *Structural Control and Health Monitoring*, *20*(1), 1-15.

[16] Kunwar, A. (2017). *System Identification Free Damage Localization* (Doctoral dissertation, Northeastern University).

[17] Li, D., Cao, M., Deng, T., & Zhang, S. (2019). Wavelet packet singular entropy-based method for damage identification in curved continuous girder bridges under seismic excitations. *Sensors*, *19*(19), 4272.

[18] Moughty, J. J., & Casas, J. R. (2017). A state of the art review of modal-based damage detection in bridges: Development, challenges, and solutions. *Applied Sciences*, *7*(5), 510.

[19] Moughty, J. J., & Casas, J. R. (2018, October). Damage identification of bridge structures using the Hilbert-Huang transform. In *Life Cycle Analysis and Assessment in Civil Engineering: Towards an Integrated Vision: Proceedings of the Sixth International Symposium on Life-Cycle Civil Engineering (IALCCE 2018)* (pp. 28-31).

[20] Newmark, N. M. (1959). A method of computation for structural dynamics. *Journal of the engineering mechanics division*, *85*(3), 67-94.

[21] Oñate, E. (2013). *Structural analysis with the finite element method. Linear statics: volume 2: beams, plates and shells*. Springer Science & Business Media.

[22] Pines, D. J., & Salvino, L. W. (2002, July). Health monitoring of one-dimensional structures using empirical mode decomposition and the Hilbert-Huang transform. In *Smart Structures and Materials 2002: Smart Structures and Integrated Systems* (Vol. 4701, pp. 127-143). International Society for Optics and Photonics.

[23] Rao, S. S. (2017). *The finite element method in engineering*. Butterworth-heinemann.

[24] Reddy, D. M., & Krishna, P. (2015). Innovative method of empirical mode decomposition as spatial tool for structural damage identification. *Structural Control and Health Monitoring*, *22*(2), 365-373.

[25] Roveri, N., & Carcaterra, A. (2012). Damage detection in structures under traveling loads by Hilbert–Huang transform. *Mechanical Systems and Signal Processing*, *28*, 128-144.

[26] Roy, T. B., Banerji, S., Panigrahi, S. K., Chourasia, A., Tirca, L., & Bagchi, A. (2019). A novel method for vibration-based damage detection in structures using marginal Hilbert spectrum.

In *Recent Advances in Structural Engineering, Volume 1* (pp. 1161-1172). Springer, Singapore.

[27] Salvino, L. W., Pines, D. J., & Fortner, N. A. (2003, September). Extracting instantaneous phase features for structural health monitoring. In *Proceedings of the 4 th International Workshop on Structural Health Monitoring, Stanford University* (pp. 666-674).

[28] Salvino, L. W., Pines, D. J., Todd, M., & Nichols, J. M. (2014). EMD and instantaneous phase detection of structural damage. In *Hilbert–Huang Transform and Its Applications* (pp. 301-336).

[29] Shi, C. X., Luo, Q. F., & Shi, W. X. (2005). Hilbert-Huang transform based approach for structural damage detection. *Journal of TongJi University*, *33*(1), 16-20.

[30] Spiridonakos, M. D., Chatzi, E. N., & Sudret, B. (2016). Polynomial chaos expansion models for the monitoring of structures under operational variability. *ASCE-ASME Journal of Risk and Uncertainty in Engineering Systems, Part A: Civil Engineering*, *2*(3), B4016003.

[31] Tatsis, K., & Chatzi, E. (2019). A numerical benchmark for system identification under operational and environmental variability. In *8th International Operational Modal Analysis Conference (IOMAC 2019)*.

[32] Wining, M., & Klein, M. (1996, March). Modal selection by means of effective masses and effective modal forces an application example. In *Proc. Conf. on Spacecraft Structures, Materials & Mechanical Testing, The Netherlands* (pp. 751-759).

[33] Wu, S. P., Qin, G. J., Zou, J. H., & Sun, H. (2009). Structure health monitoring based on HHT of vibration response from unknown excitation. In *Proceedings of the 8th International Symposium on Test and Measurement* (Vol. 1, p. 6).

[34] Yang, Y. B., Li, Y. C., & Chang, K. C. (2014). Constructing the mode shapes of a bridge from a passing vehicle: a theoretical study. *Smart Structures and Systems*, *13*(5), 797-819.

6. Appendix

Table A.1. The first 20 natural frequencies with their corresponding effective modal mas participation factors (expressed in %).

Mode	Natural frequency, f [Hz]	Mode Shape Description	Participation Factor		Effective Modal Mass Participation Factor	
			L_{ix} (kg)	L_{iy} (kg)	F_{ix} (%)	F_{iy} (%)
1	18.6	1st asymmetric longitudinal translation	-97.057	0.000	~ 100	4.013E-22
2	26.1	1st symmetric vertical bending	-0.095	0.000	9.506E-05	1.418E-19
3	28.9	1st asymmetric vertical bending	0.000	81.559	2.507E-22	70.61
4	74.1	2nd symmetric vertical bending	0.100	0.000	1.066E-04	2.216E-29
5	80.5	2nd asymmetric vertical bending	0.000	-2.758	8.864E-21	0.0807

6	132.5	1st symmetric longitudinal translation	0.000	0.607	2.816E-29	3.912E-03
7	146.1	3rd symmetric vertical bending	0.009	0.000	7.779E-07	1.090E-32
8	156.0	3rd asymmetric vertical bending	0.000	33.739	1.541E-28	12.08
9	239.1	4th symmetric vertical bending	0.020	0.000	4.424E-06	1.768E-30
10	251.7	4th asymmetric vertical bending	0.000	-2.523	5.106E-27	0.0676
11	262.9	2nd asymmetric longitudinal translation	0.016	0.000	2.884E-06	7.642E-26
12	349.5	5th symmetric vertical bending	-0.002	0.000	5.931E-08	3.546E-20
13	363.8	5th asymmetric vertical bending	0.000	20.924	1.104E-28	4.65
14	392.9	2nd symmetric longitudinal translation	0.000	0.325	3.969E-29	1.118E-03
15	473.9	6th symmetric vertical bending	0.008	0.000	6.145E-07	2.118E-28
16	489.0	6th asymmetric vertical bending	0.000	-2.293	9.258E-24	0.0558
17	523.8	3rd asymmetric longitudinal translation	0.018	0.000	3.350E-06	1.474E-22
18	609.4	7th symmetric vertical bending	-0.001	0.000	1.097E-08	7.214E-31
19	623.9	7th asymmetric vertical bending	0.000	-15.397	1.811E-27	2.52
20	654.3	3rd symmetric longitudinal translation	0.000	0.745	3.370E-27	5.893E-03
Sum					~ 100.00 %	~ 90.08%

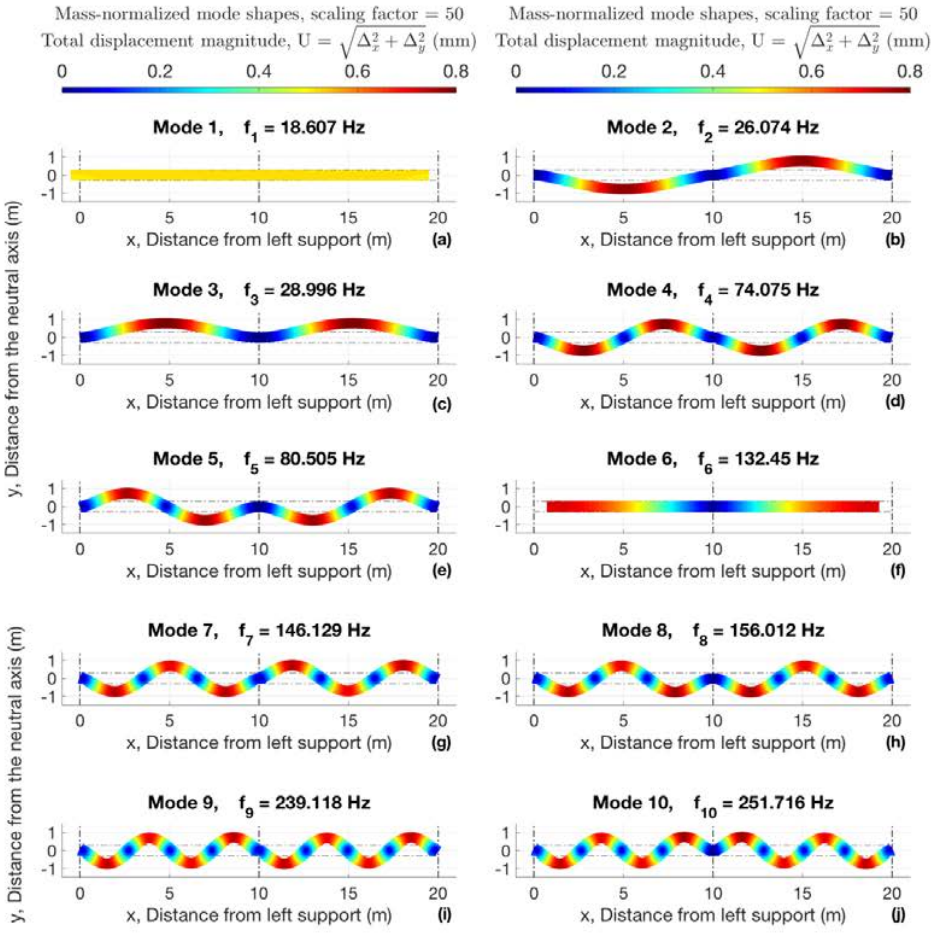

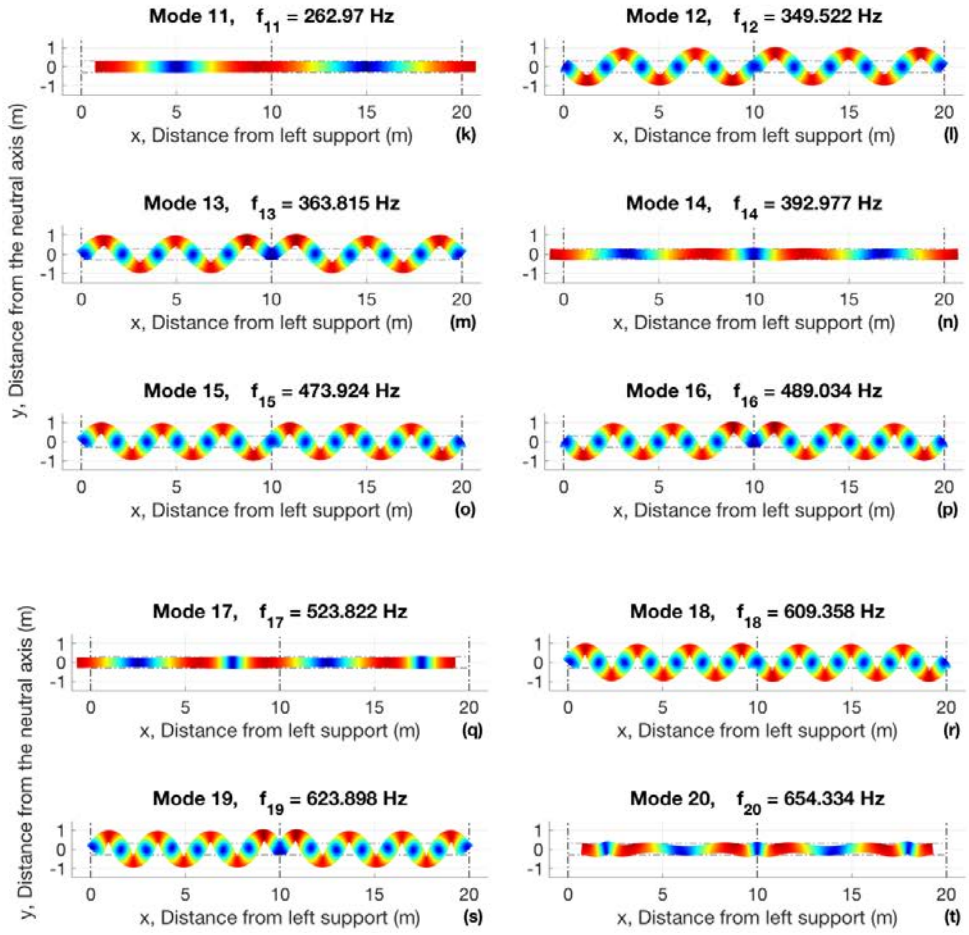

Figure A.1. The first 20 natural frequencies and mass-normalized mode shapes using a scaling factor of 50 to represent the magnitude of the total displacement vector, U (mm).

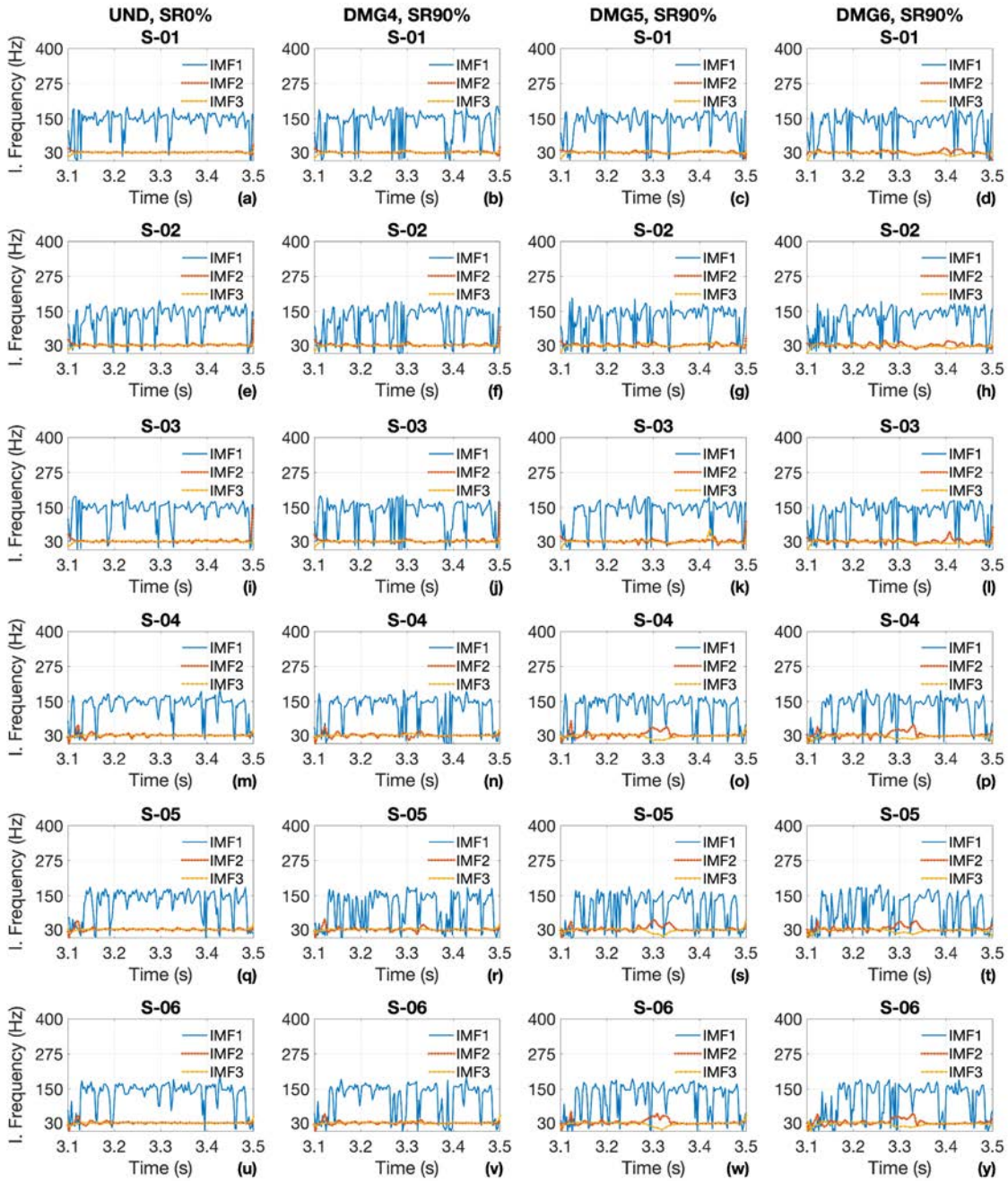

Figure A.2. Instantaneous frequency for all sensors and for Group of damage 2 (GPD2).

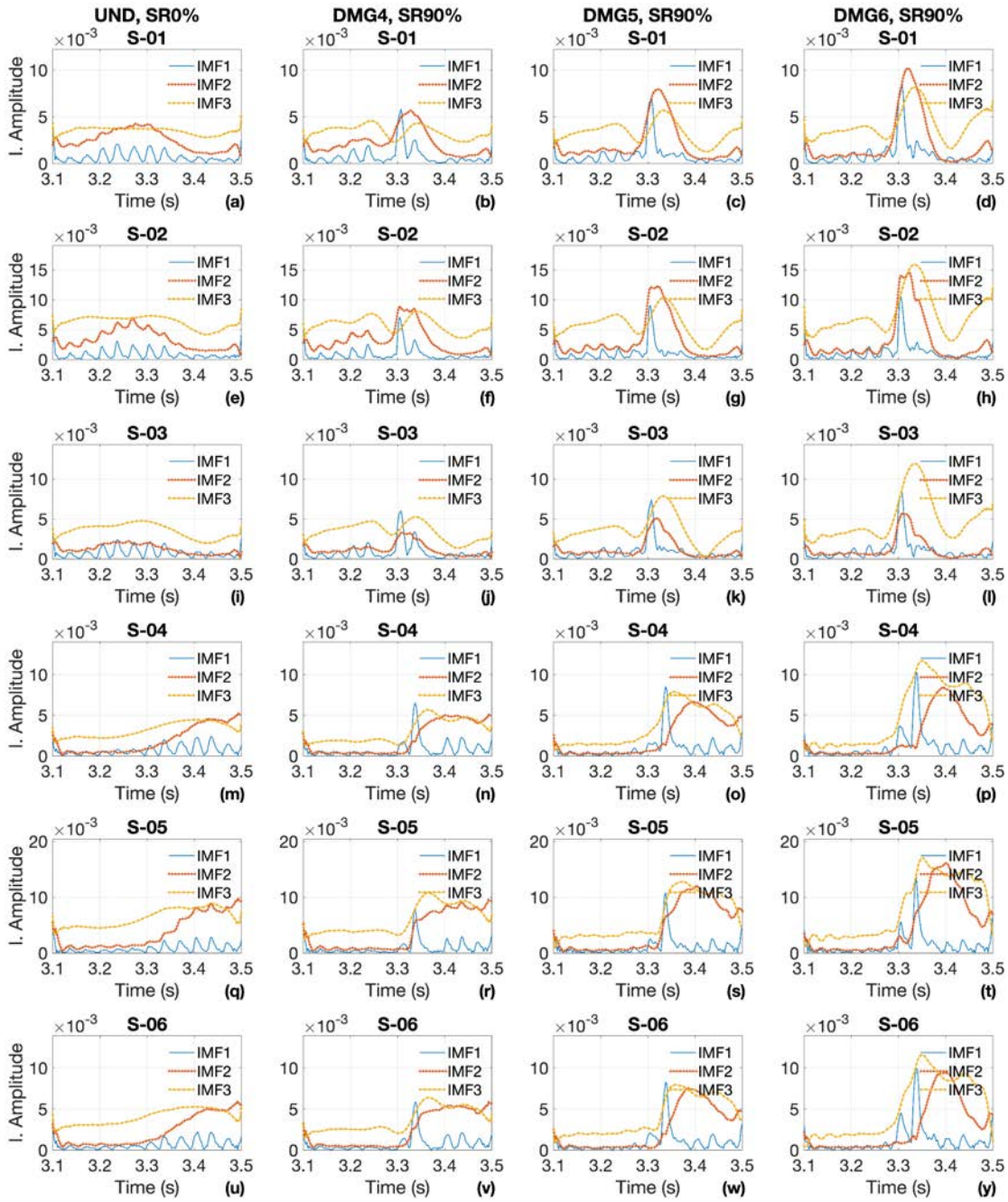

Figure A.3. Instantaneous amplitude for all sensors and for Group of damage 2 (GPD2).

5.3. Conference paper

A combined kernel-PCA with clustering analysis for bridge damage detection under changing environmental conditions

Published in Life-Cycle Civil Engineering: Innovation, Theory and Practice. CRC Press, IALCCE 2021. p. 1362-1370.

Rick M. Delgadillo [1], Joan R. Casas [1]

[1]Department of Civil and Environmental Engineering, Technical University of Catalonia (UPC), c/ Jordi Girona 1-3, 08034 – Barcelona, Spain

Realized: 27 – 30 October 2020, Shanghai, China

Abstract: Damage caused in bridges can be hidden by the service conditions mainly due to environment effects as temperature and traffic loading. The literature review indicates that the majority of investigations are limited since they do not consider these effects or they are applied under laboratory conditions and not to real bridges. The temperature effects on the natural frequencies of bridges have shown to be non-linear. In this context, this article presents a damage detection strategy considering a more robust kernel-based method (KPCA) which is the nonlinear extension of the principal component analysis (PCA) to take into account the environmental conditions of the bridge such as the non-linearity of the temperature effects in the natural frequencies. This method is combined with a clustering analysis in order to group the data with similar features both for undamaged and damaged conditions, and in this way the structural damages can be identified. The main contribution is a novel damage detection methodology based on advance statistical and machine learning algorithms to account for the non-linear environmental effects. The method is checked using measurements from the Z24 bridge, which was subjected to progressive structural damages while monitored for almost a year. The results show good performance of the proposed algorithm and highly reducing the computational cost.

Keywords: Kernel, symbolic data analysis, damage detection, environmental conditions, operational conditions.

1. Introduction

Bridge structures are present in all countries, regardless of culture, economic and geographical conditions. Almost 40 percent of the bridges in the world are at least a half century old and a lot vehicles cross structurally deficient bridges every day (Cardno 2016). In addition, they are in constant degradation due to operational and environmental changes. For this reason, a robust structural health monitoring (SHM) should be dedicated to maintaining and improving bridges and extending their service life.

During the past decades, several researchers have developed different techniques for damage detection using numerical and experimental model structures. However, difficulties have arisen in implementing them for structural health monitoring on real bridges. Delgadillo & Casas (2019) proposed novel empirical parameters for damage identification on two real bridges under different real conditions. Furthermore, the majority of vibration properties used as damage sensitivity features are affected by the changes due to the environmental factors (e.g. humidity, ambient temperature, wind), (Sohn 2006). According to (Farrar et al., 1997; Alampalli 1998; Peeters & Roeck 2001), the temperature plays an important role in the variation of vibration properties for bridge structures. It is shown that temperature can cause up to 5% - 10% variation in the natural frequencies of highway bridges, that can be confused by the changes produced by structural damages (Ko & Ni 2005).

Many researchers have developed algorithms increasingly sophisticated and with great performance for damage detection on bridges. For instance, (Figueiredo et al., 2012) proposed an approach to damage detection in two bridges considering the vibration response data like damage sensitive parameters (Output-only method). Firstly, several progressive damage tests carried out during one-year in a post-tensioned concrete box girder bridge called Z24 (Peeters & Roeck 2001), were analyzed. It was assumed that the bridge operates within its undamaged condition (baseline condition) under operational and environmental conditions. As a first step, the unsupervised learning stage was carried out to infer the heterogeneity of the data in different operational and environmental conditions. Then, the next step was to establish a procedure to incorporate prior knowledge of the baseline data into the damage detection process. A daily Damage Index (DI) was implemented, corresponding to the minimum Mahalanobis Squared-Distance (MSD) coefficient of two models with a defined threshold for the 95% confidence region. Therefore, the performance of the classifier was observed taking into account the existence of known damaged structural responses. Secondly, a supposed undamaged bridge called Tamar was evaluated. Since the real structural condition of the bridge was not known a priori, 50% of the observations were used to find the number of normal components. As a result, the multi-normal distribution indicated that the structure changes very little during the time and a good result of DI was obtained, that considering the four MSD together models with a confidence threshold of 95 %. (Yan et al., 2005) developed a comparison analysis between linear PCA and local PCA for damage identification in the Z24 bridge. This study considers the non-

linear cases, which can be encountered in the majority of real and complex structures. The comparison of the results obtained by linear PCA with those obtained by using local PCA shows two enhancements. (i) The anomaly present in a monitoring period disappears as the non-linearity is taken into account by the local PCA-based method. (ii) The novel index values increase slightly for damage states with respect to those in the reference state; it means that the local PCA-based method is more sensitive to the damage. (Reynders et al., 2014) developed an improved output-only method based on the KPCA in order to eliminate nonlinear operational influences and environmental conditions on Z24 bridge. For this reason, the authors used two parameters automatically determined from the learned model based on Gaussian KPCA. The results demonstrated satisfactory improvements in data normalization for damage identification. (Moughty & Casas 2017) assessed the performance of some outlier detection algorithms such as Principal Component Analysis (PCA) from a progressive damage in an Austrian bridge subject to ambient excitation. Moreover, the incorporation of an estimator called Minimum Covariance Determinate (MCD) improved the PCA performance significantly to identify and remove erroneous data from the training sets, and it reduces uncertainties caused by external sources of excitation.

Nowadays, Data mining have been employed in SHM field due to their powerful computational ability to detect damage in structural systems like bridges. It can be categorized as cluster analysis, group classification, prediction and association. Clustering is a set of multi-variable statistical analysis techniques and the most common unsupervised machine learning approach that finds hidden patterns or intrinsic structures in data. The purpose of clustering is to classify and identify the variables or objects into groups with related behavior (Bishop 2006), which is used in pattern recognition, image analysis and bioinformatics. There are basically two types of clustering techniques: hierarchical and non-hierarchical. Hierarchical clustering has two types: divisive (top-down) and agglomerative (bottom-up). For the second type, K-means, Principal Component Analysis (PCA), Gaussian Mixture Models (GMM), Support Vector Clustering (SVC) and Self-Organizing Maps (SOM) algorithms are the most representative examples for statistical modeling and feature classification in SHM (Santos et al., 2015a). (Figueiredo & Cross, 2013) developed algorithms based on PCA, Gaussian mixture models (GMMs) and MSD to model the main clusters that correspond to the normal or undamaged state conditions in the measured vibration data sets of Z24 bridge. Nonetheless, the PCA and MSD linear algorithms might not be appropriate for long-term monitoring as they are not able to model the nonlinear patterns from the baseline condition data during the training process, which leads to relatively high number of false alarms. Yu et al. (2013) adopted PCA and KPCA algorithms for data compression and the median values of principal components were defined for damage feature extraction in a six-bay truss bridge model. Afterwards, a fuzzy c-means (FCM) clustering algorithm is used to categorize these features for structural damage detection. This method could effectively identify the bridge damages simulated by loosening the bolted joints of the truss bridge structure. (Santos et al., 2013) implemented a new strategy to detect structural damage from vibration-data. The

authors proposed a cluster analysis to achieve baseline independence using the concept of symbolic data analysis to reduce raw vibration data through a statistical process able to detect damage in real-time. (Santos et al., 2015b) developed cluster algorithms with symbolic data to achieve a single-value novelty index (NI) able to detect structural changes in multi-sensor data-sets from a real bridge.

The present paper aims for damage detecting by an exhaustive analysis of the natural frequencies, estimated from acceleration time series. In order to achieve this objective, a promising strategy for SHM in changing environmental conditions like temperature variation is proposed. For this study, an improved machine learning algorithm named kernel principal component analysis (KPCA) was implemented. Likewise, a statistical clustering algorithm named *k*-means in conjunction with a cluster-based damage detection strategy is proposed.

2. Mathematical formulation

2.1. Covariance driven stochastic subspace identification

The covariance-driven stochastic subspace identification (SSI-COV), is one of the most robust methods applied in real civil structures for dynamic structural identification (Kvåle et al., 2015; Magalhaes et al., 2009). The basic idea was proposed by (Juang 1994), and is used to identify the modal parameters assuming the excitation as a white noise. Mathematically it can be written in its discrete form as:

$$x_{n+1} = Ax_n + w_n \tag{1}$$

$$y_n = Cx_n + v_n \tag{2}$$

Where x_n = discrete-time state vector at instant n; y_n = vector with the sampled outputs; A = discrete state matrix; C = discrete output matrix; and w_n = process noise; and v_n = measurement noise.

The starting point for the analysis of the SSI-COV method is the block-Hankel matrix H_i, where the sub-matrices represent the correlation between varying time shifts and all the measurement channels, as follows:

$$H_i = \begin{bmatrix} R_1 & R_2 & \cdots & R_i \\ R_2 & R_3 & \cdots & R_{i+1} \\ \vdots & \vdots & \ddots & \vdots \\ R_i & R_{i+1} & \cdots & R_{2i+1} \end{bmatrix} \tag{3}$$

In this matrix, *2i* represents the maximum number of time lags; and *i* = number of block rows. The following formula define the correlation matrices:

$$R_k = \frac{1}{N-i} \sum_{n=0}^{N-i-1} y_{n+k} . y_n^T \tag{4}$$

Where N = number of points of the time series.; Finally, the modal parameters are easily obtained from matrices A and C. (Magalhaes et al., 2009).

2.2. Kernel principal component analysis (KPCA)

The KPCA algorithm is the nonlinear extension of the linear principal component analysis (PCA) developed by (Schölkopf et al., 1998). This KPCA algorithm is a statistical tool commonly used to fit a nonlinear model to the features sensible to damages in the undamaged state. Besides, the model predictions and the observed features in a bridge structure are compared (Reynders et al., 2014).

Note that a training data matrix $X \in \sim^{mxn}$ is considered for normal condition data. Where n = feature vectors; m = environmental and operational factors when the bridge is undamaged. Moreover, $Z \in \sim^{kxn}$ represents a test data matrix, where k = number of feature vectors from the undamaged or/and damage states. The data normalization consists as follows: (i) the loadings matrix, U, is obtained from X; (ii) the test matrix Z is mapped onto the feature space $\sim^{r}$ and reversed back to the original space $\sim^{n}$, where r = number of factors or principal components. Finally, (iii) the residual matrix E is obtained as the difference between the original and the reconstructed test matrix.

For the feature classification, a feature vector f *(f = 1, 2,...,l)* is considered and its residual uncorrelated with environmental and operational conditions can be expressed as:

$$e_f = U_1 U_2^T \Phi(\mathrm{z}_f) \qquad (5)$$

Where U_1 = contains the r largest eigenvectors; U_2 = comprises the *(m - r)* shortest eigenvectors and the compact form $U = [U_1\ U_2]$ represents the eigenvectors matrix partitioned. Furthermore, $\Phi(z_f)$ represents a nonlinear mapping of the output sequence, z_f, onto a possible very high-dimensional.

Additionally, the r principal components can be obtained by test the minimal percentage of the variance Γ (0.99 can be adopted) to explain the variability in the matrix X (Reynders et al., 2014). Note that due high-dimensional in feature space of the KPCA, the Γ and r may be larger than the values used in linear PCA. Then, an eigenvector matrix A can be used in order to determine Φ.

$$U = \tilde{\Phi}\, A \qquad (6)$$

$$\tilde{\Phi} = \frac{1}{\sqrt{m}}\left[\Phi(\mathrm{x}_1)...\Phi(\mathrm{x}_m)\right] \qquad (7)$$

In general, all solutions are summarized in solve a standard eigenvalue problem as mentioned in equation 8, where Λ = diagonal matrix containing the ranked eigenvalues λ_i and K = kernel matrix expressed as equation 9.

$$KA = A\Lambda \qquad (8)$$

$$K = \tilde{\Phi}^{T} \tilde{\Phi} \in \sim^{mxm} \quad (9)$$

A kernel function can be represented by the inner product of the form $\Phi(x_i)^T \Phi(x_j)$ and a Gaussian kernel or radial basis function (RBF) defines a single parameter by the equation 10. Where $\sigma > 0$ is the bandwidth of the RBF kernel and can be obtained using the Shannon's information entropy in the inner product matrix K.

$$k(\mathrm{x}_i, \mathrm{x}_j) = \exp\left(-\frac{\left\| \mathrm{x}_i - \mathrm{x}_j \right\|^2}{2\sigma^2} \right) \quad (10)$$

Finally, as mentioned in (Reynders et al., 2012), the d_k parameter can be used as a damage indicator:

$$d_k = \left\| e_k \right\| = \sqrt{\Phi(\mathrm{z}_f)^T \tilde{\Phi} A_2 A_2^T \tilde{\Phi}^T \Phi(\mathrm{z}_f)} \quad (11)$$

2.3. Statistical classification and clustering method

Clustering is an unsupervised statistical data analysis method, which nowadays is widely used in several fields such as bioinformatics, data mining and pattern recognition. The basic idea involved in the clustering methods is their capability of classifying data objects into separated similar subsets (or clusters) (Bishop 2006). Unlike supervised machine learning algorithms, clustering techniques do not require the previously definition of training or reference data. They can understand the behavior of a data set and then try to obtain the most separated and compact set of clusters (Rendón et al., 2011). Whereby, mathematically it can be written by equation 12. Where a given partition containing K clusters is considered, $P_K = \{C_{1, \ldots,} C_K\}$; $c(i)$ = many-to-one allocation rule that assigns object i to cluster k, based on a dissimilarity measure d_{ij} defined between each pair of data objects, i and j.

$$W(\mathrm{P}_k) = \frac{1}{2} \sum_{k=1}^{K} \sum_{c(\mathrm{i})=\mathrm{k}} \sum_{c(\mathrm{j})=\mathrm{k}} d_{ij} \quad (12)$$

One of the most descriptive partitioning clustering algorithms is the k-means (Forgy 1965), which is used herein with a cluster-based damage detection developed by (Santos et al., 2016). The k-means is capable of automatically distinguish between undamaged and damaged bridge structural conditions. For this purpose, the equation 13 shows a damage parameter DC based on computing the average dissimilarity between clusters:

$$DC = \frac{1}{\mathrm{K}(\mathrm{K}-1)} \sum_{k=1}^{K} \sum_{\substack{c=1 \\ c \neq k}}^{K} d_{ck} \quad (13)$$

Where K = number of clusters defined with the highest global silhouette index (SIL) (Rousseeuw 1987); c and k are two of the K clusters; d_{ck} = Gowda-Diday dissimilarity parameter measured between their centroids (Gowda & Diday 1991). Furthermore, when the clusters are generated in undamaged condition, the k-mean algorithm can identify these groups clearly and will generate small values of DC. Conversely, if damages are presented, the k-means method generates separate clusters and therefore will generate large values of DC.

3. Case study – Z24 Bridge

The methodology proposed in this article will be demonstrated in the benchmark bridge called Z24 (Switzerland), shown in Figure 1(a). It was a post-tensioned concrete box girder bridge with a main span of 30 m and two side-spans of 14 m (Figure 1b). The Z24 bridge was demolished in 1998, but instead a railway near to the highroad was built. This bridge was monitored for approximately one year and a long-term continuous monitoring program between November 1997 and August 1998 was carried out. The bridge was monitored by a long-term continuous vibration system, where the data was acquired hourly through two kinds of measurements: ambient vibration response and environmental conditions. For this purpose, 16 acceleration sensors were used to measure the ambient vibration responses located in different points and directions, three of them were collocated on one of the piers and the rest in the deck, as shown in Figure 2(a). All accelerometers were programmed to collect the data in a sequence of 65,536 samples by hour. Additionally, 49 sensors to measure environmental conditions were installed, such as humidity, air temperature, wind characteristics, bridge expansion soil temperatures at the boundaries and bridge concrete temperatures (Peeters & Roeck 2001). Likewise, the measurements of the environmental variables were obtained each hour. The Figure 2(b) shows the temperature sensor in the deck. The foundation temperatures were measured near one of the piers.

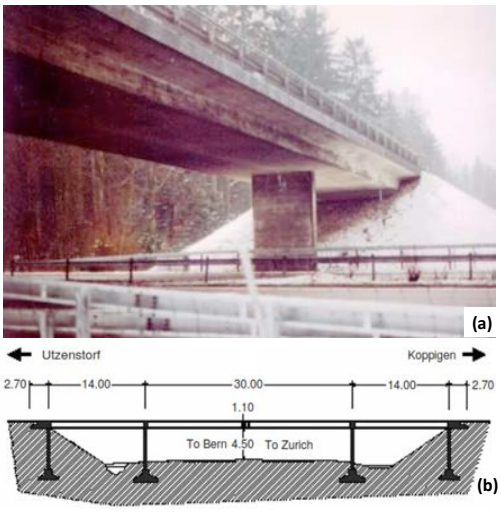

Figure 1. The Z-24 Bridge (a) side view and (b) longitudinal section (Adapted from Peeters & Roeck 2001).

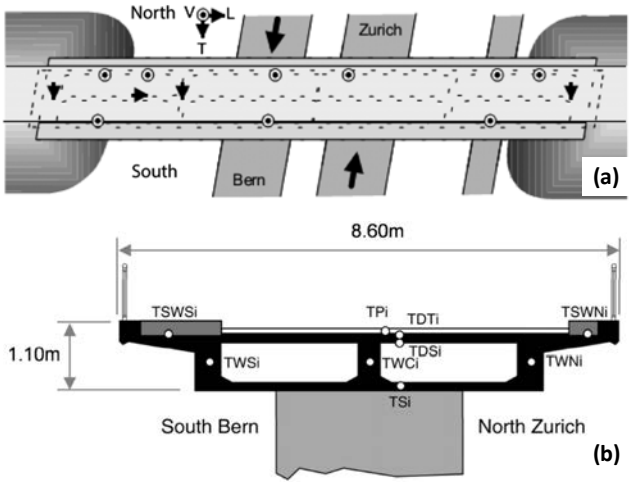

Figure 2. Acceleration sensors locations (a); cross-section and location of the thermocouples (b) (Adapted from Peeters & Roeck 2001).

During the long-term monitoring test, several progressive damage scenarios were imposed to the structural system of the bridge before its demolition (Peeters & Roeck 2001; Reynders & Roeck 2009). The damage scenarios imposed to Z24 bridge are classified as: (i) losses of stiffness both in the structure and in its boundary conditions; (ii) controlled displacements. These damage scenarios represented several types of possibilities present in a vulnerability analysis, which are easy to find in a typical operational evaluation on bridges. As a summary, Table 1 depicts all damages.

Table 1. Types of artificial damaged induced on Bridge Z24.

Number	Date (1998)	Damage type
1	4 August	Undamaged state (1st reference)
2	9 August	Second reference measurement
3	10 August	Lowering of pier, 20 mm
4	12 August	Lowering of pier, 40 mm
5	17 August	Lowering of pier, 80 mm
6	18 August	Lowering of pier, 95 mm
7	19 August	Lifting of pier, tilt of foundation
8	20 August	Third reference measurement
9	25 August	Spalling of concrete, 24 m^2
10	26 August	Spalling of concrete, 12 m^2
11	27 August	Landslide of 1 m at abutment
12	31 August	Failure of concrete hinge
13	2 September	Failure of 2 anchor heads
14	3 September	Failure of 4 anchor heads
15	7 September	Rupture of 2 out of 16 tendons
16	8 September	Rupture of 4 out of 16 tendons
17	9 September	Rupture of 6 out of 16 tendons

4. Analysis of the results

4.1. Determination of modal parameters

The vibration frequencies analyzed herein are related to the first three mode shapes and were automatically obtained from the stabilization diagrams generated by the covariance driven stochastic subspace identification method (SSI-COV). Figure 3 provides the variations of the first three natural frequencies with time over the whole monitoring period, which are identical to those obtained by (Reynders et al., 2014). These frequencies represent the mode shapes such as vertical bending mode around 4 Hz, a lateral bending mode (5 Hz), and one mode combining vertical bending and torsion (10 Hz). The dashed vertical line divides the undamaged state period (10th of November 1997 to the 9th of august 1998) and the period in which structural artificial damages were imposed (9th of august 1998 to the 10th of September 1998). Moreover, the figure plots some short periods of time without data, due to fail of the monitoring system.

Figure 3 shows that the frequencies decrease as artificial damages appear. Nevertheless, during normal operating conditions (undamaged state) and due to environmental effects, the variation of these sensible features in comparison with damaged state is much higher. Just analyzing the change in frequencies is not enough for damage detection, since it could produce false alerts.

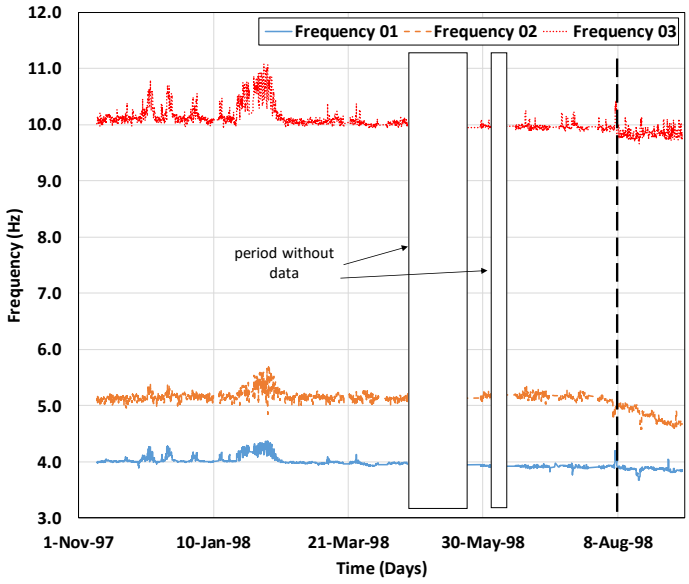

Figure 3. Modal frequencies obtained from the Z24 bridge: first, second and third natural frequency.

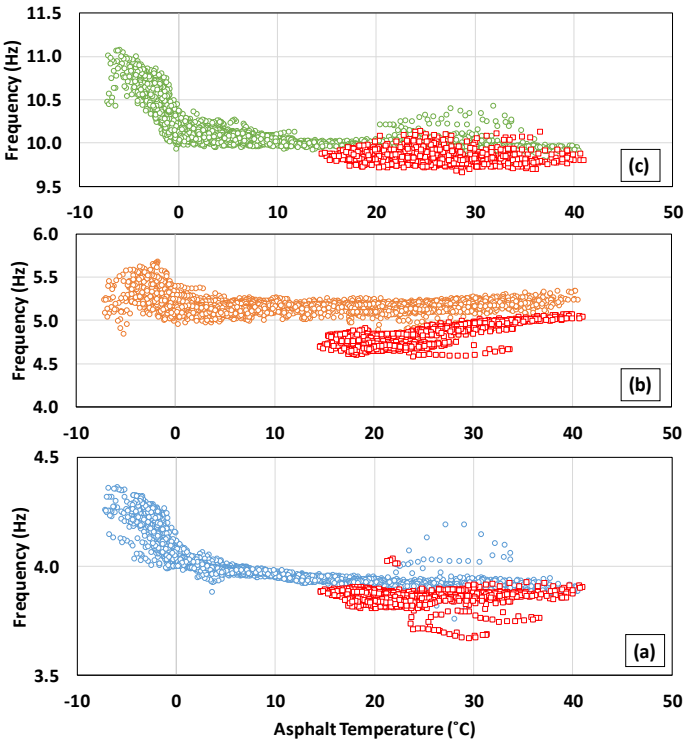

Figure 4. Correlation between modal frequencies and temperature (a) first frequency (b) second frequency (c) third frequency.

Note that even though several environmental factors were measured, not all were used because only the temperature showed an important influence on the modal frequencies (as can be shown in Figure 4). The correlation between the three modal frequencies and the temperature measured in the surface asphalt layer reveals a high influence of the temperature on the dynamic properties. In addition, the non-linear relationship becomes evident in figure 4, The red squares show the monitoring data in the damaged state, which has an additional influence on frequencies. As mentioned (Reynders et al., 2014), the interpretation to this behavior can be explained by the variation of Young's modulus of the material with temperature. This is presumably due to extremely temperatures recorded (below 0 ºC and above 40 ºC) during the monitoring period of the Z24 bridge.

4.2 Output-only monitoring using KPCA

Many researchers have pointed out the issues and limitations of PCA method, since it does not correctly consider the effects of environmental factors because this relationship is in general nonlinear (Peeters et al., 2001; Moser & Moaveni 2011; Reynders et al., 2014). Hence, in pursuit of better damage detection the kernel principal component analysis (KPCA) has been used in the present study. For this purpose, the data sets were divided in three groups: training data, monitoring data in undamaged state and monitoring data in damaged condition. The model was constructed using 3500 data points for training phase and the rest of the data were used for monitoring in undamaged and

damaged state. In fact, the amount of data points represent an average compared to what other researchers have found and, it was chosen considering the good results obtained by (Reynders et al., 2012) and (Reynders et al., 2014).

Figure 5 shows the gradual development of the damage indicator (equation 11). The red squares correspond to the artificial damages imposed to Z24 bridge during the last month of monitoring (9th of august 1998 to the 10th of September 1998), shown through the misfit depicted in Figure 5.

The proposed method is able to predict the behavior of the dynamic parameter variations under undamaged and damaged conditions underhanging environmental conditions. In addition, the misfit both for the validation data in undamaged condition as for the training data are lower. This is because the 3500 training data points entered in the model cover a wider range under normal environmental factors. Therefore, the normal variability of modal parameters is better predicted using the kernel-PCA and also increases the damage detection capability of the model. Likewise, when a new artificial damage is imposed to the bridge, the prediction error grows very significantly, in this way, these undesirable effects can be clearly and easily detected, either visually or with a novelty detection algorithm. In this study, a novelty detection technique based on machine learning algorithms was utilized as presented in the next section.

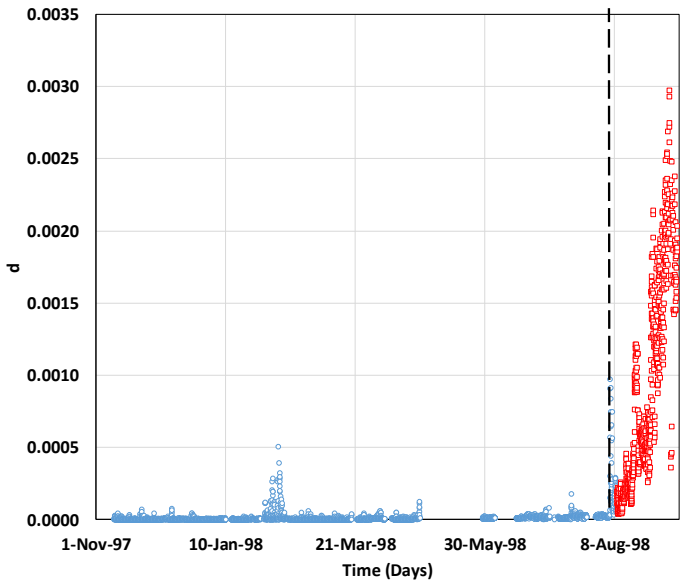

Figure 5. Damage indicator from the undamaged/baseline and damaged condition using the nonlinear kernel-based algorithm in the Z24 bridge.

4.3. Statistical classification

The strategy in statistical classification and clustering consists on modeling and classifying the structural response of the bridge taking into account the existence of artificial damages. For this purpose, a time-series of DC values (equation 13) were obtained considering mobile time windows, using the algorithms described in 2.3. Figure 6 plots the damage detection procedure before artificial

damages occurs. Firstly, the Figure 6(a) depicts a mobile window that contains the samples of undamaged condition only, although highly affected by environmental effects. The results in the figure confirm that all the samples are in healthy condition (undamaged), because there is not the presence of any misfit, despite for this period of time an important change in the frequencies was obtained because of the temperature effects, as shown in figure 3. This confirms the efficiency of the proposed KPCA in eliminating the temperature effects from the data set. All the damage indicators along time can be seen in Figure 6(b), where the vertical dashed line indicates the instant in which the damage appears due to the stiffness reduction. Furthermore, the figure shows the first mobile windows considered during the monitoring period in the undamaged state where the cluster analysis is applied. For each of these windows, the sequential application of the k-means algorithm automatically generates the DC values shown in Figure 6(c), which were obtained for a scenario of healthy condition (undamaged). In this case, all DC values are informative by themselves, about the undamaged condition.

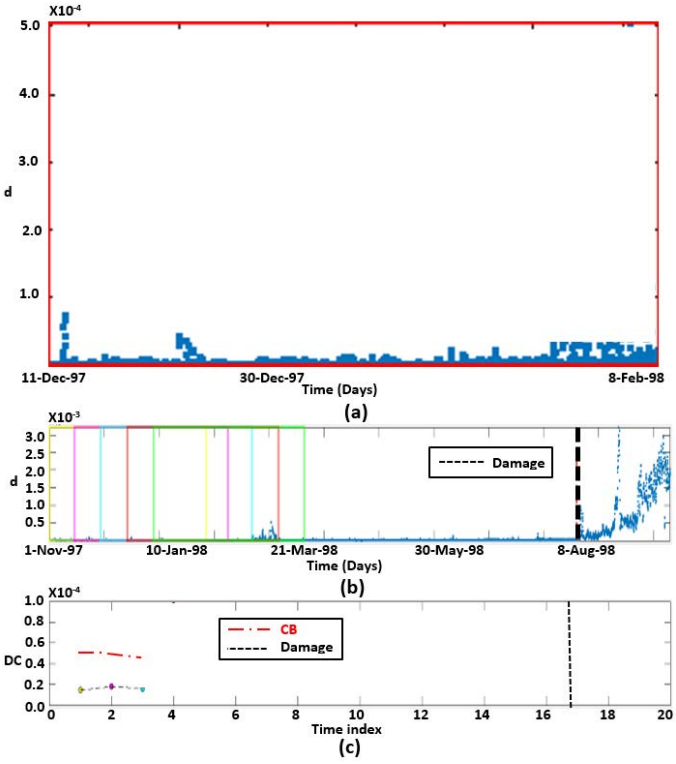

Figure 6. Damage detection procedure before the damages occurs (a) damage indicator (b) sequence of mobile windows (c) DC values obtained from each window.

In addition, Figure 7 provides the damage detection procedure after artificial damage. Figure 7(a) gives a mobile window that contains samples in the two conditions of the bridge: undamaged and damaged. The vertical dashed line indicates the instant in which the artificial damages occurs, since it separates the healthy and unhealthy conditions and on the right of this line, several misfits can

be found visually. Figure 7(b) plots the damage indicators and all the mobile windows during the whole monitoring period. Then, the clustering *k*-means algorithm generates the DC values for each mobile window, as shown in Figure 7(c). In this case the values of DC demonstrate the real behavior of the bridge differentiating the loss of stiffness from the healthy condition. Furthermore, the proposed strategy involves an additional step to detect the existence of damage. It consists on defining a confidence boundary (CB), which is an indicator that warns about structural damage if crossed by the damage feature indicator. This CB is obtained by statistically testing the DC distribution of the mobile windows, which is generally associated with the use of the Normal distribution. For example, in this study the *t*-student distribution was used taking as reference the good results obtained by (Santos et al., 2016). Thus, Figure 7(c) plots the values of CB to show the atypical values of DC. As seen there, four values exceed the threshold line, indicating the presence of structural damages. In conclusion, the cluster analysis is considered a powerful tool capable of automatically distinguish between structural conditions on bridges.

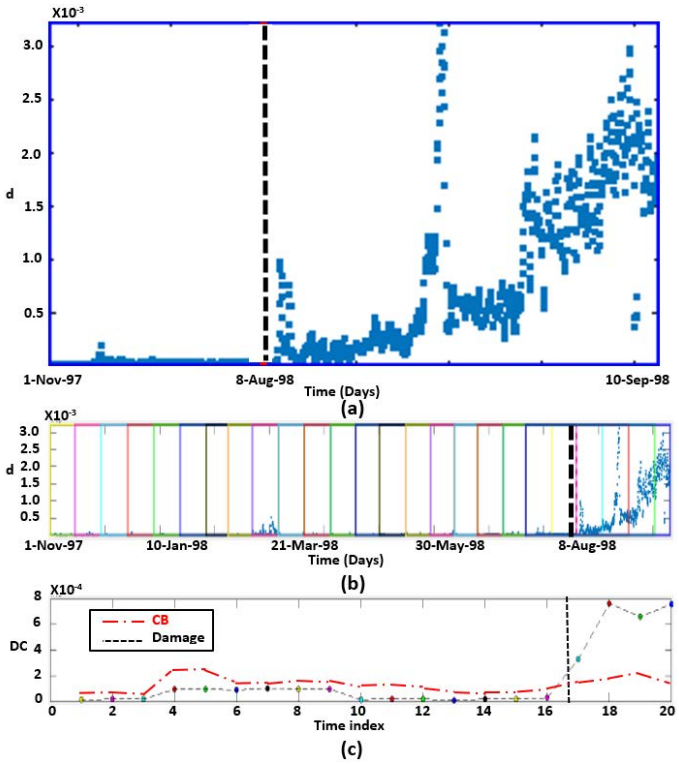

Figure 7. Damage detection procedure after the damages occurs (a) damage indicator (b) sequence of mobile windows (c) DC values obtained from each window.

5. Conclusions

The present paper presents the online automatic identification of the modal parameters of bridge Z24 using the SSI-COV method. This method showed a good efficiency in the identification of the bridge first three natural frequencies. The results show the evolution along time of the natural

frequencies, which allows a better understanding of the influence of environmental factors (temperature) on the bridge dynamics.

The application of the proposed methodology includes the identification of the modal parameters as outputs in a global system model. The kernel PCA algorithm presented good performance and capability for output-only damage detection. Its capability to identify the non-linear behavior of modal parameters due to changes in environmental conditions is fully proven. Therefore, KPCA-based method provides promising results when applied to real-world data sets from existing bridges.

With regard to the statistical machine learning algorithms and clustering, this paper obtained a good capability for damage identification using the k-means algorithm to the monitored data. The proposed strategy demonstrates the success for detecting misfits without generating false detections. Finally, this methodology presented good performance in terms of computation effort, robustness and prediction accuracy.

Acknowledgements

The first author acknowledges the financial support received from Ministry of Education of Peru with the National Scholarship and Educational Loan Program PRONABEC - President of the Republic Scholarship. The authors also would like to thank Professors Guido De Roeck, Edwin Reynders and Geert Lombaert from the Katholieke Universiteit Leuven, for the generous sharing of the Z-24 bridge data assessed within this study.

References

[1] Alampalli, S. (1998, February). Influence of in-service environment on modal parameters. In *Proceedings-SPIE The International Society for Optical Engineering,*Vol. 1, pp. 111-116.

[2] Bishop, C.M., 2006. *Pattern Recognition and Machine Learning*. USA: Springer.

[3] Cardno, C. A. (2016). Analysis reveals 58,495 US bridges are structurally deficient. *Civil Engineering*.

[4] Delgadillo, R.M., & Casas, J. R. 2019. Non-modal vibration-based methods for bridge damage identification. *Structure and Infrastructure Engineering*, 1-22.

[5] Farrar, C. R., Doebling, S. W., Cornwell, P. J., & Straser, E. G. (1997). Variability of Modal Parameters Measured on the Alamosa Canyon Bridge. In *Proceedings of the 15th International Modal Analysis Conference* (Vol. 3089, p. 257).

[6] Figueiredo, E., Radu, L., Westgate, R., Brownjohn, J., Cross, E., Worden, K., & Farrar, C. (2012, July). Applicability of a Markov-Chain Monte Carlo method for damage detection on data from the Z-24 and Tamar suspension bridges. In *Proceedings of the 6th European workshop on structural health monitoring* (pp. 747-754).

[7] Figueiredo, E., & Cross, E. (2013). Linear approaches to modeling nonlinearities in long-term monitoring of bridges. *Journal of Civil Structural Health Monitoring*, 3(3), 187-194.

[8] Forgy, E. W. (1965). Cluster analysis of multivariate data: efficiency versus interpretability of classifications. *biometrics*, 21, 768-769.

[9] Gowda, K.C., & Diday, E. 1991. "Symbolic clustering using a new dissimilarity measure," *Pattern Recognition*, 24(6):567-578.

[10] Juang, J. N. (1994). *Applied system identification*. Prentice-Hall, Inc.

[11] Ko, J. M., & Ni, Y. Q. (2005). Technology developments in structural health monitoring of large-scale bridges. *Engineering structures*, 27(12), 1715-1725.

[12] Kvåle, K. A., Øiseth, O., Rønnquist, A., & Sigbjörnsson, R. (2015). Modal analysis of a floating bridge without side-mooring. In *Dynamics of Civil Structures, Volume 2* (pp. 127-136). Springer, Cham.

[13] Magalhaes, F., Cunha, A., & Caetano, E. (2009). Online automatic identification of the modal parameters of a long span arch bridge. *Mechanical Systems and Signal Processing*, 23(2), 316-329.

[14] Moser, P., & Moaveni, B. (2011). Environmental effects on the identified natural frequencies of the Dowling Hall Footbridge. *Mechanical Systems and Signal Processing*, 25(7), 2336-2357.

[15] Moughty, J. J., & Casas, J. R. (2017). Damage sensitivity evaluation of vibration parameters under ambient excitation. In *International Conference on Experimental Vibration Analysis for Civil Engineering Structures* (pp. 249-260). Springer, Cham.

[16] Peeters, B., Maeck, J., & De Roeck, G. (2001). Vibration-based damage detection in civil engineering: excitation sources and temperature effects. *Smart materials and Structures*, 10(3), 518.

[17] Peeters, B. & Roeck, G. de, (2001). One-year monitoring of the Z24 Bridge environmental effects versus damage events. *Earthquake Engineering and Structure Dynamics*, 30(2), pp.149–171.

[18] Rendón, E., Abundez, I., Arizmendi, A., & Quiroz, E. M. (2011). Internal versus external cluster validation indexes. *International Journal of computers and communications*, 5(1), 27-34.

[19] Reynders, E. & Roeck, G. De, 2009. Continuous vibration monitoring and progressive damage testing on the Z24 bridge. In *Encyclopedia of Structural Health Monitoring*. Chichester, UK: John Wiley & Sons, pp. 2149–2158.

[20] Reynders, E., Wursten, G., & De Roeck, G. (2012). Nonlinear system identification for vibration-based structural health monitoring. In *Proceedings of the National Congress on Theoretical and Applied Mechanics* (pp. 9-11).

[21] Reynders, E., Wursten, G., & De Roeck, G. (2014). Output-only structural health monitoring in changing environmental conditions by means of nonlinear system identification. *Structural Health Monitoring*, 13(1), 82-93.

[22] Rousseeuw, P. J. 1987. "Silhouettes: A graphical aid to the interpretation and validation of cluster analysis," *Journal of Computational and Applied Mathematics*, 20, 53-65.

[23] Santos, J.P., Cremona, C., Orcesi, A.D., & Silveira, P., 2013, Baseline-free real-time novelty detection using vibration-based symbolic features. *Experimental Vibration Analysis for Civil Engineering Structures (EVACES),* 28-30 October, Ouro, Brazil.

[24] Santos, A., Figueiredo, E., & Costa, J. (2015a). Clustering studies for damage detection in bridges: A comparison study. *Structural Health Monitoring, 2015*.

[25] Santos, J. P., Orcesi, A. D., Crémona, C., & Silveira, P. (2015b). Baseline-free real-time assessment of structural changes. *Structure and Infrastructure Engineering*, 11(2), 145-161.

[26] Santos, J. P., Crémona, C., Calado, L., Silveira, P., & Orcesi, A. D. (2016). On-line unsupervised detection of early damage. *Structural Control and Health Monitoring*, 23(7), 1047-1069.

[27] Schölkopf, B., Smola, A., & Müller, K. R. (1998). Nonlinear component analysis as a kernel eigenvalue problem. *Neural computation*, 10(5), 1299-1319.

[28] Sohn, H. (2006). Effects of environmental and operational variability on structural health monitoring. *Philosophical Transactions of the Royal Society A: Mathematical, Physical and Engineering Sciences*, 365(1851), 539-560.

[29] Yan, A. M., Kerschen, G., De Boe, P., & Golinval, J. C. (2005). Structural damage diagnosis under varying environmental conditions—part II: local PCA for non-linear cases. *Mechanical Systems and Signal Processing*, 19(4), 865-880.

[30] Yu, L., Zhu, J. H., & Yu, L. L. (2013). Structural damage detection in a truss bridge model using fuzzy clustering and measured FRF data reduced by principal component projection. *Advances in Structural Engineering*, 16(1), 207-217.

5.4. Journal Paper III

Bridge damage detection via Improved Completed Ensemble EMD with Adaptive Noise and machine learning algorithms

Accepted for publication in Structural Control and Health Monitoring, January 2022.

Rick M. Delgadillo [1], Joan R. Casas [1]

[1]Department of Civil and Environmental Engineering, Technical University of Catalonia (UPC), c/ Jordi Girona 1-3, 08034 – Barcelona, Spain

Abstract: Structural health monitoring field is growing in the use of more modern techniques and tools in order to identify damages in civil structures. The improvements in signal processing techniques and data mining have, recently, been employed due to their powerful computational ability to detect damage in bridges. Despite the majority of researchers have been studying laboratory-scale implementations and theoretical developments, the limited data to identify structural faults in real bridges is still a problem. The current study presents a novel approach for damage identification by using two improved methods such as decomposition techniques and machine learning algorithms. Since the data obtained from the traffic vibration in real bridges is non-linear and time varying, the Hilbert-Huang transform is used to process the vibration data. Additionally, a phenomenon of mode mixing is presented in the current decomposition methods, such as empirical mode decomposition (EMD). Therefore, a novel Improved Completed Ensemble EMD with Adaptive Noise (ICEEMDAN) was adopted. After the signal decomposition and identification of the damage parameter, a symbolic data analysis and clustering-based approach were developed. Additionally, an unsupervised machine learning algorithm was used to group substructures with similar behavior and then detect damages. This learning method was used for automatically classifying the damages using a moving windows process sequentially applied to the structural response of the bridge. The validity of the approach is demonstrated using real data collected from a truss bridge. The results show that the proposed mixed method was effective and can endow better results in bridge health monitoring.

Keywords: Hilbert-Huang Transform; Empirical Mode Decomposition; ICEEMDAN; instantaneous frequency; damage detection; symbolic data analysis; unsupervised machine learning; cluster analysis.

1. Introduction

Road transportation plays an important role in the world both as passenger and freight transportation. Bridges are the most critical structural component in transport infrastructures, due to their importance both in life-safety as in the economy of the countries. The design, construction and management of bridges are factors that must be taken care of. However, failures can appear due to inappropriate design, material degradation and poor maintenance. In this context, bridge health monitoring-based approaches have been increasingly developed during the last decades.[1] For instance, the most efficient and sophisticated monitoring systems, various techniques to collect data and analysis methods are being implemented[2,3].

To achieve good results in the damage identification, experimental data obtained must be transformed to meaningful information and then from damage-sensitive features a statistical analysis should be developed to identify the actual structural condition. In this context, there are currently several methods for signal decomposition to identify the modal sensitive parameters in bridges, such as Fourier transform and Wavelet transform (WT). Nonetheless, during the preceding decade, the use of empirical mode decomposition (EMD) has received considerable attention[4], because it is an adaptive signal decomposition technique and also due to its ability to decompose and analyze the non-stationary and non-linear signals.[5-7] Considering the real-world applications, most of the signals are not only non-linear but also non-stationary, thus new methods in signal processing are required. However, EMD method presents some shortcomings like the recurrent emergence of mode mixing due to signal intermittence and a single intrinsic mode function (IMF)[7]. Huang et al.[8] developed a new method called Hilbert Huang Transformation (HHT) to analyze non-stationary and non-linear signals and is considered a pioneer in this field. This method consists in two parts, that is, Hilbert Transform (HT) and Empirical Mode Decomposition (EMD). The principal idea of the EMD is to decompose the mean signal into Intrinsic Mode Functions (IMF) since the EMD is based on the local characteristic time scale of the original data, so this decomposition method is easily applied and highly efficient. The HHT method has been employed in many researches and in practical engineering analyzing cases of study in different fields, such as biomedical, structural engineering and now the application of HHT especially define SHM has attracted increasingly attention.[9] However, there is little information in the study of HHT applied to real bridges. Therefore, this investigation aims to demonstrate the feasibility of this method applied to real bridges.

Yan and Miyamoto[10] developed a comparative investigation between the improved HHT and WT in order to identify the modal parameters. They used ambient vibration data from the Z24-bridge benchmark. The results showed that both methods identified the modes correctly when the time-frequency resolutions are clear. Qu & Lian[11] developed an approach based on HHT to damage detection in a transmission tower and EMD is used to decompose response signals. In this case, a shape factor is used to analyze the response signal of the structural IMFs and it could detect the

damage on the structure intuitively. A modal identification procedure for the Tsing Ma Bridge was performed using the HHT, and the modal damping ratios and natural frequencies were clearly identified from both stationary and non-stationary records[12]. Huang et al.[13] carried out several damage detection applications using laboratory experiments and numerical simulations and they proposed an HHT-based bridge structural health-monitoring method. The dynamic condition assessment in a bridge was carried out utilizing HHT approach and three damaged scenarios (intact, minor and severe) in one concrete pile substructure were evaluated. Piles were excavated and broken to simulate flood and earthquake damage to a bridge substructure. As a result, the HHT method revealed the quantitative difference in instantaneous frequency of sound and the damaged components[14].

There are still many challenges and difficulties concerning the HHT based damage detection. To this end, many improvements of EMD were developed over time. A new method named Ensemble EMD (EEMD) based on the studies of white noise was developed by Wu & Huang[7]. This new approach determines the IMF component like a mean of an ensemble of traces having signal and white noise of finite amplitude. However, Wu & Huang[15] showed some drawbacks in EEMD method like the creation of extra modes and the phenomenon of mode mixing. For this reason, the calculation capability and the ensemble average results could be importantly reduced. Yeh et al.[16] proposed the Complimentary EEMD (CEEMD) in order to reduce the residual noise. Nevertheless, the number of added white noise and the selection of amplitude remain unresolved, and most of the times the IMF obtained by CEEMD does not fulfil the IMF criterion. In addition, the advantage of this method is that it improves the calculation efficiency. Lin[17] define ICEEMD to select an ensemble number as 100 for the EEMD method, although, this gave inconsistent results since the important information was ignored. Zheng et al.[18] presented the Partly EEMD by introducing the permutation entropy (PE), but the PE threshold such as size selection and number of added white noise were not defined. The issues of spurious high frequency modes were studied by Torres et al.[19], who presented a method named Complete Ensemble Empirical Mode Decomposition with Adaptive Noise (CEEMDAN). The ability of the CEEMDAN was demonstrated in building energy consumption, biomedical engineering and seismology. Furthermore, a decomposition improved method ICEEMDAN, was used in a real bridge structure[20]. Colominas et al.[21] developed an Improved CEEMDAN implementing two major improvements: (i) the avoidance of the spurious modes and (ii) the physical meaning of the results is achieved with the reduction in the amount of noise included in the modes. Considering the applications of this method in SHM, some authors[22,23] verified its efficiency for damage identification in a real steel bridge.

On the other hand, nowadays, generated models based on machine learning analysis, statistical pattern recognition and data mining are being widely used to identify structural damage. The data mining approach uses the information of the different structural health conditions from the database (e.g. undamaged or healthy and damaged) and then, the relationship between intrinsic properties in the form of patterns are studied. Effective damage detection methods and applications based in

clustering and unsupervised learning approaches can be found in[24]. Besides, the data sets obtained from SHM of bridge monitoring systems are named "big data" due to complexity, diversity and sheer volume[25]. The most common algorithms of clustering-based approaches for statistical modeling and feature classification are Gaussian Mixture Models (GMM), Support Vector Clustering (SVC), *K*-means and Self-Organizing Maps (SOM). For example, a clustering approach named fuzzy c-means (FCM) was used by Yu et al.[26] for structural damage detection, besides, the authors utilized data projection algorithms such as principal component analysis (PCA) and its nonlinear version like kernel principal component analysis (KPCA) in order to extract the significant features. Several dimensionality reduction methods such as PCA, Curvilinear Component Analysis and Random Projection were used by Toivola et al.[27] in order to reduce high-dimensional vibration measurements in conjunction with nearest neighbor algorithm. They implemented this novelty detection in a real-life data from a wooden bridge model, which was subjected to simulated damages with small added weights. Cho et al.[28] used a hierarchical parameter clustering technique to group acceleration data from the Jindo cable-stayed bridge in South Korea.

A cluster analysis technique was proposed by Santos et al.[29] for damage identification in a real bridge, and they utilized a statistical process considering interquartile ranges as part of symbolic data analysis. The algorithms used are able to allocate data objects to any number of predefined clusters, irrespective of whether this amount has really been observed in the structural system. This strategy was applied to vibration data (frequencies, mode shapes and damping ratio). Besides, Santos et al.[30] implemented two approaches together: cluster algorithms and symbolic data to achieve a single-value novelty index (NI) to be able to detect structural changes in multi-sensor data-sets. To achieve the capability of NI and to corroborate the proposed theory, data obtained from Samora Machel bridge was used. During structural monitoring, refurbishment works were performed, such as repairing/replacement of concrete, replacement of suspension cables, hangers and supports. The methodology was implemented to perform a real-time assessment using a single-value NI for multiple time windows. A cable-stayed bridge was utilized as case of study for damage identification[31], the authors used a combination of two statistical learning methods such as neural networks and clustering methods in order to detect early damages. Diez et al[32] proposed a clustering-based approach to join datasets with similar behaviors and then detect structural changes on the Sydney Harbour Bridge. The approach presented has a peculiarity of considering the vibration signals caused by passing vehicles to detect and locate damaged junctions using *K*-means clustering algorithm. The results showed correlations between joints, locating a damaged joint and another with a defective instrumented sensor.

The current investigation aims to evaluate the performance and possibilities of the combination of ICEEMDAN-Hilbert Huang Transform with an unsupervised machine learning algorithm (clustering, K-means), to detect and locate damage in the case of bridges under operational traffic, where recorded signals are non-linear and non-stationary.

ICEEMDAN and clustering-based methods have been used separately in SHM for vibration analysis and damage detection in other scientific disciplines. In particular, the clustering techniques used in the present paper were already applied to bridges in other works. However, their validation was limited to the case of ambient data (the input action was the temperature change) and of the static type (in the sense that no vibration data was examined). Also, the data came from a numerical model of the bridge, due to the difficulties in real bridges to find experimental results for original and damaged scenarios. As a novelty, in the present paper the clustering techniques are used to detect damage in the case of vibration data that does not come from an ambient excitation, but from a forced vibration due to traffic, what justifies the adoption of HHT improved with ICEEMDAN technique. In addition, the vibration data is coming from a dynamic test on a real bridge with a real vehicle, and is not numerically simulated. This is also a main novelty of this research that shows the feasibility of the proposed approach not only in simulated scenarios, but in real world applications.

In summary, the novelties presented in the paper are:

• The new methodology presents a mixed of two approaches such as Hilbert-Huang Transform and machine learning algorithms, that is able to detect and localize damages in a real bridge by using non-linear and non-stationary data coming from the forced-vibration data recorded under traffic.

• The proposed methodology is checked with data from a real bridge under undamaged and damaged conditions and not from the simulation on a numerical model

• ICEEMDAN, a technique that was initially developed in biomedical signals, is applied for the first time to the civil engineering field, demonstrating its performance in the case of the acceleration signals from a real bridge.

The main steps of the methodology are graphically explained in detail in Figure 1. The vibration responses of the bridge excited by a passing vehicle, are measured and recorded in several points within the bridge using accelerometers. For every event, raw acceleration data are transformed into an unique damage feature in the frequency domain.

The content of the paper is the following. Section 2.1 explains the improved methodology to decompose the complex traffic-induced signals to obtain the instantaneous frequency (IF), used as damage feature. In section 2.2 are presented the symbolic data analysis and cluster algorithms that allow to obtain a single-value damage parameter (DC) in order to detect and localize damage. Chapter 3 describes the real steel bridge where the proposed methodology is checked, the monitoring programme, the damage scenarios and the acquired data. In chapter 4 the proposed strategy is applied and the main results discussed. Finally, the main conclusions from the detailed analysis are drawn in chapter 5.

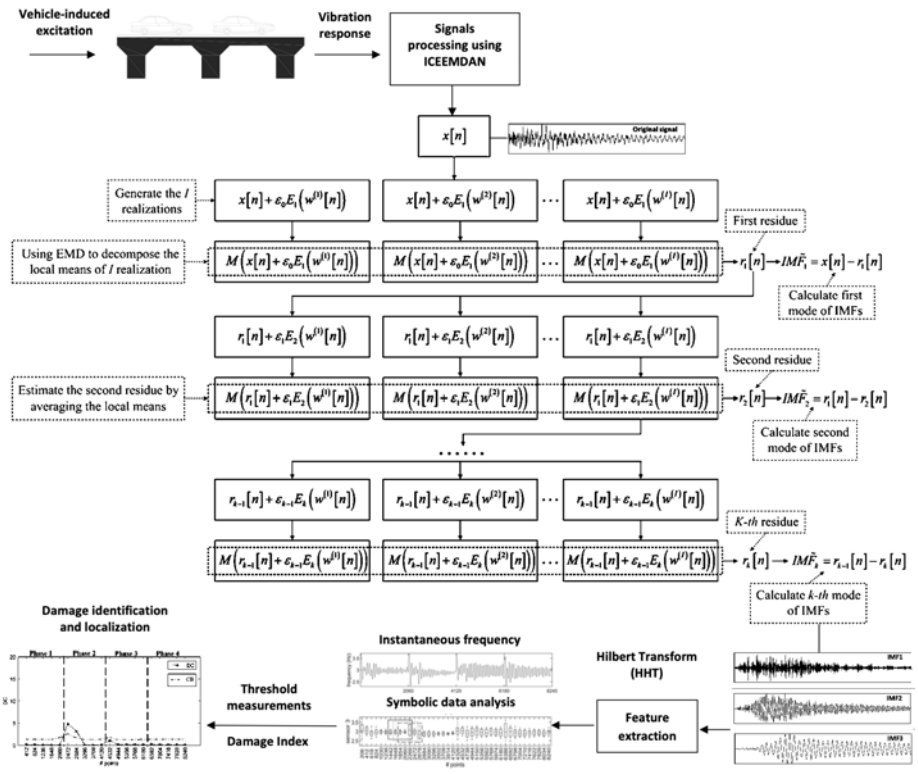

Figure 1. Schematic view of proposed method

2. Theoretical background

2.1 Novel improved ICEEMDAN method

2.1.1 Empirical Mode Decomposition (EMD)

In 1996, EMD was proposed by Huang et al.[5] as a time-series decomposition method for non-linear and non-stationary data. The original signal can be reconstructed by summation of intrinsic mode functions (IMF), where $x(t)$ = original signal, I_i represent the ith IMF and the residue $r_n(t)$ is generally a monotonic function or a constant. Therefore:

$$x(\mathrm{t}) = \sum_{i=1}^{n} I_i(\mathrm{t}) + \mathrm{r}_n(\mathrm{t}) \tag{1}$$

This method is adaptive and offers physical representation and no harmonics. EMD uses all the extrema to construct the envelopes and the problem arises when the signal contains intermittent processes, since the phenomenon of mode mixing can occur. The ability of this method to overcome the mode mixing problem in the SHM field has been surpassed by other modern decomposition methods[33].

The evolution of methods that emerged from EMD describe a successive improvement. For example, the Ensemble EMD (EEMD) method defines the IMF component as a mean of ensemble of

trails, having white noise as well as signal. The statistical characteristics of white noise of finite amplitude to improve the scale separation problem is introduced. It helps all possible solutions to be examined in the ensemble and the effect of the included white noise is removed by utilizing ensemble mean. In CEEMD method, the white noise residue present in the IMF is eliminated in a considerable way and its calculation efficiency increases. The other method called CEEMDAN solves the EEMDs' faults, achieving a negligible reconstruction error and solving the problem of different number of modes for different realizations of signal plus noise. Finally, in the present investigation the improved method that currently exists ICEEMDAN[21] is used, which is explained in detail in Section 2.1.2.

2.1.2 Improvements on Complete Ensemble Empirical Mode Decomposition with Adaptive Noise (ICEEMDAN)

Many authors have made an attempt to solve the problem of the appropriate selection for the addition of white noise to solve the mode mixing problem. However, many proposed techniques were not really successful and effective, especially for the signals obtained from real bridges. Hence, in pursuit of better performance of this technique applied to real bridges, a novel-based Improved CEEMDAN method developed by Colominas et al.[21] was proposed.

Taking into account the weaknesses of the variations of EMD explained above, a controlled noise should be added to the original signal in order to create new extrema. In this regard, the ICEEMDAN method considers two improvements such as residual noise in modes and the spurious modes, as it is explained herein. The next mathematical formulation details the algorithms used in ICEEMDAN method. $E_k(.)$ is an operator which produces the k-th mode obtained by EMD, $M(.)$, is also an operator which produces the local mean of the signal and $w^{(i)}$ = is a realization of zero mean unit variance white noise.

Considering, $x^{(i)}=x+w^{(i)}$ being x the original signal and $\langle\cdot\rangle$ the action of averaging throughout the realizations, then the modes for the first EEMD[7] and original CEEMDAN[21] can be written as:

$$\tilde{d}_1 = \left\langle E_1\left(x^{(i)}\right)\right\rangle = \left\langle x^{(i)} - M\left(x^{(i)}\right)\right\rangle = \left\langle x^{(i)}\right\rangle - \left\langle M\left(x^{(i)}\right)\right\rangle \tag{2}$$

In order to estimate only the local mean and subtract it from the original signal, the formula can be expressed as:

$$\tilde{d}_1 = x - \left\langle M\left(x^{(i)}\right)\right\rangle \tag{3}$$

Taking into account Equations 2 and 3, a reduction in the amount of noise present in the modes is obtained, because the estimation of modes was replaced by the local mean estimations, which

demonstrated the best performance previously explained. With respect to spurious modes, analogously to the previous methods like EMD, EEMD obtained a strong overlapping in the scales for the first two modes (first one extracted adding white noise and the second one adding $E_1(w^{(i)})$). Then, in order to reduce this overlapping, Colominas et al.[21] proposed to use $E_k(w^{(i)})$ and not directly use the white noise to extract the *k*th mode. The sequence of this improved CEEMDAN method consists in:

Step 1. Calculate by EMD the local means of *I* realizations $x^{(i)}=x+\beta_0 E_1(w^{(i)})$, taking account that *I* is the number of realizations of Gaussian white noise added to the signal of interest (*I* is consider usually a few hundred[21]). Then the first residue can be expressed as

$$r_1 = \left\langle M(\mathrm{x}^{(\mathrm{i})}) \right\rangle \tag{4}$$

Fig Where $\beta_0 = \varepsilon_0\, std(x)/std(E_1(w^{(i)}))$; β_0 is chosen such that ε_0 is exactly the reciprocal of the desired signal-to-noise ratio (SNR) between the first added noise and the analyzed signal; the SNR is considered as a quotient of standard deviations.

Step 2. At the first stage *(k=1)* calculate the first mode:

$$\tilde{d}_1 = x - r_1 \tag{5}$$

Step 3. Estimate the second residue as the average of local means of the realizations $r_1+\beta_1 E_2(w^{(i)})$ and define the second mode:

$$\tilde{d}_2 = r_1 - r_2 = r_1 - \left\langle M(r_1 + \beta_1 \mathrm{E}_2(w^{(\mathrm{i})})) \right\rangle \tag{6}$$

Step 4. For $k=3,\ldots,N$ calculate the *k*th residue

$$r_k = \left\langle M(r_{k-1} + \beta_{k-1} \mathrm{E}_k(w^{(\mathrm{i})})) \right\rangle \tag{7}$$

Step 5. Compute the *k*th mode

$$\tilde{d}_k = r_{k-1} - r_k \tag{8}$$

Step 6. Go to step 4 for next *k.*

Constants $\beta_k=\varepsilon_k\, std(r_k)$ are chosen to obtain a desired SNR between the added noise and the residue to which the noise is added.

2.1.3 Hilbert-Huang Transform

The Hilbert Huang Transform (HHT) of a signal x(t) is defined by Huang et al.,[5] and it has been used for linear and nonlinear vibration systems identification for a long time. However, HHT is being developed and recently applied in the field of SHM during last years[34-37]. The main feature of Hilbert–Huang Transform (HHT) is its capability to deal with nonlinear and non-stationary vibrations. The HHT method involves two distinct steps: Firstly, the decomposition of signals into intrinsic mode functions (IMF), where its components are obtained from the original signal through an empirical procedure. Secondly, the HHT approach is implemented applying the Hilbert Transform (HT) to each IMF component. Then, relevant parameters such as the instantaneous amplitude, instantaneous frequency and instantaneous phase can be determined. In this study, HHT utilizes ICEEMDAN to extract IMFs from the original signals and the Hilbert transform is applied on IMFs to find instantaneous frequencies, which are later on used to define a damage feature.

The resulting IMFs $\{c_i(\tau)\}$ obtained as explained in 2.1.2 are introduced into the Hilbert Transform (Equation 9). The resulting Hilbert Transform $H[c_i(t)]$ is grouped with $\{c_i(\tau)\}$ to form an analytic signal $z(\mathrm{t})$ (Equation 10) whose constituents $a_i(\mathrm{t})$ and $\theta_i(\mathrm{t})$ (instantaneous amplitudes and phases), can be expressed by Equation (11) & Equation (12) respectively. Instantaneous frequencies $\{\varpi_i(\mathrm{t})\}$ of each IMF are determined by differentiating the instantaneous phase function in Equation (13).

$$H[c_i(t)] = \frac{1}{\pi}\int_{-\alpha}^{\alpha}\frac{c_i(\tau)}{t-\tau}d\tau \tag{9}$$

$$z(\mathrm{t}) = c_i(\mathrm{t}) + \mathrm{jH}\left[c_i(\mathrm{t})\right] = a_i(\mathrm{t})\,\mathrm{e}^{j\theta_i(\mathrm{t})} \tag{10}$$

$$a_i(\mathrm{t}) = \sqrt{c_i^{\,2}(\mathrm{t}) + \mathrm{H}^2\left[c_i(\mathrm{t})\right]} \tag{11}$$

$$\theta_i(\mathrm{t}) = \arctan\left(\frac{\mathrm{H}\left[c_i(\mathrm{t})\right]}{c_i(\mathrm{t})}\right) \tag{12}$$

$$\varpi_i(\mathrm{t}) = \frac{d\theta_i(\mathrm{t})}{dt} \tag{13}$$

2.2 Feature extraction and clustering-based approach

2.2.1 Symbolic feature extraction

In this paper, the feature extraction is carried out using a symbolic data analysis. This analysis consists in the reduction of the data in more generic types and less voluminous information in contrast with classical data used in SHM applications[38]. Symbolic data objects (SDO) use time intervals in statistical quantities such as interquartile intervals (IQR) or histograms[30]. According to Diday and Noirhomme-Fraiture[39] the IQR intervals manage a greater degree of data fusion than histograms. Therefore, interquartile intervals are used in this investigation.

Mathematically, the SDO described by p interquartile intervals of multiple sensors can be written as

$$T = \left[(\mathrm{T}_{\mathrm{inf}}^{(1)}; \mathrm{T}_{\mathrm{sup}}^{(1)}) \ldots (\mathrm{T}_{\mathrm{inf}}^{(\mathrm{i})}; \mathrm{T}_{\mathrm{sup}}^{(\mathrm{i})}) \ldots (\mathrm{T}_{\mathrm{inf}}^{(\mathrm{p})}; \mathrm{T}_{\mathrm{sup}}^{(\mathrm{p})}) \right] \tag{14}$$

Where p = number of modal quantities describing the symbolic object (for instance, modal parameters, static variables, etc.). The parameter studied in the present investigation is the instantaneous frequency. Furthermore, for the case of an interquartile type object, each sensor measurement is transformed into an interquartile pair $(T_{inf}^{(r)}, T_{sup}^{(r)})$. Assuming that the data associated with the *r-th* sensor are ordered in ascending order, the value $T_{inf}^{(r)}$ corresponds to the data that has 25% below it. Similarly, $T_{sup}^{(r)}$ corresponds to the value that has 75% of the data below it. For this reason, this type of object is called interquartile, since the representation excludes the data located in the lower and upper quartiles, while the interval $(T_{inf}^{(r)}, T_{sup}^{(r)})$ contains within it the 50% of all data. In addition, the symbolic data in conjunction with statistical learning methods can be applied to reveal the structural changes on bridges[29,30]. The SDO uses the distance between pairs of concepts and considers their intrinsic features, since when the values are lower, the objects can be more similar. Hence, the Normalized Euclidean Ichino-Yaguchi distance[40] is used in this study and is defined as

$$d_{ij} = \left\{ \frac{1}{p} \sum_{r=1}^{p} \varphi_r(\mathrm{T}_i, \mathrm{T}_j)^2 / |Y_r| \right\}^{1/2} \tag{15}$$

Where T_i and T_j = two symbolic objects obtained from a data set of $s = 1, \ldots, N$ objects, N is the number of symbolic objects defined for the analyzed data-set; r=interquartile intervals like $(\mathrm{T}_{\mathrm{i,inf}}^{(\mathrm{r})}; \mathrm{T}_{\mathrm{i,sup}}^{(\mathrm{r})})$ and $(\mathrm{T}_{\mathrm{j,inf}}^{(\mathrm{r})}; \mathrm{T}_{\mathrm{j,sup}}^{(\mathrm{r})})$ obtained from $r=1,\ldots,p$ instantaneous frequency, φ_r is the Ichino-Yaguchi dissimilarity measure given by

$$\varphi_r(\mathrm{T}_i,\mathrm{T}_j)=\left|T_i^{(\mathrm{r})}\oplus T_j^{(\mathrm{r})}\right|-\left|T_i^{(\mathrm{r})}\otimes T_j^{(\mathrm{r})}\right|+\gamma\left(2\left|T_i^{(\mathrm{r})}\otimes T_j^{(\mathrm{r})}\right|-\left|T_i^{(\mathrm{r})}\right|-\left|T_j^{(\mathrm{r})}\right|\right) \tag{16}$$

The symbols $\oplus$ and $\otimes$, as well as the norm $\left|\left[\ldots\right]\right|$, are defined by

$$T_i^{(\mathrm{r})}\oplus T_j^{(\mathrm{r})}=\left\{\min\left[T_{i,\mathrm{inf}}^{(\mathrm{r})},T_{\mathrm{j,inf}}^{(\mathrm{r})}\right],\max\left[T_{i,\mathrm{sup}}^{(\mathrm{r})},T_{\mathrm{j,sup}}^{(\mathrm{r})}\right]\right\} \tag{17}$$

$$T_i^{(\mathrm{r})}\otimes T_j^{(\mathrm{r})}=\left\{\max\left[T_{i,\mathrm{inf}}^{(\mathrm{r})},T_{\mathrm{j,inf}}^{(\mathrm{r})}\right],\min\left[T_{i,\mathrm{sup}}^{(\mathrm{r})},T_{\mathrm{j,sup}}^{(\mathrm{r})}\right]\right\} \tag{18}$$

$$\left|T_i^{(\mathrm{r})}\right|=\left|\left[T_{i,\mathrm{inf}}^{(\mathrm{r})},T_{\mathrm{i,sup}}^{(\mathrm{r})}\right]\right|=T_{\mathrm{i,sup}}^{(\mathrm{r})}-T_{i,\mathrm{inf}}^{(\mathrm{r})} \tag{19}$$

The factor γ is generally taken as 0.5 and the normalizing factor $\left|Y_r\right|$ is defined as:

$$\left|Y_r\right|=\left|\max(T_{\mathrm{sup}}^{(\mathrm{r})})-\min(T_{\mathrm{inf}}^{(\mathrm{r})})\right| \tag{20}$$

2.2.2 Cluster analysis

Symbolic data analysis can serve to catch several structural behaviors in a big data-set. Nonetheless, the strategy for SHM used herein requires the use of machine learning algorithms, which arise as an effective tool to aid in the data analytic. Therefore, a powerful tool of unsupervised machine learning like cluster analysis is addressed herein. Clustering is a technique to divide a dataset into separated similar clusters according to common feature patterns[30].

Clustering methods provide a variety of algorithms with desirable characteristics for the discovery of intrinsic properties contained in the data. As an un-supervised machine learning algorithm, clustering does not require the definition of reference/training data. Instead, they have the capability to "understand" the intrinsic features by trying to find the most compact and separated set of clusters[41]. In this study, the *K*-means clustering is used to characterize the structural behavior of the bridge. According to Arthur & Vassilvitskii[42], *K*-means algorithm minimizes within-cluster sum of squares and mathematically can be written as:

$$\mathrm{argmin}_S\sum_{i=1}^{n}\sum_{j:x_j\in S_i}d(\mathrm{x}_j,\mu_i)^2 \tag{21}$$

Where n = number of clusters; $x_1, x_2, \ldots$ = observations, $S=\{S_i:i=1,\ldots,n\}$ is set of clusters, $\mu_i, i=1,\ldots,n$ are cluster centers and $d(*,*)$ is Euclidean metric obtained from Equation 15. When the

K-means algorithm is used, it does not necessarily mean to obtain optimal results, since a kind of heuristic is incorporated in order to find the solution. Furthermore, each time the algorithm is executed, a slightly different solution can be obtained. The reason is the randomness of the initial selection of the grouping centers.

As mentioned, the objective proposed in the clustering analysis is to minimize the within-cluster distance, which, consequently, maximizes the between-cluster distance. This can be expressed as:

$$W(\mathrm{P}_k) = \frac{1}{2}\sum_{k=1}^{K}\sum_{\mathrm{C(i)=k}}\sum_{\mathrm{C(j)=k}} d_{ij} \tag{22}$$

Where a given partition containing *K* clusters is considered, $P_K = \{C_{1, \ldots,} C_K\}$; $C(i)$ = many-to-one allocation rule that assigns object *i* to cluster *k*, based on a dissimilarity measure d_{ij} defined between each pair of data objects, *i* and *j*. This $d_{ij\ is}$ obtained using Equation 15.

2.2.3 Cluster validity

Clustering procedures define a certain number of partitions in data irrespective of whether this number of clusters really exists. In this way, high values of within cluster dissimilarity and solutions that are not optimal can be obtained. Therefore, it is necessary to estimate the optimal number of clusters in the studied data. For this reason, a quantitative evaluation known as cluster validity is employed to find the appropriate number of clusters. In the present work, a validity index called silhouette statistic (SIL) was employed[43]. The construction of silhouette statistic consists in assigning a fixed number of clusters *K* to the *i*th observation, with the following value:

$$s(\mathrm{x}_i) = \frac{b(\mathrm{x}_i) - \mathrm{a}(\mathrm{x}_i)}{\max\{a(\mathrm{x}_i), \mathrm{b}(\mathrm{x}_i)\}} \in [-1,1] \tag{23}$$

Where $b(x_i)$ = distance to nearest neighbouring cluster's centre and $a(x_i)$ is the average distance between the *i*th object of cluster *C* and the remaining *j* objects. The silhouette index of clusters and the average of silhouette widths for all samples are respectively given by Equation 24 and 25. Where $(1 \leq M_k \leq N)$, *N* = set of objects, *K* = clustering partitions and the value of silhouette coefficient varies from 0 to 1. A larger silhouette width indicates better clustered data.

$$s(\mathrm{x}) = \frac{1}{M_k}\sum_{i=1}^{M_k} s(\mathrm{x}_i) \tag{24}$$

$$SIL = \frac{1}{K}\sum_{k=1}^{K} s(\mathrm{x}) \tag{25}$$

2.3 Strategy for damage identification and localization

As shown in Section 2.2.2 and in the references[29-31], clustering methods can be applied for structural assessment considering the changes of the measured structural behaviours (classifying in clusters). The majority of researches need expert judgment to detect structural damage in SHM, especially in bridges. Nonetheless, expert judgment is not always available, therefore a robust strategy that includes the evaluation of SHM in real time should be implemented. For instance, many investigations of this type were developed on bridges.[29-31,44]. In the present study, a novelty index that has been widely studied by Santos[29-31,44] is used because it demonstrated a good performance and efficiency in many complex bridge structures under ambient vibration. The damage parameter DC based on computing the average dissimilarity between clusters can be expressed as:

$$DC = \frac{1}{\mathrm{K}(\mathrm{K}-1)}\sum_{k=1}^{K}\sum_{\substack{c=1 \\ c\neq k}}^{K} G_{ck} \tag{26}$$

Where K = number of clusters defined with the highest global silhouette index (SIL)[42]; c and k are two of the K clusters; G_{ck} = Gowda-Diday dissimilarity parameter measured between their centroids[45]. The Gowda-Diday dissimilarity measure, $G_{ck} = G(T_c, T_k)$, defined between the pair of objects T_c and T_k, is obtained by the following equations:

$$G_{ck} = \sum_{r=1}^{p} \varphi_r(\mathrm{T}_c, \mathrm{T}_k) \tag{27}$$

$$\varphi_r(\mathrm{T}_c, \mathrm{T}_k) = \frac{\left|\left|T_{c,\mathrm{sup}}^{(\mathrm{r})} - T_{\mathrm{c,inf}}^{(\mathrm{r})}\right| - \left|T_{\mathrm{k,sup}}^{(\mathrm{r})} - T_{\mathrm{k,inf}}^{(\mathrm{r})}\right|\right|}{k_r} \tag{28}$$

$$\varphi_r(\mathrm{T}_c, \mathrm{T}_k) = \frac{\left|\left|T_{c,\mathrm{sup}}^{(\mathrm{r})} - T_{\mathrm{c,inf}}^{(\mathrm{r})}\right| - \left|T_{\mathrm{k,sup}}^{(\mathrm{r})} - T_{\mathrm{k,inf}}^{(\mathrm{r})}\right|\right|}{k_r} + \frac{\left(\left|T_{c,\mathrm{sup}}^{(\mathrm{r})} - T_{\mathrm{c,inf}}^{(\mathrm{r})}\right| - \left|T_{\mathrm{k,sup}}^{(\mathrm{r})} - T_{\mathrm{k,inf}}^{(\mathrm{r})}\right| - 2\,\mathrm{I}_r\right)}{k_r} + \frac{\left|T_{c,\mathrm{inf}}^{(\mathrm{r})} - T_{\mathrm{k,inf}}^{(\mathrm{r})}\right|}{\left|Y_r\right|} \tag{29}$$

Where: $k_r = \left|\max(T_{c,\mathrm{sup}}^{(\mathrm{r})}, T_{\mathrm{k,sup}}^{(\mathrm{r})}) - \min(T_{c,\mathrm{inf}}^{(\mathrm{r})}, T_{\mathrm{k,inf}}^{(\mathrm{r})})\right|$, $I_r = \left|\max(T_{c,\mathrm{inf}}^{(\mathrm{r})}, T_{\mathrm{k,inf}}^{(\mathrm{r})}) - \min(T_{c,\mathrm{sup}}^{(\mathrm{r})}, T_{\mathrm{k,sup}}^{(\mathrm{r})})\right|$ and

$$|Y_r| = \left| \max_s (\mathrm{T}_{\mathrm{sup}}^{(\mathrm{r})}) - \min_s (\mathrm{T}_{\mathrm{inf}}^{(\mathrm{r})}) \right|.$$

When the clusters are generated in undamaged condition, the *K*-means algorithm can identify these groups clearly and will generate small values of DC. Conversely, if damages are present, the *K*-means method generates separate clusters and therefore will generate large values of DC. In addition, the proposed strategy evaluated herein used a successive time-windows (TW) technique in order to identify and localize the structural damages.

The value of DC by itself is not considered informative since the structural changes cannot be detected with a pre-defined confidence level. For this reason, the methodology considers an additional step in order to test a statistical procedure to evaluate the DC values obtained in each time window. A confidence boundary (CB) was implemented in the statistical test of each set of DC values. It means that if the structural system presents changes, then this CB will allow to identify those changes as damages. Using a statistical testing for the DC distribution at each time window, the CB is obtained under the premise that residual errors in undamaged conditions are only influenced by random effects. This premise generally uses the Normal statistical distribution as shown in many investigations of SHM[29-31,44]. Nonetheless, if the number of DC values is small, then the *t*-student distribution will be more adequate for describing small samples extracted from Gaussian populations[31]. The paper[31] suggests the confidence boundaries (CB) for each time window as below:

$$CB = E\left[DC\right] + (t_{S-1,\frac{1}{2}+\frac{\beta}{2}}) E\left[DC - E\left[DC\right]\right] / \sqrt{S} \tag{30}$$

Where $t_{S-1,1/2+\beta/2} = 1/2+\beta/2$ percentile of a *t*-student distribution with $S-1$ degrees of freedom and β is the confidence level (99.9%); $E[DC]$ = the expected value of the DC sample contained within each time window and $E[DC-E[DC]]$ = variability estimates of each DC. The statistical parameters such as mean and standard deviation are used to obtain $E[DC]$ and $E[DC-E[DC]]$ in the baseline reference data because this state does not contain outliers related to damage. These statistical indicators were used due to their accuracy to estimate the samples with an outlier incidence up to 25%, as a reference[46] suggests.

3. Case study – Warren truss bridge

3.1 Description of the bridge and vehicle

The Warren truss bridge was located in Japan and all the experimental study was carried out by Chang & Kim[47]. The structure consists of a single span 59.2m, 8.2 m maximum height, and 3.6 m width, designed for a single lane. Figure 2 (a) depicts the real bridge that was constructed in 1959, besides, after 2012 it was demolished and replaced by a new one. A dynamic load test was carried

out before the bridge was removed, using artificial damages, and during the experiment, all the traffic was prohibited and only a one van-type vehicle crossed along the bridge. Figure 2 (b) illustrates the recreation vehicle used for the experiment, which is a two-axle vehicle (Serena; Nissan Motor Co. Ltd.) with total weight of about 21 kN.

3.2. Experimental programme and damage scenarios

The experimental setup consists of a sensor network to measure vertical accelerations. Acceleration data are collected using eight uniaxial accelerometers, labelled sensors A1, A2,…A8 which, respectively, are mounted to the joint in left, middle, right and the exact positions where damages occur, as shown in Figure 2 (c). The three sensors located at the opposite side (A6-A8) serve to offer a clue to the judgment of torsion modes. The sampling rate was set as 200 Hz for all sensors. Acceleration data are collected during and after the van-type recreation vehicle drive over the deck where the sensors are located. Figure 3 plots the sequence of the five artificial damages imposed to the bridge, and it is briefly presented in Table 1. Firstly, the undamaged scenario denoted by UND show the healthy state. Secondly, two damage scenarios were applied sequentially such as: (i) Figure 3 (b) shows a half cut in a vertical member at the midspan of the bridge using an oxyacetylene cutting torch, it is considered like the first damage (DMG1); (ii) Figure 3 (c) depicts a full cut applied to the same vertical member that represented the second damage (DMG2). The previously damages explained herein can represent the corrosion and the overloading. After the DMG1 and DMG2, the full cut was recovered welding some steel plates, this damage scenario was denoted as the RCV state (as shown in Figure 3 (d)). Furthermore, despite the fact that the bridge has been not restored to its original state, the RCV state only served as a reference to the last damage scenario. Finally, a full cut was applied in the vertical member located at the 5/8th-span and was labelled as DMG3, as shown in Figure 3 (a).

Figure 2. Illustration of (a) the Warren truss bridge (b) recreation vehicle used in the test (c) location of the 8 accelerometers and artificial damages. Adapted from reference[47].

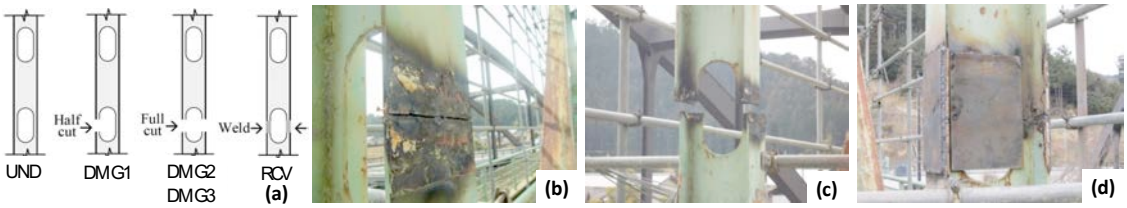

Figure 3. Experimental programme of the artificial damage (a) sequence of the damages (b) half cut (c) full cut (d) recovery. Adapted from reference[47].

Table 1. Damage actions conducted on the Steel Truss Bridge

Damage states	Description of damage actions
1	Undamaged
2	Half cut in vertical member at mid-span
3	Full cut in vertical member at mid-span
4	Mid-span member reconnected
5	Full cut in vertical member at 5/8th span

4. Results and discussion

4.1. Signal decomposition

In order to validate the effectiveness of the proposed method, all vertical accelerometers were utilized and analyzed. Figure 4 presents the time series of sensor 1 (A1) before and after severing the member for each damage scenarios, such as UND, DMG1, DMG2, RCV, DMG3 acquired from the experiment. This sensor was located at the bridge left part, representing a sensor away from artificial damages (Figure 2c). According to the nature of the excitation (forced vibration due to a crossing vehicle within the bridge), the dashed rectangle in Fig. 4 shows the part of the total acceleration record that is non-linear and non-stationary. If the frequency components change in time, the analyzed signal can be considered like non-linear[5]. The non-stationarity comes from the fact that the average amplitude of the signal also changes with time depending on the closeness of the vehicle to the location of measurement. These signals can be divided into two parts: (i) bridge forced signals that includes ten seconds from 5 s to 15 s; (ii) free vibration signals that includes from 15 s onwards. The first part of the signal, corresponding to the vehicle in the bridge is used in this paper.

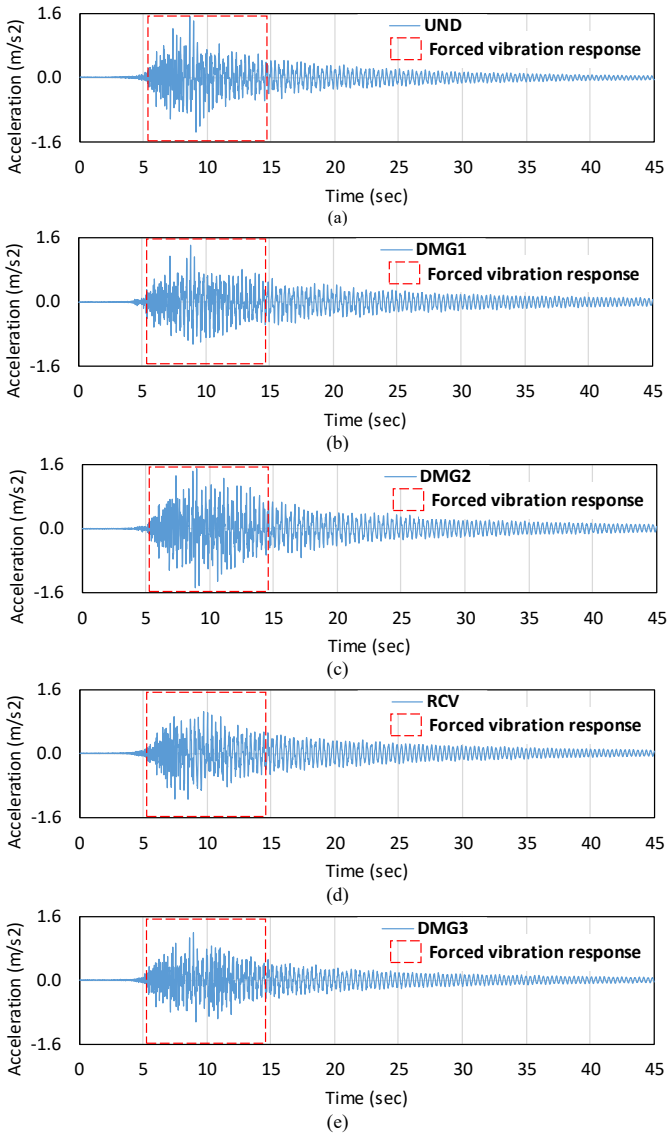

Figure 4. The forced and the free vibration of the bridge for sensor 1 in each damage scenario (a) undamaged (UND) (b) damage 1 (DMG1) (c) damage 2 (DMG2) (d) recovery (RCV) (e) damage 3 (DMG3).

One of the most challenging steps of the methodology is the frequency extraction. Although the forced and the free vibration are both time domain signals, they represent different processes: the forced vibration is a non-stationary process, while free vibration is a stationary process. To extract the instantaneous frequency of the forced signals, a proper time-frequency method is required. To this end, firstly, the non-stationary signals should be decomposed into a set of mono-component signals extracting the corresponding Intrinsic Mode Functions (IMF). Different methods have been described in Section 2.1 to extract the IMF, however the more advanced and improved EMD method named ICEEMDAN was used herein. Furthermore, the latest research claims that this improved empirical decomposition method is very robust for damage identification in bridges[20,23,48,49]. The original signal

was decomposed into three IMF considering only those that have physical meaning as shown in Figure 5. These three IMF are clearly identified in terms of its frequency content.

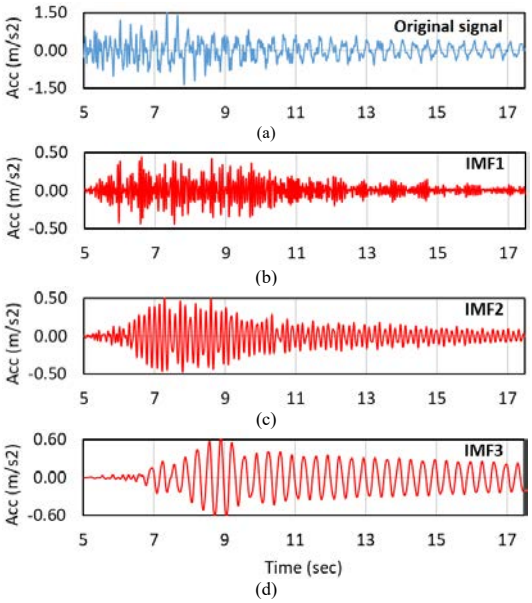

Figure 5. Decomposition results from ICEEMDAN (a) original signal (b) IMF1 (c) IMF2 (d) IMF3.

After the decomposition, Hilbert-Huang transform (HHT) has been applied to obtain the instantaneous frequency, using the mathematical formulation explained in Section 2.1.3. This analysis was carried out for each damage scenario and for all sensors. Figure 6 shows the three instantaneous frequencies estimates obtained by MATLAB for sensor 1 in undamaged state (UND). These three extracted frequencies are very stable, more pronounced and its trend is more regular and compact. In addition, the frequencies obtained are close to the theoretical natural frequencies of the bridge, which represent the bending modes obtained by Kim et al[50] who found that the first fundamental frequency is 3.0 Hz, second is 6.8 Hz and fifth is 13.3 Hz.

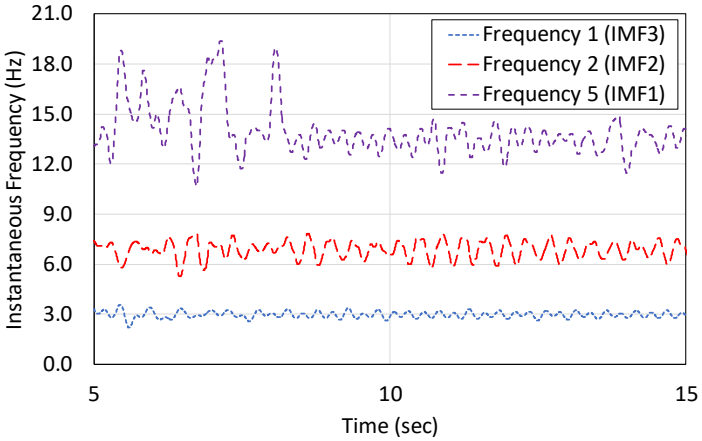

Figure 6. Instantaneous frequencies obtained by Sensor 1 in undamaged condition: first (IMF3), second (IMF2) and fifth (IMF1).

In order to verify the performance of the method, the bridge fundamental instantaneous frequency (corresponding to IMF3) is calculated along time for all the eight sensors as per Figure 7. Figure 7 (a) depicts the instantaneous frequency variation of sensor 1, located away from the three damages, and this situation is very clear since in undamaged condition (UND) the average frequency is approximately 3.0 Hz. Whereas when the damage 2 (DMG2) occurs, this average decrease slightly from 3.0Hz to 2.90 Hz. Then, this instantaneous frequency increases a little bit from 2.90 Hz to 2.97 Hz, what shows the exact behavior when the bridge changes from damaged to recovered state (RCV). Finally, considering the damage 3 (DMG3), the instantaneous frequency shows a slight decrease from 2.97 Hz to 2.94 Hz. In the case of sensor 2, the average of the instantaneous frequency for all damage states is depicted in Figure 7 (b). Firstly, the average frequency in an undamaged condition presents 2.99 Hz, which is considered close to the numerical values obtained by Kim et al[50]. Besides, the damages 2, 3 (DMG2 and DMG3) and the recovered state (RCV) show a similar behavior to that obtained in sensor 1. When the damages occur the instantaneous frequency decrease slightly (from 2.99 Hz to 2.90 Hz for DMG2 and from 2.97 Hz to 2.93 Hz for DMG3) and when the structure recovers (RCV) then the frequency increase a little bit (from 2.90 Hz to 2.97 Hz).

The Figure 7 (c) plots a particular behavior captured by sensor 3, the average of the frequency begins with 3.00 Hz for an undamaged state, nonetheless when the first damage 2 occurs (DMG2), this value decreases to a more significant value of 2.85 Hz. Therefore, this indicates that the structure has suffered a considerable damage, since sensor 3 was located in the same position where damage 2 occurs. After the DMG2 occurs, the recovered state was carried out and the average of instantaneous frequency increase from 2.85 Hz to 2.95 Hz. Furthermore, other interesting behavior was presented when the damage 3 occurred (DMG3). The frequency dropped to a not very far value (from 2.95 Hz to 2.90 Hz). Sensor 4 is deployed in a particular location as sensor 3. This behavior is exemplified in Figure 7 (d). In a first undamaged condition, the average frequency is 3.00 Hz. However, the damage 3, the most severe, caused an important drop of the average frequency down to 2.86 Hz. It can be explained because sensor 4 was located in the exact position of damage 3 (See Figure 2c). According to these results, the instantaneous frequencies decrease to a smaller value in sensors 3 and 4 when damages 2 and 3 are considered. For this reason, these sensors are able to locate the damage on the bridge.

On the other hand, the average instantaneous frequencies of sensors 5, 6, 7 and 8 are presented in Figures 7 (e) – (h) respectively. These results show a similar behavior to sensors 1 and 2. As a summary, Table 2 gives the average instantaneous frequency values obtained in all sensors. In conclusion, all the sensors are capable of capturing structural changes, however sensors 3 and 4 managed to better capture the structural changes, due to their deployment in the exact places where the damage occurred. Furthermore, the analysis of this first vibration pattern, reported accurate results regarding detection and localization of structural damages in the bridge. Therefore, a more detailed analysis of sensors 3 and 4 is carried out throughout the article.

Table 2. Average of the first instantaneous frequency (IMF3) considering all damages and sensors.

Damage states	Frequency (Hz)							
	sen1	sen2	sen3	sen4	sen5	sen6	sen7	sen8
Undamaged	3.00	2.99	3.00	2.98	3.00	2.96	2.98	3.00
Damage 02	2.90	2.90	2.85	2.91	2.90	2.89	2.89	2.89
Recovered	2.97	2.97	2.95	2.97	2.97	2.97	2.98	2.98
Damage 03	2.94	2.93	2.90	2.86	2.93	2.92	2.93	2.93

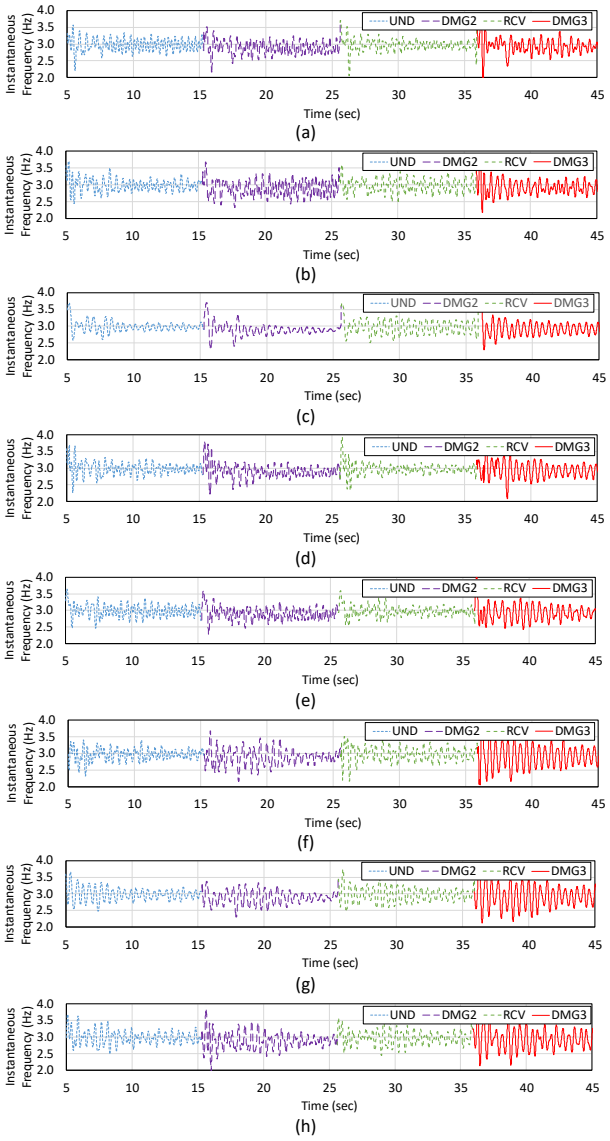

Figure 7. Variation of the first instantaneous frequencies (IMF3) at each damage state (a) sensor 1 (b) sensor 2 (c) sensor 3 (d) sensor 4 (e) sensor 5 (f) sensor 6 (g) sensor 7 (h) sensor 8.

The variation of the instantaneous frequency 2 (corresponding to IMF2) was analysed for all sensors too. Results are shown in Figure 8. The average instantaneous frequency was calculated (Table 3).

Table 3. Average of the second instantaneous frequency (IMF2) considering all damages and sensors.

Damage states	Frequency (Hz)							
	sen1	sen2	sen3	sen4	sen5	sen6	sen7	sen8
Undamaged	6.80	7.00	6.63	7.09	6.88	7.07	7.10	6.90
Damage 02	6.88	6.87	7.13	7.56	6.88	6.87	6.65	6.88
Recovered	7.04	7.12	6.50	8.08	7.02	6.94	8.01	6.81
Damage 03	7.49	7.49	6.47	6.42	7.01	5.41	8.46	8.54

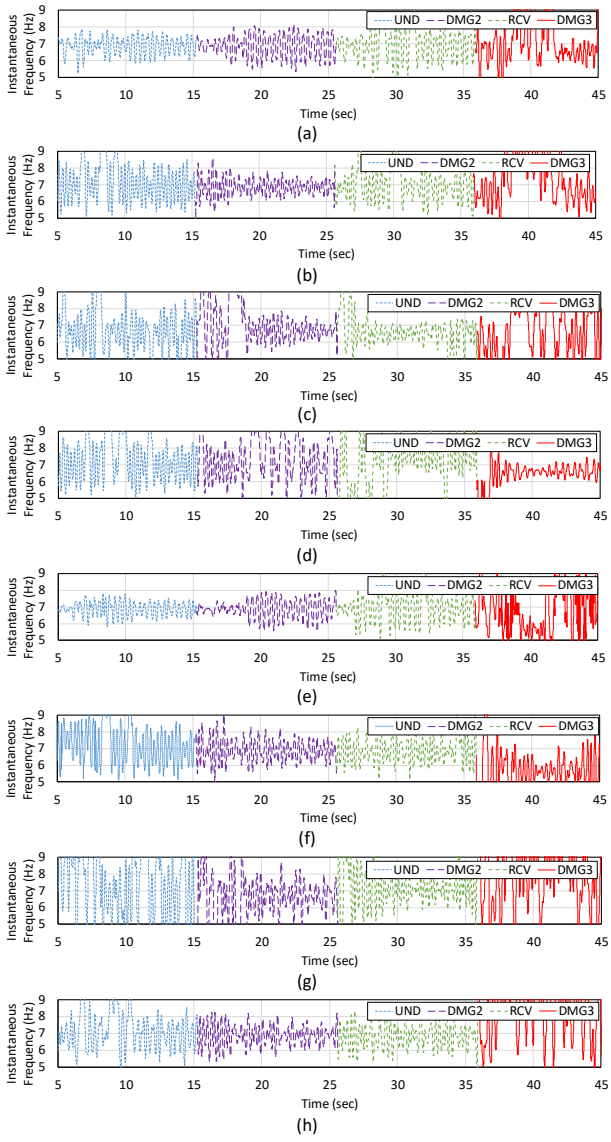

Figure 8. Variation of the second instantaneous frequencies (IMF2) at each damage state (a) sensor 1 (b) sensor 2 (c) sensor 3 (d) sensor 4 (e) sensor 5 (f) sensor 6 (g) sensor 7 (h) sensor 8.

Additionally, Figure 9 depicts the variation of the instantaneous frequency 5 (corresponding to IMF1) for all sensors. In the same way, Table 4 shows the average instantaneous frequency. For IMF2 and IMF1, the changes in the average instantaneous frequency do not help to clearly identify the artificial damage on the bridge. Therefore, these IMF´s are not further used to identify and locate structural damage in the bridge and only IMF 3 is further analysed.

Table 4. Average of the fifth instantaneous frequency (IMF1) considering all damages and sensors.

Damage states	Frequency (Hz)							
	sen1	sen2	sen3	sen4	sen5	sen6	sen7	sen8
Undamaged	13.30	14.00	13.80	13.90	13.50	13.00	14.10	14.50
Damage 02	13.29	14.34	14.49	12.89	13.98	14.06	14.54	14.57
Recovered	14.58	14.17	16.03	13.94	15.73	14.61	13.84	15.89
Damage 03	13.57	14.71	14.56	13.30	14.07	14.89	13.80	15.10

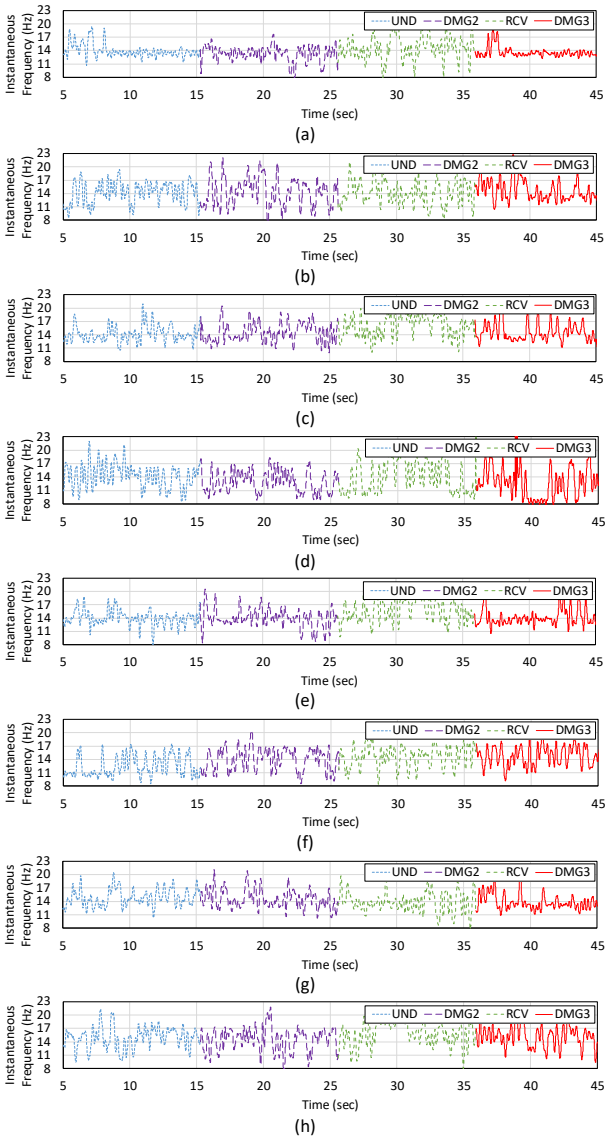

Figure 9. Variation of the second instantaneous frequencies (IMF1) at each damage state (a) sensor 1 (b) sensor 2 (c) sensor 3 (d) sensor 4 (e) sensor 5 (f) sensor 6 (g) sensor 7 (h) sensor 8.

In addition, the first instantaneous frequencies (IMF3) obtained from sensors 1, 2, 5, 6, 7 and 8 do not represent substantial changes allowing to detect or to locate the damage. Therefore, in the following only sensors 1, 3 and 4 will be analyzed. The first one is selected to show that the method

does not detect damage when damage is far from the sensor, and the other two, to show how the method is able not only to detect but also to locate damage.

4.2 Feature extraction

In Section 2.2.1 the symbolic data analysis was explained in detail with the objective to reduce the big data into more generic types of information and less voluminous. For this reason, in this work, the feature extraction is addressed using symbolic data analysis (interquartile intervals). The first instantaneous frequency (corresponding to IMF3) considering the 40 seconds of data by adding the 10 seconds window of forced vibration from undamaged and damaged scenarios was studied. With this analysis, the trend and distribution of the data groups for each damage scenario are clearly identified. The original data was converted in symbolic objects like interquartile intervals considering that the four damage scenarios (UND, DMG2, RCV and DMG3) are plotted for a time of 40 s. The sampling frequency was 200 Hz and the number of points is 8240 as shown in Figure 10. A window length of 206 points was considered and the respective boxplots were plotted for each instantaneous frequency of all sensors. Figure 10a and b give the symbolic data objects for sensor 3 and sensor 4 respectively. In this case, this type of data does not present a substantial loss of information related to structural changes.

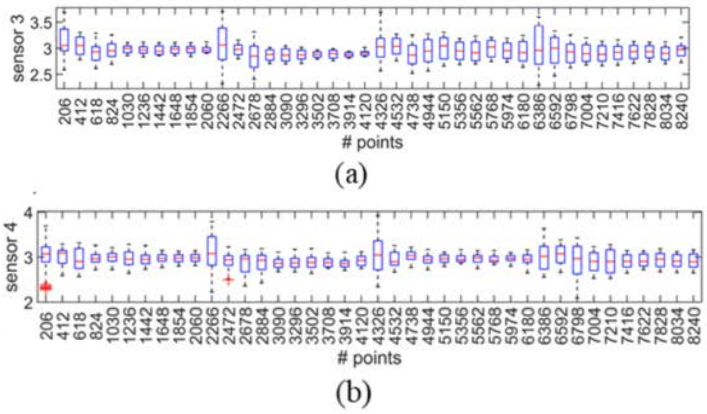

Figure 10. Time-series of IQR intervals for instantaneous frequency (a) sensor 3 (b) sensor 4.

4.3 Cluster analysis and damage novelty index

The sequence of the damage detection procedure is shown in Figures 11 and 12. Figure 11 (a) plots the instantaneous frequency obtained in sensor 3. Secondly, an algorithm of time-window (TW) described in Section 2.3 was used to successively model, classify and identify the several damage scenarios, as shown in Figure 11 (b). The sequential application of the *K*-means algorithm described in Section 2.2.2 is used to analyze each time window. Symbolic objects describing 40 seconds of normalized instantaneous frequency were considered along with time windows (5 SDO per TW[30,31,44]). Then, these time windows were used to obtain the DC values through Equation 26. The

use of the DC greatly reduces false detections with a high degree of reliability as Santos[31] indicates. All data analyzed in undamaged and artificial states for each time window is shown in Figure 11 (c). The vertical dashed lines indicate the division between all damage states along time present on the bridge. From zero to 2060 points, the results confirm that all the samples are in healthy condition (undamaged), because there is not the presence of any misfit. After point 2060, the figure shows a misfit that indicates a change in the structural response due to the presence of damage (DMG2). This behavior is more evident since damage 2 occurred at the same location of sensor 3 (Figure 2 (c)). Then, all DC values obtained show a constant trend up to the point 4532 where there is the presence of a slight misfit, that shows that the structure stabilizes at its recovered condition. The method shows a high sensitivity for damage detection and localization, as previously noted by other authors[29-31,44,51]. Furthermore, the analysis obtained of the DC values from point 6529 to 8240 (during the damage 3) showed a smooth trend with no major changes or any mismatch. This shows that damage 3 (DMG3) cannot be clearly detected by sensor 3 as this damage occurred in a location not so close to sensor 3.

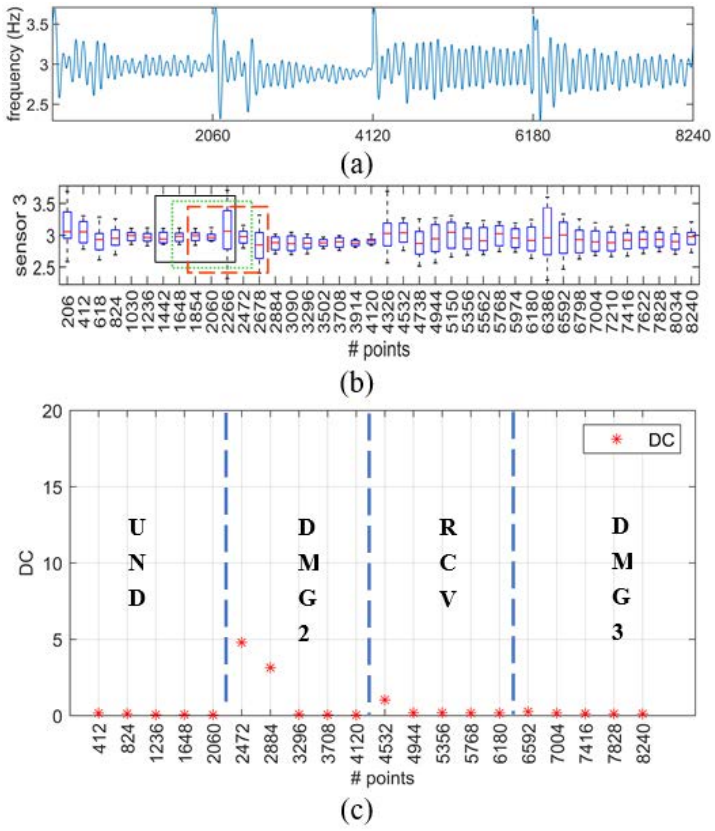

Figure 11. Damage detection procedure (a) instantaneous frequency for sensor 3 considering all damage states (b) sequence of mobile windows (c) DC values obtained from each window.

Figure 12 provides a similar damage detection procedure in sensor 4. Figure 12 (a) shows the first identified instantaneous frequency as a result of signal decomposition procedure (ICEEMDAN) and Hilbert-Transform. Figure 12 (b) gives the symbolic data analysis of the frequency and mobile

window technique that evaluates the obtained samples during the damage and healthy states of the bridge. Considering the sequential application of the *K*-means algorithm for each mobile window, both algorithms together managed to obtain the DC values in Figure 12 (c). Opposite to what is obtained in sensor 3, for sensor 4 the biggest mismatch occurs at point 6592, where DMG3 appears, whereas a small change is observed in relation to DMG2 (point 2472). This clearly shows the ability of the method not only to detect but also to locate damage, as sensor 4 is deployed where DMG3 is created.

Finally, for both sensor 3 and sensor 4 the algorithm *K*-means partitions data into k=2 mutually exclusive clusters, and returns the index of the cluster to which it has assigned each observation. On the other hand, the cluster analysis using the *K*-means algorithm for the other sensors shows SIL indices different than 2, thus revealing that the clusters are randomly assigned over time. This allocation suggests that no change in the bridge occurred during the analyzed period in the location of these sensors. In this regard, no damage was monitored by these sensors. Therefore, these results conclude the ability of *K*-means to distinguish structural conditions (undamaged and damaged state) without requiring any reference input. This can be seen in Section 4.4.

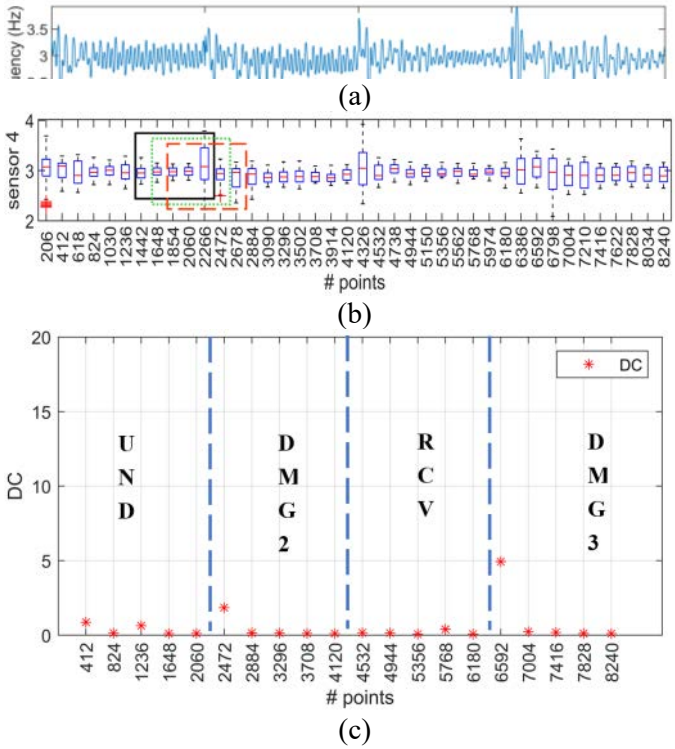

Figure 12. Damage detection procedure (a) instantaneous frequency for sensor 4 considering all damage states (b) sequence of mobile windows (c) DC values obtained from each window.

4.4 Cluster validity

In order to obtain an objective evaluation of the number of structural changes on the truss bridge, the global silhouette index (SIL) was obtained for the partitions considered in Section 4.3. In this case, this index was used to evaluate the two damage states: UND and DMG2 for sensor 3 and RCV and DMG3 for sensor 4. The SIL index was obtained for 10 possible partitions (number of clusters) as shown in Figure 13 (a) and (b) for sensor 3 and 4 respectively. Time windows are defined with fixed time length equal to DL, where L is the time between each data sample (1/200 s) and D is the number of samples in the window. For all cases, time windows comprising D = 824 samples are used, resulting in time windows of 4.12 s. 5 symbolic objects have been considered for each time window.

The validity index (SIL) was calculated for each time window and for each sensor at the intersection of the undamaged and damaged state. The time windows analyzed are the same as those used in Figures 11 and 12 for sensors 3 and 4 respectively. That is, the 20 symbolic objects comprising the undamaged state (UND) and damage 2 (DMG2) for sensor 3, and the 20 ones comprising the recovered state (RCV) and damage 3 (DMG3) for the sensor 4. The Figure 13 shows a maximum value of SIL such as 0.65 and 0.63 for sensor 3 and sensor 4 respectively, corresponding to the case of 2 clusters. In fact, each of these indices suggests that two structural behaviors (clusters) can be clearly observed in the data acquired, taking into account the analysis of undamaged and damaged scenarios. In conclusion, during the monitoring period, the structural changes have been well analyzed and identified, since this index was able to "understand" the structural behavior intrinsically present in the real bridge data[29-31,44]. For the rest of the sensors, the values of SIL were between 0.4 and 0.5 for any number of clusters.

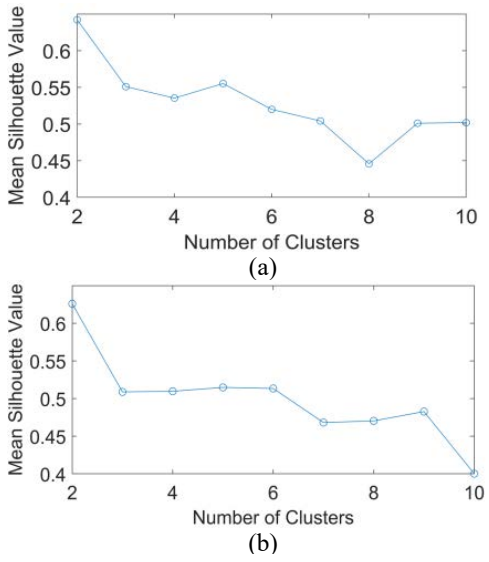

Figure 13. Cluster validity index (SIL) in undamaged and damage scenarios (a) sensor 3 (b) sensor 4.

Considering the advance in the machine-learning algorithms and its diversity in many techniques, the symbolic dissimilarities and distances have assumed especial attention because they are able to distinguish large data-sets. The dissimilarity matrices have been obtained and shown in

Figure 14 for the 20 symbolic objects comprising the undamaged and damaged state (figures 11b and 12b) for each sensor. In Figure 14, "data points" stands for the samples drawn from the time series depicted in Figures 11b and 12b for sensor 3 and 4 respectively. 100 points were considered in the change from the undamaged state (50 points from UND) to damage 2 (50 points from DMG2) for sensor 3, and from the recovered state (50 points from RCV) to damage 3 (50 points from DMG3) for sensor 4. The dissimilarity matrices contain the pair-wise dissimilarities between all 100 data points between the undamaged (UND) and damaged state, and constitute the input for cluster analysis. They present a clear difference between the undamaged and damage states (DMG2 and DMG3) for sensor 3 and 4 respectively. This information is very useful, since the structural damages can be represented by changes in the colors. In both cases, the matrices are able to distinct two groups of data. Bearing in mind that darker colors represent the discrepant pairs of symbolic modal features while brighter colors outline the similar ones, the existence of two groups well defined suggests the existence of two scenarios (healthy and unhealthy state), which are dissimilar among themselves. As a final caveat, the Ichino-Yaguchi dissimilarity obtained a good sensitivity and performance in the damage identification.

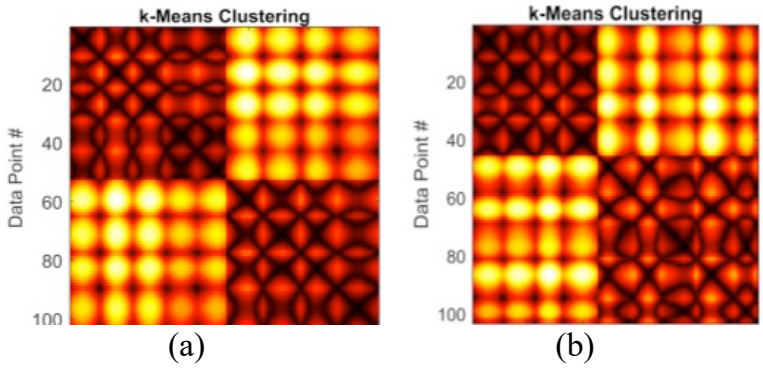

Figure 14. Distance matrix obtained from damaged structure in (a) dissimilarity matrix of sensor 3 (b) dissimilarity matrix of sensor 4.

4.5 Strategy for damage identification and localization

The DC and confidence boundary (CB) values as defined in Equation 30 obtained at each TW and for each analyzed set in sensor 3 are shown in Figure 15. The figure clearly shows a damage detection (mismatch that exceeds the confidence boundary CB) when DMG2 occurs at a position close to sensor 3. However, no damage is detected by this sensor when DMG3 takes action. Figure 15b depicts the values of DC and CB obtained at each time window for sensor 4. In this plot, the value of the DC exceeds its corresponding CB only in the intersection between phases 3 and 4 (DC values outlined with red circle). This misfit demonstrates that there is evidence of structural damage, since the damage 3 (DMG3) occurred in the exact location of sensor 4. However, in this case, the sensor is not able to detect the damage corresponding to DMG2.

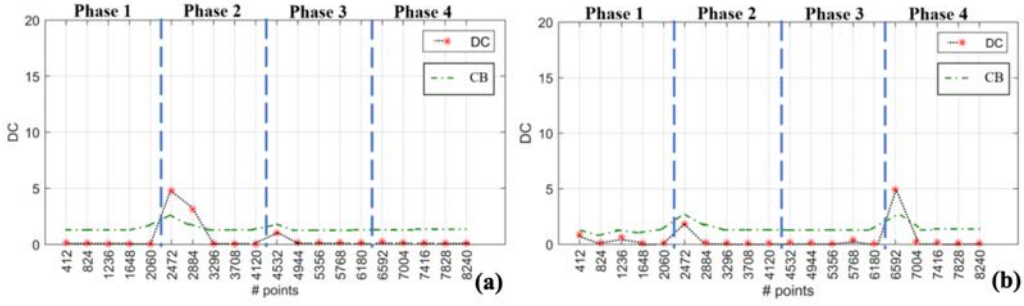

Figure 15. DC series from the sets of windows and the definition of confidence boundary (CB) within each window for: (a) sensor 3 (b) sensor 4.

Additionally, a damage localization analysis was carried out for the sensor 1 to corroborate the effectiveness of the proposed method in locating damage. Sensor 1 is located away from the artificial damages (see Figure 2c). In the Figure 16a, the DC values and confidence boundary (CB) are obtained for this sensor. As seen, DC values do not exceed the CB during the four phases (UND, DMG2, RCV and DMG3), which shows that this sensor is not capable of locating structural damage in the bridge. Similar results were obtained for sensors 2,5,6,7 and 8 (see figures 16b, 16c, 16d, 16e, 16f respectively).

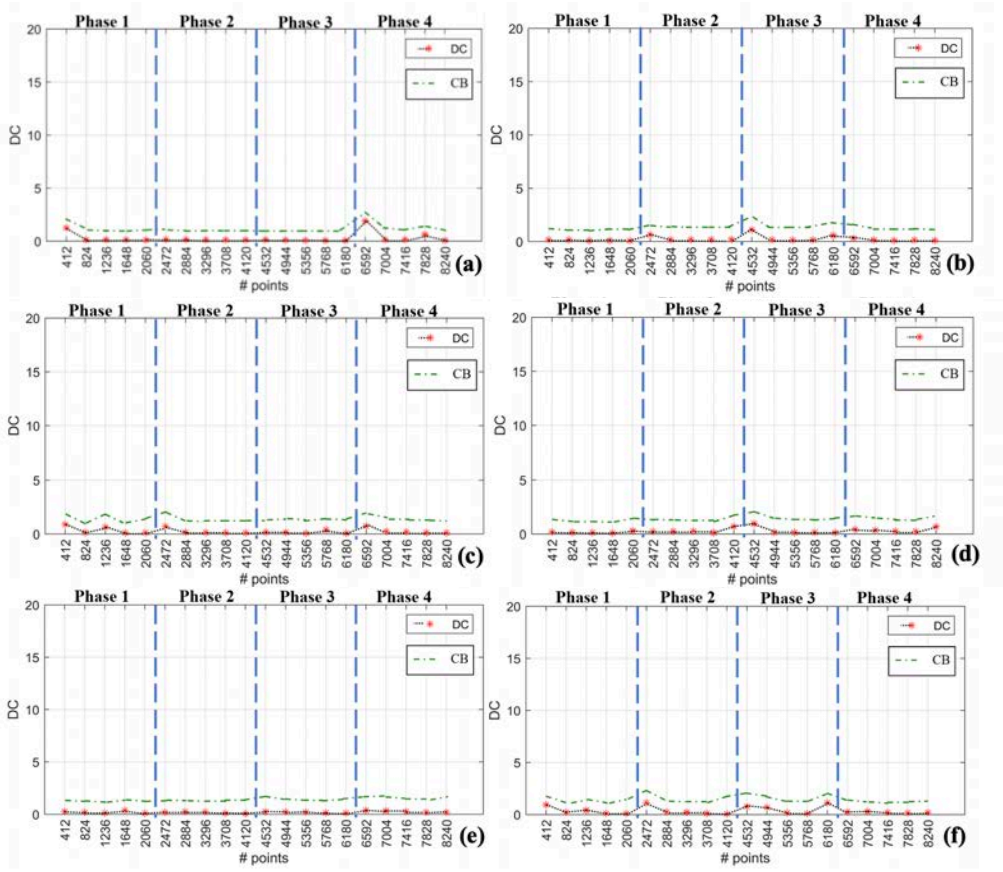

Figure 16. DC series from the sets of windows and the definition of confidence boundary (CB) within each window for: (a) sensor 1 (b) sensor 2 (c) sensor 5 (d) sensor 6 (e) sensor 7 (f) sensor 8.

In conclusion, these results suggest that the proposed novel strategy does not have limitations to choose the sensible damage parameters and confirms its performance to detect and localize structural damages immediately after their occurrence when using force-induced non-stationary vibration data coming from existing traffic in a bridge.

5. Conclusions

In this article, a promising new strategy that combines algorithms for signal processing and machine learning is proposed to conduct damage detection and localization in bridges by using the traffic-induced vibration data. Its effectiveness was assessed on the transient vibration monitoring data acquired on a Warren steel bridge crossed by a vehicle. Due to the characteristics of the acquired acceleration data in terms of non-linearity and non-stationarity, the proposed damage feature used is the instantaneous frequency obtained by HHT on previous decomposed signals obtained by the Improved Complete Ensemble Empirical Mode Decomposition with Adaptive Noise (ICEEMDAN). HHT yields improved frequency extraction based on ICEEMDAN, since dispersion in frequencies is considerably reduced. In addition, the phenomenon of mode mixing that exist in the previously studied methods specially for experimental and numerical cases has been very effectively eliminated by a suitable addition of white noise considering a good performance of the decomposition of Intrinsic Mode Function (IMF). The improvements in EMD provided by ICEEMDAN gave good results and can be considered as a reference method for the noise-assisted variation of empirical mode decomposition.

In this analysis, a clustering-based approach to group data of frequencies with similar behavior on bridge was developed, and then used to detect and localize structural damages. The *K*-means clustering algorithm was capable to allocate data objects to any number of predefined clusters. Additionally, the symbolic data objects (SDO) based on interquartile intervals were able to accurately generalize the data-set of instantaneous frequencies. The Ichino-Yaguchi distance like a judge clustering visually, was found to be sensitive to hidden structural changes in symbolic data-sets. The SIL cluster validity index demonstrated its ability to suggest the number of distinct structural behaviors (clusters in the analyzed data set) monitored on the bridge.

Finally, the clustering algorithms were employed to classify the structural conditions in the bridge and the mobile windows techniques with a confidence boundary (CB) were able to identify and localize the damages from the data-set, which shows that they are very effective and reliable in the field of bridge structural health monitoring by using traffic-induced acceleration data.

In this work, the impact of variations in operational and environmental conditions on the performance of the algorithm was not taken into account. This is due to the lack of experimental data

comprising several vehicles crossing bridges in un-damaged and damaged scenarios and with changing environmental conditions, in contrast with the case of ambient vibrations.

Acknowledgements

The first author would like to thank Ministry of Education of Peru with the Educational Credit Program PRONABEC – Bicentennial Generation Scholarship for the great support as part of the work on his PhD diploma thesis. The authors also wish to thank the Prof. Chul-Woo Kim, Department of Civil and Earth Resources Engineering, Kyoto University, Kyoto, Japan for giving us the data as well as documentation from the steel truss bridge utilized in this research work.

References

[1] An Y, Chatzi E, Sim SH, Laflamme S, Blachowski B, Ou J. Recent progress and future trends on damage identification methods for bridge structures. Structural Control and Health Monitoring. 2019 Oct;26(10):e2416.

[2] Azim MR, Gül M. Damage detection of steel girder railway bridges utilizing operational vibration response. Structural Control and Health Monitoring. 2019 Nov;26(11):e2447.

[3] Huang J, Li D, Li H, Song G, Liang Y. Damage identification of a large cable-stayed bridge with novel cointegrated Kalman filter method under changing environments, Structural Control and Health Monitoring, 25.5 (2018): e2152.

[4] Chen B, Zhao SL, Li PY. Application of Hilbert-Huang transform in structural health monitoring: a state-of-the-art re-view. Mathematical Problems in Engineering. 2014;2014.

[5] Huang NE, Shen Z, Long SR, Wu MC, Shih HH, Zheng Q, Yen NC, Tung CC, Liu HH. The empirical mode decomposition and the Hilbert spectrum for nonlinear and non-stationary time series analysis. Proceedings of the Royal Society of London. Series A: mathematical, physical and engineering sciences. 1998 Mar 8;454(1971):903-995.

[6] Huang NE, Shen Z, Long SR. A new view of nonlinear water waves: The Hilbert spectrum. Annual Review of Fluid Mechanics. 1999 Jan;31(1):417-457.

[7] Wu Z, Huang NE. A study of the characteristics of white noise using the empirical mode decomposition method. Proceedings of the Royal Society of London. Series A: Mathematical, Physical and Engineering Sciences. 2004 Jun 8;460(2046):1597-1611.

[8] Huang NE, Long SR, Shen Z. The Mechanism for Frequency Downshift. Advances in Applied Mechanics. 1996 May 9:59.

[9] Vincent HT, Hu SL, Hou Z. Damage detection using empirical mode decomposition method and a comparison with wavelet analysis. In Proceedings of the 2nd International Workshop on Structural Health Monitoring 1999 Sep (pp. 891-900). Stanford Univeristy, Standford.

[10] Yan B, Miyamoto A. A comparative study of modal parameter identification based on wavelet and Hilbert–Huang transforms. Computer-Aided Civil and Infrastructure Engineering. 2006 Jan;21(1):9-23.

[11] Qu CZ., Lian XW. Damage identification for transmission towers based on HHT. Energy Procedia. 2012 Jan 1;17:1390-4.

[12] Chen J, Xu YL, Zhang RC. Modal parameter identification of Tsing Ma suspension bridge under Typhoon Victor: EMD-HT method. Journal of Wind Engineering and Industrial Aerodynamics. 2004 Aug 1;92(10):805-827.

[13] Huang NE, Huang K, Chiang WL. HHT-based bridge structural health-monitoring method. InHilbert–Huang transform and its applications 2014 (pp. 337-361).

[14] Zhang RR, King R, Olson L, Xu YL. Dynamic response of the Trinity River Relief Bridge to controlled pile damage: modeling and experimental data analysis comparing Fourier and Hilbert–Huang techniques. Journal of Sound and Vibration. 2005 Aug 6;285(4-5):1049-1070.

[15] Wu Z, Huang NE. Ensemble empirical mode decomposition: a noise-assisted data analysis method. Advances in Adaptive Data Analysis. 2009 Jan;1(01):1-41.

[16] Yeh JR, Shieh JS, Huang NE. Complementary ensemble empirical mode decomposition: A novel noise enhanced data analysis method. Advances in Adaptive Data Analysis. 2010 Apr;2(02):135-156.

[17] Lin J. Improved ensemble empirical mode decomposition and its applications to gearbox fault signal processing. International Journal of Computer Science. 2012 Nov 1;9(6):194-199.

[18] Zheng J, Cheng J, Yang Y. Partly ensemble empirical mode decomposition: An improved noise-assisted method for eliminating mode mixing. Signal Processing. 2014 Mar 1; 96:362-374.

[19] Torres ME, Colominas MA, Schlotthauer G, Flandrin P. A complete ensemble empirical mode decomposition with adaptive noise. In2011 IEEE international conference on acoustics, speech and signal processing (ICASSP) 2011 May 22 (pp. 4144-4147). IEEE.

[20] Delgadillo RM, Casas JR. SHM of bridges by improved complete ensemble empirical mode decomposition with adaptive noise (ICEEMDAN) and clustering. Enabling Intelligent Life-cycle Health Management for Industry Internet of Things (IIOT). Proceedings of IWSHM. 2019:2111-2118.

[21] Colominas MA, Schlotthauer G, Torres ME. Improved complete ensemble EMD: A suitable tool for biomedical signal processing. Biomedical Signal Processing and Control. 2014 Nov 1;14:19-29.

[22] Moughty JJ, Casas JR. Damage identification of bridge structures using the Hilbert-Huang transform. InLife Cycle Analysis and Assessment in Civil Engineering: Towards an Integrated

Vision: Proceedings of the Sixth International Symposium on Life-Cycle Civil Engineering (IALCCE 2018) 2018 Oct (pp. 28-31).

[23] Delgadillo RM, Casas JR. Non-modal vibration-based methods for bridge damage identification. Structure and Infrastructure Engineering. 2019 Aug 8:1-22.

[24] Fugate ML, Sohn H, Farrar CR. Unsupervised learning methods for vibration-based damage detection. In Proceedings of 18th International Modal Analysis Conference–IMAC 2000 Feb 7 (p. 18).

[25] Cremona C, Santos J. Structural health monitoring as a big-data problem. Structural Engineering International. 2018 Jul 3;28(3):243-254.

[26] Yu L, Zhu JH, Yu LL. Structural damage detection in a truss bridge model using fuzzy clustering and measured FRF data reduced by principal component projection. Advances in Structural Engineering. 2013 Jan;16(1):207-217.

[27] Toivola J, Prada MA, Hollmén J. Novelty detection in projected spaces for structural health monitoring. InInternational Symposium on Intelligent Data Analysis 2010 May 19 (pp. 208-219). Springer, Berlin, Heidelberg.

[28] Cho S, Jo H, Jang S, Park J, Jung HJ, Yun CB, Spencer Jr BF, Seo JW. Structural health monitoring of a cable-stayed bridge using wireless smart sensor technology: data analyses. Smart Structures and Systems. 2010;6(5_6):461-480.

[29] Santos J, Crémona C, Orcesi A, Silveira P. Baseline-free real-time novelty detection using vibration-based symbolic features. EVACES'13. 2013 Oct 28:1-8.

[30] Santos JP, Orcesi AD, Crémona C, Silveira P. Baseline-free real-time assessment of structural changes. Structure and Infrastructure Engineering. 2015 Feb 1;11(2):145-161.

[31] Santos JP, Crémona C, Calado L, Silveira P, Orcesi AD. On-line unsupervised detection of early damage. Structural Control and Health Monitoring. 2016 Jul;23(7):1047-1069.

[32] Diez A, Khoa NL, Alamdari MM, Wang Y, Chen F, Runcie P. A clustering approach for structural health monitoring on bridges. Journal of Civil Structural Health Monitoring. 2016 Jul 1;6(3):429-445.

[33] Zhu L, Malekjafarian A. On the Use of Ensemble Empirical Mode Decomposition for the Identification of Bridge Frequency from the Responses Measured in a Passing Vehicle. Infrastructures. 2019 June;4(2):32.

[34] Yang JN, Lei Y, Lin S, Huang N. Hilbert-Huang based approach for structural damage detection. Journal of engineering mechanics. 2004 Jan;130(1):85-95.

[35] Khan I, Shan D, Li Q, Jie H. Continuous modal parameter identification of cable-stayed bridges based on a novel improved ensemble empirical mode decomposition. Structure and Infrastructure Engineering. 2018 Feb 1;14(2):177-191.

[36] Kunwar, A, Jha, R, Whelan, M, & Janoyan, K. Damage detection in an experimental bridge model using Hilbert–Huang transform of transient vibrations. Structural Control and Health Monitoring, 20(1), 2013, 1-15.

[37] Reddy M, Krishna P. Innovative method of empirical mode decomposition as spatial tool for structural damage identification. Structural Control and Health Monitoring 22.2 (2015): 365-373.

[38] Cury, A. Techniques d'anormalité appliquées à la surveillance de santé structurale. Paris: Université Paris-Est. 2010.

[39] Diday, E, and Noirhomme-Fraiture M. Symbolic data analysis and the SODAS software. John Wiley & Sons, 2008.

[40] Ichino, M, and Yaguchi H. Generalized Minkowski metrics for mixed feature-type data analysis. IEEE Transactions on Systems Man and Cybernetics 24.4 (1994): 698-708.

[41] Rendón E., Abundez I., Arizmendi A., Quiroz EM. Internal versus external cluster validation indexes. International Journal of computers and communications 5.1 (2011): 27-34.

[42] Arthur D, and Vassilvitskii S. k-means++: The advantages of careful seeding. Proceedings of the Eighteenth Annual ACM-SIAM Symposium on Discrete Algorithms. Stanford, 2006. pp 1027–1035.

[43] Rousseeuw, PJ. Silhouettes: a graphical aid to the interpretation and validation of cluster analysis. Journal of computational and applied mathematics. 20 (1987): 53-65.

[44] Santos JP., Cremona C., Silveira P., Calado L. Real-time damage detection based on pattern recognition. Structural Concrete, 17(3), (2016): 338-354.

[45] Gowda, KC, Diday E. Symbolic clustering using a new dissimilarity measure. Pattern recognition 24.6 (1991): 567-578.

[46] Rousseeuw, PJ and Croux, C. Alternatives to the median absolute deviation. Journal of the American Statistical association 88.424 (1993): 1273-1283.

[47] Chang KC and Kim CW. Modal-parameter identification and vibration-based damage detection of a damaged steel truss bridge. Engineering Structures. 122 (2016): 156-173.

[48] Mousavi, A. A., Zhang, C., Masri, S. F., & Gholipour, G. Structural damage localization and quantification based on a CEEMDAN Hilbert transform neural network approach: a model steel truss bridge case study. Sensors, 2020, 20(5), 1271.

[49] Mousavi, A. A., Zhang, C., Masri, S. F., & Gholipour, G. Structural damage detection method based on the complete ensemble empirical mode decomposition with adaptive noise: a model steel truss bridge case study. Structural Health Monitoring, 2021, 14759217211013535.

[50] Kim CW, Chang KC, Kitauchi S, McGetrick PJ, Hashimoto K, Sugiura K. Changes in modal parameters of a steel truss bridge due to artificial damage. Safety, Reliability, Risk and Life-Cycle Performance of Structures and Infrastructures: Proceedings of ICOSSAR. 2014:16-20.

[51] Santos J, Cremona C, Orcesi A, Silveira P. Multivariate statistical analysis for early damage detection. Engineering Structures 56 (2013): 273-285.

Chapter 6 – Conclusions and future research lines

In this chapter, the main conclusions of this thesis related to the results achieved and limitations encountered are presented. It also discusses future research topics for which the methods proposed in this study can be the fundamental basis or integrating parts. In general, several conclusions can be drawn from this thesis, highlighting the advantages from the application of proposed methods.

6.1. Conclusions

In this doctoral thesis it was proposed to develop and assess the performance of a methodology for damage detection, location and quantification that can be applied to vibration data coming from real bridges, taking into account the influence of environmental and operational effects on the experimentally recorded signals. The proposed methodology has to be suitable for any kind of external excitation, from ambient to forced vibration. To this end, new vibration-based parameters were defined as damage features, and advanced tools for signal decomposition and analysis as well as machine learning algorithms were developed and their reliability in the damage detection, location and quantification in 3 real bridges was demonstrated. The following conclusions are based on the main findings in the work.

1. Nowadays, bridges that present a structural health monitoring system during in-service stage present a great challenge in SHM technology to separate changes in characteristics caused by structural damage from those caused by normal variability (operational and environmental). In addition, according to various investigations, the changes caused by normal variability can be even greater than those caused by damage. In this sense, if a correct extraction of characteristics and data normalization is not carried out, the changes in the characteristics sensitive to the structural response caused by both operational and environmental influences can result in false detections of damage and consequently a taking of wrong decisions. According to the literature review, output-only methods are a highly accurate approach to solving this problem.
2. Nonlinear and non-stationary data, which are nowadays available in modern SHM systems of bridge and civil engineering structures, should be thoroughly studied. For this reason, the fundamental objective of this thesis was to utilize HHT method to analyze the nonlinear and nonstationary response signals of several real bridges. The advanced EMD procedure like Improved on Complete Ensemble Empirical Mode Decomposition with Adaptive Noise (ICEEMDAN) and Variational Mode Decomposition (VMD) have shown a good performance in the decomposition of nonlinear and non-stationary vibration data to be further applied in the Hilbert Transform.
3. A set of novel vibration parameters such as CAV, CAD, DVI, MCVI, IVI and AIVI were proposed and their feasibility as damage features to detect damage using ambient and forced vibrations in two real bridges was analyzed. In the first bridge analyzed, the signals are linear and stationary, however in the second case, the bridge is subjected to a forced vibration, which produces non-linear and non-stationary signals. The developed strategy on using non-modal vibration-based methods and the results demonstrated that these novel empirical vibration parameters are suitable for damage identification (detection, localization & quantification in the case of ambient vibration).
4. Additionally, two parameters such as the marginal Hilbert spectrum (MHS) and the instantaneous phase difference (IPD) are proposed as damage indicators for bridges under traffic loads, where recorded data is characterized by high non-linearity and non-stationarity. These parameters were

obtained from the Hilbert Huang Transform (HHT). The efficiency of the ICEEMDAN-HHT method and the feasibility of MHS and IPD as damage indicators are demonstrated in the case of a numerical model of a bridge and a real steel arch bridge subjected to traffic loading. Results for damage detection obtained in both cases are very satisfactory. On one hand, for all sensors, the peak frequencies extracted from the Hilbert marginal spectrum are reduced when damage occurs due to stiffness loss. On the other hand, all sensors detect a reduction of the instantaneous phase difference when damage occurs due to the decrease in the wave speed of the response measurements. Both damage features present an excellent performance in detecting, localizing and quantifying damage in bridges under operational loads.

5. A promising new strategy that combines algorithms for signal processing (ICEEMDAN and HHT) and machine learning (k-means) is proposed to conduct unsupervised damage detection and localization in bridges by using the traffic-induced vibration data. Its effectiveness was assessed on the transient vibration monitoring data acquired on a Warren steel bridge crossed by a vehicle taking account the instantaneous frequencies as damage parameter. In this analysis, a clustering-based approach to group data of instantaneous frequencies with similar behavior on the bridge was developed. The K-means clustering algorithm was capable to allocate data objects to any number of predefined clusters. Besides, the symbolic data objects (SDO) based on interquartile intervals were able to accurately generalize the data-set of instantaneous frequencies. The clustering algorithms were employed to classify the structural conditions in the bridge and the mobile windows techniques with a confidence boundary (CB) were able to identify and localize the damages from the data-set in an unsupervised way, which shows that they are very effective and reliable in the field of bridge structural health monitoring by using traffic-induced acceleration data. The possibility of false detections is greatly reduced by the proposed approach
6. The evolution along time of the natural frequencies were studied for the well-known Z24 bridge, which allowed a better understanding of the influence of environmental factors (temperature) on the bridge dynamics. The application of the proposed methodology includes the identification of the modal parameters as outputs in a global system model. The kernel PCA algorithm was used for output-only damage detection and gave a good performance and capability when applied to real-world data sets from an existing bridge. Its capability to identify the non-linear behavior of modal parameters due to changes in environmental conditions (temperature) is fully proven.

6.2. Future Developments

The author suggests further research work following the results and conclusions derived in this thesis. Considering the observed limitations and aspects of improvement, those identified as more relevant are presented here.

1. While the successful outcome of the proposed method for damage detection has been here demonstrated, the author does admit that at this point the empirical mode decomposition and its improvements, as used in this thesis, are not the most powerful kind of non-stationary signals decomposition methods presently available. With the advancement in signal processing, the potential use of more advanced mode decomposition is an interesting venue to explore, especially in a context of Bridge Health Monitoring (BHM) since very little work o nothing exists. It will then be possible to compare between different kinds of mode decomposition techniques in terms of their advantages and disadvantages to a certain end.
2. More robust unsupervised damage detection methodology should be implemented, capable of automatically extracting compact and meaningful information related to the condition of the bridge evaluated, since the majority of damage detection techniques reviewed under machine learning (ML) applications are based on supervised ML algorithms, which require labeled data for training. However, the data-sets for pre-damage and post-damage cases are rarely available in real civil structures as bridges, therefore, researchers should come up with more sophisticated methodologies and algorithms.
3. Actually, the advancement in Deep Learning is drawing the attention of researchers, therefore, comparisons should be made between clustering-based methods with other un-supervised learning methods as Variational Autoencoder (VA) and Generative Adversarial Networks (GAN). The results of the present thesis recommend that these comparisons will be made using many real bridge cases. Variational Auto-encoder (VAE) should be studied with major detail, because the last investigations have demonstrated more robustness and good applicability to structural damage detection on bridges
4. In cases where the real data on damaged bridges are missing, a numerical finite element (FE) model can be a good option to generate artificial data in large quantities (big data). In addition, a numerical model can generate damages of different magnitudes, in different locations of the structure, and in different types, which allows a more extensive investigation. For this case, neural networks are causing great attention in the research world for their high performance in damage identification.
5. Development of an output-only approach that combines both operational and environmental variability to detect, localize and quantify structural damage is of interest. The motivation is that all real bridges are subject to these changes during their useful life and these factors can mask the structural damage, therefore, these problems should be studied in major detail not just in a separate way but in combination and robust and accurate methodologies should be proposed.

References

[1] S. W. Doebling, C. R. Farrar, M. B. Prime, and D. W. Shevitz, "Damage identification and health monitoring of structural and mechanical systems from changes in their vibration characteristics: A literature review". United States, Los Alamos National Laboratory report LA-13070-MS, 1996.

[2] Z. W. Chen, Y.L. Xu, and X.M. Wang, “SHMS-based fatigue reliability analysis of multiloading suspension bridges”. Journal of Structural Engineering, vol. 138, no. 3, pp. 299-307, 2011.

[3] C. R. Farrar, K. Worden, "An introduction to structural health monitoring". Philosophical Transactions of the Royal Society: Mathematical, Physical & Engineering Sciences, vol. 365, no. 1851, pp. 303–315, 2007.

[4] Z. W. Chen, Y.L. Xu, Q. Li, and D.J. Wu, “Dynamic stress analysis of long suspension bridges under wind, railway, and highway loadings”. Journal of Bridge Engineering, vol. 16, no. 3, pp. 383-391, 2011.

[5] J. J. Sinou, "A review of damage detection and health monitoring of mechanical systems from changes in the measurement of linear and non-linear vibrations". In Mechanical Vibrations: Measurement, Effects and Control; Nova Science: Hauppauge, NY, USA, 2009; pp. 643–702.

[6] H. Sohn, "Effects of environmental and operational variability on structural health monitoring". Philosophical Transactions of the Royal Society of London A: Mathematical, Physical and Engineering Sciences, vol. 365, no. 1851, pp. 539–560, 2007.

[7] J. Kullaa, "Distinguishing between sensor fault, structural damage, and environmental or operational effects in structural health monitoring". Mechanical Systems and Signal Processing, vol. 25, no. 8, pp. 2976–2989, 2011.

[8] E. J. F. Figueiredo, “Damage Identification in Civil Engineering Infrastructure under Operational and Environmental Conditions”. Ph.D. Thesis (Doctor of Philosophy in Civil Engineering) — Faculdade de Engenharia, Universidade do Porto, Porto, Portugal, 2010.

[9] C. R. Farrar, N. A. J. Lieven. Damage prognosis: the future of structural health monitoring. Philosophical Transactions of the Royal Society of London A: Mathematical, Physical and Engineering Sciences, The Royal Society, vol. 365, no. 1851, pp. 623–632, 2007.

[10] A. Diez, N. L. Khoa, M. M. Alamdari, Y. Wang, F. Chen, P. Runcie. A clustering approach for structural health monitoring on bridges. Journal of Civil Structural Health Monitoring, vol. 6, no. 3, pp. 429-445, 2016.

[11] A. C. Neves, “Structural Health Monitoring of Bridges”. Doctoral Thesis, KTH Royal Institute of Technology, Stockholm, Sweden, 2020.

[12] J. P. Santos, C. Crémona, L. Calado, P. Silveira, A. D. Orcesi, On-line unsupervised detection of early damage. Structural Control and Health Monitoring, vol. 23, no. 7, pp. 1047-1069, 2016.

[13] K. Worden, G. Manson, "The application of machine learning to structural health monitoring". Philosophical Transactions of the Royal Society: Mathematical, Physical & Engineering Sciences, vol. 365, no. 1851, pp. 515–537, 2007.

[14] O. Avci, O. Abdeljaber, S. Kiranyaz, M. Hussein, M. Gabbouj and D. J. Inman, "A review of vibration-based damage detection in civil structures: From traditional methods to Machine Learning and Deep Learning applications," Mechanical Systems and Signal Processing, 147 (2021), 107077.

[15] A. Santos, E. Figueiredo, M.F.M. Silva, C.S. Sales, J.C.W.A. Costa, Machine learning algorithms for damage detection: Kernel-based approaches, Journal of Sound and Vibration, vol. 363, pp. 584–599, 2016.

[16] M. Kubat, in: An introduction to machine learning. Springer, Cham, 2017.

[17] E. Figueiredo, G. Park, C. R. Farrar, K. Worden, J. Figueiras, Machine learning algorithms for damage detection under operational and environmental variability. Structural Health Monitoring, vol. 10, no. 6, pp. 559-572, 2011.

[18] B. Yegnanarayana, Artificial Neural Networks, Prentice-Hall, New Delhi, India, 1999.

[19] P. C. Chang, A. Flatau, S. C. Liu, "Review Paper: Health Monitoring of Civil Infrastructure". Structural Health Monitoring, vol. 2, no. 3, pp. 257–267, 2003.

[20] D. Inaudi, L. Manetti, B. Glisic, "Integrated Systems for Structural Health Monitoring". In: Proceedings of the fourth International Conference on Structural Health Monitoring on Intelligent Infrastructure. Zurich, Switzerland: Empa-Akademie, 2009.

[21] ASCE, "Infrastructure report card," ASCE News, vol. 53, October 2021.

[22] M. D. Spiridonakos, E. N. Chatzi and B. Sudret, "Polynomial Chaos Expansion Models for the Monitoring of Structures under Operational Variability". ASCE-ASME Journal of Risk and Uncertainty in Engineering Systems, Part A: Civil Engineering, vol. 2, no. 3, pp. B4016003, 2016.

[23] M. R. Azim, M. Gül, "Damage detection of steel girder railway bridges utilizing operational vibration response". Structural Control and Health Monitoring, vol. 26, no. 11, pp. e2447, 2019.

[24] J. Santos, C. Crémona and P. Silveira, "Automatic Operational Modal Analysis of Complex Civil Infrastructures", Structural Engineering International, vol. 30, no. 3, pp. 365-380, 2020.

[25] A. Meixedo, J. Santos, D. Ribeiro, R. Calçada, M. Todd, "Damage detection in railway bridges using traffic-induced dynamic responses", vol. 238, p. 112189, 2021.

[26] Italy bridge collapse: what might have caused it? BBC, August 2018, https://www.bbc.com/news/world-europe- 45188668.

[27] A. C. Neves, I. González, R. Karoumi and J. Leander, "The influence of frequency content on the performance of artificial neural network–based damage detection systems tested on numerical and experimental bridge data". Structural Health Monitoring, vol. 20, no. 3, pp. 1331–1347, 2021.

[28] R. Horgan, "Fatal Taiwan bridge collapse is latest example of maintenance failings," New Civil Engineer. [Online]. Available: https://www.newcivilengineer.com/latest/fatal-taiwan-bridge-collapse-is- latest-example-of-maintenance-failings-07-10-2019/.

[29] GLOBO. Justiça faz em BH terceira audiência sobre queda de Viaduto Guararapes. October 2016. Available from Internet: <http://g1.globo.com/minas-gerais/noticia/2016- /10/justica-faz-em-bh-terceira-audiencia-sobre-queda-de-viaduto-guararapes.html>. Access on: 15.02.2017.

[30] El colapso del puente que unía Cañete y Chincha. El comercio, July 2015, https://elcomercio.pe/peru/ica/colapso-puente-unia-canete-chincha-fotos-179864 noticia/?ref=ecr.

[31] J. Santos. Smart Structural Health Monitoring techniques for novelty identification in civil engineering structures. PhD Thesis. Instituto Superior Técnico - University of Lisbon; 2014.

[32] F. Salazar. A machine learning based methodology for anomaly detection in dam behaviour. PhD Thesis. Universitat Politècnica de Catalunya; 2016.

[33] A. Santos. Output-only methods for damage identification in structural health monitoring. PhD Thesis. Institute of technology - Federal University of Pará; 2017.

[34] J. Li, H. Hao, "A review of recent research advances on structural health monitoring in Western Australia". Struct Monitor Maintenance, vol. 3, no. 1 pp. 33-49, 2016.

[35] P. Gudmundson, "Eigenfrequency changes of structures due to cracks, notches or other geometrical changes". Journal of the Mechanics and Physics of Solids, vol. 30, pp. 339-353, 1982.

[36] J. R. Casas, J. J. Moughty, Bridge damage detection based on vibration data: past and new developments. Frontiers in Built Environment, vol. 3, pp. 4, 2017.

[37] J. J. Moughty, J. R. Casas, A state of the art review of modal-based damage detection in bridges: Development, challenges, and solutions. Applied Sciences, vol. 7, no 5, pp. 510, 2017.

[38] F-L. Zhang, Y-P. Yang, H-B. Xiong, J-H. Yang, Z. Yu, Structural health monitoring of a 250-m super-tall building and operational modal analysis using the fast Bayesian FFT method. Structural Control and Health Monitoring, vol. 26, no. 8, pp. e2383, 2019.

[39] I. Yesilyurt, H. Gursoy, Estimation of elastic and modal parameters in composites using vibration analysis. Journal of Vibration and control, vol. 21, no 3, pp. 509-524, 2015.

[40] B. Chen, S-L. Zhao, P-Y. Li, Application of Hilbert-Huang transform in structural health monitoring: a state-of-the-art review. Mathematical Problems in Engineering, 2014.

[41] T. H. Yi, H. N. Li, and H. M. Sun, "Multi-stage structural damage diagnosis method based on energy-damage theory," Smart Structures and Systems, vol. 12, no. 3-4, pp. 345–361, 2013.

[42] K. Gurley and A. Kareem, "Applications of wavelet transforms in earthquake, wind and ocean engineering," Engineering Structures, vol. 21, no. 2, pp. 149–167, 1999.

[43] Y. L. Xu and B. Chen, "Integrated vibration control and health monitoring of building structures using semi-active friction dampers. Part I: methodology," Engineering Structures, vol. 30, no. 7, pp. 1789–1801, 2008.

[44] B. Chen and Y. L. Xu, "Integrated vibration control and health monitoring of building structures using semi-active friction dampers. Part II: numerical investigation," Engineering Structures, vol. 30, no. 3, pp. 573–587, 2008.

[45] D. J. Ewins, Modal Testing: Theory and Practice, John Wiley, New York, NY, USA, 2nd edition, 2000.

[46] K. Balafas, A. S. Kiremidjian, R. Rajagopal. The wavelet transform as a Gaussian process for damage detection. Structural Control and Health Monitoring, vol. 25, no. 2, pp. e2087, 2018.

[47] L. Dayang, C. Maosen, D. Tongfa, Z. Shixiang, Wavelet packet singular entropy-based method for damage identification in curved continuous girder bridges under seismic excitations. Sensors, vol. 19, no. 19, pp. 4272, 2019.

[48] S. Mahato, M. V. Teja, A. Chakraborty, Combined wavelet–Hilbert transform-based modal identification of road bridge using vehicular excitation. Journal of Civil Structural Health Monitoring, vol. 7, no. 1, pp. 29-44, 2017.

[49] R. M. Delgadillo, J. R. Casas, Non-modal vibration-based methods for bridge damage identification. Structure and Infrastructure Engineering, vol. 16, no. 4, pp. 676-697, 2020.

[50] E. Reynders, G. Wursten, G. D. Roeck, Output-only structural health monitoring in changing environmental conditions by means of nonlinear system identification. Structural Health Monitoring, vol. 13, no. 1, pp. 82–93, 2014.

[51] C. R. Farrar, S. W. Doebling, P. J. Cornwell and E. G. Straser, "Variability of Modal Parameters Measured on the Alamosa Canyon Bridge". In Proceedings of the 15th International Modal Analysis Conference, vol. 3089, pp. 257, 1997.

[52] S. Alampalli, "Influence of in-service environment on modal parameters". In Proceedings-SPIE The International Society for Optical Engineering, vol. 1, pp. 111-116, 1998.

[53] B. Peeters, J. Maeck, G. De Roeck, "Vibration-based damage detection in civil engineering: excitation sources and temperature effects". Smart materials and Structures, vol. 10, no. 3, pp. 518, 2001.

[54] G. D Roeck, The state-of-the-art of damage detection by vibration monitoring: the SIMCES experience. Structural Control and Health Monitoring, vol. 10, no. 2, pp. 127–134, 2003.

[55] R. M. Delgadillo, J. R. Casas, SHM of Bridges by Improved Complete Ensemble Empirical Mode Decomposition with Adaptive Noise (ICEEMDAN) and Clustering. In Proceedings of the Twelfth International Workshop on Structural Health Monitoring, September 10–12, Stanford University, USA, 2019.

[56] A. A. Mousavi, C. Zhang, S. F. Masri, G. Gholipour, Structural damage detection method based on the complete ensemble empirical mode decomposition with adaptive noise: a model steel truss bridge case study. Structural Health Monitoring, pp. 14759217211013535, 2021.

[57] K. Dragomiretskiy, D. Zosso, Variational mode decomposition. IEEE transactions on signal processing, vol. 62, no. 3, pp. 531-544, 2014.

[58] X. Yan, M. Jia, A novel optimized SVM classification algorithm with multi-domain feature and its application to fault diagnosis of rolling bearing. Neurocomputing, vol. 313, pp. 47-64, 2018.

[59] F. J. Tenelema, R. M. Delgadillo, J. R. Casas, Damage identification in a benchmark bridge under a moving load using Hilbert-Huang Transform of transient vibrations. In proceedings 10th International Conference on Structural Health Monitoring of Intelligent Infrastructure, 30 June to 2 July, Porto, Portugal, 2021.

[60] K. Tatsis, E. Chatzi, A numerical benchmark for system identification under operational and environmental variability. In 8th International Operational Modal Analysis Conference (IOMAC 2019), 2019.

[61] F. L. Wang, T. H. T. Chang, D. P. Thambiratnam, A. C. C. Tan, C. J. L. Cowled, Correlation-based damage detection for complicated truss bridges using multi-layer genetic algorithm. Advances in Structural engineering, vol. 15, no. 5, pp. 693-706, 2012.

[62] Centre for Research on the Epidemiology of Disasters (CRED), “Natural disasters in 2017: Lower mortality, higher cost,” 2018.

[63] J. Tan, K. Elbaz, Z. Wang, J. Shen and J. Chen, "Lessons Learnt from Bridge Collapse: A View of Sustainable Management," Sustainability, vol. 12, no. 3, 2020.

[64] K. Gkoumas, F. Marques dos Santos, M. Van Balen, A. Tsakalidis, A. Ortega, M. Grosso, A. Haq and F. Pekár, "Research and innovation in bridge maintenance, inspection and monitoring - A European perspective based on the Transport Research and Innovation Monitoring and Information System (TRIMIS)," EUR 29650 EN, Publications Office of the European Union, Luxembourg, 2019.

[65] H. Sohn, C. R. Farrar, F. M. Hemez, J. J. Czarnecki, A Review of Structural Health Review of Structural Health Monitoring Literature 1996–2001; Los Alamos National Laboratory: Los Alamos, NM, USA, 2002.

[66] J. Ko and Y. Ni, Technology developments in structural health monitoring of large-scale bridges, Engineering Structures, vol. 27, pp. 1715–1725, 2005.

[67] V. Karbhari and F. Ansari, Structural Health Monitoring of Civil Infrastructure Systems, Woodhead Publishing, 2009.

[68] A. Rytter, "Vibrational based inspection of civil engineering structures." PhD thesis. Department of Building Technology and Structural Engineering, Aalborg University, Denmark, 1993.

[69] K. Worden, J. M. Dulieu Barton, An overview of intelligent fault detection in systems and structures. Structural Health Monitoring, vol. 3, no. 1, pp. 85-98, 2004.

[70] D. M. Siringoringo, Y. Fujino, T. Nagayama, Dynamic characteristics of an overpass bridge in a full-scale destructive test. Journal of Engineering Mechanics, vol. 139, no. 6, pp. 691-701, 2013.

[71] B. Chen, X. Wang, D. Sun and X. Xie, Integrated system of structural health monitoring and intelligent management for a cable-stayed bridge. The Scientific World Journal, 2014, vol. 2014.

[72] V. H. Nguyen, J. Mahowald, S. Maas, J. -C. Golinval, Use of time-and frequency-domain approaches for damage detection in civil engineering structures. Shock and Vibration, 2014, vol. 2014.

[73] J. P. Santos, C. Crémona, A. D. Orcesi, P. Silveira, Multivariate statistical analysis for early damage detection. Engineering Structures, vol. 56, pp. 273-285, 2013.

[74] J. P. Santos, A. D. Orcesi, C. Crémona, P. Silveira. Baseline-free real-time assessment of structural changes. Structure and Infrastructure Engineering, vol. 11, no. 2, pp. 145-161, 2015.

[75] W. Fan, P. Qiao, Vibration-based damage identification methods: a review and comparative study. Structural health monitoring, vol. 10, no. 1, pp. 83-111, 2011.

[76] J. J. Moughty, J. R. Casas, A state of the art review of modal-based damage detection in bridges: Development, challenges, and solutions. Applied Sciences, vol. 7, no. 5, pp. 510, 2017.

[77] Y. An, E. Chatzi, S. -H. Sim, S. Laflamme, B. Blachowski, J. Ou, Recent progress and future trends on damage identification methods for bridge structures. Structural Control and Health Monitoring, vol. 26, no. 10, pp. e2416, 2019.

[78] K. Worden, C. R. Farrar, G. Manson, G. Park, The fundamental axioms of structural health monitoring. Proceedings of the Royal Society A: Mathematical, Physical and Engineering Sciences, vol. 463, no. 2082, pp. 1639-1664, 2007.

[79] T. H. Ooijevaar, Vibration based structural health monitoring of composite skin-stiffener structures, PhD Thesis (PhD) — University of Twente, 2014.

[80] S. J. S. Hakim, H. Abdul Razak, S. A. Ravanfar, Fault diagnosis on beam-like structures from modal parameters using artificial neural networks, Measurement, vol. 76, pp. 45–61, 2015.

[81] V. Meruane, Online sequential extreme learning machine for vibration-based damage assessment using transmissibility data, Journal of Computing in Civil Engineering, vol. 30, no. 3, pp. 4015042, 2015.

[82] J. Y. Longyuan Li, H. Wang, Y. Jin, Anomaly detection of time series with smoothness-inducing sequential variational auto-encoder. IEEE transactions on neural networks and learning systems, vol. 32, no. 3, pp. 1177-1191, 2020.

[83] MA. Xirui, L. Yizhou, N. Zhenhua, MA. Hongwei, Structural damage identification based on unsupervised feature-extraction via Variational Auto-encoder. Measurement, vol. 160, pp. 107811, 2020.

[84] R. M. Delgadillo, J. R. Casas, A combined kernel-PCA with clustering analysis for bridge damage detection under changing environmental conditions. In Life-Cycle Civil Engineering: Innovation, Theory and Practice. CRC Press, IALCCE 2021. pp. 1362-1370, 2021.

[85] E. Reynders, G. Wursten, G. D. Roeck, Nonlinear system identification for vibration-based structural health monitoring. En Proceedings of the National Congress on Theoretical and Applied Mechanics, pp. 9-11, 2012.

[86] M. Silva, A. Santos, R. Santos, E. Figueiredo, C. Sales, & J. C. Costa, "Agglomerative concentric hypersphere clustering applied to structural damage detection". Mechanical Systems and Signal Processing, vol. 92, pp. 196-212, 2017.

[87] M. Fallahian, F. Khoshnoudian, V. Meruane, Ensemble classification method for structural damage assessment under varying temperature, Structural Health Monitoring, vol. 17, no. 4, pp. 747-762, 2017.

[88] M. Fallahian, F. Khoshnoudian, S. Talaei, V. Meruane, F. Shadan, Experimental validation of a deep neural network—sparse representation classification ensemble method, The Structural Design of Tall and Special Buildings, vol. 27, no. 15, pp. e1504, 2018.

[89] C. S. N. Pathirage, J. Li, L. Li, H. Hao, W. Liu, P. Ni, Structural damage identification based on autoencoder neural networks and deep learning, Engineering structures, vol. 172, pp. 13-28, 2018.

[90] A. A. Mousavi, C. Zhang, S. F. Masri, G. Gholipour, Structural damage localization and quantification based on a CEEMDAN Hilbert transform neural network approach: a model steel truss bridge case study. Sensors, vol. 20, no. 5, pp. 1271, 2020.

[91] R. M. Delgadillo, J. R. Casas, Bridge damage detection via Improved Completed Ensemble EMD with Adaptive Noise and machine learning algorithms. Structural Control and Health Monitoring, Accepted for publication, January, 2022.

[92] R. M. Delgadillo, F. J. Tenelema, J. R. Casas, Marginal Hilbert spectrum and instantaneous phase difference as total damage indicators in bridges under operational traffic loads. Structure and Infrastructure Engineering, pp. 1-21, 2021.

[93] R. M. Delgadillo, J. R. Casas, Damage detection in a real truss bridge using Hilbert-Huang Transform of transient vibrations. In Bridge Maintenance, Safety, Management, Life-Cycle Sustainability and Innovations (IABMAS). CRC Press, pp. 890-898, 2021.

[94] F. J. Tenelema, R. M. Delgadillo, J. R. Casas, Damage detection of bridges considering environmental variability using Hilbert-Huang Transform and Principal Component Analysis. In proceedings 10th International Conference on Structural Health Monitoring of Intelligent Infrastructure, 30 June to 2 July, Porto, Portugal, 2021.

[95] F. J. Tenelema, R. M. Delgadillo, J. R. Casas, Bridge damage detection and quantification under environmental effects by Principal Component Analysis. 1st Conference of the European association on quality control of bridges and structures - EUROSTRUCT, August 29 to September 1, University of Padova, Italy, 2021.

[96] J. P. Santos, C. Cremona, A. D. Orcesi, P. Silveira, Early damage detection based on pattern recognition and data fusion. Journal of Structural Engineering, vol. 143, no. 2, pp. 04016162, 2017.

[97] J. Santos, C. Crémona, A. Orcesi, P. Silveira, Baseline-free real-time novelty detection using vibration-based symbolic features, EVACES'13. October, vol. 28, pp.1-8, 2013.

[98] J. Santos, P. Silveira, L. Calado, C. Crémona, Identificação de dano baseada em métodos numéricos e de inteligência artificial. Revista Portuguesa de Engenharia de Estruturas. Ed. LNEC. Série III, no. 1. ISSN 2183-8488, pp. 81-89, julho 2016.

[99] J. Santos, C. Crémona, P. Silveira, L. Calado, Real-time damage detection based on pattern recognition. Structural Concrete, vol. 17, no. 3, pp. 338-354, 2016.

[100] S. L. Kramer, Geotechnical earthquake engineering. Upper Saddle River, NJ: Prentice-Hall, 1996.

[101] J. J. Moughty, J. R. Casas, Damage identification of bridge structures using the Hilbert-Huang transform. In Life Cycle Analysis and Assessment in Civil Engineering: Towards an Integrated Vision: Proceedings of the Sixth International Symposium on Life-Cycle Civil Engineering (IALCCE 2018), pp. 28-31, 2018.

[102] H. Li, Y. Zhang, H. Zheng, Hilbert-Huang transform and marginal spectrum for detection and diagnosis of localized defects in roller bearings. Journal of mechanical science and technology, vol. 23, no. 2, pp. 291-301, 2009.

[103] C. -Z., Qu, X. -W., Lian. Damage identification for transmission towers based on HHT. Energy Procedia, vol. 17, pp. 1390-1394, 2012.

[104] K. Fua, J. Qua, Y. Chaia, T. Zoub, Hilbert marginal spectrum analysis for automatic seizure detection in EEG signals. Biomedical Signal Processing and Control, vol. 18, pp. 179-185, 2015.

[105] N. T. Trung, Application of the Hilbert–Huang transform to identify the dynamic characteristics of a caisson foundation during liquefaction. Structural Control and Health Monitoring, vol. 26, no. 10, pp. e2427, 2019.

[106] I. Khan, D. Shan, Q. Li, H. Jie, Continuous modal parameter identification of cable-stayed bridges based on a novel improved ensemble empirical mode decomposition. Structure and Infrastructure Engineering, vol. 14, no. 2, pp. 177-191, 2018.

[107] Z. Wu, N. E. Huang, A study of the characteristics of white noise using the empirical mode decomposition method. Proceedings of the Royal Society of London. Series A: Mathematical, Physical and Engineering Sciences, vol. 460, no. 2046, pp. 1597-1611, 2004.

[108] N. E. Huang, S. R. Long, Z. Shen, The mechanism for frequency downshift in nonlinear wave evolution. Advances in applied mechanics, vol. 32, pp. 59-117C, 1996.

[109] N. E. Huang, Z. Shen, S. R. Long, M. C. Wu, H. H. Shih, Q. Zheng, N.-C. Yen, C. C. Tung and H. H. Liu. The empirical mode decomposition and the Hilbert spectrum for nonlinear and non-stationary time series analysis. Proceedings of the Royal Society of London. Series A: mathematical, physical and engineering sciences, vol. 454, no. 1971, pp. 903-995, 1998.

[110] W. Yang, R. Court, P. J. Tavner, C. J. Crabtree, Bivariate empirical mode decomposition and its contribution to wind turbine condition monitoring. Journal of Sound and Vibration, vol. 330, no. 15, pp. 3766-3782, 2011.

[111] N. Roveri, A. Carcaterra, Damage detection in structures under traveling loads by Hilbert–Huang transform. Mechanical Systems and Signal Processing, vol. 28, pp. 128-144, 2012.

[112] I. Antoniadou, G. Manson, W. J. Staszewski, T. Barszcz, K. Worden, A time–frequency analysis approach for condition monitoring of a wind turbine gearbox under varying load conditions. Mechanical Systems and Signal Processing, vol. 64, pp. 188-216, 2015.

[113] D. M. Reddy, P. Krishna, Sathesa, Innovative method of empirical mode decomposition as spatial tool for structural damage identification. Structural Control and Health Monitoring, vol. 22, no. 2, pp. 365-373, 2015.

[114] E. J. OBrien, A. Malekjafarian, A. González, Application of empirical mode decomposition to drive-by bridge damage detection. European Journal of Mechanics-A/Solids, vol. 61, pp. 151-163, 2017.

[115] J. N. Yang, Y. Lei, S. Lin, N. Huang, Hilbert-Huang based approach for structural damage detection. Journal of engineering mechanics, vol. 130, no. 1, pp. 85-95, 2004.

[116] L. Zhu, A. Malekjafarian, On the use of ensemble empirical mode decomposition for the identification of bridge frequency from the responses measured in a passing vehicle. Infrastructures, vol. 4, no. 2, pp. 32, 2019.

[117] Z. Wu, N. E. Huang, Ensemble empirical mode decomposition: a noise-assisted data analysis method. Advances in adaptive data analysis, vol. 1, no. 01, pp. 1-41, 2009.

[118] J. R. Yeh, J. S. Shieh, N. E. Huang, Complementary ensemble empirical mode decomposition: A novel noise enhanced data analysis method. Advances in adaptive data analysis, vol. 2, no. 02, pp. 135-156, 2010.

[119] M. E. Torres, M. A. Colominas, G. Schlotthauer, P. Flandrin, A complete ensemble empirical mode decomposition with adaptive noise. In 2011 IEEE international conference on acoustics, speech and signal processing (ICASSP), May 22, pp. 4144-4147, IEEE, 2011.

[120] M. A. Colominas, G. Schlotthauer, M. E. Torres, Improved complete ensemble EMD: A suitable tool for biomedical signal processing. Biomedical Signal Processing and Control, vol. 1, no. 14, pp. 19-29, 2014.

[121] A. Bagheri, O. E. Ozbulut, and D. K. Harris, "Structural system identification based on variational mode decomposition," Journal of Sound and Vibration, vol. 417, pp. 182-197, 2018.

[122] R. R. Zhang, L. D. Olson, Dynamic bridge substructure condition assessment with Hilbert-Huang transform: Simulated flood and earthquake damage to monitor structural health and security. Transportation research record, vol. 1892, no. 1, pp. 153-159, 2004.

[123] R. R. Zhang, R. King, R. Olson, Y. L. Xu, “Dynamic response of the Trinity River Relief Bridge to controlled pile damage: modeling and experimental data analysis comparing Fourier and Hilbert-Huang techniques,” Journal of Sound and Vibration, vol. 285, no. 4-5, pp. 1049–1070, 2005.

[124] A. Kunwar, R. Jha, M. Whelan, K. Janoyan, Damage detection in an experimental bridge model using Hilbert-Huang transform of transient vibrations. Structural Control and Health Monitoring, vol. 20, no. 1, pp.1–15, 2013.

[125] C. Bao, H. Hao, Z. X. Li, Multi-stage identification scheme for detecting damage in structures under ambient excitations. Smart materials and structures, vol. 22, no. 4, pp. 045006, 2013.

[126] N. E. Huang, K. Huang, W. -L. Chiang, HHT-based bridge structural health-monitoring method. In Hilbert-Huang transform and its applications. pp. 263-287, 2005.

[127] L. W. Salvino, D. J. Pines & N. A. Fortner, Extracting instantaneous phase features for structural health monitoring. In: Proceedings of the 4th International Workshop on Structural Health Monitoring, Stanford University, pp. 666–674, 2003.

[128] D. J. Pines & L. W. Salvino, Health monitoring of one-dimensional structures using empirical mode decomposition and the Hilbert-Huang transform. Smart Structures and Materials 2002: Smart Structures and Integrated Systems, International Society for Optics and Photonics, vol. 4701, 2002.

[129] A. Entezami, H. Sarmadi, B. Behkamal and S. Mariani, Big data analytics and structural health monitoring: a statistical pattern recognition-based approach. Sensors, vol. 20, no. 8, pp. 2328, 2020.

[130] C. Cremona, J. Santos, Structural health monitoring as a big-data problem. Structural Engineering International, vol. 28, no. 3, pp. 243-254, 2018.

[131] Y. J. Kim, L. B Queiroz, Big Data for condition evaluation of constructed bridges. Engineering Structures, vol. 141, pp. 217-227, 2017.

[132] W.-H. Hu, D.-H. Tang, J. Teng, S. Said and R. G. Rohrmann, Structural health monitoring of a prestressed concrete bridge based on statistical pattern recognition of continuous dynamic measurements over 14 years. Sensors, vol. 18, no. 12, pp. 4117, 2018.

[133] Mathworks, Statistics and Machine Learning Toolbox™: User's Guide (r2021b), 2021.

[134] C.M. Bishop, Pattern Recognition and Machine Learning. USA: Springer, 2006.

[135] I. Jolliffe, Principal component analysis. 2nd. ed. New York, United States: Springer-Verlag, 2002.

[136] K. Pearson, "Philosophical Magazine," On Lines and Planes of Closest Fit to Systems of Points in Space, vol. 2, no. 11, pp. 559–572, 1901.

[137] H. Hotelling, "Analysis of a complex of statistical variables into principal components," Journal of Educational Psychology, vol. 24, no. 6, pp. 417, 1933.

[138] W. Soo Lon Wah, Y.-T. Chen, G. Wyn Roberts and A. Elamin, Separating damage from environmental effects affecting civil structures for near real-time damage detection. Structural Health Monitoring, vol. 17, no. 4, pp. 850-868, 2018.

[139] F. J. Tenelema Muñoz, Bridge damage identification under operational and environmental variability, Master thesis, Technical University of Catalonia (UPC-BarcelonaTech), 2020.

[140] B. Schölkopf, A. Smola, K. R. Müller. Nonlinear component analysis as a kernel eigenvalue problem. Neural computation, vol. 10, no. 5, pp. 1299-1319, 1998.

[141] E. Figueiredo, L. Radu, R. Westgate, J. Brownjohn, E. Cross, K. Worden & C. Farrar. Applicability of a Markov-Chain Monte Carlo method for damage detection on data from the

Z-24 and Tamar suspension bridges. In Proceedings of the 6th European workshop on structural health monitoring, pp. 747-754, 2012.

[142] L. Yu, J. H. Zhu, L. L. Yu. Structural damage detection in a truss bridge model using fuzzy clustering and measured FRF data reduced by principal component projection. Advances in Structural Engineering, vol. 16, no. 1, pp. 207-217, 2013.

[143] Y. Changxi, L. Yang, S. Yaqi, Damage detection of bridges considering environmental temperature effect by using cluster analysis. Procedia engineering, vol. 161, pp. 577-582, 2016.

[144] P. J. Rousseeuw, Silhouettes: a graphical aid to the interpretation and validation of cluster analysis. Journal of computational and applied mathematics, vol. 20, pp. 53-65, 1987.

[145] VCE. Progressive Damage Test S101 Flyover Reibersdorf (draft), Tech. Report 08/2308, 2009.

[146] M. Döhler, F. Hille, L. Mevel, W. Rücker, Structural health monitoring with statistical methods during progressive damage test of S101 Bridge. Engineering Structures, vol. 69, pp. 183-193, 2014.

[147] K.C. Chang and C. W. Kim, Modal-parameter identification and vibration-based damage detection of a damaged steel truss bridge. Engineering Structures, vol. 122, pp. 156-173, 2016.

[148] P. Moser, B. Moaveni, Environmental effects on the identified natural frequencies of the Dowling Hall Footbridge. Mechanical Systems and Signal Processing, vol. 25, no. 7, pp. 2336-2357, 2011.